NUREG/CR-2331
BNL-NUREG-51454
VOL. 7, NO. 2 AND NO. 3

SAFETY RESEARCH PROGRAMS SPONSORED BY OFFICE OF NUCLEAR REGULATORY RESEARCH

PROGRESS REPORT
APRIL 1 — SEPTEMBER 30, 1987

Date Published — June 1988

DEPARTMENT OF NUCLEAR ENERGY, BROOKHAVEN NATIONAL LABORATORY
UPTON, NEW YORK 11973

Prepared for the U.S. Nuclear Regulatory Commission
Office of Nuclear Regulatory Research
Contract No. DE-AC02-76CH00016

NUREG/CR-2331
BNL-NUREG-51454
VOL. 7, NO. 2 AND NO. 3
AN, R-1,4,5,7,8, RD

SAFETY RESEARCH PROGRAMS SPONSORED BY OFFICE OF NUCLEAR REGULATORY RESEARCH

PROGRESS REPORT
APRIL 1 — SEPTEMBER 30, 1987

Herbert J.C. Kouts, Department Chairman
Walter Y. Kato, Deputy Chairman

Principal Investigators:

R.A. Bari	W.J. Luckas, Jr.
J.L. Boccio	K.R. Perkins
J.F. Carew	A.J. Philippacopoulos
C.J. Czajkowski	W.T. Pratt
R. Fitzpatrick	U.S. Rohatgi
T. Ginsberg	J.H. Taylor
G.A. Greene	G.J. van Tuyle
J.G. Guppy	S.D. Unwin
R.E. Hall	W. Wulff
M. Khatib-Rahbar	

Compiled by: Allen J. Weiss

Manuscript Completed May 1988

DEPARTMENT OF NUCLEAR ENERGY
BROOKHAVEN NATIONAL LABORATORY, ASSOCIATED UNIVERSITIES, INC.
UPTON, NEW YORK 11973

Prepared for the
OFFICE OF NUCLEAR REGULATORY RESEARCH
U.S. NUCLEAR REGULATORY COMMISSION
CONTRACT NO. DE-AC02-76CH00016
FIN NOS. A-3014,-3024,-3215,-3227,-3230,-3242,-3252,-3268,
-3270,-3281,-3282,-3286,-3290,-3293,-3294,-3295,-3298,-3302,-3305,-3705,
-3772,-3786,-3788,-3801,-3806,-3821,-3825,-3827,-3828,-3829,
-3849,-3861,-3952,-3954,D-1679

Printed in the United States of America
Available from
National Technical Information Service
U.S. Department of Commerce
5285 Port Royal Road
Springfield, VA 22161

NTIS price codes:
Printed Copy: A12; Microfiche Copy: A01

FOREWORD

The Advanced and Water Reactor Safety Research Programs Quarterly Progress Reports have been combined and are included in this report entitled, "Safety Research Programs Sponsored by the Office of Nuclear Regulatory Research - Progress Report." This progress report will describe current activities and technical progress in the programs at Brookhaven National Laboratory sponsored by the Division of Regulatory Applications, Division of Engineering, Division of Reactor Accident Analysis, and Division of Reactor and Plant Systems of the U. S. Nuclear Regulatory Commission, Office of Nuclear Regulatory Research following the reorganization in February 1987. The projects reported are the following:

Division of Regulatory Applications -

Advanced Reactor Review/LMRs of HTGRs

Division of Engineering -

Standard Problems for Structural Computer Codes, Fire Protection Research, Characterization and Detection of Age-Related Failures of Selected Components and Systems With Consideration for Aging/Seismic Interactions, Failure Analysis and Nuclear Industry Practice, Evaluation of the Adequacy of Current Reactor Coolant Pump Seal Instrumentation and Operator Responses to Possible Reactor Coolant Pump Seal Failures, Adequacy of Current Valve In-Service Testing Methods, and Regulatory Guide for Reactor Dosimetry

Division of Reactor Accident Analysis -

Thermal-Hydraulic Reactor Safety Experiments, Protective Action Decisionmaking, MELCOR Verification and Benchmarking, Uncertainty Analysis of the Source Terms (QUASAR), Source Term Code Package Verification and Benchmarking, Risk and Risk Reduction for Zion, Thermodynamic Core-Concrete Interactions Experiments and Analysis, Containment Performance Design Objective, Review of the Core-Melt Evaluation for the Westinghouse Standard Plant (SP-90), Review of Containment Response Analyses in the Shoreham Probabilistic Risk Assessment, Fission Product Releases and Radiological Consequences of Degraded Core Accidents, and Review of the Accident Sequence Evaluation for the Westinghouse Standard Plant (SP-90)

Division of Reactor and Plant Systems -

Code Maintenance (RAMONA-3B), Assessment and Application of TRAC-BF1 Code, Plant Analyzer Development of BWR/2 and BWR/6 and Maintenance for BWR/4, Procedures for Evaluating Technical Specifications (PETS), Operational Safety Reliability Research, Risk-Based Performance Indicators, Study of Beyond Design Basis Accidents in Spent Fuel Pools (Generic Issue 82), Development of Technical Basis for Severe Accident Guidelines and Procedural Criteria for Existing BWR Plants, Development of Technical Basis for Severe Accident Guidelines and General Criteria for Existing BWR Plants, Interfacing Systems LOCA at LWRs, Improved Reliability of Residual Heat Removal Capability in PWRs as Related to Resolution of Generic Issue 99, Support for Containment Loading Studies, and Support for TRAC-PF1/MOD1 Uncertainty Analysis

The previous reports have covered the period October 1, 1976 through March 31, 1987.

TABLE OF CONTENTS

TABLE OF CONTENTS (cont'd.)

TABLE OF CONTENTS (cont'd.)

TABLE OF CONTENTS (cont'd.)

TABLE OF CONTENTS (cont'd.)

FIGURES

FIGURES (cont'd.)

FIGURES (cont'd.)

FIGURES (cont'd.)

TABLES

TABLES (cont'd.)

I. DIVISION OF REGULATORY APPLICATIONS

SUMMARY

Advanced Reactor Review/LMRs & HTGRs

The Advanced Reactor Review Safety Research Program is directed toward enchancing analytical tools for applications to the new generation of advanced reactors. In April 1987, as a result of an NRC reorganization, the Accident Analysis and Safety Review of Liquid Metal and High Temperature Gas Reactors (LMRs and HTGRs) Program was transferred from Regulation to Research. Therefore, both programs (which are coordinated to meet a common objective) are discussed here.

In the part of the effort originally supported by Research, efforts are underway to improve (1) our LMR reactivity modeling for metal fuel cores, and (2) our representation of HTGR systems during postulated water ingress events. In LMRs with metal fuels, changes in core geometry (mostly due to thermal expansion) are proportionately more important than for oxide fuel cores, largely due to the much smaller Doppler contribution in the metal cores. Appropriate reactivity feedbacks have recently been implemented into SSC, and results compare favorably to those cited by GE. Similar models have been developed for MINET. The revised numerics for tracking HTGR moisture ingress in MINET have been implemented, and testing is near completion.

In the effort to analyze the advanced LMRs and HTGRs, good progress continued to be made. A series of postulated severe accidents for the MHTGR has been analyzed, and the results are provided within. It appears that, with a fair margin, the MHTGR can survive heatup transients with and without RCCS functioning. On the LMR side, three significant findings were made: (1) breaking a primary pipe in PRISM of SAFR appears to have little safety importance, (2) the reactivity changes due to radial expansion claimed by GE and RI for PRISM and SAFR, respectively, appear to be correct - within 10% of a "hand calculated" value, and (3) the performance of the air-cooled vessel systems, RVACS and RACS, should be at least as effective as GE and RI claim.

1. Advanced Reactor Review/2. LMRs & HTGRs (Combined) (C. J. Van Tuyle)

The Advanced Reactor Review Safety Research Program has continued under NRC Research funding since October 1986. In April 1987, as a result of an NRC reorganization, the Accident Analysis and Safety Review of Liquid Metal and High Temperature Gas Reactors (LMRs and HTGRs) Program was transferred from Regulation to Research. Therefore, both programs are discussed here under the "Research" title of Advanced Reactor Review.

The combined programs are focused to help NRC accomplish the review of advanced reactor (LMR and HTGR) designs over the next one and one-half years. Technical assistance in the following areas is provided: (1) review, adaptation, and implementation of analytical tools and models for application to the design submittals, (2) independent analysis of specific accidents and plant conditions and characteristics for the designs, (3) developing and evaluating appropriate source terms, (4) reviewing DOE reports on safety issues, (5) review of those aspects of DOE's base technical program related to the areas described in (1) through (4), and (6) assistance in assessing PRAs submitted for review.

1.1 Advanced Reactor Review Efforts

1.1.1 LMR Reactivity Modeling (H. S. Cheng, G. C. Slovik, G. J. Van Tuyle)

The use of metallic fuel causes significant changes in the importance of the various reactivity feedbacks. The hard neutronic spectrum and the small temperature rise across (radial direction) the fuel pins act to significantly reduce the importance of Doppler feedback. The sodium density feedback is positive (undesirable), but is of only moderate importance until boiling is reached. Expansion of the core and the control rod drive lines is very important, given the small Doppler. Thus, much of our effort to modify our codes, originally developed for oxide fuels, is in the incorporation of the reactivity feedbacks due to geometric effects.

Several of the key reactivity feedbacks have now been implemented in SSC [Guppy, 1983], including metal fuel Doppler, sodium density feedbacks (was in place already), axial fuel expansion, and radial expansion at the load pads and the grid plate. Expansion of the control rods is currently being added. Bowing, which is expected to be a negative feedback (and therefore helpful), will be neglected in order to be conservative regarding this very complex response. The SSC reactivity feedbacks have been tested against results generated by GE for a postulated 3$ insertion (see later section), and the feedbacks in the SSC run appear consistent.

Similar reactivity feedback models have been developed for MINET [Van Tuyle, 1984] but have not yet been implemented. (MINET has more flexibility in representing the LMR systems, while SSC has the more detailed reactor model.)

1.1.2 HTGR Ingress Modeling (G. J. Van Tuyle, A. Aronson, J. W. Yang)

Problems with the numerical behavior of our initial water ingress model

for MINET forced us to convert to an implicit differencing scheme. Implementation of the revised numerics has taken some time, but testing is now nearly completed. In the meantime, water ingress analyses have been performed using carefully chosen reactivity boundary conditions, and results similar to those reported by ORNL have been obtained.

1.1.3 COMMIX (G. J. Van Tuyle, B. C. Chan)

Our concerns regarding the gap between the reactor and containment vessels in SAFR, which would have required COMMIX [ANL, 1985] analysis of some important transients, have been answered by RI. They have reduced the gap to seven inches, which is small enough so the IHX will remain covered in the case of a reactor vessel leak. Thus, our need for COMMIX runs is no longer immediate.

1.1.4 Assessment of DOE LMR Metal Fuels Behavior Research Plan (T. Ginsberg)

Our preliminary review of the DOE LMR Metal Fuels Behavior Research Plan has now been completed, and our findings are being documented. As the research program is still very much in process, there is considerable uncertainty regarding the metal fuel/HT9 cladding currently envisioned for PRISM and SAFR.

One area of interest is the response of LMR fuel to overpower transients. Prior thinking about fission gas release led to speculation that gas release during a transient would lead to axial fuel expansion and a rapid negative feedback effect. Recent interpretation of TREAT M-Series tests suggests that insignificant axial expansion occurred prior to the onset of fuel melting. It is now believed the observed behavior is due to a combination of two factors: (1) accommodation of gas released during the transient by the available porosity, and (2) binding of the fuel and cladding prior to eutectic formation, thus restricting axial fuel motion.

1.1.5 Validation of LMR Reactivity Modeling (G. J. Van Tuyle)

A computer code validation workshop was held at ANL on May 19th. While the ANL team that runs the EBR-II facility is doing quite well with their codes, the other efforts, e.g., SASSYS, are just beginning to benchmark their codes against EBR-II data. An effort to benchmark our codes against the EBR-II data is planned for next year.

1.2 Accident Analysis and Safety Review

1.2.1 Modular HTGR (P. G. Kroeger)

1.2.1.1 PSID Review (P. G. Kroeger)

A review of Chapter 5 of the Preliminary Safety Information Document (PSID) and the corresponding sections of the Technology Development Plan was performed. At the pursuant review meeting, a list of questions was discussed and submitted to RES.

Chapters 6, 9, 10 and 11 of the PSID were reviewed. The resulting questions were discussed with RES and passed on to DOE, where appropriate, in the review meeting.

After receipt of the requested material properties, as well as design and performance data from GA, several minor items were clarified in phone conversations with GA. Considering this information, a re-evaluation of RCCS performance was made, confirming that the computations by GA for the PSID were indeed reasonable. Modifying our RCCS model in THATCH [Kroeger, 1986] correspondingly we obtained reactor vessel temperatures and RCCS panel temperatures sufficiently close to those given in the PSID.

Based on the information submitted by GA regarding the RCCS design, our depressurized core heatup accident models were revised, including internal fin performance evaluation in the PASCOL code computations of the RCCS.

The resulting more detailed computations show that the RCCS performance data of Section 5.5 of the PSID are indeed realistic. The revised models are now being used in the evaluation of Safety Related Design Condition (SRDC-6).

Chapter 15 of the PSID was reviewed. The resulting questions were discussed with RES and passed on to DOE, where appropriate, during the review meeting. Initial water ingress evaluations during depressurized core heatup (SRDC-6) indicate, that depending on how tightly the main loop shut-off valve closes, the bypass flow through the steam generator, though small (a few kg/hr), can be larger than the in-core recirculation flow. In such cases, the total H_2O inventory could increase over previous predictions, but would still remain relatively small.

The PRA report for the Modular HTGR was reviewed. The resulting questions were discussed with RES and passed on to DOE, where appropriate, during the review meeting.

1.2.1.2 Depressurized Core Heatup Accident Scenarios in Advanced Modular High Temperature Gas-Cooled Reactors (P. G. Kroeger)

The reactor vessel (Figure 1.1) is not thermally insulated, resulting in a permanent heat loss to the RCCS of about 0.8 MW during normal full power operations (about 0.3% of full power heat generation of 350 MW). During some of the worst case licensing basis events, the reactor is scrammed, all forced circulation is lost, and the primary loop is depressurized. Thereafter, decay heat removal is from the core predominantly by conduction and radiation to the reactor vessel and from there to the RCCS.

This analysis considers the core heatup and cooldown transients resulting from the above accident scenario, with the peak fuel temperatures and also the peak vessel temperature being the items of most concern. Excessive fuel temperatures leading to fuel failures can result in increased fission product releases. Excessive vessel temperatures can affect vessel integrity and compromise restart capability after an accident transient.

The analysis was performed with the THATCH [Kroeger, 1986] code, analyzing transient conduction and radiation in the reactor vessel, coupled with

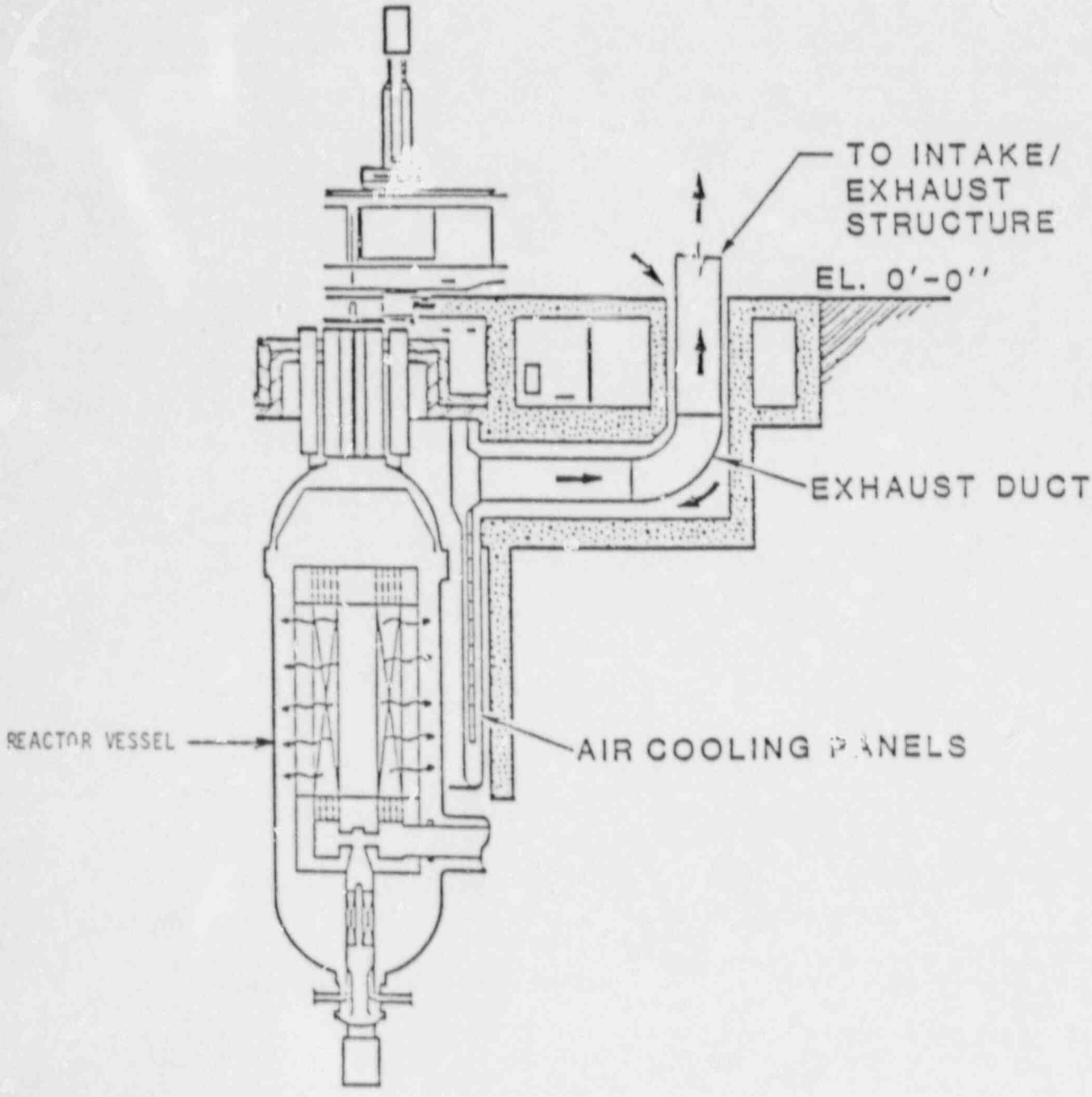

Figure 1.1 Schematic of Reactor Vessel and Reactor Cavity Cooling System (Ref. 1)

the PASCOL code, which analyzes quasi-static RCCS flow and heat transfer conditions.

The THATCH [Kroeger, 1986] code is a general purpose reactor code, which was applied here to the MHTGR reactor vessel geometry. It solves the conduction equation for all major solid capacitances, as nodalized by the user, applying an ADI numerical method, using prescribed temperature dependent property functions for all reactor components.

Heat transfer across internal gaps can be modeled as conduction, convection, and one-dimensional radiation, or any combination of these, as specified by the user. For larger internal volumes, multi-dimensional radiation can be prescribed, and is used here in the upper and lower plena.

Heat from the reactor vessel to the RCCS panel side facing the reactor is removed via natural convection and radiation. Heat transfer within the RCCS up-flow channel is by conduction and radiation to its internal fins and the back panel, and by convection from all metal surfaces to the upflowing air. The PASCOL code can, at each elevation, either model this combined conduction/convection/radiation heat transfer in detail, or use a prescribed fin effectiveness coefficient, computing local heat transfer from the panels to the coolant based on local panel temperatures. Sample applications have shown that detailed local fin conduction and radiation solutions are not warranted, since for a given design the fin effectiveness does not vary significantly in space or time during a transient. Constant user supplied fin effectiveness data, developed in a separate parametric study, were therefore applied here. Coupled with the axially nodalized heat transfer analysis, the PASCOL code also solves a one-dimensional quasi-steady momentum equation for the RCCS air flow, including ducting losses and stack effects.

Applying these codes, using best estimate input data, the results of Figures 1.2 to 1.5 were obtained. Core and fuel temperatures rise initially reaching a peak fuel temperature of about 1370°C around 60 hr, with a gradual cooldown thereafter. Figure 1.3 shows that initially the decay heat exceeds the heat removal, with excess energy being stored in the core and reflector solid capacitances. Around 70 hr, the heat absorbed by the RCCS begins to exceed the decay heat resulting in a net cooldown of the reactor.

Peak fuel temperatures of 1400°C and vessel temperatures of 420°C pose no challenge to either component and are no reason for any concern. However, the above evaluation was a best estimate transient and an important safety question still remains, i.e., whether within the uncertainty bands for some of the input parameters, significantly different results could be expected.

Therefore, a parametric study was conducted to identify those parameters that do affect performance significantly, and to establish the safety margins available in these parameters. Some of these variations are summarized in Table 1.1, showing the effects of fuel-core gaps between fuel elements, reflector irradiation, graphite annealing, as well as ambient air inlet temperature and vessel and RCCS panel thermal emissivity. Variation of none of these parameters had any significant effect on the transient, except that Case 6 (i.e., reduced thermal emissivity), showed the importance of maintaining a

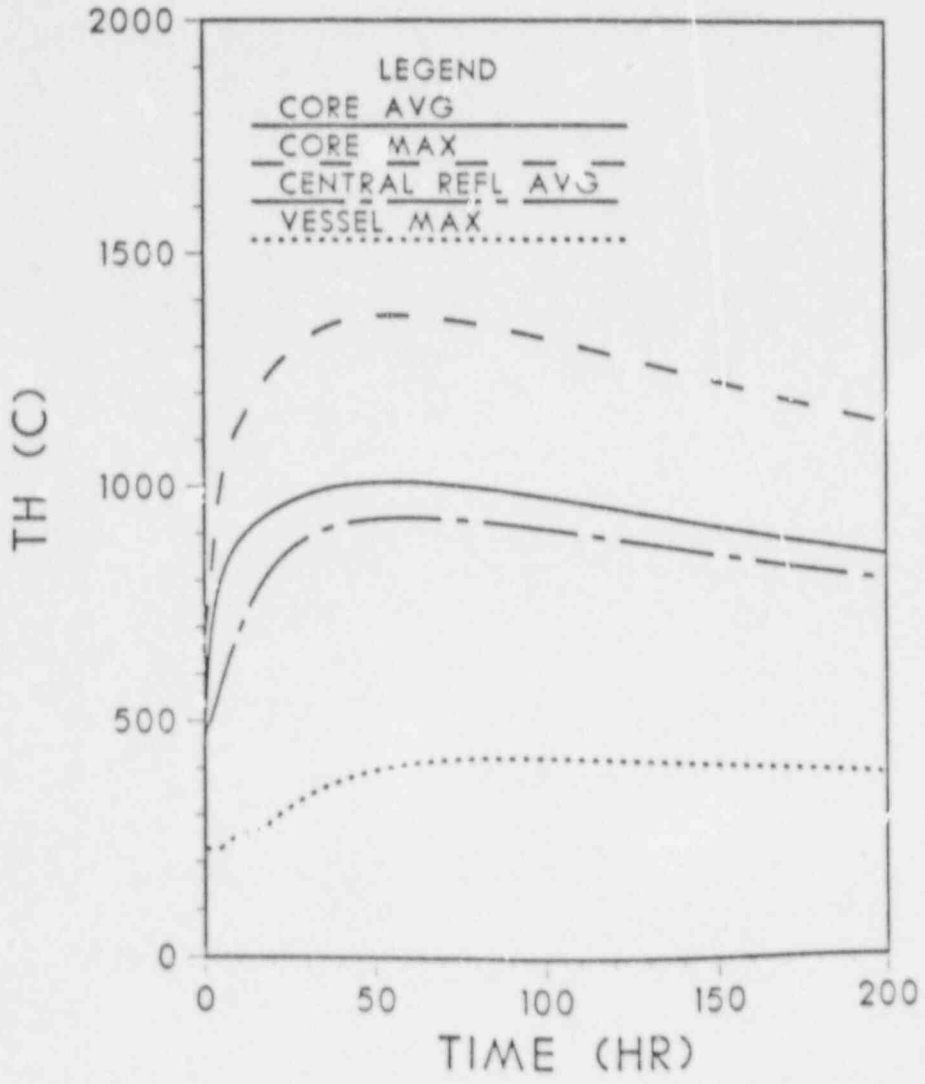

Figure 1.2 Best Estimate Core and Reactor Vessel Temperatures During Depressurized Core Heatup Accident Conditions

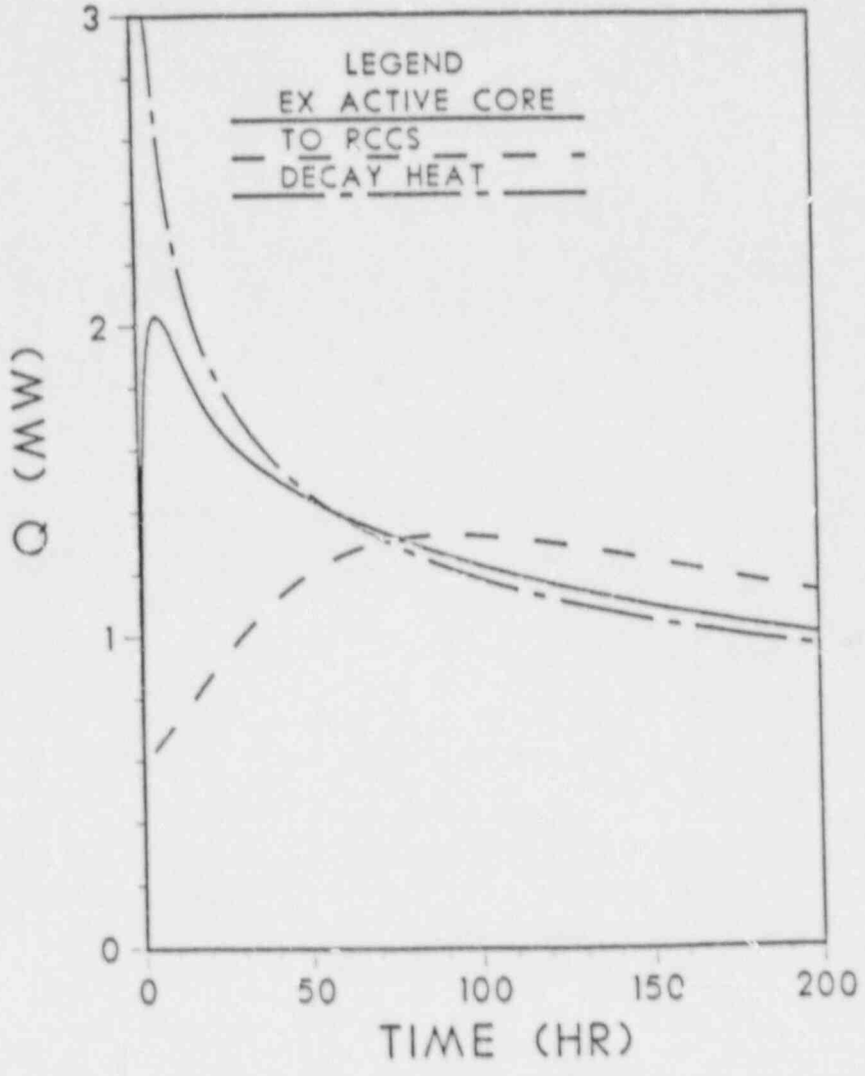

Figure 1.3 Best Estimate Heat Flows During Depressurized Core Heatup Accident Conditions

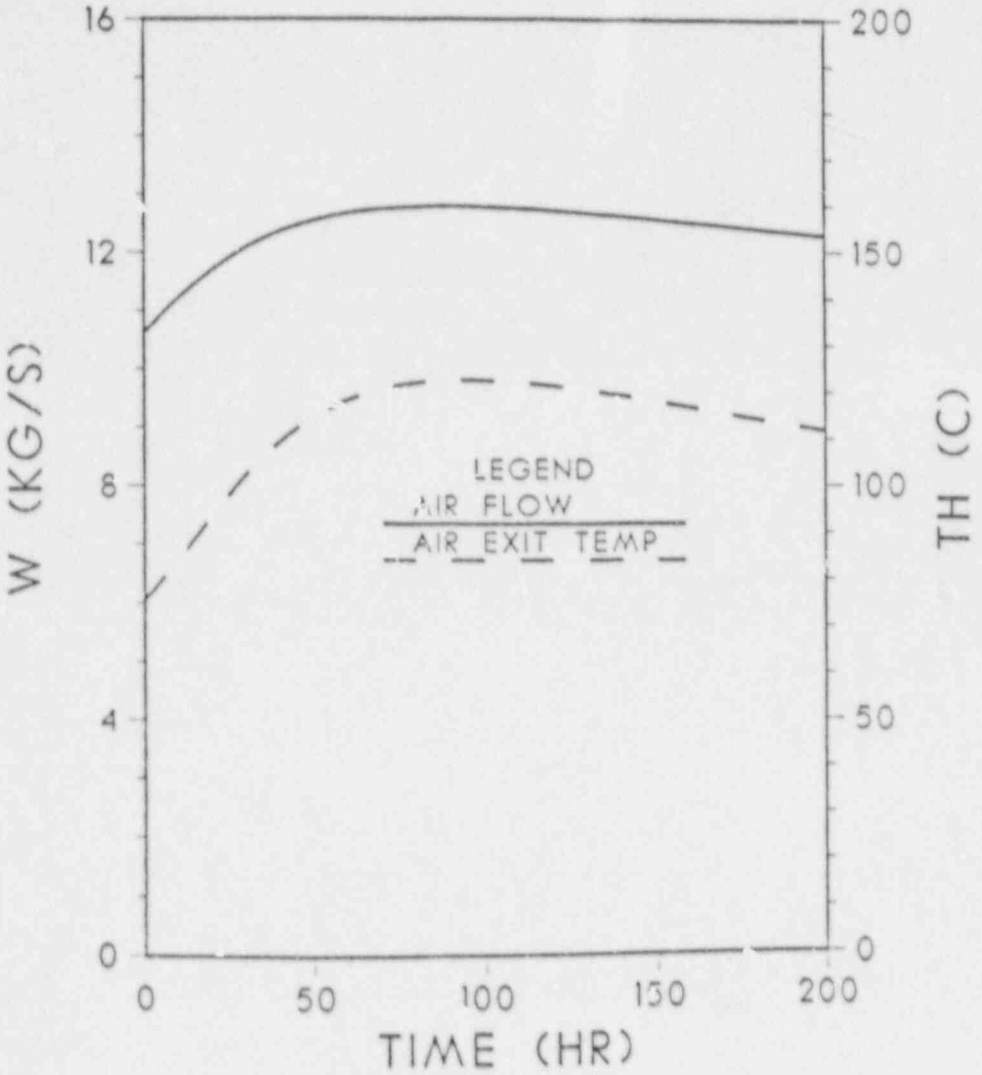

Figure 1.4 Best Estimate RCCS Performance During Depressurized Core Heatup Accident Conditions

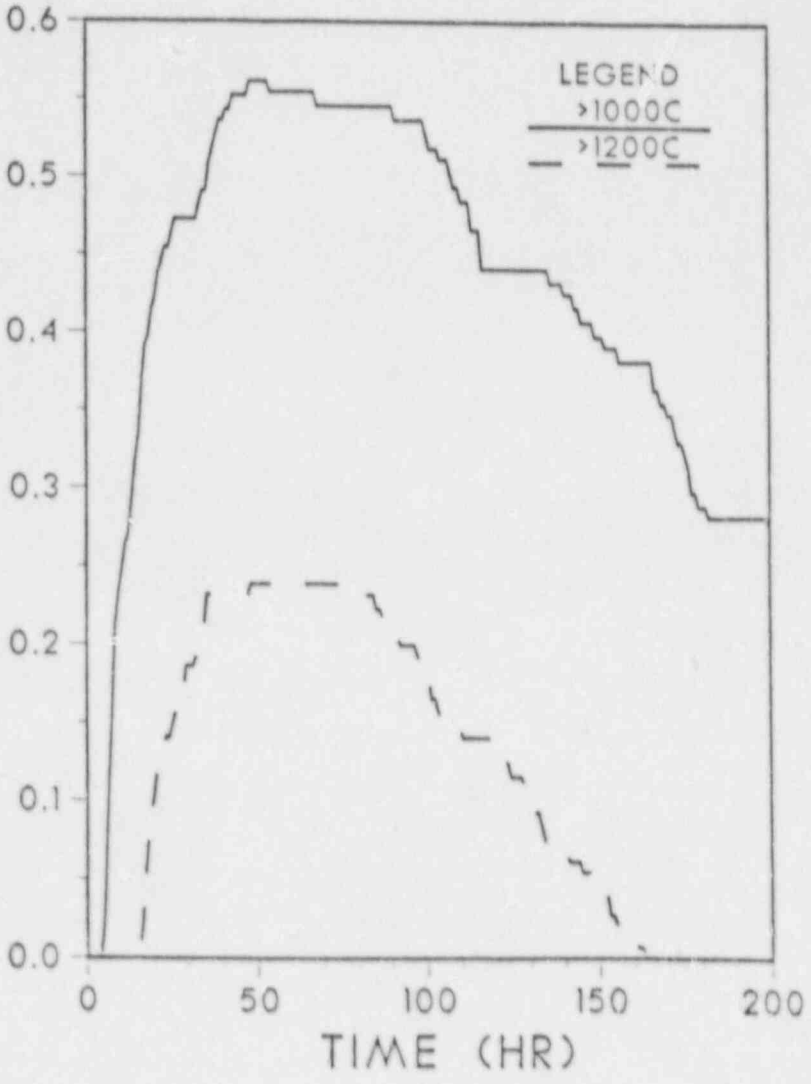

Figure 1.5 Fractions of Active Core Exceeding Specified Temperature During Depressurized Core Heatup Accident Conditions

Table 1.1 Parametric Comparison of Several Depressurized Core Heatup Transients with Operating RCCS

Case No.	Description	Peak Fuel Temperature			Peak Vessel Temperature			Vessel Cross Over Time* hr
		Value °C	At Time hr	Variation From Base Case °C	Value °C	At Time hr	Variation From Base Case °C	
1	Base Case	1320	58	-----	425	89	-----	73
2a	Without Any In-Core Gaps	1272	56	-48	433	82	+8	66
2b	In-Core Gap Widths Doubled	1339	59	+19	423	92	-2	76
3a	All Reflector Graphite Unirradiated	1261	54	-59	421	83	-4	68
3b	Replaceable Side Reflectors Plus One Row Each of Top and Bottom Reflectors Irradiated to Saturation	1354	63	+34	427	95	+2	78
4	Suppress Graphite Annealing	1405	67	+85	423	92	-2	74
5	RCCS Air Inlet Temperature 43°C	1321	59	+1	436	90	+11	75
6	RCCS and Vessel Emmissivity 0.6	1324	61	+4	474	97	+49	82

*Time at which heat leaving vessel exceeds decay heat, i.e., net cooldown of reactor vessel and internals begins.

reasonably high emissivity on the vessel and RCCS panels to avoid hot spots. The results of Case 4 point out that inclusion of a complete graphite annealing process in the model did affect the results significantly.

However, the two parameters which were found to be of major concern are the decay heat function and the core effective thermal conductivity. Both of these can significantly affect the peak fuel temperatures. Current fuel failure data indicate that there is virtually no fission product release due to core heatup up to 1600°C peak fuel temperature, with very little increase in the range of 1600 to 1800°C. At about 2200°C, massive fuel failures would be expected to occur. By varying the best estimate decay heat function it was found that a 30% increase in decay heat would cause peak fuel temperatures to reach 1600°C, and a 110% increase would be required to reach peak fuel temperatures of 2200°C. Similarly, by arbitrarily varying the core thermal conductivities, it was found that a reduction to 63% of best estimate values raised peak fuel temperatures to 1600°C, and a reduction to 30% resulted in 2200°C peak fuel temperatures.

While a reduction of core conductivities affected the vessel temperatures only very little, increased decay heat also raised the peak vessel temperatures, and a 32% increase in decay heat was required to reach the peak vessel temperature to 480°C, a value beyond which restart capability might be compromised.

These investigations have shown that typical expected depressurized core heatup transients do not result in excessive core and vessel temperatures, and that there are at least 30 to 40% margins in the decay heat function and core thermal conductivities, before temperature levels of concern are being reached. However, the evaluations also indicate the necessity to establish a high degree of confidence in the best estimate decay heat and thermal conductivity data.

1.2.1.3 Severe Accident Core Heatup Transients in Modular High Temperature Gas-Cooled Reactors without Operating Reactor Cavity Cooling Systems (P. G. Kroeger)

In this hypothetical severe accident, all forced cooling is lost, the primary loop is scrammed and depressurized, and, in addition, the completely passive RCCS is also lost.

The RCCS, with two separate stacks and four independent, but cross connected inlet and outlet ducts incorporates a significant amount of redundancy. Partial failures of the ducting or cooling panels have been shown to result in minor decreases of performance only. Thus, a complete failure of all air flow is an extremely unlikely event, and even a 90% loss of air flow scenario would be an accident of significantly lower severity than the one to be considered here.

To protect the reactor cavity concrete under normal operating conditions, thermal insulation is provided in the reactor cavity on the back side of the RCCS panels, as well as in the ceiling and floor regions of the cavity. In

case of an RCCS failure this insulation becomes the most significant heat transfer barrier, retarding heat rejection to the surrounding concrete structures and to the soil. This insulation is assumed to remain in place. Thus, the assumed accident scenario is a most conservative one, assuming that a major catastrophic event completely destroys and blocks all air ducting and stacks, but leaves all thermal insulation in place.

The analysis of this accident was conducted using the THATCH code. For the current application, the nodalization of the top and bottom regions of the reactor vessel and its surroundings had to be refined. Additionally, the thermal insulation and the concrete structures of the silo and the surrounding soil were added. As reactor cavity temperatures are much higher than in-core heatup transients with RCCS, a two-dimensional radiation model was used for the reactor cavity.

Since this accident is well beyond the design basis, neither the concrete structure nor the surrounding soil are currently planned to be controlled during design and construction of the plant. Therefore, the Base Case for the current accident evaluations makes rather pessimistic property selections for both concrete and soil. Concrete properties can vary widely and a set of properties which had been used in previous gas-cooled reactor safety studies was adopted from [General Atomic, 1978]. However, at temperatures between 1[illegible]C and 400°C, concrete typically first looses its physically bound moisture, and then also some of its chemically bound moisture, resulting in a lower thermal conductivity. Therefore, our Base Case evaluations use the above thermal conductivity only up to 200°C. Beyond 400°C a "dry" thermal conductivity of 0.5 W/mK was applied, with linear transition between the two models between 200°C and 400°C. For the surrounding soil, a relatively low conductivity clay was assumed with k = 1.28 W/mK.

About 70% of the reactor vessel is faced by five feet concrete walls which face other side cavities, then three feet of concrete and ultimately the soil. Only 30% of the vessel faces three feet concrete walls and soil directly. As the code currently cannot model this peripheral non-symmetry, these two geometries were modeled separately. It was found that the differences between the two models were not very significant, and since some average of the two configurations would represent the real situation, implementation of a model including this non-symmetry was not justified.

In evaluating the resulting Base Case transient the temperature and heat flow responses of Figure 1.6 and 1.7 were obtained. The peak fuel temperatures of almost 1400°C were reached at about 80 hr. This value is only about 30°C higher than the corresponding peak fuel temperatures with operating RCCS. Thus, even this pessimistic accident scenario is not expected to cause any significant fuel failures or fission product releases. However, the peak reactor vessel temperatures now reach 750°C, while they were around 420°C for the case with operating RCCS. Also, while the core begins a gradual but slow cooldown after 80 hr, the vessel temperatures remain within 10°C of their peak temperature from 770 hr to 800 hr (Note that the results of Figures 1.6 and 1.7 cover a time period of 2 months!).

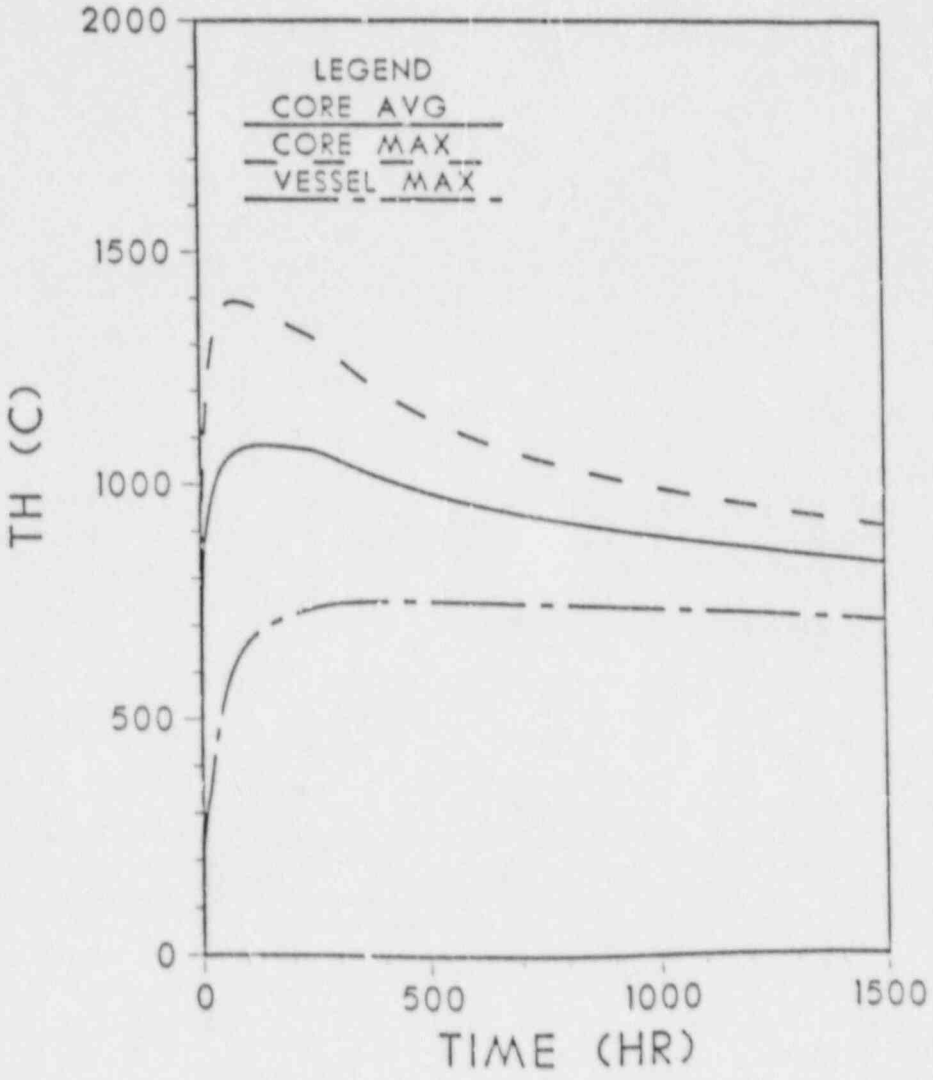

Figure 1.6 Core and Vessel Temperatures for Depressurized Core Heatup Accident without Operating RCCS

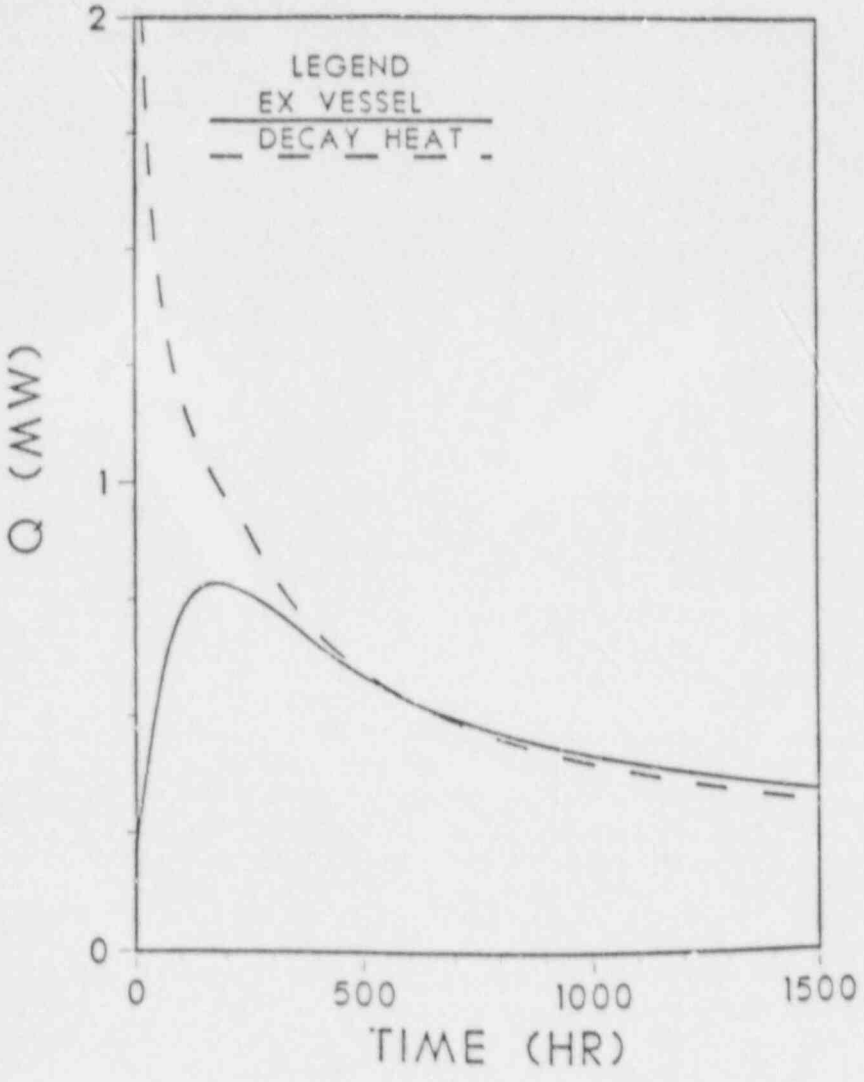

Figure 1.7 Heat Generation and Heat Flow for Depressurized Core Heatup Accident without Operating RCCS

Beyond the Base Case, several variations in concrete and soil properties and configurations were employed. Some of these are shown in Table 1.2. The Base Case considered heat rejection to the more typical configuration of 5 ft concrete wall, side cavities and then to outer walls. Case 2 models the configuration of direct heat rejection to outer walls and soil. At the time of peak fuel temperatures hardly any of the concrete and none of the soil has heated up. Therefore, the peak fuel temperature is independent of concrete and soil configuration and properties. The peak vessel temperatures were slightly higher, but occurred much later. Even when the soil conductivity was reduced by a factor of two (Case 4) the vessel temperature only rose by another 30°C. Thus, it is seen that pessimistic assumptions on concrete and soil configuration and properties do not raise the peak vessel temperature very much, but they do extend the transient significantly in time, delaying the ultimate cooldown.

During the transient, some of the surrounding concrete was found to reach excessive temperatures, 600 to 700°C at the side of the cavity, and close to 500°C at the bottom surface of the top floor. Depending on the type of concrete, such temperatures can lead to structural collapse.

To establish safety margins under such accident scenarios the decay heat function and the core thermal conductivities were varied. An increase of about 27% in decay heat level and a loss of thermal conductivity of about 30% would be required before the peak fuel temperatures would reach 1600°C.

The same decay heat increase of 27% that raised the peak fuel temperatures to 1600°C would cause vessel temperatures of about 930°C. Beyond this level of decay heat, scenarios are possible where some fuel failures occur at about 100 hr into the transient and the vessel would subsequently fail, but only after several weeks, at which time core temperatures have already returned to the range of 1200 to 1300°C.

Thus, even in a most pessimistic RCCS failure scenario, the resulting fuel temperatures and safety margins are very close to those for depressurized core heatup accidents with RCCS. However, vessel temperatures and some of the surrounding concrete temperatures are such that some component failures several weeks after the beginning of the accident are not impossible.

1.2.1.4 Hypothetical Air Ingress Scenarios in Advanced Modular High Temperature Gas-Cooled Reactors (P. G. Kroeger)

One of the potentially dangerous accident scenarios for high temperature gas-cooled reactors (HTGR) has always been the case of air ingress. Reaction of oxygen with the graphite of the core and support structure can lead to weakening of the structure, egress of combustible gases (CO), and to further core heatup and fuel failures. As in previous designs, the current modular HTGR (MHTGR) design precludes significant air ingress from being a credible event. It would require the simultaneous failure of the reactor vessel in top and bottom locations, or a complete double guillotine break of the short cross duct, which is built to vessel specification. While such accident scenarios are considered to be of extremely low probability, they have been evaluated to establish whether any traumatic consequences are to be expected.

Table 1.2 Peak Fuel and Vessel Temperatures for Several Concrete/Soil Configurations and Properties During Depressurized Core Heatup Accidents without Operating FCCS

Case No.	Description	Peak Fuel Temperature			Peak Vessel Temperature			Vessel Cross Over Time* hr	Maximum Core Temp. at 1500 hr	Maximum Vessel Temp. at 1500 hr
		Value °C	At Time hr	Variation From Base Case °C	Value °C	At Time hr	Variation From Base Case °C			
1	Base Case	1393	78	----	754	425		610	914	710
2	Heat Transfer to Exterior Concrete Wall and Clay Soil	1393	78	0	767	1105	+13	1250	966	764
3	Concrete Properties of [General Atomic, 1978] without Assuming Reduced Thermal Conductivity with Dryout	1393	78	0	739	310	-15	345	**	**
4	As Case 2, but Surrounding Soil with 1/2 of Case 2 Thermal Conductivity	1393	78	0	793	1680	+39	1790	994	792

* Time at which heat leaving vessel exceeds decay heat, i.e., net cooldown of reactor vessel and interval begins.

** Case was not run to 1500 hr.

To evaluate a massive air ingress scenario, it was assumed, non-mechanistically, that the cross duct had suffered a double guillotine break, and the steam generator side of the duct had disappeared. A scenario achieving this would require extremely destructive forces, and it may not be credible to stipulate such an event without considering also destruction of reactor vessel supports and reactor internal components. However, such an event is stipulated here, to serve as an upper bound on potential air ingress scenarios. Following such a cross duct break, gas would enter the inner part of the annular cross duct, flow upward through the core, downward at the core barrel, and discharge through the outer section of the cross duct. At this exit significant recirculation would occur, with part of the inflowing gas being exhaust gas. Again, non-mechanistically, this recirculation as well as the fact that the fresh air inventory in the silo cavities is very limited are being disregarded, and pure air inflow into the inner section of the cross duct is assumed.

Following such a break, the gas flow through the active core is determined by a balance of buoyancy and friction forces, which are in turn dominated by the temperature field of the large thermal capacitances of the core. Depending on the temperature level, the chemical reaction between oxygen and core graphite is governed predominantly by the chemical reactivity of the graphite (low temperature region), by the in-pore diffusion of gas through graphite coupled with the chemical reactivity (intermediate temperatures), or by the coolant to graphite surface mass transfer (high temperature region).

The analysis of gas flow through the reactor with mass transfer and chemical reaction in the core is carried out in the FLOXI code, which uses a depressurized core heatup temperature profile computed by the THATCH code. This quasi-static model neglects the thermal energy release from the exothermal carbon/oxygen reaction, which is always small with respect to decay heat. It does, however, include the effect of additional gas generation from the chemical reaction and its effect on the total flow field. Following [Katscher, 1986] the effects of in-pore diffusion and chemical reaction are modeled by a single semi-empirical Langmuir-Hinshelwood type expression. For mass transfer in the coolant channels the binary diffusion coefficients of oxygen in nitrogen were based on Chapman-Enskog kinetic theory. Only the reaction of C and O_2 to CO was considered here. At the prevailing temperature levels any CO_2 formed initially would typically react to CO in the hotter core regions. For the total burn-off, as well as the amount of combustible gases formed, neglecting any small CO_2 fractions in the exhaust gas is conservative.

Applying the FLOXI code to a typical core heatup transient resulting from the assumed cross duct failure the core gas flow and graphite oxidation transients of Figure 1.8 were obtained. The gas flow process and the amount of graphite oxidized are under all conditions completely limited by the in-core friction pressure drop. The coolant holes are about 15 mm in diameter and almost 10 m long, and in-core flow rates are always extremely laminar with typical Reynolds numbers between 20 and 100. As the core heats up the air inlet flow rapidly decreases from about 500 kg/hr to about 250 kg/hr for most of the transient. In very early portions of the transient the exhaust gas still contains about 6 vol % of air, but as the core heats up, after a few hours all air reacts in the lower portions of the core, and most of the reactor sees a

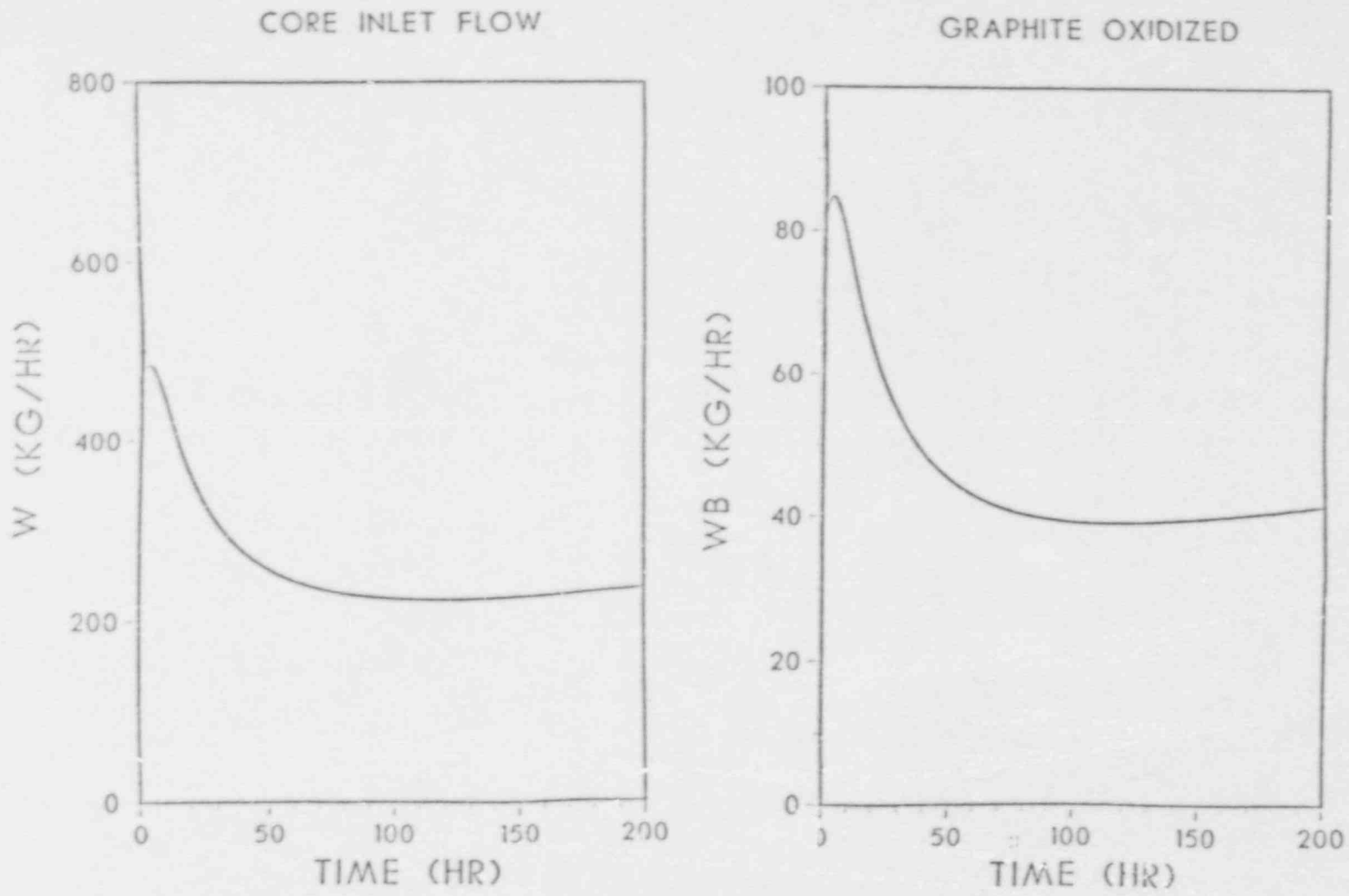

Figure 1.8 Core Air Inlet Flow, and Graphite Oxidation Transient Subsequent to Complete Cross Duct Failure

gas stream of 35 vol % CO and 65 vol % N_2. The resulting graphite oxidation rates decrease from an initial value of 80 kg/hr to about 40 kg/hr for most of the transient.

To assess the uncertainties in the graphite reactivity and the diffusion coefficients used, both were varied by up to two orders. In each case, only the length of the reaction zone was affected. With lower reactivity and/or diffusion coefficient, some of the oxidation shifted from lower elevations to the center of the core. Except in the first few hours, virtually all oxygen was converted to CO, and the total in-core flow did not vary significantly, as it remained dominated by the in-core friction pressure drop. When a 50/50 gas mixture of helium and air was assumed instead of pure air inflow, the gas mass flow rates and graphite oxidation rates were about one-third of those for pure air flow. The energy release from the chemical reaction amounted to about 6% of the decay heat, justifying the assumption of neglecting this effect as well within the uncertainties of the analysis, in particular since the temperature field used here was computed with a conservative decay heat function.

The air inflow into the core and the subsequent graphite oxidation rates under extremely pessimistic accident assumptions remain limited by the in-core friction pressure drop of the long and narrow coolant channels. All air entering the core will be oxidized except during the first few hours of the transient. As the air supply in the reactor cavity is in general limited, the reactions would come to a halt well before the 200 hr transient considered here. Significant loss of strength of the graphite structures could become a concern only if an unlimited air supply would be available for hundreds of hours. Also, during the initial phases of such an accident, as the available air in the reactor cavity is burnt and CO is emitted from the reactor, local burning in the reactor cavity would not be impossible.

Thus, even under the above extreme assumptions, such an accident could not lead to any rapid destruction of the core or to significant fission product releases.

1.2.1.5 Water Ingress Analysis (J. W. Yang, A. Aronson, G. J. Van Tuyle)

The MINET [Van Tuyle, 1984] representation of the HTGR system has been extended to include the reactor structures, secondary side of the steam generators, and transient boundary conditions. The steady-state calculations have resulted in system pressures, temperatures, and flows similar to GA's projected steady-state conditions.

A MINET analysis of the event involving the loss of HTS and SCS cooling has been completed. The event represents the early transient of DBE-6. Interpretation of the preliminary results are in progress.

Several improvements of the MINET representation of the HTGR system were made. The flow oscillation and minor inconsistency at the beginning of the transient were eliminated. Preliminary results indicate that the system response is sensitive to the time of main circulator coastdown, isolation of the steam generator, and the startup of the SCS heat exchanger and circulator. Parametric studies are in progress.

1.2.2 LMRs - PRISM and SAFR (G. J. Van Tuyle)

1.2.2.1 Review of PRISM and SAFR PSIDs (G. J. Van Tuyle, G. C. Slovik, T. Ginsberg, H. S. Cheng)

The LMR PSID Chapter 4 review meeting at NRC was quite fruitful in that many questions raised by BNL reviewers were resolved. In the area of reactivity feedback, the following problems are still outstanding:

- It appears to be impractical for an LMR to reduce the positive sodium void reactivity coefficient. This remains a point of concern for a hypothetical accident involving massive sodium boiling. However, this is highly unlikely because of very large sodium subcooling in an LMR.

- There is a real potential for limited axial fuel expansion due to fuel-clad lockup at high burnup (>2 a/o). The modeling of this feedback mechanism should take this into account.

- The radial bowing effect on reactivity can be important but very difficult to predict. It appears to be prudent to treat the radial bowing reactivity as an input function table with a large uncertainty (~50%) assigned to it.

- The definition of Doppler coefficient being used for LMR designs appears to be inappropriate for metal fuels. The more correct definition has been brought to the attention of LMR designers.

- The use of 1$ as shutdown margin by PRISM is nonconservative because it is of the same order of magnitude as various uncertainties (e.g., criticality prediction, fissile tolerance).

The thermal-hydraulics (i.e., Chapter 5 of the PSID) of PRISM [Berglund, 1987] and SAFR [Oldenkamp, 1987] were also reviewed. A list of questions was given to each designer to supply more information about specific issues which were unclear or not in the PSID. The vendors will include the formal responses to the questions asked in appendices of the PSIDs.

Chapters 6-13 and 17 cover a range of topics, including, containment, plant protection and control, electric power, auxiliary systems, balance of plant, radiation protection, waste management, and conduct of operations. Both GE and RI are citing less frequent scrams (perhaps one per year), despite the presence of a fairly standard power conversion system (the source of most transients leading to scrams in light water reactors). The explanation to this apparent contradiction is that GE and RI plan on having the control systems initiate "power runbacks" in response to many problems starting in the steam systems. Another interesting development is RI's decision to reduce the gap between the reactor and containment vessels, which should allow continued functioning of the IHX under a worst-case leak from the reactor vessel.

The PRISM and SAFR Safety Test Plans, covered in PSID Chapter 14 and supporting documents were also reviewed. GE and RI took very different approaches in this area. The GE Test Plan for PRISM focused entirely on testing the

first module, and contained little regarding supporting work that must be done by ANL and HEDL. The RI Test Plan for SAFR focused largely on the long term R&D program, and placed little emphasis on testing of the initial unit. The position taken by RI is consistent with 1) their need to make the first unit a power producer and therefore licensable, and 2) problems in running worst case events on the first unit (fear of damaging the unit so it can't then be operated to meet a 60 year design lifetime).

The GE/PRISM situation can easily be corrected by simply considering their needs for long term R&D support as stated elsewhere than "Chapter 14" as part of their overall Safety Test Plan. The RI/SAFR situation is more difficult, and there will be several open items before tests are performed on the first unit, and limits on testing would be undesirable.

On a similar note; some means of routinely testing the SAFR Curie-point SASS will have to be found before high reliability can be assured. One particular concern is that ferretic material, such as the HT9 clad, that breaks loose into the coolant system will tend to accumulate on the surface of the SASS magnets. Perhaps a means of electrically heating the sodium flowing past the magnets can be worked out as a means for routine testing.

1.2.2.2 PRISM and SAFR PRA Review (L. Chu, T. Ginsberg, G. J. Van Tuyle)

A review of the advanced LMR PRAs is in process, and clarification is being sought from GE and RI in many areas. Many of the failure probabilities assumed in the PRAs seem very optimistic, but the potential impact of substituting more conservative estimates is not yet known.

An IBM-PC program that can be used to assemble the results of the event trees in the PRISM PRA was developed. It can be used to reproduce the risk estimates of PRISM, and to perform sensitivity calculations.

1.2.2.3 SSC Analysis of PRISM and SAFR ATWS Events (G. C. Slovik, (R. J. Kennett)

A 35¢ ramp insertion TOP in PRISM was simulated and the results were compared to those provided by GE. As was indicated under modeling activities in Section 1.1.1, the two obvious differences were: 1) GE's large bowing feedback was not in our SSC [Guppy, 1983] analysis, as we have chosen to be conservative and neglect this complex behavior, and 2) the control rod expansion was not yet incorporated in SSC so it is missing in the BNL run. Otherwise, the SSC and GE runs show similar behavior, i.e., for sodium density, Doppler, axial expansion, and radial expansion. This work is summarized in a paper submitted for the Safety of Next Generation Power Reactors conference.

1.2.2.4 MINET Analysis of Leaks into Containment (B. C. Chan, G. J. Van Tuyle)

A MINET [Van Tuyle, 1984] model that can be used to simulate primary sodium leaks into the containment for the SAFR design has been completed. The leak location is at the bottom of the cold-pool. Any leaks from the

containment into the atmosphere are assumed to be much smaller compared to the leak from the reactor into the containment. A simulation under normal operation (without scram and primary pump coast down) has been performed. The resulting thermal and hydraulic behavior are consistent with engineering judgement. More testing is in progress.

1.2.2.5 RACS/RVACS Modeling in MINET (B. C. Chan, A. L. Aronson)

The PASCOL code has been coupled with the RACS/RVACS overflow model in MINET. This modification to the MINET code provides the capability to simulate the RACS/RVACS system in SAFR/PRISM designs.

1.2.2.6 Evaluation of Postulated LOF Events in PRISM and SAFR (B. C. Chan, G. J. Van Tuyle, G. C. Slovik, A. L. Aronson)

Both PRISM and SAFR are pool-type designs, with all primary components submerged in a large volume of sodium in the primary tank. The approximate configuration of the components within the reactor vessel can be inferred from Figure 1.9, which is a schematic drawing of our current MINET representation of both systems (conceptually they are very similar). Primary sodium flows upward inside the core, heats up and enters the hot pool. Hot primary sodium transfers heat into the intermediate loop sodium while flowing down through the IHXs into the cold pool. The pumps (four electromagnetic in PRISM and two centrifugal in SAFR) draw sodium from the cold pool and drive it through headers and eight pipes into the inlet plenum and on into the core. There are no valves in the primary system, and all valves shown in Figure 1.9 are solely for simulating postulated breaks. (There are additional features in the MINET representation for simulating the RVACS/RACS overflow, and leaks into and out of the containment vessel, but they are irrelevant to this analysis.)

The analyses reported here are more refined, at least for the pipe breaks, than those in the initial calculations, reported in [Van Tuyle, 1987] which used estimates for the variation of pump head versus flow rate. For the centrifugal pumps in SAFR, the estimated head curve was similar to the head curve that has since been provided by RI, so the results are little changed. For the electromagnetic (EM) pumps used in PRISM, the assumption that the head varies little with flow proved to be erroneous. GE now states that they plan to operate well out on the head curve, so that the head varies sharply with flow, assuring a nearly constant flow rate through the pumps. As a result, the surging of flow through the pumps reported in [Van Tuyle, 1987] no longer occurs, making the pipe break a more severe occurrence (although still acceptable, apparently).

In the case of pipe break accident, the diameters of the discharge pipes are small compared to the space in the cold pools, so that the discharged fluid is assumed to expand freely into the pools, and the postulated break occurs near the inlet plenum in one of the pump discharge pipes. The break model is the double end guillotine break (DEG) with large separation distance, in which the interaction between the flow discharge from the two sides of the break is neglected.

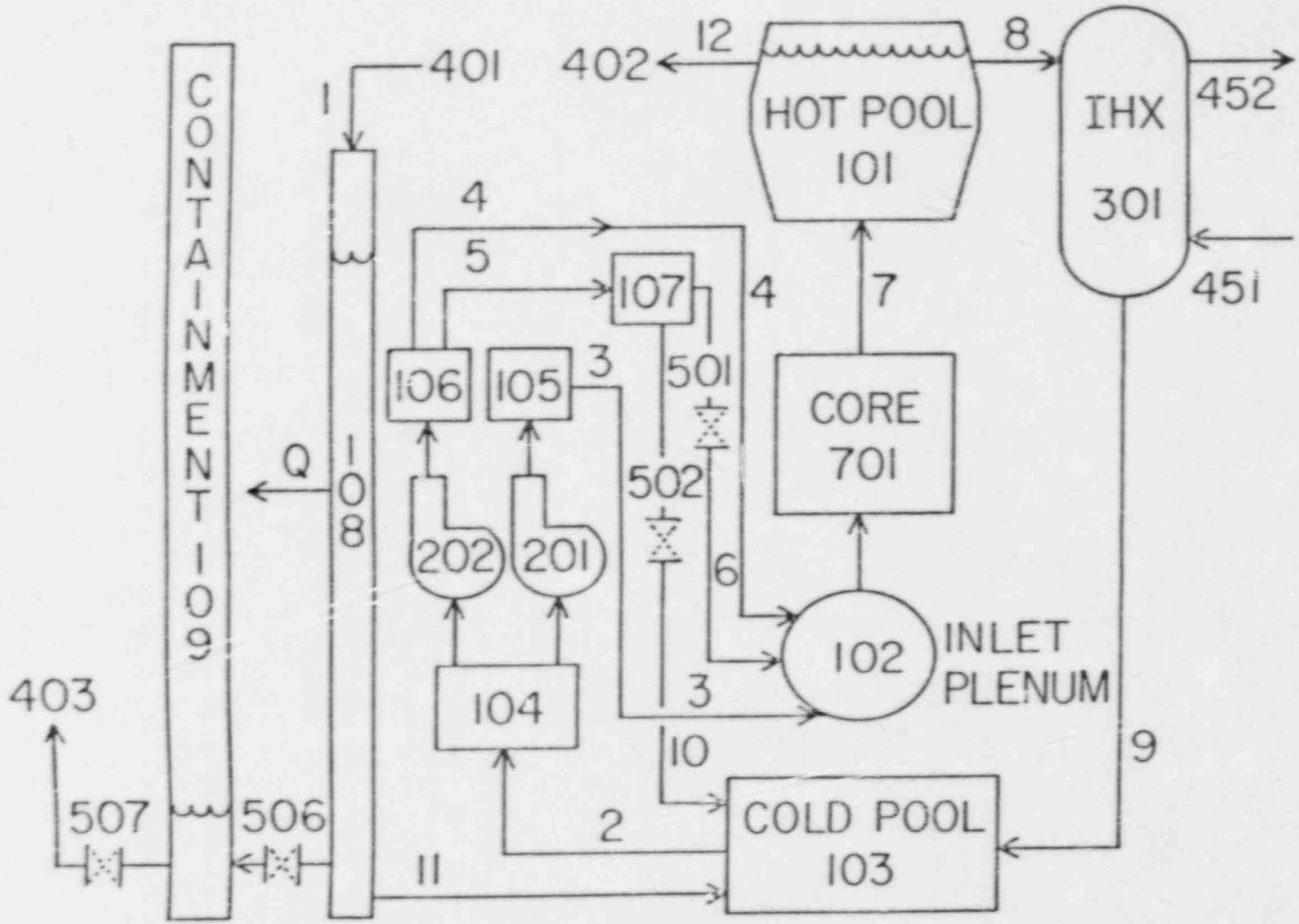
PRISM & SAFR PLANTS SCHEMATIC
CONTAINMENT 109
401
402
12
8
HOT POOL
101
IHX
301
452
451
1
4
5
107
4
7
106
105
3
501
CORE
701
Q
108
502
202
201
6
102
INLET
PLENUM
403
104
3
10
9
507
506
2
COLD POOL
103
11

Figure 1.9

The pump seizure events assume the instantaneous loss (without coastdown) of one of the pumps in each design. For PRISM, that means one of the cables from the synchronous machines to the EM pumps is assumed severed.

The calculated core flow rates in PRISM and SAFR for the three transients are shown in Figure 1.10 and Figure 1.11, respectively. In the calculations, the pipe break and the pump seizure occur rapidly in 0.1 seconds. Both PRISM and SAFR would experience a rapid reduction in the reactor flow. In the event of a pipe break, large flows through "valve" 502 come from both the pump outlet header and from the inlet plenum (reversing the flow in pipe 6). In partial compensation, the flows through the seven unaffected pipes (labelled 3 and 4 in Figure 1.9) increased somewhat. However, this was limited, as the head drops off with increasing flow. Thus, for the pipe breaks, the reactor flow in PRISM is reduced to 58% full flow, and for SAFR it falls to 73%. In the pump seizure event PRISM (one of four pumps seize), the reactor flow is reduced to 53% and, for SAFR (one of two pumps seize), to 35%. PRISM thus benefits from having four, rather than two pumps. In the results of the pump trip and coastdown, both PRISM and SAFR have similar reduction in core flow.

The significance of this study is that the loss of power to the pumps is not necessarily the worst case loss-of-flow event. The reactivity feedbacks require time to bring the power down in the PRISM and SAFR LOF events. Analyses by GE and RI have indicated that the feedbacks do have sufficient time to work in the coastdown events, although BNL has not yet performed confirmatory analyses. Of the pipe break and pump seizure events covered in Figures 1.10 and 1.11, one stands out as a potential problem; that being the pump seizures in SAFR, which quickly reduces the reactor flow to 35%. (The other three cases would require little reduction in power for survivability.) Our next step will be to feed this reactor flow history into our detailed core model to determine whether the SAFR reactivity feedbacks can act fast enough to make this event benign even without scram.

1.2.2.7 Radial Expansion Reactivity for PRISM and SAFR (H. S. Cheng)

Relatively simple and straightforward calculations have been performed in order to independently evaluate the radial expansion reactivity for PRISM and SAFR. The feedback model for radial expansion was developed sometime ago, but the lack of precise input data prevented a meaningful quantitative evaluation. Since sufficient information has been obtained from the recent LMR review meeting, we can now evaluate the radial expansion reactivity with fewer uncertainties. An interactive program called "RHORX" has been written in FORTRAN to run on a PDP-11/34 minicomputer.

The physical model for the radial expansion reactivity is based on a non-leakage probability representation of the effective neutron multiplication factor:

$$k_{eff} = k_{\infty} e^{-B^2 M^2} .$$

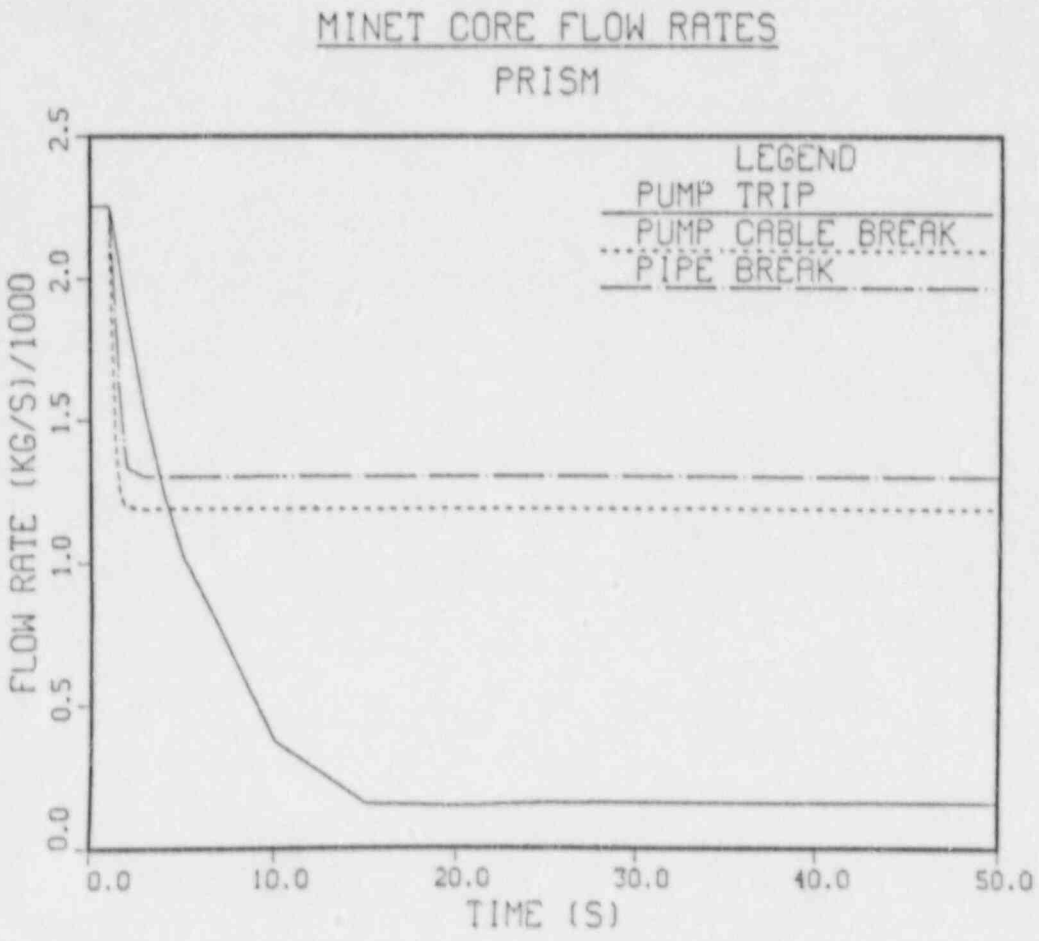
MINET CORE FLOW RATES
PRISM
LEGEND
PUMP TRIP
PUMP CABLE BREAK
PIPE BREAK
FLOW RATE (KG/S)/1000
0.0
0.5
1.0
1.5
2.0
2.5
0.0
10.0
20.0
30.0
40.0
50.0
TIME (S)

Figure 1.10

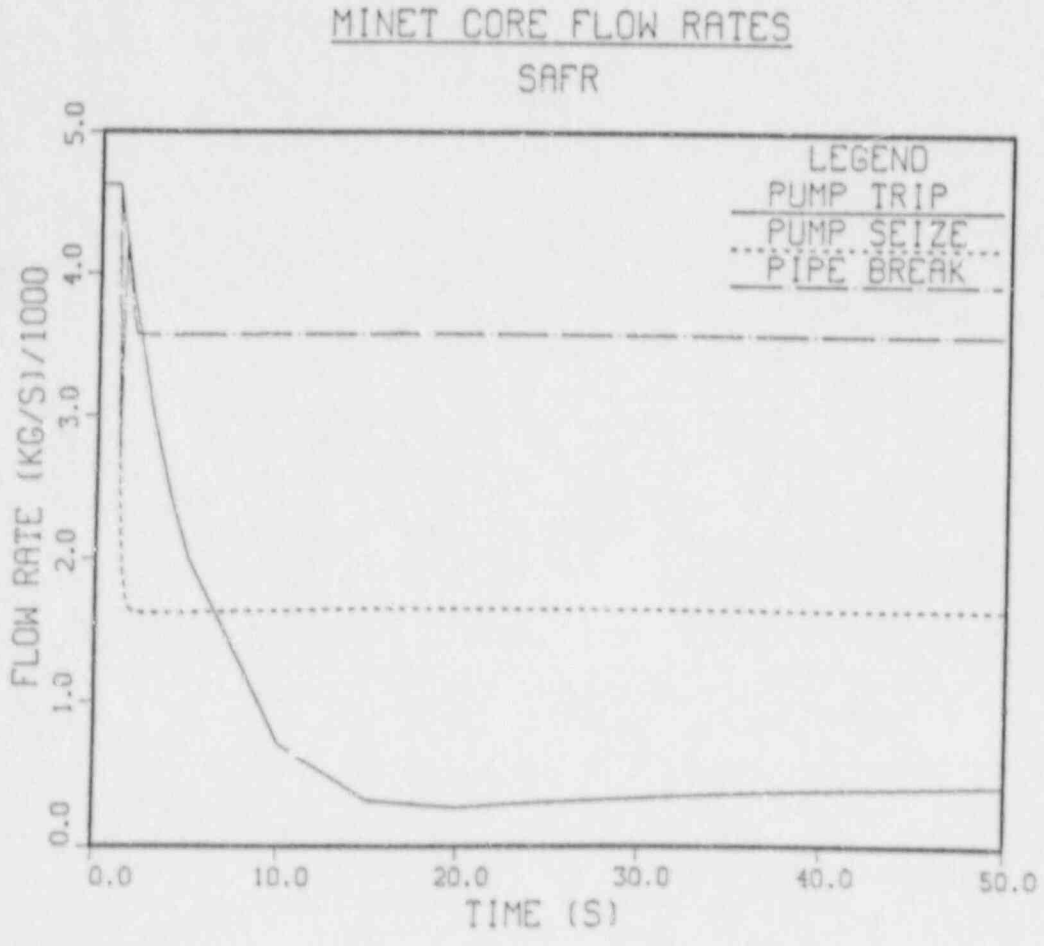
MINET CORE FLOW RATES
SAFR
LEGEND
PUMP TRIP
PUMP SEIZE
PIPE BREAK
FLOW RATE (KG/S)/1000
0.0
1.0
2.0
3.0
4.0
5.0
0.0
10.0
20.0
30.0
40.0
50.0
TIME (S)

Figure 1.11

Under the assumption that the radial expansion has no effect on k_∞ (the effect is primarily on the atom density which appears in both the numerator and denominator of k_∞, thus cancels out) and that the material mass in the core remains unchanged during the radial expansion (this is a good assumption since, as temperature increases, the material density decreases and the volume increases so that the material mass tends to stay constant), it can be shown that the radial expansion reactivity for a cylindrical core is given by:

$$\rho_{RX} = 1 - e^{\Delta B^2 M^2},$$

where $\Delta B^2 M^2 = C_1*((1+\alpha\Delta T)^4 - 1) + C_2*((1+\alpha\Delta T)^2 - 1)$

$C_1 = \pi^2 R^4 * C$

$C_2 = 5.784 R^2 H^2 * C$

$C = \frac{1}{3\sigma_{tr}\sigma_a} \left(\frac{\pi A}{M_c N_o}\right)^2$

$A = \sum_n W_n A_n$

$M_c = \sum_n \rho_n V_n$ = total material mass in the core

$V_n = \sum_i N_i VF_{n,i} V_t$

$V_t = 0.86602 * H * b^2$ = Volume of a hexagonal assembly

H = Active core height

b = Flat-to-flat duct outside of the hexagonal assembly

W_n = Weight fraction of n^{th} material composition

A_n = Atomic weight of n^{th} material composition

N_i = Number of assembly type i (e.g., driver fuel, internal blanket, etc.

ρ_n = Density of material n

$VF_{u,i}$ = Volume fraction of material u in assembly type i

N_o = 0.6023

σ_{tr} = Average microscopic transport cross section (barns) in the core

σ_a = Average microscopic absorption cross section (barns) in the core

ΔT = Temperature change relative to the reference

α = Thermal expansion coefficient of structure (HT-9):

$$= 10^{-6}*(4.286596+0.0209651T-1.0624x10^{-5}T^2) \quad \text{for } 293\ K \leq T \leq 650\ K$$

$$= 14.587x10^{-6} \quad \text{for } T \leq 650\ K$$

(Note: α is in K^{-1} and T in K, and it has been assumed that HT-9 is principally responsible for radial expansion)

ρ_n = Density of core materials. The following densities were used:

$$\rho_{HT9} = 7.76*(1.00634834-1.285972x10^{-5}T-3.144763x10^{-8}T^2 +1.06236x10^{-11}T^3)$$

$$\rho_{fuel} = 16.06509 - 8.12202x10^{-4}T-1.01005x10^{-7}T^2$$

$$\rho_{Na} = 1.0118 - 0.22054x10^{-3}T-1.9226x10^{-8}T^2+ 5.6371x10^{-12}T^3$$

where ρ's are in g/cc and T in °K.

The program RHORX was utilized to obtain the radial expansion reactivity as a function of temperature change (relative to a reference temperature) for both PRISM and SAFR. The temperature dependence of the thermal expansion coefficient and density for the structural material (HT-9) were taken into account. The microscopic cross sections of core materials averaged over the reactor spectrum were obtained from Ref. [Wirth, 1978], which were used for both PRISM and SAFR. All the assembly types in the core were taken into account.

The results indicate that the radial expansion reactivity exhibits a fairly linear behavior. The reactivity vs radial expansion data were least-square fitted with a straight line using the curve-fitting program CURFIT on a PDP-11/34. The slopes of these fitted curves are summarized below along with the reported values by vendors (GE and RI):

	PRISM ($/cm)	SAFR ($/cm)
This Work	-2.368	-1.706
GE	-2.294	
RI		-1.630

The agreement is quite good (+3% for PRISM and +5% for SAFR).

1.2.2.8 Analysis of RVACS and RACS (P. G. Kroeger, G. J. Van Tuyle)

Both PRISM and SAFR include a passive air cooling system for final decay heat removal under accident conditions. To be completely passive, these cooling systems are operative at all times, causing a minor parasitic energy loss during normal operation.

In these designs, as schematically shown in Figure 1.12, air is supplied to the bottom of the guard vessel, flowing upward along the guard vessel due to natural convection and being discharged through a stack providing sufficient draft to remove the decay heat under accident conditions.

In either concept, the heat rejection from the reactor vessel to the air cooling system is by radiation and convection across a gas gap between the reactor vessel and the guard vessel, and by radiation from the guard vessel to the opposite air cooling system surface (collector surface), and ultimately by convection from both surfaces to the rising air. Additionally, the SAFR concept includes fins on the collector surface. For this concept the simultaneous effects of radiation and conduction on the collector surface are considered.

The evaluation of the passive air cooling system was performed with the PASCOL code, which was originally developed for analyzing a similar passive air cooling system in the modular high temperature gas-cooled reactor program. This code can either be applied as a free standing program, given a spatial reactor vessel temperature distribution, or coupled to the relevant code for accident analysis. It solves simultaneously the quasi-steady momentum and energy equations for the air, coupled with simultaneous radiation, conduction and convection from the reactor vessel via the guard vessel and the other air cooling system surfaces to the coolant.

The performance evaluation reported here considers the operation under accident conditions. For the PRISM reactor the heat transfer surfaces were not finned. As the vendor specified data did not include sufficient details to compute the inlet and exit ducting pressure drops, the system was evaluated parametrically with inlet and exit loss coefficients being varied between 1 and 10. The results, shown in Figure 1.13, indicate that the vendor's claimed performance can readily be obtained, if ducting is such that inlet and exit losses each amount to about four velocity heads. The vendor assumed solid surface emissivities of only 0.7, while values of 0.85 are readily achievable. Our evaluations showed that an increase in the heat removal rate of 16% is possible with such an increase in emissivity.

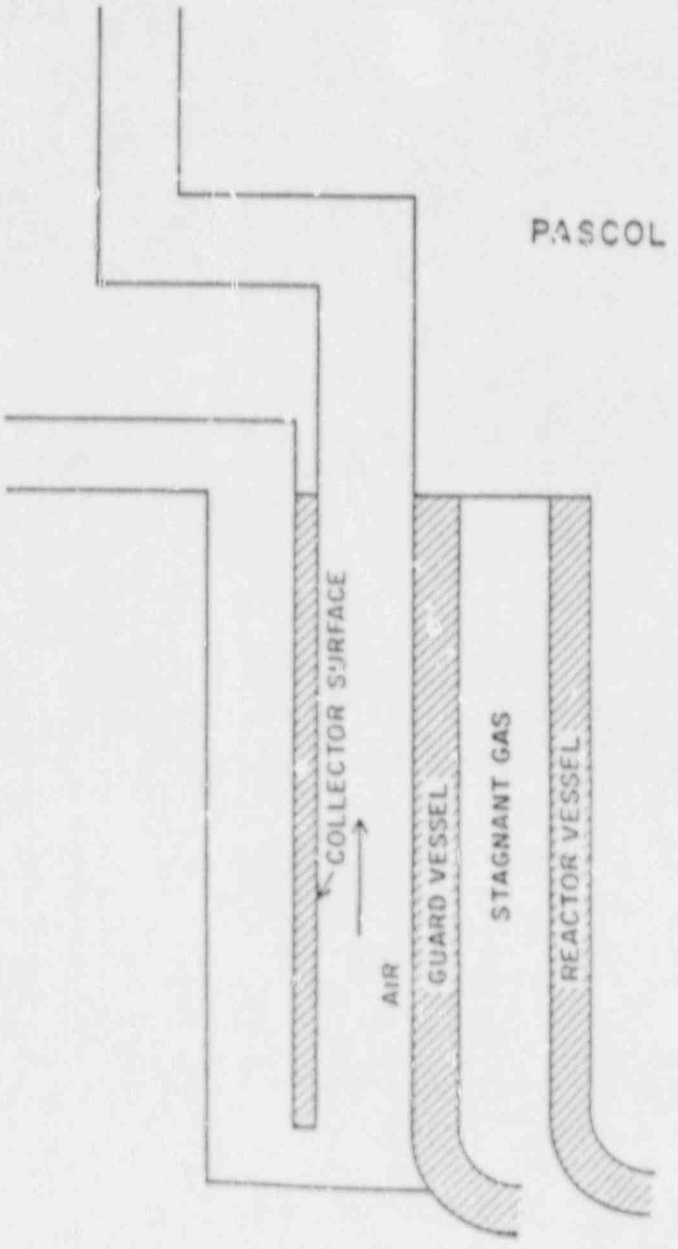

Figure 3.12 Schematic of Passive Air Cooling System for Advanced Liquid Metal Reactors

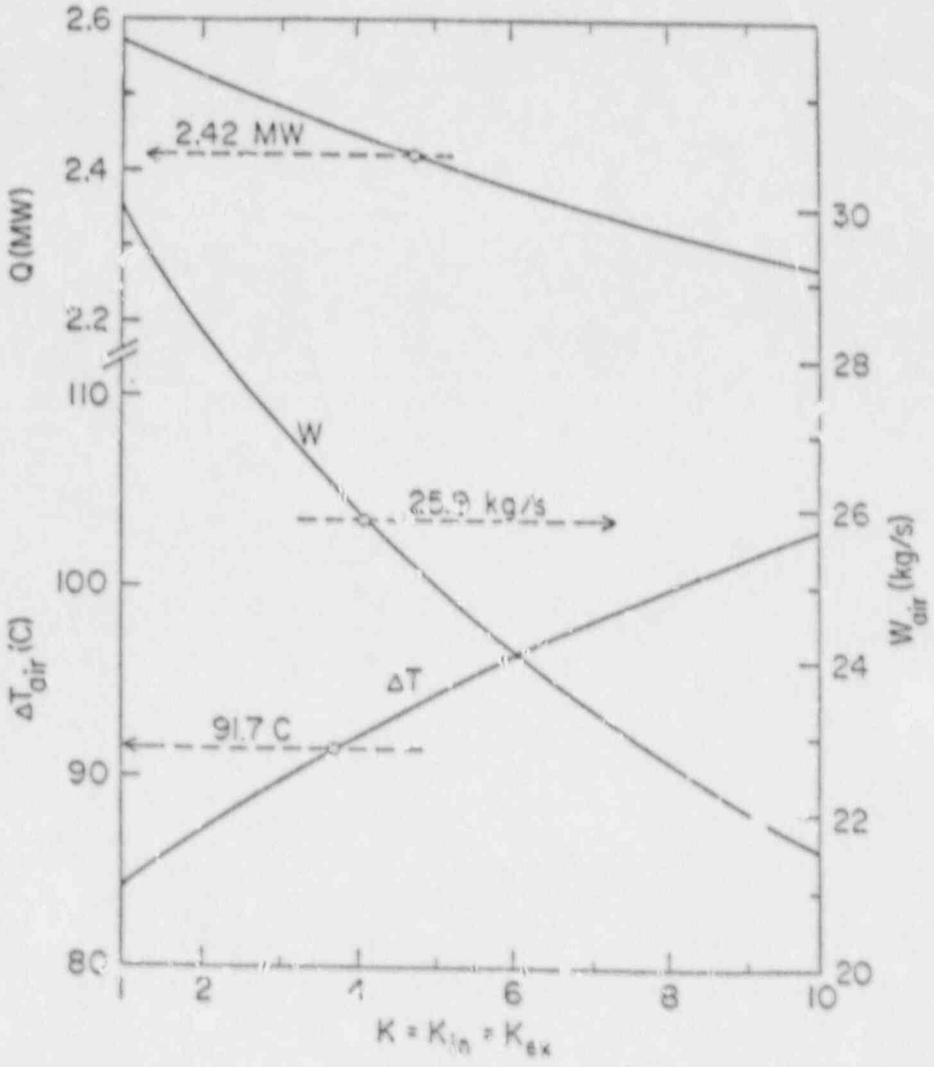

Figure 1.13 PRISM Passive Air Cooling System Performance During Decay Heat Removal as Function Inlet and Outlet Ducting Flow Resistances

For the SAFR air cooling system an evaluation of the simultaneous conduction and radiation in the collector surface had to be made. Defining a performance factor:

$$\phi = \frac{\text{total convective heat transfer to air}}{\text{convective heat transfer to air from guard vessel}}$$

it was found that a value of $\phi = 1.8$ to 2.5 can be expected under accident conditions. The vendor's claimed performance can be reached down to a value of $\phi = 1.5$. Increasing the emissivity from the vendor's value of 0.65 to 0.85 resulted in higher performance.

A comparison of our results and the vendors claimed performance for both concepts is shown in Table 1.3. As can be seen, both systems can readily achieve the required decay heat removal rate. Further increases in performance could readily be achieved. However, such performance increases may not be desirable, since they would raise the parasitic heat losses under normal operating conditions.

Table 1.3 Advanced Liquid Metal Reactor Passive Air Cooling System Performance During Decay Heat Removal

	PRISM-GE	PRISM-BNL	SAFR-RI	SAFR-BNL
Emissivity	0.7	0.7	0.85	0.65
Surface Effectiveness		≈1.7		1.5*
$K_{air_{in}} + K_{air_{ex}}$		8.0	10	10
W_{air} (Kg/s)	25.9	26.0	39	37.2
Q (MW)	2.42	2.45	3.90	3.96
$\Delta\theta$ (C)	92.2	91.7	99.4	102.5

*Surface effectiveness is likely much higher than 1.5. At best estimate value of 2.2, Q is estimated to be 4.85 MW.

REFERENCES

BECHTEL NATIONAL, Inc. et al., "HTGR Concept Descriptive Report," DOE-HTGR-86-118, October 1986.

BERGLUND, R.C. et al., "Design of PRISM, An Inherently Safe, Economic, and Testable Liquid Metal Fast Breeder Reactor Plant," Proceedings of the International Conference on Experience Gained and Path to Economical Power Generation, September 13-17, 1987, Richland, WA.

COMMIX-1B: A Three-Dimensional Transient Single-Phase Computer Program for Thermal-Hydraulic Analysis of Single and Multi-Component Systems," NUREG/CR-4348 (ANL-85-42), September 1985.

GENERAL ATOMIC, "HTGR Accident Initiation and Progression Analysis, Status Report, Phase II: Risk Assessment," General Atomic, GA-A-150000, 1978.

GLUEKLER, E.L. et al., "Safety Characteristics of a Small Modular Reactor," Proceedings of the Int. Topical Meeting on Fast Reactor Safety, 1, pp. 69-74, 1985.

GUPPY, J.G. et al., "Super System Code (SSC, Rev. 2) An Advanced Thermohydraulic Simulation Code for Transients in LMFBRs," Brookhaven National Laboratory Report, NUREG/CR-3169, BNL-NUREG-51650, April 1983.

KATSCHER, W., MOORMANN, R., "Graphite Corrosion Under Severe HTR Accident Conditions," Paper presented at the IAEA Specialists' Meeting on Graphite Component Structural Design, JAERI, Tokai-mura, Japan, September 8-11, 1986.

KROEGER, P.G. and COLMAN, J., "THATCH Input Description," Brookhaven National Laboratory Memo, 1986.

LANCET, R.T. and MARCHATERRE, J.F., "Inherent Safety of the SAFR Plant," Proceedings of the Int. Topical Meeting on Fast Reactor Safety, 1, pp. 43-50, 1985.

Nuclear Engineering and Design, Special Issue 101, No. 1, April 1987.

OLDENKAMP, R.D., GUENTHER, E., and GOLAN, S., "The Sodium Advanced Fast Reactor," Proceedings of the International Conference on Experience Gained and Path to Economical Power Generation, September 13-17, 1987, Richland, WA.

VAN TUYLE, G.J., "A Momentum Integral Network Method for Thermal-Hydraulic Systems Analysis," Nuclear Engineering and Design, 91, pp. 17-28, 1986.

VAN TUYLE, G.J., CHAN, B.C., and SLOVIK, G.C., "Initial Pipe Break Analyses for Advanced LMR Concepts Using MINET," Transactions of the American Nuclear Society, Los Angeles Conference, November 1987, also BNL-NUREG-39956.

VAN TUYLE, G.J., NEPSEE, T.C., and GUPPY, J.G., "MINET Code Documentation," Brookhaven National Laboratory Report, NUREG/CR-3668, BNL-NUREG-51742, February 1984.

WIRTZ, K., Lectures on Fast Reactors, American Nuclear Society, LaGrange Park, Illinois, 1978.

PUBLICATIONS

VAN TUYLE, G.J., B.C., and SLOVIK, G.J., "Initial Pipe Break Analyses for Advanced LM[illegible] [illegible]pts Using MINET," Transactions of the American Nuclear Society, Los Ange[illegible] [illegible] Meeting, November 1987, also BNL-NUREG-39956.

KROEGER, P.J. and VAN TUYLE, G.J., "Evaluation of Advanced Liquid Metal Reactor Passive Air Cooling Systems," Transactions of the American Nuclear Society, Los Angeles Winter Meeting, November 1987, also BNL-NUREG-39957.

CHAN, B.C., VAN TUYLE, G.J., SLOVIK, G.C., and ARONSON, A.L., "Evaluation of Postulated LOF Events in PRISM and SAFR," Submitted to Conference on Safety of Next Generation Power Reactors, Seattle, Washington, May 1988.

CHENG, H.S. and VAN TUYLE, G.J., "A Simple Model for Radial Expansion Reactivity in LMRs," Submitted to Conference on Safety of Next Generation Power Reactors, Seattle, Washington, May 1988.

SLOVIK, G.C., VAN TUYLE, G.J., KENNETT, R.J., and CHENG, H.S., "Evaluating Advanced LMR Reactivity Feedbacks Using SSC," Submitted to Conference on Safety of Next Generation Power Reactors, Seattle, Washington, May 1988.

KROEGER, P.G., "Depressurized Core Heatup Accident Scenarios in Advanced Modular High Temperature Gas Cooled Reactors," Submitted to Conference on Safety of Next Generation Power Reactors, Seattle, Washington, May 1988.

KROEGER, P.G., "Severe Accident Core Heatup Transients in Modular High Temperature Gas-Cooled Reactors Without Operating Reactor Cavity Cooling Systems," Submitted to Conference on Safety of Next Generation Power Reactors, Seattle, Washington, May 1988.

KROEGER, P.G., "Hypothetical Air Ingress Scenarios in Advanced Modular High Temperature Gas Cooled Reactors," Submitted to Conference on Safety of Next Generation Power Reactors, Seattle, Washington, May 1988.

YANG, J.W., KREOGER, P.G., VAN TUYLE, G.J., and ARONSON, A.L., "MINET Analysis of MHTGR Moisture-Ingress Transient," Submitted to Conference on Safety of Next Generation Power Reactors, Seattle, Washington, May 1988.

VAN TUYLE, G.J., KROEGER, P.G., KARASULU, M. (NYPA), and GROCHOWSKI, G. (NYPA), "Comparing the Inherent Safety of the Modular LMRs and HTGR and the PIUS Concept," Submitted to Conference on Safety of Next Generation Power Reactors, Seattle, Washington, May 1988.

II. DIVISION OF ENGINEERING

SUMMARY

Standard Problems for Structural Computer Codes

During this period the studies on criteria for seismic Class I structures were continued. A detailed evaluation of uncertainties related to the behavior of reinforced Category I structures was performed. In addition, various experimental programs on concrete structures were reviewed to determine benchmark problems which may be used for validating mathematical models which are employed in predictions of structural response.

Fire Protection Research

This work was initiated to provide additional fire-modeling capability to those fire-risk tasks associated with NRC's RMIEP. As such, initial efforts were directed to investigate, numerically, potential fire scenarios in the LaSalle Plant control room. The first phase of this work, namely the determination of the fire environment (1) in the control room as a whole and (2) in the exhaust plenum behind the control cabinets in Unit 2, was completed in FY 1985. Code enhancement was begun in FY 1985 to include the effects of heat conduction to and from objects in the enclosure as well as enclosure walls and ceilings.

Due to cutbacks in NRC funding, the Fire Protection Research program was curtailed in FY 1986 and terminated in FY 1987. Originally, plans had been to develop and deliver a fully documented user package incorporating modelling features developed in FY 1984-1985. Ultimately what was completed in FY 1987 was a final NUREG/CR report regarding the fire environment in the LaSalle control room.

Characterization and Detection of Age-Related Failures

During the period April 1 to September 30, 1987, the following progress was made in the Nuclear Plant Aging Research program.

- The three volumes of the phase 2 motor study were finalized and were sent for publication (NUREG/CR-4939). While volume 1 provides recommendations for improving motor reliability in nuclear power plants, the other two volumes summarize the results obtained from tests performed on a 10-hp and a 400-hp motor.

- Testing on a naturally aged inverter and battery charger was completed. Presuming normal operation and maintenance, the test results indicated that aging has not substantially affected equipment operation. On the other hand, the monitoring techniques employed were sensitive to simulated transients and degradation changes in measurable component and equipment parameters indicating the viability of detecting degradation prior to failure. The phase 2 aging assessment of battery charges and inverters was completed and a draft report, NUREG/CR-5051 was issued to NRC for comment.

- NUREG/CR-4715, "An Aging Assessment of Relays and Circuit Breakers and System Interactions" was published in June 1987. This phase 1 report describes the effects of aging on circuit breakers and relays used in safety-related systems in nuclear power plants and the resulting effects of circuit breaker and relay deterioration on the function of a safety-related system.

- The phase 1 study on motor control centers was completed. A draft report summarizing the findings was issued to NRC for comments.

- The phase 1 study on the component cooling water system in PWR facilities was completed and the draft report summarizing the results will be issued shortly for comments.

Failure Analysis and Nuclear Industry Practice

This program was initiated in order to bound the problem of erosion-corrosion in single phase piping systems at nuclear power plants and to evaluate the extent of erosion-corrosion in nuclear units.

A literature survey was performed in addition to evaluating specific instances of erosion-corrosion at nuclear units.

It was concluded that the available literature adequately assesses the problem but that discrepancies do exist. The primary discrepancies appear in the areas of temperature (maximum corrosion rate) and on the amounts and benefits of oxygen control. The current models of maximum erosion-corrosion rates were evaluated and are considered to be of qualitative rather than quanititative value at present.

Evaluation of the Adequacy of Current Reactor Coolant Pump Seal Instrumentation and Operator Responses to Possible Reactor Coolant Pump Seal Failures

The objectives of this program are to (1) evaluate the adequacy of current reactor coolant pump seal and seal cooling system instrumentation, (2) evaluate the adequacy of current automatic actions and operator responses to prevent RCP seal loss of coolant accidents, (3) propose ways to improve current RCP seal safety procedure, and (4) develop technical findings for Generic Issue 23.

A report entitled "Technical Findings Related to Generic Issue 23: Reactor Coolant Pump Seal Failures" is being prepared. A draft report on "Technical Findings" was forwarded to NRC for review.

Adequacy of Current Valve In-Service Testing Methods

A draft methodology was developed for review of benefits and costs associated with a program to maintain in-service operability assurance. The draft document was prepared to support the justification to expand the IE Bulletin 85-03 applicability to all safety related motor operated valves.

Regulatory Guide for Reactor Dosimetry

The Reactor Dosimetry Program has been established to develop a Regulatory Guide to assist vendors and licensees in performing reactor vessel damage fluence calculations. An initial draft Regulatory Guide providing guidance and a description of acceptable methods and assumptions for determining pressure vessel damage fluence for input to the 10CFR50.61 RT_{PTS} prescription has been written and is presently under review.

3. Standard Problems for Structural Computer Codes

(A.J. Philippacopoulos)

During this period the efforts under this program were focused on the review and evaluation of test data for Category I type concrete structures. The behavior of such structures is complex because of the complicated interactions between the reinforcing steel and the concrete. Such interactions are associated with many uncertainties especially when loadings close to ultimate capacities are considered. Our work concentrated on the nature of these uncertainties as well as on the availability of experimental data which can be used in order to obtain a clearer understanding of the uncertainties. Hence, one of the final products of this work is the development of a matrix which correlates a comprehensive set of experimental programs such as the 1/6 scale containment tests by Sandia National Laboratory, the shear wall tests by Los Alamos National Laboratory etc. with various uncertainties such as failure criteria, shear transfer, effects of cracks etc. In addition, the above matrix identifies needed research and tests for resolving issues pertinent to Category I reinforced concrete nuclear structures.

The study concentrates on types of structures and loadings which are associated with safety issues of nuclear power plant facilities. Two types of Category I structures are considered: shell and plate type structures such as the containment building and shear wall type structures such as the auxiliary and turbine buildings. The type of uncertainties which are investigated are those related to ultimate capacities and strength characteristics as well as structural modeling. Emphasis was placed in identifying uncertainties which are associated with predictions of structural stiffnesses. These include cracking induced either be action of loads or microcracking. In a former case, uncertainties pertaining to shear transfer and tensile hardening were examined.

During the next reporting period, a report will be prepared on the review and evaluation of uncertainties related to Category I nuclear structures. This report is expected to provide a comprehensive correlation of uncertainties with experimental data as well as recommendations for additional research needed in this area.

4. Fire Protection Research
(John L. Boccio)

4.1 Background

NRR research needs in PRA methodology were outlined in a memo from Denton to Minogue dated November 30, 1982. The recommendations in the area of external event risks included information to be generated on "equipment performance in accident environment," "suitable but simple methods ... to predict variations in environmental parameters following an accident, e.g., temperature and pressure buildup," and "fragility data relating equipment failure probabilities to environmental changes." Specifically, in the area of fire risk, RES was urged to give attention to the aspects of "systems interaction between fire protection features and safety systems," "the reliability of fire protection features" and "the likelihood of qualified equipment to withstand the effects of fire and fire suppressants."

The External Events PRA Working Group, in its recommendations for improving the capability of PRA for external events observes that "with fire, as with all the other disciplines, the insufficiency of the data base is a major problem. In addition, the validity of modeling techniques, the knowledge of fire accident sequences, and the knowledge of the reliability of the fire protection systems limits the degree of confidence in PRA results."

Both NRR and RES had initiatives underway to address these needs. The Chemical Engineering Branch of NRR awarded a contract to the Brookhaven National Laboratory to establish a methodology and a data base for probabilistic assessment of fire risks and to develop guidance for NRR evaluation of PRAs by others.

The Division of Risk Analysis and Operations of RES was engaged in the Risk Methods Integration and Evaluation Program (RMIEP). The program had as its objective the development of an improved PRA method and demonstration of the method. The Fire Risk Analysis part of the RMIEP proposed to reduce the uncertainties in the PRA models for ignition, fire growth, detection and suppression, and component fragility. The program described here complemented the RES/DRAO program by generating deterministic information, both by experimentation and by analysis. The two programs (those of DET and DRAO of RES) were coordinated so that the LaSalle fire PRA when completed would have input from an improved data base.

Future applications of PRA methods are foreseen in the assessment of fire risks arising from secondary independent initiating events such as earthquakes. The data base on equipment fragility and the analysis methodology for fire safety margins proposed to be developed in this program would be useful for that eventual application.

In the control room two major concerns exist. The first is equipment survivability and operability; the second concern, as expressed by the ACRS on several occasions, is that existing requirements to protect control room occupants in accident situations may not be adequate. One of the recommendations

of a June 1984 staff report was that "limiting environmental conditions for operation in the control room should be established and should consider human performance as well as equipment operation as the basis for selection of appropriate limits."

This program purported to address the issue by determining the fire-generated environment and the purge effectiveness of existing equipment.

The Office of Inspection and Enforcement described in Information Notice 83-41, which was addressed to all holders of operating licenses and construction permits, several instances of automatic fire suppression system actuations resulting in inoperability of safety-related equipment. Furthermore, concerns have been expressed (Michelson to Denton, dated July 28, 1982) about the degradation in the performance of equipment, including solid state devices, due to the cooling effect of spuriously released CO_2 fire suppressant. Current regulations for equipment qualification require that only equipment which would be exposed to high-energy steam line breaks classified as DBAs must be qualified for steam and humidity. The need exists to determine the effects of fire suppression agents, in addition to the effects of fire, on the operability and failure thresholds of safety shutdown equipment.

4.2 Objective

The goal of the Fire Protection Research Program was to generate test data and incorporate existing analytical capabilities to support the evaluation of:

1. the contribution of fires to the risk from nuclear power plants,
2. the effects of fires on control room equipment and operations, and
3. the effects of actuation of fire suppression systems on safety equipment.

These three goals were to be reached by implementing a common threefold research approach:

Define Fire Sources: A range of fire sources would be characterized with respect to their energy and mass evolution, including smoke, corrosion products, and electrically conductive products of combustion. The combustible content and configurations of the sources determine the energy and mass release rate characteristics of the fires.

Define Environments: Existing analytical methods for determining the environment resulting from fire would be adapted for nuclear power plant enclosure fires. This approach will account for the source characteristics, the suppression action following detection of the fire, and certain parameters specific to the plant enclosure in which the fire originates, such as the geometry of the enclosure and the ventilation rate. The developing local environment in the vicinity of safety-related equipment would be expressed in terms of temperatures, temperature rise rates, heat fluxes, and moisture and certain species content.

Define Equipment Response: The response of certain safety shutdown equipment and components to the environmental conditions would be studied. The objective was to determine the limits of environmental conditions that a component may be exposed to without impairment of its ability to function.

4.3 Summary of Prior Efforts

As a continuation of a research project initiated in FY 1982, prior efforts entailed surveys of both national and international research programs which could be a factor in formulating nuclear power plant fire protection programs and guidelines.

Additional FY 1983 efforts included a survey of enclosure fire models that specifically employs three-dimensional, transient field model techniques and criteria for the selection of those applicable to the NRC needs.

Based upon the criteria established, a computational model was selected and efforts in FY 1984 were scoped to demonstrate further the capability of the selected analytical model/numerical code. This largely entailed comparisons with cable fire/enclosure tests conducted for the Electric Power Research Institute (EPRI) and for the NRC. Comparison with both test programs were promising to the extent that the model-demonstration phase is essentially completed and that further model augmentation can proceed to study other fire-related aspects, e.g., excess pyrolozate burning and conductive and radiative heat transfer.

Work was also initiated in FY 1984 to perform a parametric study of potential fire environments within nuclear power plant control room configurations. This work was initiated to provide additional fire-modeling capability to those fire-risk tasks associated with NRC's RMIEP. As such, initial efforts were directed to investigate, numerically, potential fire scenarios in the LaSalle Plant control room. The first phase of this work, namely the determination of the fire environment (1) in the control room as a whole and (2) in the exhaust plenum behind the control cabinets in Unit 2, was completed in FY 1985. Code enhancement was begun in FY 1985 to include the effects of heat conduction to and from objects in the enclosure as well as enclosure walls and ceilings.

4.4 Work Performed During Period

Unfortunately, due to cutbacks in NRC funding, the Fire Protection Research program was curtailed in FY 1986 and terminated in FY 1987. Originally, plans had been to develop and deliver a fully documented user package incorporating modelling features developed in FY 1984-1985. Ultimately what was completed in FY 1987 was final report regarding the fire environment in the LaSalle control room. This work is summarized as follows.

4.4.1 Computational Model Parameters

The control room contains control and instrumentation cabinets and cables for LaSalle NPP Units 1 and 2. The enclosure (Fig. 1) is 120 ft x 60 ft x

16.5 ft high with concrete walls generally two feet thick or more at the room boundary. Cabinets and control consoles are shown in Fig. 1. There are a number of desks and tables located around the control room which are not depicted in Fig. 1, but which are accounted for in the computational configuration. The exhaust configuration in the control room is unique in our experience: two L-shaped exhaust plena (Fig. 2), 40 ft. long x 10 ft. wide, are delineated by fronts of cabinets and consoles and further by steel valances extending to the enclosure ceiling as shown in Fig. 3. One exhaust vent is located in each of these plena, and there are no ventilation sources in either plenum. Air flow from the room proceeds into the exhaust plena through gratings in the bottoms of the cabinets forming the L-shaped boundary. In addition to the high cable loadings in the cabinets and consoles, horizontal cable trays, shown in Fig. 3, are located above the cabinets throughout the plenum areas. The cabinets are open both in the back and on top to the general plenum area. The unique exhaust plenum configuration resulted in the simulation of two basic fire types: one outside the plena in the control room working area and one inside an exhaust plenum behind the cabinets. The locations of these source fires are indicated by "X" on Figs. 1 and 2.

Observation of the geometrical details outlined above together with the locations of the ventilation sources and the locations of internal flow obstacles, guided the set-up of the three-dimensional (x,y,z) computational grid to be analyzed.

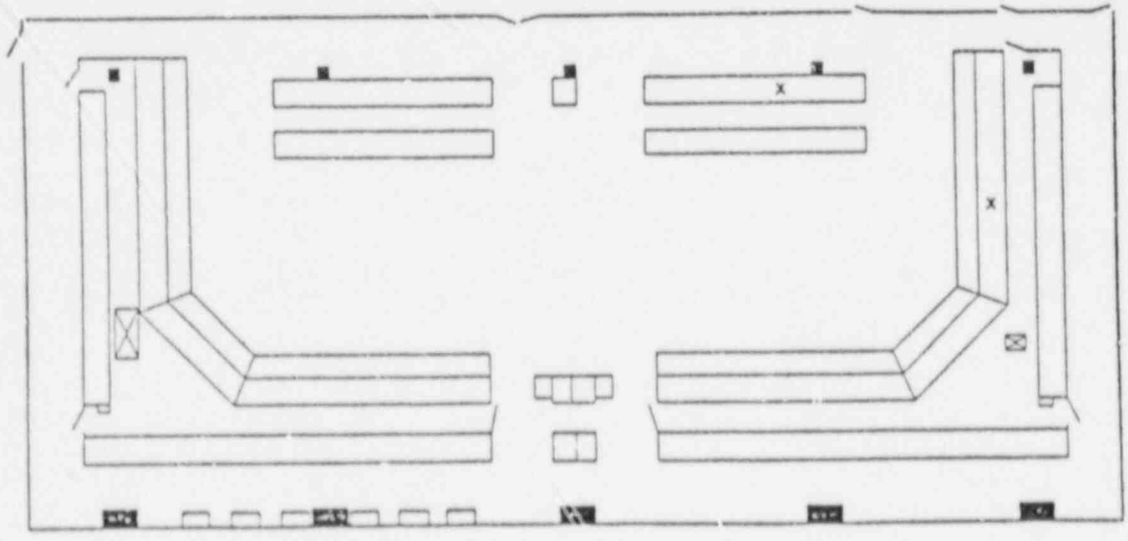

Fig. 1. LaSalle control room - plan view

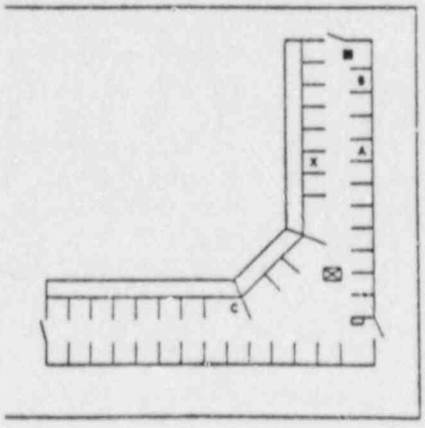

Fig. 2. LaSalle control room - exhaust plenum - unit 2

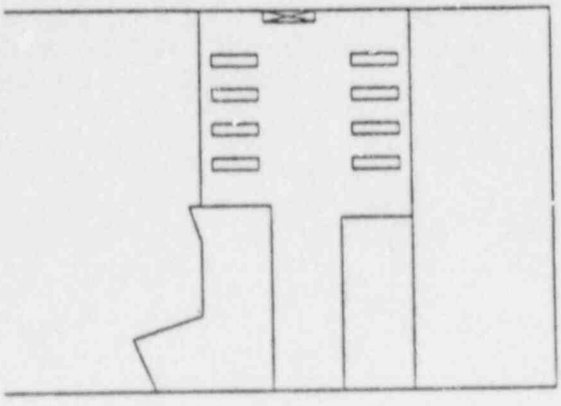

Figure 3. LaSalle control room - exhaust plenum - elevation

At the present state of evolution the model requires the heat release rate of the source fire as input to the code. The design strengths of each ventilation source are also input to the code. Total flow into the control room is distributed throughout the inlet system as per design specifications. Design leakage through the control room doors is 1500 cfm; the remaining 22520 cfm exhausts through the vents located in each exhaust plenum ceiling.

4.4.2 Simulation Results

Two separate simulations involving source fires were performed as stated above: one source fire located in the control room working area and one located in the Unit 2 exhaust plenum as shown in Figs. 1 and 2. Peak fire strength was 600 kW, while fire duration was 18 minutes. The 600 kW heat release rate was distributed in and above the cabinet in question to a flame height calculated from well-known flame-height correlations.

The first case to be examined was that of a fire in the main control room area. Fig. 4 shows the temporal variation of gas temperature at a height roughly equivalent to the tops of the cabinets (~8 ft) both at the fire location and near the center of the control room. The temperature near room center is also representative of the gas temperature at various other locations throughout the control room. Gas temperature rose linearly in six minutes to 150°C in the control room center at the 8 ft height. Gas temperature above the fire plume near the ceiling rose to 240°C in 6 minutes. There was no appreciable gas temperature increase in the exhaust plena due to this fire. Fig. 5 shows an example of perhaps the most valuable output from the simulations: an isothermal perspective of the control room. The 150°C isotherm is shown at 2, 4 and 6 minutes after fire ignition. The fire plume is clearly visible in the top view. The spread of the isotherm around the exhaust plena can be seen in the remaining two views. Notice that the 150°C isotherm only descends to the top of the cabinets at the 6 minute mark.

The second case to be investigated produces an entirely different set of results. For this case a source fire of the same strength is located within the exhaust plenum of Unit 2 as indicated on Fig. 2. Recall that the backs and the tops of these consoles/cabinets are open. In the case of a fire inside the exhaust plenum, temperature rise near the cabinet tops was more pronounced than in the previous case. Gas temperature rose to 200°C near cabinet level in about two minutes, as shown in Fig. 6. The three positions at which temperature is determined are indicated on Fig. 2.

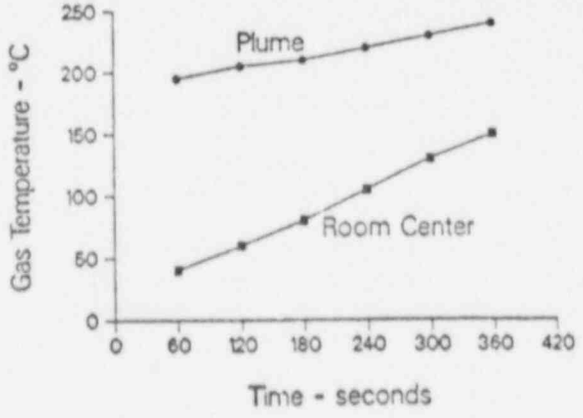

Fig. 4. Gas temperature at cabinet level - fire case 1

Note that the gas temperature at position B at the plenum end is the most sensitive to the source fire. Mention must be made here that the gas temperature is a measure of the convective heat flux only; no radiation effects were included in the model. Fig. 7 shows the temporal evolution of the 150°C isotherm. The fire plume is clearly visible as is the dead-end effect generated by the plenum boundary and swirling flow pattern.

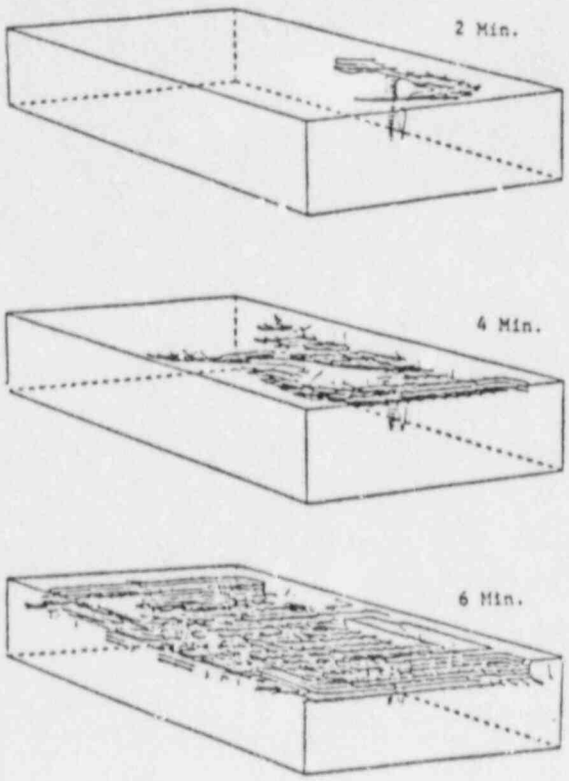

Fig. 5 150°C isotherm - fire case 1

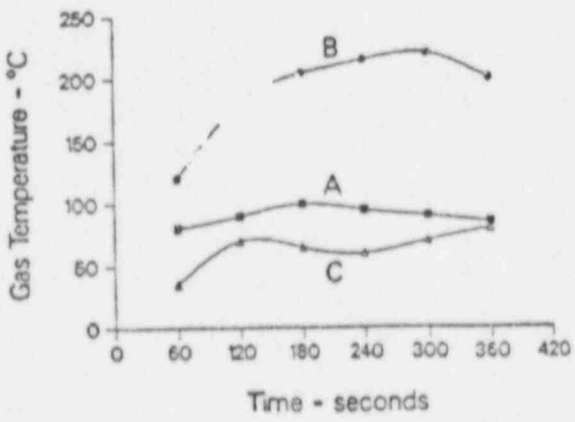

Fig. 6 Gas temperature at cabinet level - fire case 2

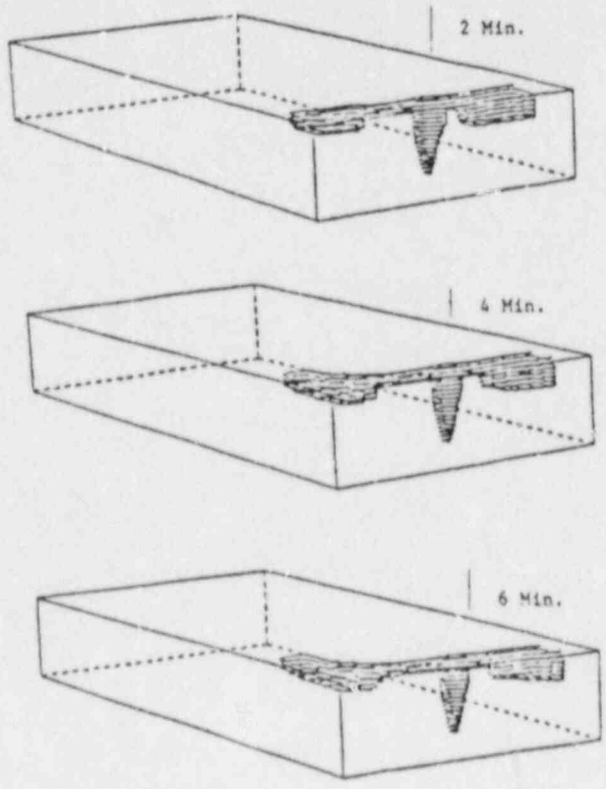

Fig. 7. 150°C isotherm - fire case 2

4.4.3 Conclusions

Conclusions were reached regarding the two separate fire simulation examples, inside and outside the exhaust plenum. The fire in the control room working area did not produce temperatures higher than 150°C in the area of the control cabinets/consoles over the time frame considered. These temperatures are probably not sufficient to cause equipment damage in the time scales noted. There is, however, concern in the area of habitability due to the fact that the temperature in the control room working area at cabinet level rose above 50°C in 15 minutes. Smoke may well descend in a manner analogous to the 50°C isotherm driven by the effects of room filling and the location of the exhaust gratings at the bottoms of the cabinets. The control room may become uninhabitable in this time frame. In the case of a fire in one of the exhaust plena, different conclusions are reached. Temperatures rose above

200°C at the cabinet level in 2 minutes, which may indicate when equipment or cable damage would begin to occur. Equipment in the dead-end area of the plenum may be most sensitive to this potential damage from high gas temperatures. Conversely, the environmental effects outside the plenum in the working area are negligible for this fire scenario; only the plenum area environment becomes inhospitable. There is also evidence that fires larger than 600 kW can occur in cabinets/consoles, which would correspondingly increase the damage potential of the fire. It was assumed in the course of these simulations that no secondary fires occurred; this may not be the case in the plenum area in view of the fact that cable trays pass through the upper portion of the fire plume (Fig. 3). Any of these effects would exacerbate equipment/cable damage potential.

4.5 References

"Fire Environment Determination in the LaSalle Nuclear Power Plant Control Room," J.L. Usher and J.L. Boccio, NUREG/CR-5037, October 1987.

"Fire Environment Determination in the LaSalle Nuclear Power Plant Control Room," J.L. Usher, et. al., BNL-NUREG-38839, presented at ANS Topical Meeting on Operability of Nuclear Power Systems in Normal and Adverse Environments, Albuquerque, New Mexico, October 1986.

"The Use of a Field Model to Assess Fire Behavior in Complex Nuclear Power Plant Enclosures: Present Capabilities and Future Prospects," J.L. Boccio and J.L. Usher, NUREG/CR-4479, December 1985.

"The Use of a Field Model to Assess Fire Behavior in Complex Nuclear Power Plant Enclosures," J.L. Boccio, et. al., ANS Transactions, Vol. 49, p. 297, June 1985.

"The Use of a Field Model to Assess Fire Behavior in Complex Nuclear Power Plant Enclosures," Boccio, J.L., et. al., Heat Transfer in Fire and Combustion Systems, HTD-Vol. 45, pp. 159-166, 1985.

5. Characterization and Detection of Age-Related Failures of Selected Components and Systems with Consideration for Aging/Seismic Interactions

(J. H. Taylor)

Under the auspices of the NRC Nuclear Plant Aging Research (NPAR) Program, BNL is currently performing aging assessments of nuclear components such as electric motors, battery chargers and inverters, relays and circuit breakers, and Motor Control Centers (MCCs). The system studies include a Component Cooling Water System for PWR plants, and a Residual Heat Removal System for BWR plants. The goals of this program are to resolve issues related to the aging and service wear of equipment and systems at operating reactor facilities and to assess their possible impact on plant safety. The progress achieved during the reporting period April 1 to September 30, 1987 is described below.

5.1 Electric Motors (M. Subudhi and R. Lofaro)

A 10-hp industrial motor with 12 years of service in a commercial nuclear power plant and a 400-hp failed motor with over 20 years of service life in a nuclear research reactor facility were tested. The 10-hp motor was subjected to plug reverse cycling to induce accelerated aging while various insulation and bearing test parameters were monitored. Stator coils from the 400-hp motor were tested to diagnose age-related deterioration of insulation dielectric properties. The test objectives were to identify the motor testing methods or functional indicators which are cost-effective and provide adequate feedback to detect degradation in motor components. It was found that monitoring and testing methods are available to detect degradation at an incipient stage. Therefore, implementing such methods in conjunction with plant maintenance activities should reduce catastrophic motor failures caused by aging and service wear in nuclear facilities.

NUREG/CR-4939, comprised of three volumes, contains the above test results, as well as recommendations for improving the current maintenance practices in nuclear power plants. The reports are expected to be published during the next quarter.

5.2 Battery Chargers and Inverters (W. Gunther and M. Subudhi)

5.2.1 Testing of Naturally Aged Equipment

Naturally aged inverters and battery chargers obtained from the Shippingport facility were tested as part of the Nuclear Plant Aging Research (NPAR) Program. The objectives of this testing were to evaluate the naturally aged equipment state, determine the effectiveness of condition monitoring recommendations, and to obtain insight into the practicality of preventive maintenance and monitoring methods.

The two primary monitoring techniques employed were temperature measurements and electrical waveform observation. Internal panel temperature as well as individual subcomponent temperatures were recorded at regular intervals during steady state and transient operations. Thermo-couples imbedded within the transformer and inductor windings and attached to silicon controlled rectifier (SCR) and capacitor surfaces provided a non-obtrusive means of monitoring component operation. Readings taken were compared to original acceptance test data. Based on a twenty percent increase in SCR case temperatures, it is concluded that some SCR heat transfer degradation has occurred with age. Similarly, an increase in output filter capacitor case temperature could be attributed to an increase in capacitor equivalent series resistance (ESR), which has been established as a capacitor aging characteristic.

Circuit waveforms were observed on an hourly basis during steady state operation and at the time load transients were applied. The inverter output voltage and the SCR gate current waveforms remained relatively constant regardless of the applied loads. On the other hand, when circuit degradation was intentionally induced (i.e., input filter capacitance change) waveform characteristic changes were evident. This indicates the usefulness of circuit monitoring to detect impending failure in the incipient stage.

Testing indicates that individual fusing of filter capacitors be considered in order to preclude a capacitor failure in the short circuit mode from rendering the inverter inoperable. Also, equipment acceptance testing should be modified to obtain the most limiting design operating conditions for all major subcomponents. It was observed that the acceptance test was conducted under a high input voltage condition only, while the testing revealed that the highest input choke winding temperatures were obtained when a low input voltage was applied.

5.2.2 Phase 2 Report

The phase 2 aging assessment of battery chargers and inverters was completed and a draft report, NUREG/CR-5051, "Detecting and Mitigating Battery Chargers and Inverter Aging," was issued to the NRC for comment. Consisting of a two-phased approach, this report achieved the second phase of the NPAR goals which are to: (1) identify inspection, surveillance, or monitoring methods which will assure timely detection of inverter and battery charger aging effects, and (2) evaluate the effectiveness of storage, preventive maintenance, repair, and replacement practices in mitigating aging effects.

A review of recent operating data (1984-1986 LER) supports the conclusions reached in the phase 1 report (NUREG/CR-4564) regarding the operational and safety importance of battery chargers and inverters. In addition to the 57 scrams resulting from an inverter failure in the last three years (1984-1986), other challenges to safety systems, abnormal transients, and loss of control or indication provide the impetus to improve inverter reliability through the maintenance and monitoring methods discussed.

Current uninterruptible power systems (ups) designs found outside of the nuclear industry incorporate inverter and battery charger design arrangements, which, when coupled with component level technological advances and increased electrical transient suppression and monitoring capabilities, can minimize the effects of aging and improve vital power availability in nuclear power plants. For instance, electrical transients are one of the direct causes of inverter and battery charger failure in a nuclear power plant. They can also indirectly result in premature equipment failures because of the stresses applied to sensitive electronic components. Electrical transient suppression techniques in large data processing centers include using line regulation/isolation transformers. These transformers have the basic capability to eliminate a large percentage of the transients experienced in a power plant environment. Determining the type and source of electrical transients existing at a specific site can be accomplished by using currently available monitoring instrumentation.

Improving reliability through redundancy or increased maintenance intervals is feasible. Fault trees were constructed for the battery charger and inverter to illustrate dominant failure modes. A sample reliability improvement calculation for the installation of an automatic transfer switch, which is a specific form of redundancy, reveals a sevenfold increase in vital bus availability.

The ability of the battery charger and the inverter to perform their intended functions under normal and emergency conditions can be enhanced through the implementation of a cost effective maintenance and surveillance program. This program should incorporte inspection, monitoring, testing, and repair activities as described in this report.

To mitigate inverter and battery charger aging effects, maintenance must be performed periodically to refurbish and/or replace those subcomponents which exhibit aging. In addition to discrete subcomponents such as capacitors, transformers, and semiconductors, the integrity of other entities such as cable connectors, wiring, and structural fasteners must also be maintained to assure proper equipment operation under normal operating and postulated accident conditions.

Relying on periodic component replacement as a means of maintaining the performance standards of inverters and chargers is not an optimum technique. Testing and monitoring methods which are utilized on a limited basis for inverters at most plants, offer the greatest potential for enhancing a preventive maintenance program and reducing or eliminating periodic component changeout.

In developing recommendations for a long-term program to maintain a high reliability for inverters and battery chargers, utilities should seek and evaluate manufacturer input. The manufacturer's literature often reflects "generic" maintenance requirements. Since reactor safety and availability are

at stake, more detailed, site-specific recommendations for optimum performance should be solicited from the manufacturers and incorporated into the maintenance program.

Corrective maintenance practices for inverters and chargers should be defined. For example, specific torque requirements exist when replacing silicon-controlled rectifiers (SCRs). Root-cause evaluation as to why a component failed may lead to the conclusion that other stressed components also must be replaced.

The testing of a naturally aged inverter and battery charger proved that temperature monitoring can be an effective condition monitoring technique. The installation of thermocouples on component surfaces and inside the panel offers insight into component operation. For example, SCR heat transfer degradation can be detected by monitoring its junction temperature, and electrolytic capacitor degradation, as reflected by the increase in internal resistance, may be reflected by an increase in case temperature. In addition, transformer and inductor winding temperatures are responsive to internal degradation such as turn to turn shorts.

The monitoring of circuit waveforms to assess equipment condition was found to be feasible, however, the information obtained is more difficult to assess than component temperatures. The waveforms which provided pertinent indication of the equipment's operational readiness are the inverter output sine wave, the battery charger output ripple voltage, the SCR gating current, and the commutating capacitor voltage waveform.

5.3 Circuit Breakers and Relays (W. Gunther and Franklin Research Center)

NUREG/CR-4715, "An Aging Assessment of Relays and Circuit Breakers and System Interactions," was published. This report satisfies the phase 1 NPAR objectives for these components in presenting the following information:

- a detailed description of the aging mechanisms and failure modes;
- an assessment of the LER, NPRDS, and IPRDS data bases;
- molded-case and metal-clad circuit breaker operations are described and related to specific failure modes experienced at nuclear power plants, including reactor trip breaker problems;
- the aging interaction relating to circuit breakers and relays in safety injection system is described in detail. Consideration of system operation under varying external influences, including seismic and LOCA conditions, is also presented. The study concludes that failure of a safety injection train is possible from circuit breaker and relay failure if adequate maintenance and testing are not performed;

- recommendations are given for development of monitoring methods to evaluate the susceptibility of continuously energized relays and diagnostic techniques for evaluating the condition of the control circuits and operating mechanisms of metal-clad circuit breakers.

5.4 Motor Control Centers (W. Shier and M. Subudhi)

A draft report describing the Phase 1 aging assessment of motor control centers (MCCs) has been completed and submitted for NRC staff comments. This report follows the established NPAR strategy and investigates the operational performance, the design and manufacturing methods, and the current maintenance, surveillance and monitoring techniques associated with MCCs. A significant result described in this report concerns the identification of important MCC failure modes, causes, and mechanisms from plant operational experience. Failure frequencies determined for the various MCC subcomponents are also described. In addition, recommendations on functional indicators that could be useful in monitoring MCC performance prior to failure are provided. These functional indicators will be evaluated during Phase 2 of the program.

Several sources of operating plant experience were reviewed in detail to examine the more important failue modes, causes, and mechanisms. The results of this review indicated that circuit breakers, relays, and coils accounted for more than 50% of the reported MCC failures. The dominant failure cause that was identified was the sticking of electrical contacts due to the accumulation of foreign substances. The subcomponents that were identified as contributing to MCC failures are shown in Figure 1. Figure 2 summarizes the failure causes that were identified. An important result that was also identified from the failure analysis was that approximately 44% of the failures were discovered during surveillance testing or maintenance. For a standby system that operates on demand, this result indictes that the MCC was found in a failed condition when the maintenance or surveillance was initiated.

The reported failure events in the Nuclear Power Reliability Data System, maintained by the Institute of Nuclear Power Operations, were organized on a component basis and a failure frequency was determined. For the dominant subcomponents (circuit breakers and relays), these results were in agreement with the results obtained in another NPAR program related to circuit breakers and relays. Other reported results include:

- A survey of the dominant failure modes;
- A summary of the safety systems affected by the MCC failures;
- A summary of the plant operating status at the time of failure identification:

- A review of the physical process or mechanism causing the particular MCC failures.

An interim review of current industry standards, manufacturers recommendations, and regulatory guides and information bulletins was completed to provide a basis for the Phase 2 work. In addition, the results of this Phase 1 work are summarized in a preliminary recommendation of functional indicators of MCC performance. The purpose of these proposed functional indicators is to provide an indication of age-related deterioration of MCC subcomponents prior to failure. Phase 2 of this program will provide a verifiction or elimination of the various functional indicators through testing of naturally aged MCCs that have been obtained from the Shippingport facility.

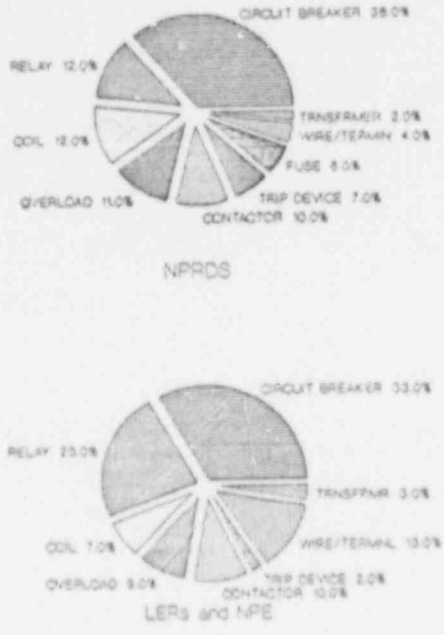

Figure 1 Subcomponent Failures

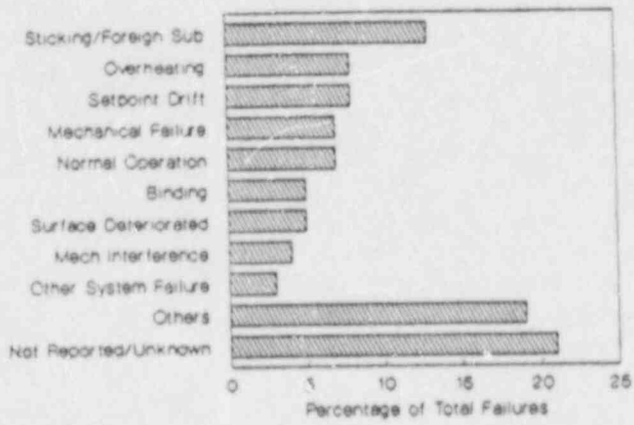

Figure 2 Failure Causes - NPRDS

5.5 Component Cooling Water System (R. Lofaro and M. Subudhi)

The CCW system is common to all pressurized water reactors although it may be known by different names. Its function is to remove heat from various plant loads and transfer it to an open loop cooling system, such as the service water system. The CCW system also acts as a barrier between the radioactive loads it services and the open loop cooling systems. Typical loads serviced by the CCW system include reactor coolant pump seals, shutdown heat exchangers, residual heat removal heat exchangers, safety injection pumps and others.

The most common CCW system design includes several pumps, heat exchangers and a surge tank. Piping, instrumentation, and numerous valves are also significant components in the CCW system which enable it to perform its many diverse functions. In some plants several systems may be used to perform the CCW function, while at other plants one system may be shared by two units.

Typical operating conditions for the CCW system include a pressure of approximately 100 psig and a temperature ranging from 75°F to 150°F. The process fluid is deminearlized water with corrosion inhibitors. A significant characteristic of CCW systems is that they are normally operating even when the reactor is down. This increases component operating time and exposure to aging mechanisms.

As part of the deterministic work performed, CCW system failure data from various national data bases were reviewed and analyzed. Results showed that over 70% of the failures reported were aging related. The dominant failure cause was "normal service" while the major failure mechanism was "wear." These findings show that aging is a significant factor in CCW system failures.

The failure data also showed that "leakage" was the most common failure mode. This is a typical failure mode for valves and pumps which were the components most frequently failed. Valve failures included both internal seat leakage and external seal leakage. Pump failures included external seal leakage as well as bearing failures. Instrumentation/controls and heat exchangers were also found to have a significant number of failures.

Of the failures reviewed, 50% resulted in degraded CCW system performance while [illegible] -esult- in a loss of redundancy. The remainder either had no effec[illegible] ystem operation or its effect was unknown. Complete loss of CCW syste[illegible] tion was only found once, and the failure was not aging related. This shows that CCW failures are typically detected before they become serious enough to cause a complete loss of system function, but not always before system performance has been affected. Current monitoring methods detect only 2/3 of all failures. The remaining 1/3 are not detected until some operational abnormality is observed. Improvements to current monitoring methods should, therefore, be considered.

To supplement the information obtained from the data bases, actual plant data from Indian Point 2 was obtained and reviewed. Results showed a large percentage of age related failures (80% to 100%). Pumps and valves were found to provide the predominant number of failures, which is consistent with previous results.

Component failure rates were calculated from both the data base information and from the actual plant data. Results showed good agreement with failure rates from commonly used sources, but were higher than failure rates used in PRA studies. Also, a trend toward increasing failure rate with component age was seen, thus indicating that system unavailability increases with age. It should be noted that current PRA techniques assume constant failure rates and, therefore, predict constant system unavailabilities throughout plant life.

The probabilistic work included a review and analysis of the Indian Point 2 PRA. The CCW system from this plant was modeled and a PC based computer program called PRAAGE was developed to perform PRA calculations as a function of age for the CCW system. Time dependent failure rates were input to the program, and system unavailability and component importance were calculated for various ages. The Indian Point 2 CCW system was modeled for this study since it is representative of other plant designs and an existing PRA was available for it.

The PRA calculations showed that if interaction between various plant systems is considered, CCW unavailability is dominated by loss of the service water system. Looking at the CCW system, valves in critical locations dominate system unavailability followed by pumps. These results are expected to be typical for most CCW systems, however, individual design variations must be considered.

When the effects of aging from the data analysis were included in the PRA calculations, two significant results were observed: 1) CCW system unavailability increased with age, and 2) component importances changed with time. Using the time dependent failure rates calculated from the data, pumps were found to become more important than valves after the first 20 years of plant life. This is due to pump failure rate increasing more rapidly with age than valve failure rate. From these results it is seen that improvements to current maintenance and/or monitoring methods may be required to prevent system unavailability from reaching an unacceptable level during the later years of plant life. It also indicates that more attention may need to be focussed on pumps as they age.

Sensitivity studies were performed to examine the effect of the uncertainties in the time dependent failure rates on the PRA results. In general, it was found that the results were not particularly sensitive to variations in the data. It was observed, however, that heat exchangers and piping have the potential to become very important to system unavailability during later years of plant life. This should be considered in assessing present monitoring/maintenance practices and in evaluating plant life extension concerns.

This work has shown that aging is a concern for CCW systems and can adversely affect system performance and reliability. Good functional indicators are, therefore, required to detect and mitigate aging degradation at an incipient stage. Proposed functional indictors for the major CCW components are presented. System level functional indicators are also discussed.

Results from this work have also provided a technical basis for evaluating current inspection, surveillance and monitoring methods and verifying that they properly address aging effects. From the failure characteristics observed it is seen that monitoring methods must be diverse to detect the various aging mechanisms present in CCW systems. As plants age, the importance placed on certain components may need to be re-evaluated due to increasing failure rates.

A draft report was prepared summarizing all the above findings and the report will be sent for comment during the next quarter.

6. Failure Analysis and Nuclear Industry Practice
(C. J. Czajkowski)

After the Surry Unit 2 (Virginia Electric Power Co.-VEPCO) catastrophic failure of a pipe in the "A" feedwater suction line, the U. S. Nuclear Regulatory Commission (USNRC) initiated a program to:

1. Evaluate Surry failure results and identify generic applicability;

2. Identify extent of erosion-corrosion problem in nuclear plants;

3. Evaluate data supplied by Office of Inspection and Enforcement and identify any trends or correlations; and

4. Identify problem areas that may need additional research to bound the problem.

A review of the controlling variables in the erosion-corrosion phenomenon was prepared as a background information for further research. This effort was completed on November 1987 closing out this task.

6.1 Erosion-Corrosion Definition

Erosion-corrosion is usually defined as the acceleration or increase in the rate of corrosion caused by the relative movement between a corrosive fluid and the metal surface. In principle, it should be distinguished from the effort of fluid flow that accelerates general corrosion by increasing the rate of mass transport of reactive species (i.e., a cathodic reactant, such as oxygen) to the metal surface, or the rate of removal of corrosion products from the metal surface. As illustrated schematically in Figure 1, at a given critical flow rate, a rather abrupt increase in the corrosion rate occurs within the turbulent flow regime. The critical fluid velocity, V_c, sometimes called erosional or breakaway velocity, depends on hydrodynamic parameters and the corrosion characteristics of the alloy/environment system. Below the critical fluid velocity the corrosion rate increases less abruptly due to an increase in the rate of mass transport of electroactive species. Within this regime the corrosion rate is governed by electrochemical and hydrodynamic phenomena under conditions varying from laminar to turbulent flow (Figures 2(a) and (b)). It should be noted, however, that for many alloy/environment systems the boundary between what is called flow-assisted corrosion and erosion-corrosion is not so well defined as suggested in Figure 1. This is precisely the case of carbon steel in high temperature deoxygenated water, as discussed in detail below.

Erosion-corrosion can also be distinguished from forms of erosion such as cavitation and impingement damage. Impingement damage involves the impact of liquid droplets present in a gaseous fluid through forces generally perpendicular to the metal surface, whereas cavitation arises from the collapse of gas bubbles contained in a fast flowing liquid phase, also through

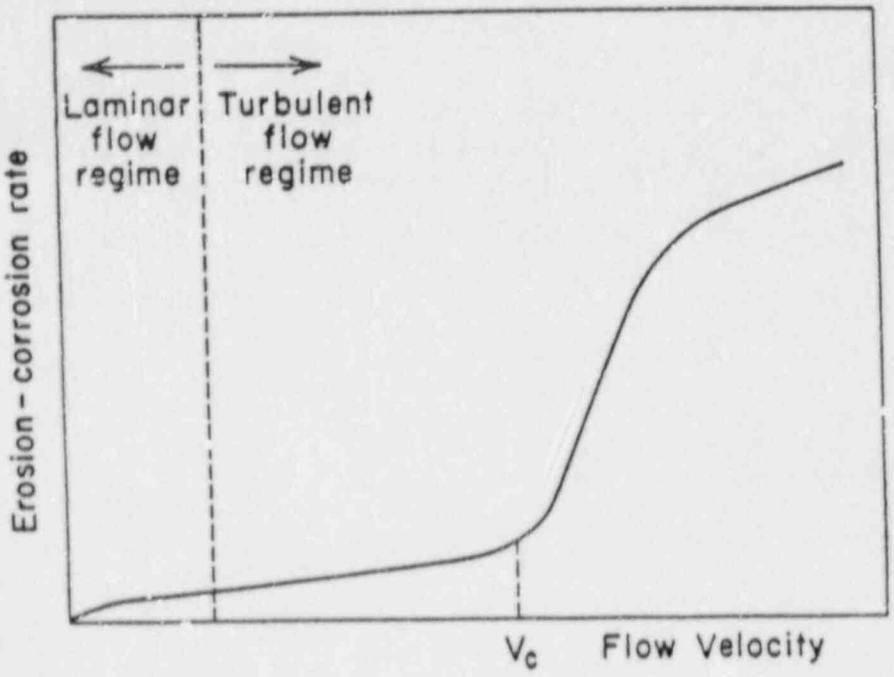

Figure 6.1 Schematic Plot Showing the Effect of Flow Velocity on Erosion-Corrosion Rate

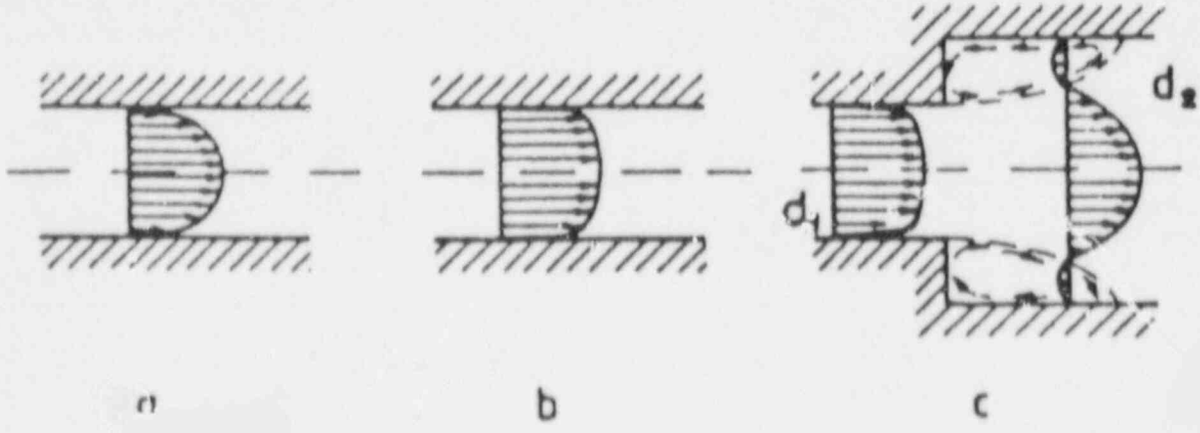

Figure 6.2 ocity Profile of Fluid Flow Inside a Pipe: a) Established Laminar Flow, b) Turbulent Flow with Logarithmic Velocity Profile, c) Turbulent Pipe with Separation (Complex Velocity Field with Reverse Flow)

perpendicular pulsive forces. Wear of last-stage turbine blades by water droplets and cavitation damage of pumps by steam bubbles are typical examples of these phenomena. Together with erosion by solid particles, they are essentially mechanical forms of metal deterioration, because the contribution of corrosion usually is thought to be almost negligible. In these three phenomena, direct damage of the metal occurs when the forces involved in the impact are higher than the material strength.

6.2 Conclusions from the Investigation

From the available literature, which has been almost completely covered in this review, it can be concluded that a qualitative assessment of the major influential factors in erosion-corrosion of carbon steel in high temperature flowing water is now complete. However, there are many discrepancies in the experimental results when studies conducted by different authors are compared. Furthermore, as the recent observations of Tomlinson and Ashmore[1,2] show, erosion-corrosion could be extremely severe even at temperatures above 250°C. Several years ago Berge and Kahn[3] noted that the commonly accepted statement that erosion-corrosion does not occur beyond 200°C should be considered cautiously. In this regard it seems that differences between results of different authors could be assigned to the presence of residual elements that are not properly identified. In most of the studies on erosion-corrosion it is uncommon to have a full description of the chemical composition of the steel. As discussed before, residual amounts of elements such as chromium may have a strong beneficial effect.

For these reasons, the most effective countermeasure against erosion-corrosion is the choice of sufficiently resistant materials. In most of the applications under single phase conditions, low alloy steels containing 2% Cr seem to be a cost effective solution if modifications in design to reduce flow rates and local turbulences are difficult to implement. Under two-phase flow (wet steam) more highly alloyed materials are needed.

Under particular conditions, modifications in the water chemistry by rising the pH or by adding oxygen to the feedwater may be extremely effective to inhibit erosion-corrosion damage, as suggested by the experience in the U.K. and West Germany. In this case again, these types of countermeasures are more successful under single phase conditions.

Regarding the modeling efforts, it can be concluded that the prediction of accurate erosion-corrosion rates on the basis of laboratory data is still very limited. These models are capable of metal loss predictions within the range of data on which they are based. It should be noted, however, that small variations in the environmental conditions (dissolved oxygen concentrations varying in the range of few ppb, or presence of acidic impurities) may lead to unsuspectedly high rates of erosion-corrosion under certain circumstances. These variables, plus significant variations in the rate of mass transfer at specific locations may be the source of very large differences in erosion-corrosion rates from plant to plant, from component to component and in particular for different locations in the same component, even

though no substantial changes in the overall hydrodynamic conditions could be suspected.

6.3 REFERENCES

L. TOMLINSON and C. B. ASHMORE, Ref. 5, p. 195.

L. TOMLINSON and C. B. ASHMORE, Br. Corros. J., 22, 45 (1987).

PH. BERGE and F. KHAN, "Summary and Conclusions of the Meeting," Ref. 2.

7. Evaluation of the Adequacy of Current Reactor Coolant Pump Seal Instrumentation and Operator Responses to Possible Reactor Coolant Pump Seal Failures

(C.J. Ruger and W.J. Luckas, Jr.)

As part of resolving Generic Issue 23 entitled, "Reactor Coolant Pump Seal Failure" the objectives of this project are to (1) evaluate the adequacy of current reactor coolant pump (RCP) seal and seal cooling system instrumentation to detect RCP seal degradation and failures, (2) evaluate the adequacy of current automatic actions and operator responses to prevent RCP seal loss of coolant accidents (LOCAs) or other unacceptable events, and (3) propose possible instrumentation, automatic actions or manual operator response changes which could improve the current RCP seal safety procedures. An additional objective is to (4) develop technical findings for Generic Issue 23.

In achieving the first three objectives, namely those associated with the RCP seal instrumentation and operator response, BNL published NUREG/CR-4544 in December 1986. This document is entitled, "Reactor Coolant Pump Seal Instrumentation and Operator Responses: An Evaluation of Adequacy to Anticipate Seal Failures."

The fourth objective is being addressed by the ongoing development of a report to be entitled, "Technical Findings Related to Generic Issue 23: Reactor Coolant Pump Seal Failures." When published, the report is intended to document the findings of the appropriate technical studies developed as part of the effort to resolve Generic Issue (GI) 23. The report is structured to address the findings as they apply to each subtask of the GI 23 Task Action Plan.

During the third and fourth quarters of FY 1987, a preliminary draft of the "Technical Findings" report was developed based on the relevant seal failure research documentation available. The draft was forwarded to the NRC and other appropriate reviewers for comment.

8. Adequacy of Current Valve In-Service Testing Methods

(C.J. Ruger and W.J. Luckas, Jr.)

The objective of this project is to perform studies and related services to systematically evaluate current requirements for in-situ testing in nuclear power plants. The evaluation will be to determine if the valve testing methods, as currently invoked, are sufficient to assure valve performance under design basis accident conditions. Emphasis for the project is in the area of value-impact analyses for expanding IE Bulletin 85-03 valve operability assurance applicability to all safety related motor operated valve (MOV) actuators.

During the third and fourth quarters of FY 1987, a draft methodology was developed for the review of the benefits (value) and costs (impacts) associated with a program to maintain in-service operability assurance. This draft document was prepared to support the justification to expand IE Bulletin 85-03 applicability to all safety related MOVs.

9. Regulatory Guide for Reactor Dosimetry
(J.F. Carew, M. Todosow)

A draft Regulatory Guide for performing pressure vessel damage fluence calculations has been written. This guide provides acceptable methods and assumptions for use in determining pressure vessel damage (>1-MeV) fluence for input to the RT_{PTS} prescription given in 10 CFR 50.61. Detailed procedures for determining few-group neutron cross sections, constructing an exposure-averaged core neutron source and carrying out the required neutron transport calculations are presented. Acceptable methods for qualifying calculational techniques and a quantitative acceptance criteria are also presented.

III. DIVISION OF REACTOR ACCIDENT ANALYSIS

SUMMARY

Thermal-Hydraulic Reactor Safety Experiments

Boundary and parametric calculations to evaluate the possible extent of hydrogen generation in the Zion reactor cavity during a high pressure melt ejection accident scenario have been performed. The results show that although significant quantities of hydrogen can be produced in the cavity region, the melt exiting the cavity is likely to retain a significant fraction of the stored chemical energy.

Protective Action Decisionmaking

In this program, BNL staff are developing a technical basis for NRC guidance on protective action decisionmaking based on an evaluation of the consequences of nuclear power plant accidents. Potential actions under consideration include sheltering, evacuation, and relocation. In the past specific recommendations have been proven to be difficult to justify because of uncertainties in potential accident sequences. Consequently, BNL will establish strategies appropriate to those sequences for which emergency planning is necessary, emphasizing credible failure modes, links to emergency action levels based on in-plant observables and containment status, and other factors such as weather.

MELCOR Verification and Benchmarking

In this project, BNL staff will evaluate the potential for the MELCOR computer code to be used as a source term code. MELCOR is currently being developed for NRC by Sandia National Laboratories (SNL) to be used in probabilistic risk assessment (PRA) studies. In addition, the project will also benchmark MELCOR against more mechanistic codes and the available severe accident data.

Uncertainty Analysis of the Source Terms (QUASAR)

The first estimate of the potential release of radioactive fission products from Light Water Reactor (LWR) power plants was made in 1957 (AEC report WASH-740). Other estimates followed, including TID-14844 which gave source term magnitudes to the containment in 1962. The Reactor Safety Study (RSS/WASH-1400) published in 1975 provided estimates of the radiological source terms that might result from hypothetical severe core-damage accidents using limited phenomenological models and conservative or near-estimates of the radionuclide releases. In addition, an updated basis for estimating fission

product behavior was published in NUREG-0772 in 1981. The latter study did not actually estimate the source term, but provided a review of the state of knowledge at that time. It also led to the current NRC and Industry (IDCOR) initiatives on re-estimating the source term as embodied in the BMI-2104 documentation and the final IDCOR document.

Since publication of the RSS, and subsequently, the accident at the Three Mile Island Unit 2, substantial development and advances in the state of knowledge concerning the nature of severe accidents and associated fission product release and transport have been made. These developments and advances indicated that the source term estimates conceived previously might be highly conservative and often uncertain.

As part of the continuing source term reassessment, the United States Nuclear Regulatory Commission (USNRC) is sponsoring a demonstration procedure for mechanistic determination of source terms at Battelle Columbus Laboratories (BCL) and Sandia National Laboratories (SNL). The models for the estimation of fission product release and behavior are incorporated into computer codes referred to as the Source Term Code Package (STCP), which mathematically simulates a severe accident to predict the source terms. In order to better establish the estimates of source term from these phenomenological models, quantification of the uncertainties in the resulting source term is essential.

The objectives of the present program are: (1) to perform an uncertainty evaluation of the input parameters and phenomenological models used in the Source Term Code Package (STCP), (2) to define reasonable, technically defensible ranges and assumptions for use in the STCP, and (3) to determine the uncertainty in the source term to the environment for selected sequences in both Boiling and Pressurized Water Reactors.

Source Term Code Package Verification and Benchmarking

During accidents in Light Water Reactors (LWRs) the reactor core could be damaged and fission products may be released to the primary system. If the primary system is breached fission products could in turn be released to the containment building. In containment there are a number of systems available to help prevent the fission products from being released to the environment. If these systems fail or are compromised, a fraction of the radionuclides may be released to the atmosphere with corresponding adverse effects on the surrounding environment. There are potentially a large number of different accident sequences that could lead to core damage and ultimately to core meltdown. Each individual accident sequence could result in several possible paths for fission products to reach the environment. Each path will have a unique fission product release characteristic or "source term".

In order to define a "source term", information is needed on the amount and chemical form of the fission product species released and also on the characteristics of the release. The release characteristics are the timing of release, release duration, release height, and release energy. In the Reactor

Safety Study (RSS) models of the physical processes associated with particular accident sequences were developed to assess the magnitudes and timings associated with the release, transport, and deposition of the radioactive materials form the core through the primary system and containment and into the environment. However, it has been suggested that the methodology used to generate source terms in the RSS may contain simplifications, which would tend to over predict the release of fission products and hence result in overly conservative estimates of off-site consequences.

The Source Term Code Package (STCP) developed by Battelle Columbus Laboratories (BCL) is aimed at better quantifying the severe accident source term estimates. The interim version of the code (STCP/MOD0) has been operational at BNL since late 1985, and BNL has received the newest version (STCP/MOD1) in July 1986.

The objectives of this project are (1) to implement, verify and benchmark the STCP at BNL, (2) to provide quality assurance of the specific STCP calculations performed by BCL, (3) to perform plant specific calculations for the USNRC, and (4) to initiate a validation program based in the recent experimental data and detailed mechanistic code calculations.

Risk and Risk Reduction for Zion

Significant improvements have been made in U.S. nuclear power plants, plant models, and risk-analytical methods over the last ten years. In order to determine the impact of these improvements on severe accident risk evaluation in Light Water Reactors (LWRs), the United States Nuclear Regulatory Commission (USNRC) is undertaking a complete reassessment of severe accident risk for five reference plants, to be published in the document NUREG-1150.

The identification of important core melt accident sequences for four of the five reference plants is being undertaken in the Accident Sequence Evaluation Program (ASEP) at Sandia National Laboratories (SNL). Containment event trees (CETs) for the important accident sequences at the four plants are being formulated as part of the Severe Accident Risk Reduction Program (SARRP) also at SNL. New source term calculations using the Source Term Code Package (STCP) have been performed at Battelle Columbus Division (BCD) for important failure modes for each of the five plants. Finally, SNL will integrate the results of the above studies into a complete risk analysis for four of the five plants as a basis for NUREG-1150. BNL is applying the methods developed for the above studies to the Zion plant for input to NUREG-1150.

The technical phases of the BNL project include the following: (1) Review of the Zion accident sequence analysis provided by SNL, and adaptation of its content to the NUREG-1150 methodological framework, (2) Characterization of the Zion containment by use of the containment event tree methods under development at SNL, (3) Incorporation of the BCL Zion source term calculations into the accident progression analysis, (4) Performance of Zion-specific containment loading calculations, (5) Characterization of systems and phenomenological uncertainties through the use of expert opinion elicitation, (6) evaluation of offsite impacts, conditional upon the radiological releases predicted,

and (7) Integration of the previous phases to provide a characterization of the severe accident risk posed by operation of Zion Unit 1. In February 1987, a draft version of the BNL analysis of Zion was published (NUREG/CR-4551, Vol. 5, Draft). The analysis is currently being revised in the light of public, utility and peer panel review. BNL is providing on-call assistance to the NRC on matters relating to this study.

Thermodynamic Core-Concrete Interaction Experiments and Analysis

A survey of available models for stratified interlayer heat transfer between bubbling layers is presented. The models are compared to existing data and shown to underpredict the magnitude and trend of the data. An apparatus is described in which interlayer bubbling heat transfer experiments were performed. Three sets of experimental data are presented: 10 cs oil/mercury, 100 cs oil/mercury, and water/mercury. A dimensionless correlation is developed and the form of the correlation is reported.

Efforts taken to redesign the apparatus for film boiling from solid and porous surfaces are described. Modifications to the design to eliminate nucleate boiling, maintain constant liquid level, and cool the boiling chamber base are described. Final testing was performed to ensure proper operation of the apparatus prior to the gas injection tests. The measured boiling heat flux was found to deviate from the Berenson model prediction by approximately 10%.

Containment Performance Design Objectives

The initial objectives of this project were to develop a containment performance objective (CPO) for light water reactor (LWR) containment buildings and implementation guidance for possible incorporation into the Nuclear Regulatory Commission's Safety Goals Policy Statement. This work was completed during 1986. During the current reporting period the project was redirected to providing the NRC staff with technical support to help define what might constitute "a large release" of radioactive materials during a severe accident in a LWR.

Review of the Core-Melt Evaluation for the Westinghouse Standard Plant (SP-90)

This project involves a review of those aspects of the Probabilistic Safety Assessment (PSA) for the Westinghouse Standard Plant (SP/90) related to the core meltdown evaluation. The SP/90 PSA was performed by the Westinghouse Electric Corporation as part of the requirements for application for a preliminary design approval (PDA). The BNL effort includes a full review and requantification of the risk that could result from accidents involving core damage.

Review of Containment Response Analyses in the Shoreham Probabilistic Risk Assessment

The purpose of this work is to assist the NRC staff in reviewing the accuracy and completeness of the Shoreham probabilistic risk assessment (PRA) with regard to: core melt accident progression including containment loading and failure modes, radioisotope inventory in containment, possible release characteristics, and radiological consequences.

Fission Product Releases and Radiological Consequences of Degraded Core Accidents

To assess the radiological consequences of a degraded core accident at a nuclear power reactor, an evaluation must be made of the quantities and characteristics of releases of radionuclides (source term) from the fuel to the environment. The NRC staff has used estimates of fission product releases that are based upon the WASH-1400 methodology, estimates based upon evolving research for one reactor type (GESSAR-II), and source terms based upon TID-14844 (1962) methodology. During FY 1984, the results of ongoing research for severe accident source term estimations were made available through the Accident Source Term Program Office (ASTPO). The results consist of a number of computer codes (and guidance in the use thereof) that model the evolution, transport, and attenuation of radionuclides from fuel pins through a reactor primary system, containment, other buildings, and to the environment.

The application of the maturing Source Term Code Package (STCP) methodology will require a review, on a case-by-case basis, of specific regulatory issues, their technical basis (including relative conservatisms, or non-conservatisms), the over-all goal of regulatory action, the results of STCP calculations, and the degree of confidence that can be associated with these results. This project will provide the NRC staff with a data base for considering generic alternative regulatory actions and for considering applicant/licensee requests for departure from related current staff practice.

The objective of this project is to perform evaluations of degraded core accident source terms in order to provide the NRC staff with the technical bases necessary for considering changes in technical specifications, Standard Review Plans and Regulatory Guides, and rulemaking.

Review of the Accident Sequence Evaluation for the Westinghouse Standard Plant (SP/90)

This project involves a review of those aspects of the Probabilistic Safety Assessment (PSA) for the Westinghouse Standard Plant (SP/90) related to the accident sequence evaluation. The SP/90 PSA was performed by the Westinghouse Electric Corporation as part of the requirements for application for a preliminary design approval (PDA). The BNL effort includes a full review and requantification of the accident sequences that could lead to core damage.

10. Thermal-Hydraulic Reactor Safety Experiments

10.1 Direct Heating of Containment Atmosphere by Core Debris (N. K. Tutu and T. Ginsberg)

This task is concerned with predicting the actual extent of the direct heating of the containment atmosphere by the molten core debris following a high-pressure melt ejection accident. The general objective of the experimental part of the program is to understand the details of the melt-blowdown steam interaction in the reactor keyway and its immediate vicinity, and the development of individual phenomenological models to describe this interaction. This investigation would complement the 1/10-scale Surtsey program at SNL.

10.1.1 Parametric Calculations of Hydrogen Generation in the Zion Reactor Cavity Region

10.1.1.1 Introduction

Since it is the high-speed jet of steam (blowing down from the reactor pressure vessel) that entrains the melt and transports it out of the cavity, we have recognized from an early date, the possibility of hydrogen generation due to steam-metal chemical reactions in the reactor cavity during a high-pressure melt ejection (HPME) accident. Our preliminary calculations have shown (Tutu et al., 1985) that there is enough time available for significant zirconium-steam reactions to take place within the Zion reactor cavity. More recently, calculations performed by Williams et al. (1987) using the lumped parameter CONTAIN code have also demonstrated the possibility of significant hydrogen generation in the reactor cavity during a HPME accident. This phenomenon is now well recognized by the workers in this field. However, it must be pointed out that so far no realistic calculations to predict the actual extent of hydrogen generation in the reactor cavity during a HPME accident have been performed. Such realistic calculations (development of which is under way [Ginsberg and Tutu, 1987]) would involve modeling of all the rate processes (melt entrainment rates, melt droplet size distribution, gas-droplet interfacial drag, heat transfer, and chemical reaction) and any thermodynamic limits on the relevant chemical reactions. In the absence of these very complex calculations, hydrogen generation in the cavity region was neglected in the past; whereas now several investigators have argued that most of the potential chemical energy in the core melt could be converted into hydrogen in the reactor cavity. Therefore, to improve our understanding of the reactor cavity phenomena during HPME accidents, we have performed an equilibrium bounding calculation, which gives the maximum possible extent of hydrogen produced in the reactor cavity. We have also performed several parametric calculations to take into account the effect of transient melt dispersal rate on the magnitude of hydrogen generaion in the cavity. The calculation procedure and the results are described below.

10.1.1.2 Initial Conditions and Equilibrium Melt-Steam Chemical Reactions

The assumed initial conditions at the instant of vessel failure are based upon the Zion Standard Problem 1 (Containment Loads Working Group, 1985) and are given in Table 10.1. Let us first find the total amount of hydrogen that would be produced if the entire melt inventory were allowed to react with an infinite supply of steam. The reactions, along with the amount of hydrogen produced, are given by:

$$Zr + 2H_2O \rightarrow ZrO_2 + 2H_2 \quad (1)$$
$$(482.35 \text{ kg of } H_2)$$

$$2Cr + 3H_2O \rightarrow Cr_2O_3 + 3H_2 \quad (2)$$
$$(126.93 \text{ kg of } H_2)$$

$$3Fe + 4H_2O \rightarrow Fe_3O_4 + 4H_2 \quad (3)$$
$$(892.92 \text{ kg of } H_2)$$

$$Ni + H_2O \rightarrow NiO + H_2 \quad (4)$$
$$(37.47 \text{ kg of } H_2)$$

Therefore, the entire metallic component of the melt inventory is capable of producing 1540 kg (or 770 kg-moles) of hydrogen due to metal-steam reactions. Let us denote this amount of hydrogen in kg-moles by N_o. If n is the number of kg-moles of hydrogen calculated to be produced in the cavity region, then we define the efficiency η, of hydrogen production in the reactor cavity as:

$$\eta = \frac{n}{N_o} \quad (5)$$

Table 10.1 Assumed Initial Conditions at the Instant of Vessel Failure

Mass of Zr	1.1×10^4 kg
Mass of ZrO_2	1.486×10^4 kg
Mass of UO_2	9×10^4 kg
Mass of Fe	1.87×10^5 kg
Mass of Cr	0.22×10^4 kg
Mass of Ni	0.11×10^4 kg
Temperature of corium	2533 K
Primary system volume	340 m^3
Containment pressure at vessel failure	0.4 MPa
Ratio of partial pressure of steam to partial pressure of hydrogen in the primary system	3.893
(Hydrogen-steam mixture is assumed to be stratified)	

Since the availability of steam in the reactor cavity is limited, the actual steam-steel reaction may not follow Equation (3). As Baker et al. (1982) have pointed out, the core melt-steam reaction under thermodynamic equilibrium proceeds in the following stages.

First, all the available zirconium is oxidized in accordance with Equation (1). Next, if steam is still available, the chromium and iron in stainless steel react with steam as follows:

$$2Cr + Fe + 4H_2O \rightarrow FeO \cdot Cr_2O_3 + 4H_2 \qquad (6)$$

Considering the mass ratio of chromium to iron in the melt, as given in Table 10.1, this implies that only 6.32% of the iron inventory will be oxidized to FeO during this stage. The remaining iron in the core melt can be oxidized to FeO only if the ratio of partial pressure of steam to partial pressure of hydrogen is greater than or equal to 0.5. In other words,

$$Fe + H_2O \xrightarrow[\frac{P_{H_2O}}{P_{H_2}} \geq 0.5]{} FeO + H_2 \qquad (7)$$

where P_{H_2O} is the partial pressure of steam and P_{H_2} is the partial pressure of hydrogen in the gas phase. The oxidation of nickel and further oxidation of FeO to Fe_3O_4 is subject to the following restrictions:

$$3FeO + H_2O \xrightarrow[\frac{P_{H_2O}}{P_{H_2}} > 100]{} Fe_3O_4 + H_2 \qquad (8)$$

$$Ni + H_2O \xrightarrow[\frac{P_{H_2O}}{P_{H_2}} > 50]{} NiO + H_2 \qquad (9)$$

The partial pressure limitations for the reactions represented by Equations (7) through (9) are temperature dependent, and the reader is advised to refer to the paper by Baker et al. (1982). The values given here are the ones that we have used for the calculations that follow.

10.1.1.3 Upper Bound on Hydrogen Produced in the Reactor Cavity

Let us first find the maximum amount of hydrogen that could be generated in the reactor cavity as a function of the primary system pressure, P_o, at the instant of the vessel failure. This upper bound on hydrogen production in the cavity is given by assuming complete mixing of all the core melt and the

entire steam inventory in the primary system and evaluating the thermodynamic equilibrium state. This is indeed the procedure that we have followed for this calculation. The chemical reactions are assumed to follow Equations (1), and (6) through (9).

The results are shown in Figure 10.1 as the curve ABCDE. Note that instead of plotting the amount of hydrogen produced, we have plotted the hydrogen production efficiency as defined by Equation (5). The reason being that the departure of this efficiency (η) from unity gives us an indication of the potential chemical energy fraction that is still stored in the melt. When P_o is small, the amount of steam available for hydrogen production is small, and therefore η is small. As P_o is increased, η increases correspondingly. At point B, the reactions given by Equations (1) and (6) are complete. In other words, all the zirconium and chromium inventory, and 6.32 percent of the iron inventory have been oxidized to produce ZrO_2 and $FeO \cdot Cr_2O_3$. As P_o is further increased, there is no change in η (from B to C) because the next reaction, which is the oxidation of iron as given by Equation (7) cannot proceed since $P_{H_2O}/P_{H_2} < 0.5$. At point C the partial pressure ratio of steam to hydrogen is 0.5 and as P_o is increased further, the iron can begin to be oxidized to FeO. The conversion of the entire inventory of iron to FeO is complete at point D. As P_o is increased further (D to E) there is no change in η because the partial pressure ratio of steam to hydrogen is lower than that required (as indicated by Equations (8) and (9)) for the oxidation of FeO to Fe_3O_4 and Ni to NiO. Thus the maximum hydrogen production efficiency in the cavity region from D to E is 0.83.

10.1.1.4 Parametric Calculations to Study the Effect of Transient Melt Dispersal and Steam Blowdown Rates on the Hydrogen Production Efficiency

The equilibrium bounding calculations discussed in the last section assumed complete mixing of the entire steam inventory in the primary system and the entire melt inventory within the reactor cavity. Given infinite reaction rates, this might be a reasonable assumption if the debris dispersal time was equal to the steam blowdown time and the instantaneous melt entrainment rate in the reactor cavity was proportional to the instantaneous mass flow rate of steam flowing through the cavity. Such, however, is not expected to be the case because of two reasons. First, the melt dispersal rate is expected to be proportional to the dynamic pressure (and not the mass flow rate of steam), and secondly the equality of the steam blowdown time and the melt dispersal time can only happen for one particular value of P_o. The purpose of this section is to study the effect of these transient processes on the hydrogen production efficiency parametrically.

In order to perform these parametric calculations, we assume the following hypothetical idealized melt-steam mixing model in the reactor cavity. Let $\dot{m}_g$ be the instantaneous mass flow rate of steam leaving the pressure vessel. Then, a model for the melt entrainment rate is used to calculate the instantaneous mass flow rate $\dot{m}_d$ of the melt. This entrained mass of melt is assumed to

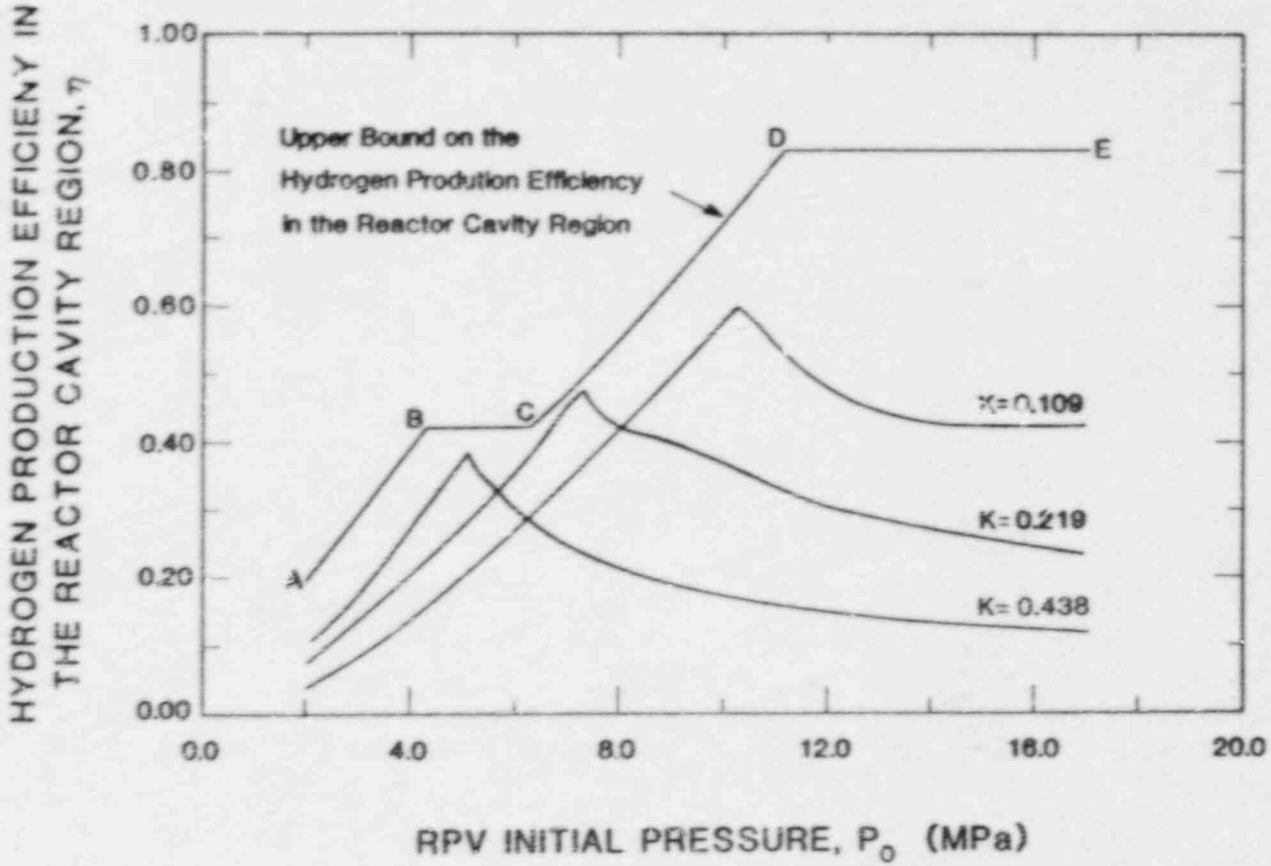

Figure 10.1 Effect of Debris Dispersal Rate and the Initial Vessel Pressure on the Hydrogen Production Efficiency for the Zion Reactor Cavity Region

flow with the steam without slip and mix with the flowing steam completely. In other words, the instantaneous hydrogen flow rate at the exit of the cavity is calculated to be given by the equilibrium value obtained from the mixing of $\dot{m}_d$ amount of core melt and m_g amount of steam. Integration of the instantaneous hydrogen flow rate for the entire duration of the steam blowdown process gives us the total amount of hydrogen produced in the cavity. It must be emphasized here that this highly idealized model is not intended to provide any estimate of the actual amount of hydrogen produced in the reactor cavity. That, as was mentioned in the Introduction, can only be provided by a much more sophisticated and detailed model. Our purpose here is only to illustrate the effect of the transient nature of melt dispersal and steam blowdown on the hydrogen production efficiency.

As indicated in Table 10.1, the gas phase in the primary system consists of a mixture of steam and hydrogen. Since hydrogen is much lighter than steam, we assume that the gas phase in the primary system is stratified. Thus the gas blowdown from the pressure vessel is modeled as the blowdown of pure steam followed by the blowdown of hydrogen. Let d be the diameter of hole in the lower head of the pressure vessel at the beginning of the steam blowdown. Then, assuming choked flow at the vessel hole, the instantaneous mass flow rate of steam, $\dot{m}_g$, leaving the vessel is given by

$$\dot{m}_g = \dot{m}_g^o \left\{1 + \frac{(\gamma - 1)}{2} \frac{\dot{m}_g^o}{M_o} At\right\}^{\frac{\gamma + 1}{1 - \gamma}} \tag{10}$$

$$\dot{m}_g^o = \frac{\pi d^2}{4} \gamma^{0.5} \left(\frac{2}{\gamma + 1}\right)^{\frac{\gamma + 1}{2(\gamma - 1)}} \frac{P_o}{\sqrt{RT_o}} \tag{11}$$

$$A = 1 - P^o_{H_2}/P_o \tag{12}$$

where t is the time (t=0 corresponds to the beginning of the gas blowdown), γ is the ratio of specific heats for the steam, M_o is the mass of steam in the primary system at t=0, R is the gas constant of steam, T_o is the temperature of steam in the pressure vessel at t=0 (assumed equal to the saturation temperature corresponding to P_o), P_o is the primary system pressure at t=0, and $P^o_{H_2}$ is the partial pressure of hydrogen in the primary system at t=0.

We assume that the instantaneous core melt debris flux, $\dot{m}_d$, leaving the cavity is given by

$$\dot{m}_d = K \rho_g u_g^2 \tag{13}$$

where ρ_g is the steam density, u_g is the steam velocity in the reactor cavity, and K is a parameter which will be varied to study the effect of debris dispersal rate. Assuming choked flow of steam at the vessel hole during the blowdown process, it can be shown that

$$\rho_g u_g^2 = \gamma \left(\frac{2}{\gamma + 1}\right)^{\frac{\gamma + 1}{\gamma - 1}} \left(\frac{A_t}{A_k}\right)^2 \left(\frac{T_\infty}{T_o}\right) \frac{P_o^2}{P_\infty} \left\{1 + \frac{\gamma - 1}{2} \frac{\dot{m}_g^o}{M_o} At\right\}^{\frac{2(\gamma + 1)}{1 - \gamma}} \tag{14}$$

where A_t is the cross-sectional area of the vessel hole ($=\pi d^2/4$), A_k is the cross-sectional area of the reactor cavity, T_∞ is the steam temperature in the reactor cavity (assumed to be equal to the melt temperature for the calculations presented here), and P_∞ is the pressure in the reactor cavity (assumed to be equal to the containment pressure).

Now we are in a position to calculate the instantaneous mass flow rate of hydrogen, $\dot{m}_h$, leaving the cavity. To do this, we assume the quasi-steady model shown in Figure 10.2. At any instant, $\dot{m}_g$ amount of steam (given by Equation (10)) and $\dot{m}_d$ amount of core melt (given by Equation (13)) are assumed to mix, react, reach equilibrium (according to Equations (1), and (6) through (9)) and exit the cavity. The instantaneous mass flow rate of hydrogen is then integrated for the entire blowdown process to yield the total amount of hydrogen produced. Equation (5) is then used to calculate the hydrogen production efficiency.

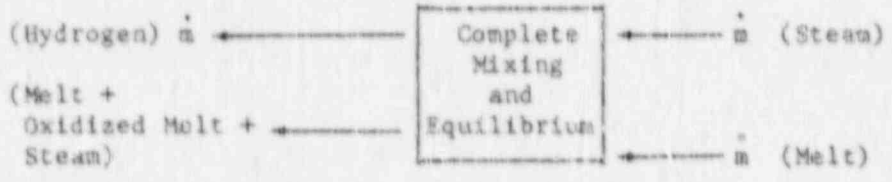

Figure 10.2 A Quasi-Steady Melt-Steam Mixing Model for Hydrogen Production Calculations in the Reactor Cavity

The results of these calculations for different values of the initial vessel pressure and the debris dispersal parameter K are shown in Figure 10.1. Let us first look at the curve corresponding to K = 0.438. When P_o is small, the amount of debris dispersed (and hence the amount of debris mixing and reacting with the steam), as well as the total amount of available steam, is small. Therefore, the hydrogen production efficiency η is small. As P_o is increased, both of these quantities increase, and hence η increases. However, the efficiency is lower than the upper bound calculation (curve ABCD%) for two reasons. First, as is evident from Equation (13), the debris flux leaving the cavity falls off (with time) much more rapidly than the steam flux, and therefore the exit conditions tend to be steam starved during the initial period of blowdown. Secondly, for small values of P_o, the fraction of debris dispersed, and hence allowed to react with steam, is less than unity. For example, for the case K = 0.438, P_o = 4 MPa, only 65.26% of the debris is dispersed from the cavity. The hydrogen production efficiency continues to increase as P_o is increased until P_o reaches a critical value P_o^*. Beyond this point (i.e., $P_o > P_o^*$) η decreases (or remains constant) with increasing P_o. The reason is as follows. Our calculations show that for the case which corresponds to the peak in the efficiency curve ($P_o = P_o^*$), two things happen. First, all of the melt is dispersed from the cavity and secondly, the supply of steam and melt is exhausted at the same instant. In other words, the time required to disperse the melt completely from the cavity (and hence react with steam) is equal to the time required to completely discharge the steam from the pressure vessel. Thus, when $P_o < P_o^*$ the fraction of melt dispersed from the cavity is less than unity. For $P_o \geq P_o^*$, the fraction of melt dispersed is unity. However, for $P_o > P_o^*$, the debris dispersal time is smaller than the steam blowdown time. Therefore, the melt does not get a chance to mix with all the steam in the cavity; as a result the hydrogen production efficiency goes down. In fact, the discrepancy between the steam blowdown time and the debris dispersal time increases rather rapidly as P_o is increased beyond P_o^*. For example, for the case corresponding to K = 0.219, we have:

P_o (MPa)	Steam Blowdown Time (s)	Debris Dispersal Time (s)
7.17 ($\approx P_o^*$)	17.84	17.84
8	17.98	7.04
11	18.59	2.46

To put the values of the debris dispersal parameter K into a physical perspective, Table 10.2 gives the values of P_o^* and the corresponding debris dispersal times for the three values of K that we have used for these calculations.

Table 10.2 Dependence of P_o^* and Debris Dispersal Times on the Parameter K

K	Values of P_o and debris dispersal times[1] at which η has a peak		
(s·m)	P_o^* (MPa)	τ (seconds)	$\tau_{0.9}$ (seconds)
0.109	10.2	18.41	10.19
0.219	7.17	17.84	9.65
0.438	5.0	17.57	9.50

[1] τ corresponds to the time at which all of the melt has been ejected from the cavity. This is also the steam discharge time from the primary system. $\tau_{0.9}$ is the time by which 90% of the melt is out of the cavity.

10.1.1.5 Concluding Remarks

We have performed two sets of calculations to evaluate the possible extent of hydrogen generation in the Zion reactor cavity during a high-pressure melt ejection accident scenario. The first set gives us an upper bound on the hydrogen production efficiency, and the second set of calculations shows the effect of the transient nature of melt dispersal and steam blowdown on the hydrogen generation in the reactor cavity.

The results show that although significant quantities of hydrogen can be produced in the cavity region, the melt exiting the cavity is likely to retain a significant fraction of the stored chemical energy. For example, if the primary system pressure at vessel failure equals 7 MPa, the bounding calculation shows that the hydrogen production efficiency in the cavity region equals 0.48. Although we do not know the true value of the debris dispersal parameter K, the results clearly indicate that the effect of variable debris dispersal rate is only to lower the hydrogen production efficiency. Thus it appears that both the cavity and the ex-cavity (intermediate subcompartments and upper dome) phenomena need to be studied in detail to evaluate the extent of direct containment heating. It is emphasized here, once again, that these bounding and parametric calculations have assumed that the melt-steam reaction times are smaller than the transit time through the cavity.

REFERENCES

BAKER, L., et al. (1982), "Hydrogen Evolution During LWR Core Damage Accidents," Proceedings of the Int. Meeting on Thermal Nuclear Reactor Safety, Aug. 29 - Sept. 2, Chicago, IL, NUREG/CP-CP0027, Vol. 2, pp. 1433-1442.

CONTAINMENT Loads Working Group (1985), "Estimates of Early Containment Loads from Core Melt Accidents," NUREG-1079, Chapter 2.

TUTU, N. K., et al. (1985), "Direct Heating of Containment Atmosphere by Core Debris," Sec. 3.2 in Safety Research Programs Sponsored by the Office of Nuclear Regulatory Research, Quarterly Progress Report, July 1 - September 30, 1985, compiled by Allen J. Weiss, NUREG/CR-2331, BNL-NUREG-51454, Vol. 5, No. 3.

WILLIAMS, D. C., et al. (1987), "Containment Loads Due to Direct Containment Heating and Associated Hydrogen Behavior," NUREG/CR-4896, SAND87-0633, R4.

GINSBERG, T AND TUTU, N. K. (1987), "DHCVIM - A Direct Heating Containment Vessel Interactions Module," AIChE Symposium Series, No. 257, Vol. 83, pp. 347-354.

11. Protective Action Decisionmaking

(W. T. Pratt and A. G. Tingle)

11.1 Background

NRC regulations require that, in the case of a major nuclear power plant accident, licensees recommend protective actions to reduce radiation dose to the public. When certain emergency action levels are exceeded, the licensee recommends protective actions to State and local officials. The nature of the protective actions recommended is determined by which emergency action levels are exceeded.

In practice drills, decisions on protective action recommendations have proven to be difficult. NUREG-0654 states that if containment failure is imminent, sheltering is recommended for areas that cannot be evacuated before the plume arrives, but evacuation is recommended for other areas. The assumption in NUREG-0654 is that there would be a greater dose savings if the population were sheltered during plume passage rather than evacuated, but this assumption has not been proven. Furthermore, the recommended protective actions must be based on estimated containment failure times, which are difficult to determine.

Alternatively, other NRC publications suggest that the appropriate response would be early evacuation of everyone within a distance of about 2 or 3 miles for all events that could lead to a major release even if containment failure is imminent or a release is underway. Those at greater distances should take shelter. Further, if a release occurs, the appropriate action would be for monitoring teams to find "hot spots" (radiation dose rate exceeding about 1 R/hr) and for people to evacuate these "hot spots."

11.2 Project Objectives

The objectives of the activities to be performed in this project are to:

(1) characterize the family of potential accident sequence for which emergency planning is necessary,

(2) establish strategies appropriate to these sequences, emphasizing credible failure modes,

(3) identify those factors which would influence the implementation of these strategies,

(4) determine how these factors should be incorporated into the decisionmaking process, and

(5) develop a guidance report on the protective actions to be recommended for combinations of these factors.

11.3 Technical Approach

The technical approach is based on an evaluation of the consequences of nuclear power plant accidents as they relate to protective action decision-making. The evaluation includes a careful review of previous work (e.g., NUREG/CR-2339, NUREG-0654, NUREG/CR-2025, NUREG-0396, and reports and memoranda by the NRC staff) and its applicability to protective action decision-making. The approach is also based on a consideration of a wide range of potential accident sequences and on up-to-date assessments of containment performance. Thus the technical basis reflects the new fission product source term information that was developed (BMI-2104) by the NRC/RES Accident Source Term Program Office (ASTPO). In addition, BNL staff participated in the activities of the SARP Containment Loads Working Group (NUREG-1079) and in the Containment Performance Working Group (NUREG-1037). The results of these various activities were described in NUREG-0956, which was published in draft form (for comment) during July 1985. This information is being integrated into our development of protective action strategies. In addition, the American Physical Society's review of the new source term methodology and the results of the review are being factored into our evaluation. Finally, the new source term methodology is being applied to five representative reactor designs, as part of an updating of nuclear accident risk and risk-reduction perspective by RES/DRAO. This effort will be repored in NUREG-1150 and it is being closely followed by BNL staff and the results are being integrated into our development of protective action strategies.

The evaluation will also be based in large part on results obtained from the MACCS (MELCOR Accident Consequence Code System) and CRAC2 (Consequence of Reactor Accident Code, version 2) computer codes. The output from these codes is being analyzed for a variety of release characterizations, weather sequences, and protective action strategies.

In accordance with the above, the following five facilities were selected to represent a range of reactor and containment designs:

Zion: PWR with a large dry containment
Surry: PWR with a subatmospheric containment
Sequoyah: PWR with an ice condenser containment
Peach Bottom: BWR with a Mark I containment
Grand Gulf: BWR with a Mark III containment

11.4 Project Status

Following review of the draft BNL report by the NRC, it was agreed that the effectiveness of protective actions would be presented as bar charts instead of numerical tabulations. It was also agreed that the evacuations be shown only for a 10 mph evacuation speed and for starting times at release and one hour after release. In addition, all calculations were rerun with version 1.3 of the MACCS code using new penetration (shielding) factors, a relocation time of four hours and an evacuation distance of ten miles.

After completion of the calculations, BNL was informed by Sandia Labs that version 1.3 contained several errors that made the results invalid. The calculations were redone using the corrected code version 1.4

Source terms used in the calculations were reviewed and in some cases improved by NRC and BNL staff. New consequence calculations were performed for the new source terms and appropriate revisions were made to the text of the BNL report.

BNL staff codified a constant weather atmospheric transport and acute health effects model to assess the accuracy of the MACCS code predictions. The model contains decay, wet and dry deposition, and multipuff capability. The solution procedure involves direct analytic integration of air concentration equations over time and position as opposed to the differential approach used in CRAC2 and MACCS. The code will also be used to rapidly carry out sensitivity and uncertainty analyses. A tentative outline for a report on this model was prepared.

Since the CDC 7600 machine was decommissioned at BNL, the CRAC2 code was made operational on the new IBM computer.

12. MELCOR Verification and Benchmarking

(M. Khatib-Rahbar and I.K. Madni)

12.1 Background (I.K. Madni)

The MELCOR code is being developed for the NRC by Sandia National Laboratories (SNL) to be used in probabilistic risk assessment (PRA) studies. It is intended to be fast running, user friendly and portable. In addition, the code models the entire plant thermal/hydraulic behavior and fission product release and transport. Therefore, MELCOR has the potential to be a unified source term/PRA code if its development incorporates up-to-date information from both technical areas. The objective of this project is to evaluate MELCOR's potential as a source term code and provide independent assessment of its modeling capabilities and limitations. In addition, the project will also benchmark MELCOR against more mechanistic codes and the Source Term Code Package.

12.2 MELCOR PWR Application (I.K. Madni, J. Maly)

An input deck was prepared for a MELCOR version 1.6 simulation of a severe accident in the Zion plant (a PWR with large dry containment). The plant model allows two-loop simulation of a multi-loop plant, with one of the loops containing the pressurizer. Each simulated loop includes both primary and secondary (steam) circuits, with common volumes at the reactor vessel and turbine-condenser. The plant is nodalized into twenty-six control volumes, with thirty-four flow paths and fifty-four heat structures. The reactor vessel has five control volumes (core, bypass, lower and upper plena, and annulus), five flow paths, and fourteen heat structures. The core is nodalized into thirty cells (five radial rings including bypass and six axial levels including lower core plate). The core barrel surrounding the core is partitioned axially into several heat structures with elevations to match those of the core cells.

Geometric, thermal-hydraulic, structural, and neutronic data were obtained from an extensive search of the FSAR and other sources, and supplemented by extensive hand calculations to achieve the desired input specifications for the various code packages. The initial Zion input deck, consisting of a few thousand executable lines of data, was completed and sent to SNL and BCL for review in July 1987.

Following completion, the input model went through a debugging phase. The intent was to test and debug the code with a steady (null) transient simulation at full power, before initiating accident calculations.

The first attempt at a null-transient run was, after a few corrections, successful through both passes of MELGEN, but aborted in MELCOR due to errors in COR and RN1 packages. The SNL staff were very helpful in resolving the apparent errors which existed in version 1.6. The run was initiated again, and was allowed to proceed through 65 timesteps. Rapid fluctuations were observed in pressure and velocity in the primary system that restricted the timestep size to its user-specified minimum value of one millisecond.

Following a careful analysis of the results, control volume pressures, flow areas and velocities were recalculated and form loss coefficients were also recalculated to give the desired pressure drop distribution. With these changes, oscillations were reduced to a bare minimum, and timestep sizes stayed at about 0.1 second. but, fuel was predicted to start melting in the hottest cell. In order to properly refine the primary system input data, an interim deck was created, where the secondary system was replaced by a constant heat loss in the steam generators equal to the energy generated in the core. The very high fuel temperatures in the hottest cell were traced to incorrect specification of radial power fractions in the core. Power fractions were recalculated, and transient results were dramatically improved. At thirty seconds into the null-transient, all primary system parameters were approaching a steady state. Pressures and flows were less than 3 percent off from input values and oscillations were minimal. Fuel temperature in the hottest cell was 1686K and rising very slowly. Timestep was, on average, 0.1 second.

Following installation of MELCOR version 1.7.0 on the VAX cluster, BNL staff began to convert the ZION input deck to the version 1.7.0 format.

12.3 MELCOR Verification (I.K. Madni, W. Bornstein)

In April 1987, the installation of MELCOR Version 1.6.0 on the BNL IBM-3090 was completed. In May the sample problem was successfully executed. Some discrepancies were noticed when the IBM results were compared to the results obtained from the SNL VAX-8650 and CRAY calculations obtained with version 1.6.0.

Version 1.7.0 of MELCOR was received from SNL in July. By August, it was installed on the BNL VAX cluster, and the sample problem was successfully run and the SNL VAX results were reproduced. Some additional updates to MELCOR 1.7.0, which increased the size of the real variable array and allowed the user to change the sizes of the main data base arrays, were received and implemented into the code during August. These updates were needed to enable the code to handle the PWR input model.

13. Uncertainty Analysis of the Source Terms (QUASAR)
(M. Khatib-Rahbar)

13.1 Probability Distributions of Input Parameters (E. Cazzoli)

Through an extended Latin Hypercube Sampling (LHS) sensitivity study of each code component of the Source Term Code Package (STCP) 43 input parameters were identified as important to the prediction of source terms. In the extended sensitivity study the code components of the STCP were grouped as: 1) MARCH (In-vessel)/CORSOR/TRAPMELT, 2) CORCON/VANESA, 3) SPARC, and 4) NAUA. The uncertainties associated with these 43 input variables were characterized using the guidance provided by expert reviewers together with methods based on information theory[1]. The proposed probability distribution functions (PDFs) were documented and sent back to the expert reviewers for further comments. Few comments were received. Table 13.1 presents a list of these 43 input variables together with then associated PDFs.

13.2 LHS STCP Calculations for a Peach Bottom TB Sequence (M. Lee, E. Schmidt, Y. Liu, E. Cazzoli)

The Source Term Code Package (STCP/MOD1.1) LHS calculations for a Peach Bottom TB sequence have been started. In all 43 variables are included and 100 STCP calculations will be made. To make the final data analyses easier, each individual code component of STCP has been modified to write data files containing the information needed for detailed analyses. The STCP has been fully automated externally by incorporating several interface programs. A job deck was set up on the IBM to execute STCP from MARCH to NAUA and save the data files for final analyses and now there is no manual intervention necessary. Since the NAUA code is a single compartment code and can only handle one compartment at a time, multiple NAUA calculations and iterations are necessary when modeling a BWR Mark I containment. In order to guarantee that the multiple NAUA calculations have reached a converged result, the job deck has the capability to check for convergence. The multiple NAUA calculations stop as the convergence criterion is satisfied. A processor was written to summarize the NAUA results from drywell, wetwell, and reactor building calculations onto a single data file for further analyses. The processor can also correct, based on mass conservation, the NAUA results to achieve a better overall mass balance for each fission product group.

In order to debug the job deck, besides the base case (case B), 3 test runs of the STCP were made. The input values of the 43 variables for the 3 test runs correspond to the 5th percentile (case L), 95th percentile (case U), and median (case M) levels associated with the PDF's specified for the QUASAR calculations.

13.3 Modification to the Codes (M. Lee, Y. Liu)

The final 43 variables included in the LHS calculations consist of several embedded constants which have fixed values in the original version of STCP and cannot be changed through user input. In order to vary these constants in the LHS calculations, the corresponding codes were modified to incorporate these constants as new input variables. The modifications made for this purpose are not discussed here.

A. MARCH3

The MARCH3 code was modified to be capable of modeling a "leak" before "break" of the containment. The threshold pressure for each containment failure mode is an input variable in the LHS calculation. For the case that containment leakage occurs prior to a massive rupture, the leak area is a linear function of containment pressure. The proportionality constant between leak area and containment pressure is also considered for variation during the QUASAR calculations.

B. TRAPMELT3

Unusually large aerosol injection rates for some of the QUASAR cases combined with the new nucleation model have resulted in initial conditions for the aerosol agglomeration equations that are significantly differenc from the equilibrium solution. The equations have become very stiff under these conditions. TRAPMELT computation times became unacceptable using the Runge Kutta integration VERK from the ISML library. The use of a GEAR integrator was found to reduce the computation times by an order of magnitude demonstrating that the stiffness was mostly due to extraneous transients. TRAPMELT has been modified to use the GEAR integrator for the core volume. The GEAR integrator is also an ISML program.

C. VANESA

In the STCP/MOD1 version of the VANESA code. the mass generation rate of gas calculated by CORCON is converted to a volumetric gas flow rate using the ideal gas law. In the calculations, VANESA assumes that the ambient pressure is always at 1 atmosphere. This assumption is only valid for cases with early containment failure. For cases with late containment failure, MCCI can occur under pressurized condition. Based on the experience gained during the STCP analysis of a BWR with Mark II containment, the containment pressure was found to have a large impact on the prediction of ex-vessel releases. The impact on the ex-vessel release can change the prediction of environmental release of fission products. The version of VANESA code used in the LHS calculation was modified to include the capability to consider the containment pressure when calculating the volumetric gas flow rate.

D. NAUA

Multiple NAUA calculations/iterations are required for a Peach Bottom TB sequence. The calculational scheme is summarized in Table 13.2. The steps 3 through 5 in Table 2 are repeated until a predetermined convergence criterion is satisfied. The NAUA code has been modified to accept a file containing decontamination factors associated with each of the two leak tapes into the compartment. To adopt the calculational scheme shown in Table 13.2, this modification is necessary.

13.4 Interface Programs (M. Lee, Y. Liu)

A. TITLE

Based on user's specification, the program TITLE picks a vector out of the 100 vectors on the LHS data file and then moves the elements of the vector to the corresponding input files of the STCP code component.

B. PRETHC

The program PRETHC processes a data file (Tape 60) written by MARCH3 to generate input data for THCCA, the interface program between MARCH3, NAUA, and SPARC. Three files are generated by PRETHC for different THCCA runs, one for SPARC in-vessel, one for SPARC ex-vessel, and one for NAUA. Tape 60 of the MARCH3 code contains the time step number and time for major events, e.g., core uncovery, start of melt, core slump, core collapse, bottom head failure, containment break, and hydrogen burn (start and end).

C. CONV

For a Peach Bottom TB sequence, multiple NAUA calculations and iterations are necessary. Steps 3 through 5 in Table 13.2 are repeated until the convergence is achieved. The program CONV checks the convergence of the multiple NAUA calculations. The converge criterion is satisfied when the difference between the transport fraction for each compartment between two successive iteration cycles is less than 1%. The transport fraction from drywell to reactor building $T_{DR}(t)_i$ is defined as:

$$T_{DR}(t)_i = \frac{M_{DR}(t)_i}{M_{WD}(t)_i + M_{RD}(t)_i + S_2(t)_i} \qquad (13.1)$$

where:

$M_{DR}(t)_i$ is the accumulated mass leaked from drywell to reactor building for species i

$M_{WD}(t)_i$ is the accumulated mass leaked from wetwell to drywell for species i

$M_{RD}(t)_i$ is the accumulated mass leaked from reactor building to drywell for species i, and

$S_2(t)_i$ is the accumulated ex-vessel release from MCCI for species i.

The transport fraction of other containment flow paths can be defined in a similar manner. The transport fractions checked by CONV are those from wetwell to drywell, drywell to reactor building, and reactor building to environment.

The data needed to calculate transport fractions are saved on tape 8 of NAUA.

D. NAUTRAS

The program NAUTRAS summarizes the data on NAUA tape 8 from drywell, wetwell and reactor building calculations on a print output file and a data file for further data analyses. To improve the overall mass balance of the multiple NAUA calculations, the program NAUTRAS also interfaces the NAUA calculations based on the following mass conservation equation for each containment flow path:

$$M_{WD}(t)_i = T_{WD}(t)_i \left(\frac{S_1(t)_1}{DF_1(t)_i} + \frac{M_{DW}(t)_i}{DF_2(t)_i}\right) \qquad (13.2)$$

$$M_{DW}(t)_i = T_{DW}(t)_i (S_2(t)_i + M_{WD}(t)_i + M_{RD}(t)_i) \qquad (13.3)$$

$$M_{DR}(t)_i = T_{DR}(t)_i (S_2(t)_i + M_{WD}(t)_i + M_{RD}(t)_i) \qquad (13.4)$$

$$M_{RE}(t)_i = T_{RE}(t)_i \, M_{DR}(t)_i \qquad (13.5)$$

$$M_{RD}(t)_i = T_{RD}(t)_i \, M_{DR}(t)_i \qquad (13.6)$$

where:

$S_1(t)_i$ is the accumulative in-vessel release up to time t for species i,

$S_2(t)_i$ is the accumulative ex-vessel up to time t for species i,

$DF_1(t)_i$ is the accumulative decontamination factor during in-vessel phase up to time t for species i,

$DF_2(t)_i$ is the accumulative decontamination factor during ex-vessel phase up to time t for species i,

$T_{XY}(t)_i$ is the transport fraction from compartment X to compartment Y for species i

$M_{XY}(t)_i$ is the accumulative mass leaked from compartment X to compartment Y up to time t for species i

and D: drywell
W: wetwell
R: reactor building
E: environment.

In the above equations, $S_1(t)_i$ and $S_2(t)_i$ are determined by TRAPMELT3 and VANESA code, respectively. $DF_1(t)_i$, $DF_2(t)_i$ are calculated by SPARC and $T_{XY}(t)_i$) are determined by NAUA calculations. Therefore, the above five equations can be solved for the five unknowns, $M_{XY}(t)_i$. Through this calculation, the overall mass balance of each fission product species is guaranteed. The data needed to formulate the above equations are saved on tape 8 of each NAUA run.

13.5 Results of the Test Runs (M. Lee)

The input values of the 43 variables varied in the LHS calculation for the test runs are given in Table 3. In the test runs, the containment failure threshold pressures were not varied. It is assumed that the containment fails at 132 psia with an opening of 7 ft^2.

Table 4 summarizes the accumulated environmental release predicted in the test runs. In the test runs, the fission products retains in the drywell, wetwell, suppression pool, reactor building is also saved. The time dependent results are also available for data analysis.

The results of the test runs are reasonable and the trends can be explained qualitatively by the input data. It seems that the variation of the predicted environmental release is dominated by the activity coefficient of VANESA code and the multiplier of the CORSOR release coefficient.

13.6 Modeling of Fission Product Revaporization Following RPV Failure (J.W. Yang)

The revaporization of the volatile fission products in the reactor coolant system after reactor vessel failure is not modeled in the current version of STCP. In order to estimate the effects of revaporization on source term to the containment, a computer subroutine REVAP is being developed. The subroutine uses the basic models of TRAPMELT, namely, the ADHOC subroutine to compute the vaporization and condensation of volatile fission products (CsI, CsOH and Te), and the FISPQ subroutine to compute the Beta and Gamma heating of structures and gases. Using the TRAPMELT computed results prior to vessel failure as the initial conditions, REVAP determines the revaporization of the volatile fission products and the density and pressure of the RCS. The density and pressure are compared with that in the cavity compartment provided by the MARCH code. The comparison determines whether a density-driven flow or pressure-driven flow would occur between the RCS and cavity compartment. The release of the volatile fission products is accompanied with an outward flow in the reactor coolant system. Testing of the model is currently in progress.

References

1. S.D. Unwin et al., "The Formulation of Probability Distributions for the QUASAR Program", BNL Technical Report A-3286, September 1987.

Publications:

1) R.E. Davis, et al., "QUASAR Screening Sensivity Analysis: Application to the CORCON and VANESA Codes", BNL Technical Report, A-3286 June, 1987.

2) H.P. Nourbakhsh, "QUASAR Screening Sensitivity Analysis: Application to the Suppression Pool Aerosol Removal Code (SPARC)", BNL Tehchnical Report, A-3286, July, 1987.

3) S.D. Unwin, "The formulation of Probability Distributions for the QUASAR Program", BNL Technical Report, A-3286, September, 1987.

4) H.P. Nourbakhsh, et al., "In-Vessel Flow Characterization Under Severe Accident Condition", Trans. Am. Nucl. Soc., 55, 1987.

5) M. Lee, et al., "Impact of Coking Reactions on the Ex-vessel Source Term Predictions of CORCON/VANESA, "National Heat Transfer Conference, Pittsburgh, PA., August 1987.

6) M. Lee, et al., "Sensitivity of In-vessel Hydrogen Generation and Fission Product Release to Parameter Variation in a Melt Progression Model", Trans. Am. Nucl. Soc., 54, 1987.

Table 13.1 Most Sensitive Input Parameters for STCP Together With Their Respective Ranges and Probability Density Functions (Uncertainty Distributions)

Code	Parameter	Definition	Range (Percentile)				Coordinate Basis
			Min.	5th	95th	Max.	
MARCH	DPART (m)	Debris particle size (in-vessel)	10^{-3}	10^{-3}	0.2	0.2	Log-Uniform
	FHEAD	Fraction of bottom head CCI	0	0.01	1.0	1.0	Uniform
	FDROP	Core slump criterion	0	0.01	0.75	0.75	Uniform
	$\Delta H_f^{(1)}$ (MJ/m^3)	Volumetric latent heat of fuel	410	410	2420	2420	Uniform
	RHOCU (MJ/m^3°k)	Volumetric heat capacity of fuel	2.96	2.96	4.44	4.44	Uniform
	TMELT (°K)	Fuel melting temperature	2120	2200	2980	3110	Uniform
	WGRID (kg)	Mass of grid plate	3.4×10^4	3.4×10^4	4.8×10^4	3.4×10^4	Uniform
	P_1(Pa)	Containment leakage pressure threshold	1.0×10^5	4.1×10^5	1.4x10	1.5×10^6	Uniform
	P_r(Pa)	Containment rupture pressure threshold	4.9×10^5	8.9×10^5	1.6x10	2.5×10^6	Uniform
	$C^{(2)}$(um^2/Pa)	Proportionality constant between Drywell leakage area and drywell pressure	4.7×10^{-2}	4.7×10^{-2}	6.1×10^{-2}	6.1×10^{-2}	Uniform
CORSOR-M	Cs, I, Te[3]	Multiplier for the pre-exponential factor	10^{-3}	10^{-2}	2	10	Log-Uniform
	Ba, Sr[3]	" " " "	10^{-3}	10^{-2}	10	10^2	Log-Uniform
	Ru, Rh, Pd[3]	" " " "	10^{-1}	1	10^2	10^3	Log-Uniform
	Mn, Cr[3]	" " " "	10^{-3}	10^{-2}	10	10^2	Log-Uniform
TRAPMELT	GAMMA	Collision shape factor	1.0	1.2	10	15	Uniform
	VTE (mm/sec)	Te deposition velocity	0	0.1	90	100	Uniform
	PDEN (kg/m^3)	Aerosol Density	1000	1000	8000	8000	Uniform
SPARC	DIAM (mm)	Mean bubble diameter	3	4	12	20	Uniform
	RATIO	Bubble aspect ratio	1	1.25	1.5	4	Uniform
	VSWARM (m/sec)	Bubble swarm rise velocity	0.2	0.25	1.0	1.2	Uniform
CORCON	RW (m)	Corium spread (radius of corium pool)	3	3	6.5	6.5	Uniform
	TDC (°k)	Concrete decomposition temperature	1200	1690	1875	1950	Uniform
	EVAP	Weight % of concrete evaporable water	2.3	3.9	7.8	8.0	Uniform
	EM	Metal phase emissivity	0.2	0.5	1.0	1.0	Uniform
	ES	Emissivity of Surroundings	0.1	0.1	1.0	1.0	Uniform
VANESA	SIGMA	Aerosol size distribution parameter	1.5	1.5	3.2	3.2	Uniform
	NC	Number concentration of condensed aerosol	10^7	10^7	10^9	10^9	Log-Uniform
	Mo, Te, CsI	Activity coefficient	10^{-4}	10^{-3}	1	10	Log-Uniform
	BaO_2, SrO[2]	" "	10^{-4}	10^{-3}	1	10	Log-Uniform
	La_2O_3, CeO_2[2]	" "	10^{-4}	10^{-3}	1	10	Log-Uniform
NAUA	GAMMA	Collision shape factor	1.0	1.0	10	10	Uniform
	CHI	Dynamic shape factor	1.0	1.0	5.0	10	Uniform

(1) With a correlation coefficient of 0.9 with TMELT
(2) $A=C(P-P_1)$
(3) With a correlation coefficient of 0.9

Table 13.2 Calculational Scheme of NAUA and SPARC

		Aerosol Information	D.F. of Suppression Pool
	SPARC (In-vessel)	TRAPMELT3	--
Step 1	NAUA, wetwell (in-vessel release)	TRAPMELT3	In-vessel
Step 2	NAUA, drywell	NAUA (step 1)	None
		VANESA	None
Step 3	NAUA, reactor building	NAUA (step 2)	None
Step 4	NAUA, drywell	NAUA (step 1)	None
		NAUA (step 3)	None
	SPARC (Ex-vessel)	NAUA (step 4)	--
Step 5	NAUA, wetwell	TRAPMELT3	In-vessel
		NAUA (step 4)	Ex-vessel

Table 13.3 Input of Test Runs

Variables	Case B	Case L	Case M	Case U
DPART (ft)	1.042×10^{-2}	3.3×10^{-3}	4.7×10^{-2}	0.66
FHEAD	0.0	0.1	0.55	1.0
FDROP	0.02	0.01	0.39	0.75
ΔH_f (BTU/ft^3)	6.08×10^4	1.1×10^4	3.8×10^4	6.5×10^4
RHOCU (BTU/ft^3,°F)	60.81	44.12	55.15	66.18
TMELT (°F)	4130.0	3500.0	4204.4	4900.0
WGRIDX (lb)	1.06×10^5	7.5×10^4	9.05×10^4	1.06×10^5
Cs	1.0	1.0×10^{-2}	0.139	2.0
I	1.0	1.0×10^{-2}	0.139	2.0
Te	1.0	1.0×10^{-2}	0.139	2.0
Ba	1.0	1.0×10^{-2}	0.316	10.0
Sr	1.0	1.0×10^{-2}	0.316	10.0
Ru	1.0	1.0	10.0	100.0
Rh	1.0	1.0	10.0	100.0
Pd	1.0	1.0	10.0	100.0
Mn	1.0	1.0×10^{-2}	0.316	10.0
Cr	1.0	1.0×10^{-2}	0.316	10.0
GAMMA	1.0	1.2	5.72	10.0
Vte	1.0	0.01	4.53	9.0
RHO	3.0	1.0	4.5	8.0
DIAM	0.75	4.0	8.18	12.0
RATIO	3.0	1.25	1.43	1.5
VSWARM (cm/sec)	116.0	25.0	62.9	100.0
RAD (m)	5.0	5.0	5.7	6.5
TDC (°k)	1751.7	1690.0	1772.0	1875.0
EVAP	1.0	1.0	1.5	2.0
EMM	0.5	0.5	0.743	1.0
ESUR	0.9	0.1	0.55	1.0
FRAC	1.0	0.	0.5	1.0
AMD	1.0	10^{-3}	0.0316	1.0
ABaO	1.0	10^{-3}	0.0316	1.0
ASrO	1.0	10^{-3}	0.0316	1.0
ALa_2O_3	1.0	10^{-3}	0.0316	1.0
$ACeO_2$	1.0	10^{-3}	0.0316	1.0
ACsI	1.0	10^{-3}	0.0316	1.0
ATe	1.0	10^{-3}	0.0316	1.0
NC	10^8	10^7	10^8	10^9
σ	2.0	1.5	2.35	3.2
Y	1.0	1.0	5.5	10.0
X	1.0	1.0	3.13	5.0
TUNTL	--	--	--	--
TUNTB (psi)	131.7	131.7	131.7	131.7
AUBRK	--	--	--	--

Table 13.4 Environmental Release

Species	Release (kg)			
	Case B	Case L	Case M	Case U
CsI	0.23	0.38	4.23	1.97×10^{-2}
CsOH	1.42	129.6	42.9	0.14
Te	6.85	1.29×10^{-2}	0.30	0.93
Sr	15.0	1.57×10^{-2}	0.72	17.0
Ru	5.17×10^{-4}	1.38×10^{-5}	1.87×10^{-5}	8.95×10^{-4}
Ce	8.16	1.14×10^{-2}	2.88	7.32
Ba	17.9	1.74×10^{-2}	0.82	5.08
NG	388.5	391.1	399.6	386.7

14. Source Term Code Package Verification & Benchmarking
(M. Khatib-Rahbar)

14.1 STCP Simulation of PBF Severe Fuel Damage Scoping and 1-1 Tests
(J.W. Yang)

The STCP simulation of PBF SFD scoping and 1-1 tests were performed and comparisons with the test data and SCDAP (Version 18) code results were made. The scoping test was the first large scale severe fuel damage experiment and is the only test to simulate rapid steam/water cooling of degraded core materials. The 1-1 test was designed to simulate the heating and resulting fuel damage in the upper half of a 3000-MW(t) PWR core approximately 2 to 3 hours after initiation of a small break accident.

The STCP simulation involved detailed studies of: (a) the overall thermal response of the core and associated structures, (b) the rate of hydrogen generation from the interaction of coolant with cladding and structures, (c) the release of fission products, and (d) the coolability of the damaged fuel under reflood. Some boundary and initial conditions, such as the inlet flow rate, fuel axial power distribution and shroud heat loss caused uncertainties in the MARCH3 simulation. However, the overall predictions of the STCP code are considered satisfactory. The following conclusions were made based on this study:

1) The local fuel temperature distribution exhibits some discrepancy with the test data, but the overall core average temperature response is comparable to the test results as shown in Figures 14.1 and 14.2.

2) The local oxidation and transient hydrogen generation rate exhibit some discrepancy with the test data, but the integral hydrogen production agree reasonably well with the test results as shown in Figures 14.3 & 14.4.

3) The MARCH code cannot predict the complexity of fuel liquefaction, ZrO_2 dissolution, material relocation and formation of local blockage. The rapid occurrence of these processes observed in the tests introduced a large uncertainty related to hydrogen generation and fission product release during the final stage of transient. The MARCH core meltdown and slumping models, which for the most part are non-mechanistic, cannot be tested using the SFD ST and 1-1 experiments.

4) The tests indicated no reduction or termination of hydrogen generation upon material relocation. Hence the model assumption of a Zr/steam cut-off temperature in the MARCH code cannot be justified based on these test results.

5) The lack of corrections on fuel axial power distribution during the transient caused a large uncertainty in the MARCH result. The effect could be important for the analysis of ATWS events.

6) The fraction of gap release built into the CORSOR model and the release rate coefficient of the empirical correlations are not suitable for the trace-irradiated fuel rods employed in the SFD scoping and 1-1 tests. The MARCH-CORSOR-M codes overpredicted fission product release when compared with the test data as indicated in Figure 14.5 for nobel gases.

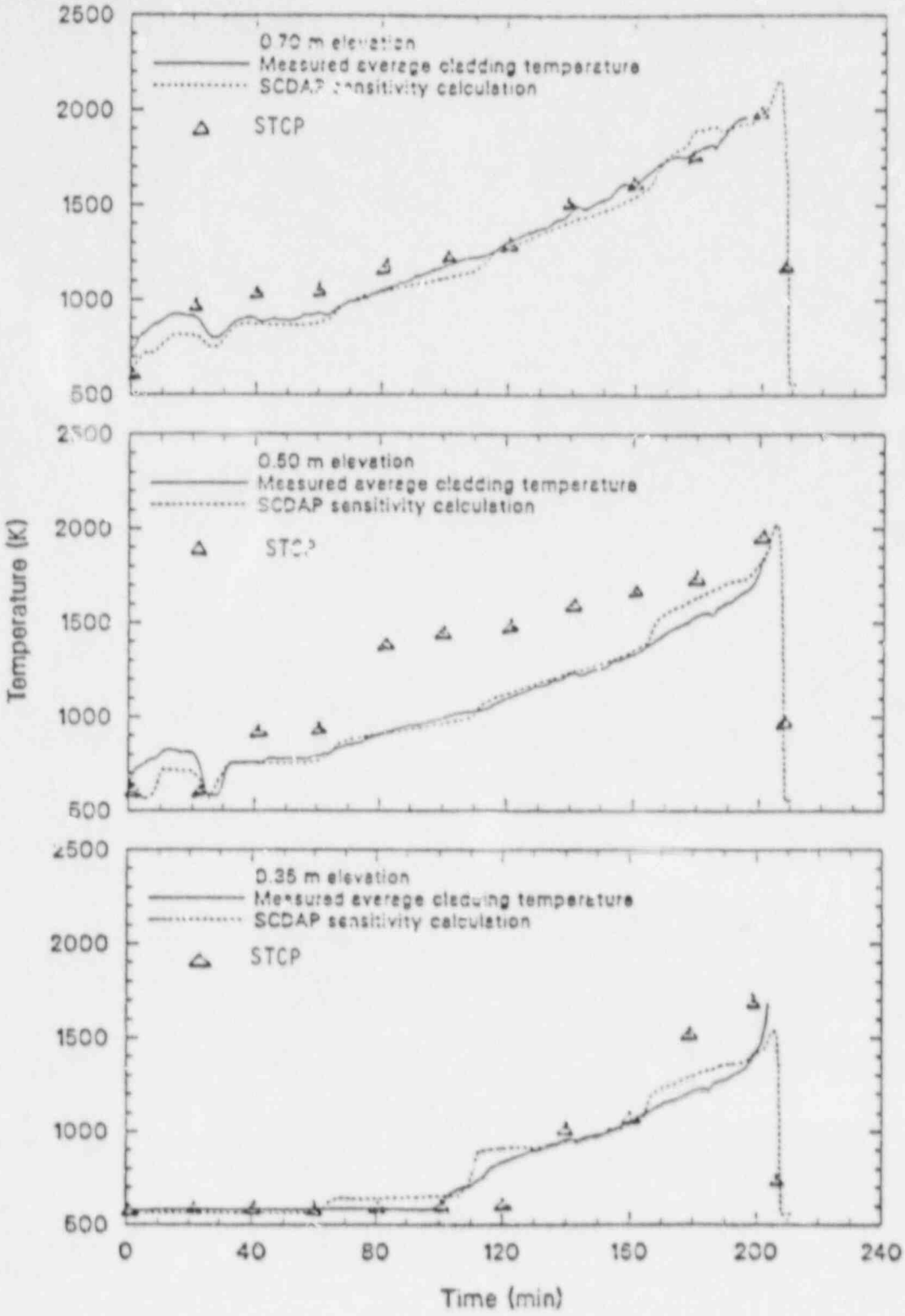

Figure 14.1 Comparison of the measured and calculated fuel temperatures of SFD-ST.

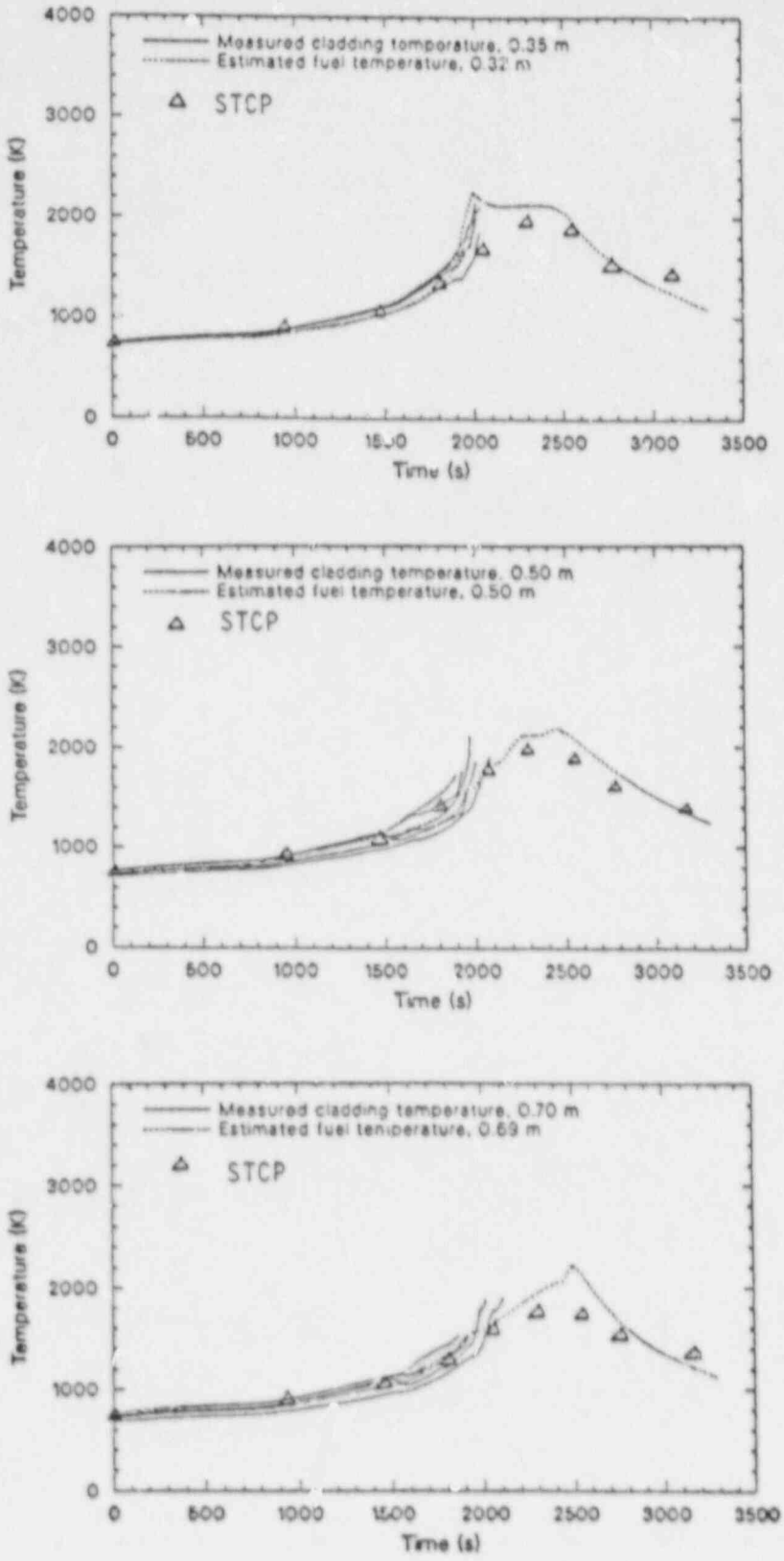

Figure 14.2 Comparison of estimated fuel temperature histories of test SFD 1-1.

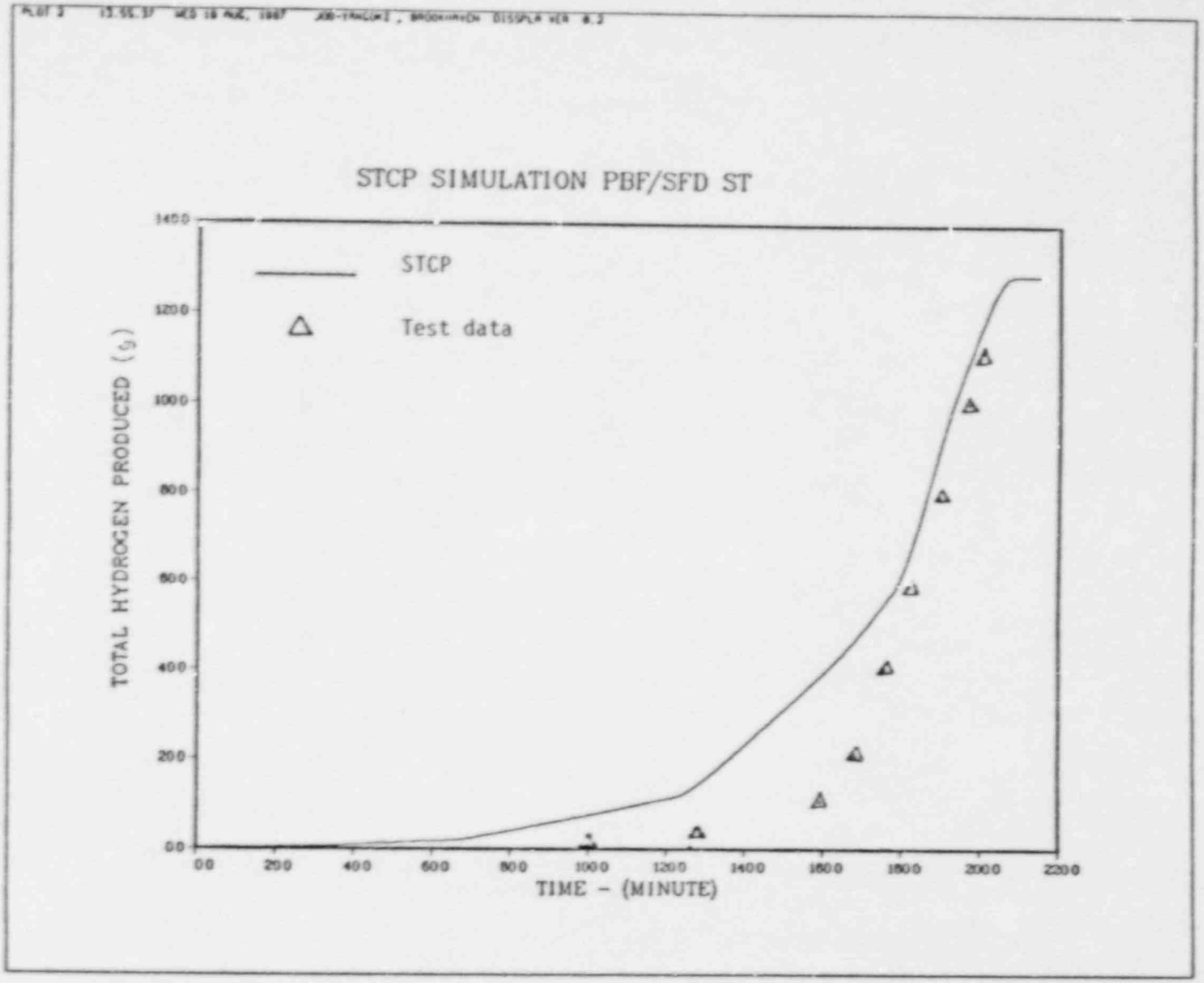

Figure 14.3 Comparison of the measured and calculated total hydrogen production of SFD-ST.

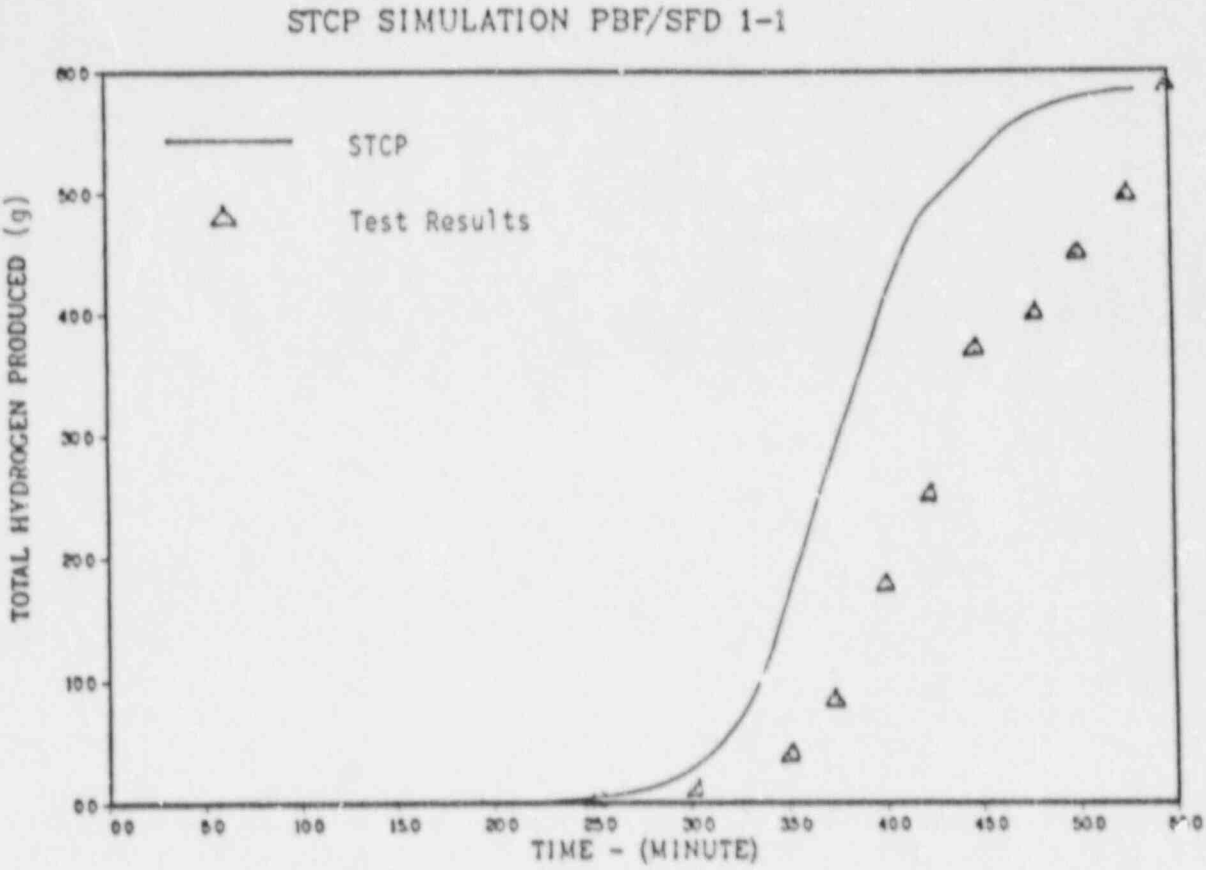

Figure 14.4 Comparison of the measured and calculated total hydrogen production of test SFD 1-1.

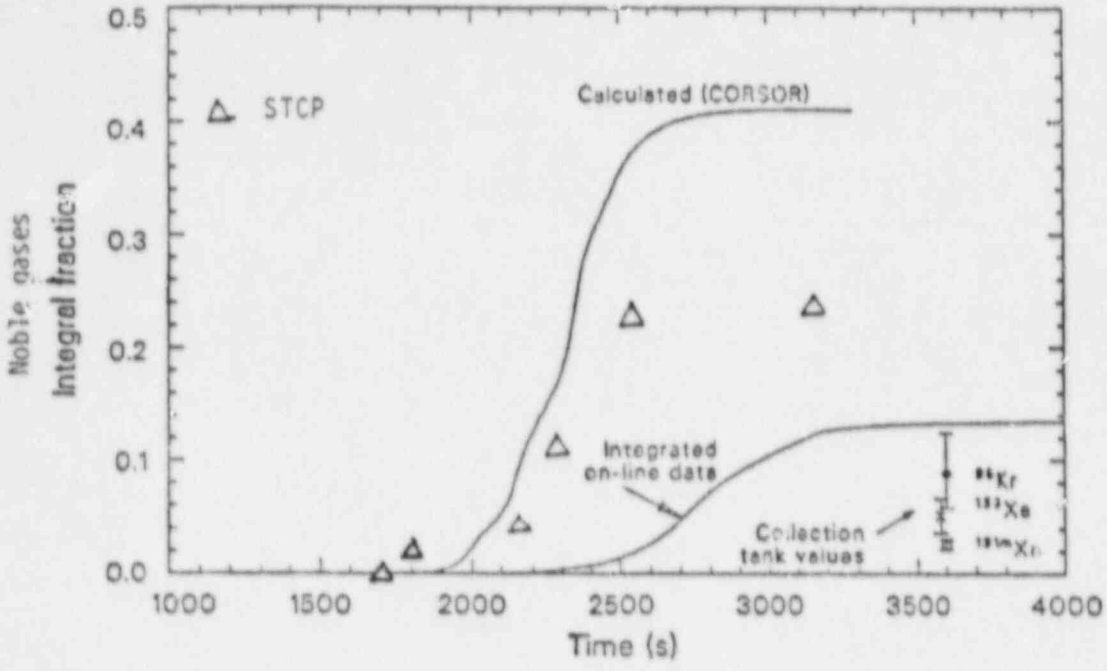

	MARCH/CORSOR-M	Test
N.G.	0.24	0.06
Cs	0.25	0.094
I	0.22	0.12
Te	0.047	0.009

Figure 14.5 Comparison of the measured and calculated noble gas integral release of test SFu 1-1.

15. Risk and Risk Reduction for Zion

(W. T. Pratt)

15.1 Introduction (W. T. Pratt, S. D. Unwin)

A draft report of the BNL Zion risk rebaselining analysis was published in February 1987 (NUREG/CR-4551, Vol. 5). As part of the NUREG-1150 effort, this analysis comprised input to the draft USNRC Reactor Risk Reference Document.

The preliminary Zion analysis differed in various respects from the remaining NUREG-1150 reference plant studies. In particular, the systems analysis was confined to consideration of the frequency-dominant sequences identified in the Sandia review (NUREG/CR-3300, Vol. 1) of the Zion Probabilistic Safety Study. Further, the containment and source term analyses were based upon adaptation of the NUREG-1150 analysis of Surry, performed at SNL. These methodological limitations have served to restrict interpretation of the results generated by the BNL study. In the ongoing analysis of Zion, certain of these limitations are being addressed through refinement of the models utilized and through the generation of Zion-related phenomenological data. The result of this effort will be greater parity between the BNL Zion study and the remaining NUREG-1150 reference plant analyses.

15.2 Information Dissemination (S. D. Unwin)

A primary objective of the draft Zion analysis publication is that of eliciting comments from industry, the public, and the nuclear safety community regarding the methodology, the models, and the results of the preliminary analysis. Such comments will provide a basis for modification of the study. Publication of the document has been complemented by a series of BNL presentations intended to clarify the content of the report with respect to various methodological and technical areas. Amongst such presentations were those to the Kouts' Review Committee, the Kastenberg Review Committee, and to the Commonwealth Edison Company of Chicago. Additionally, BNL participated in a briefing of the Tennessee Valley Authority regarding NUREG-1150 methodology.

15.3 Work Performed During Period (S. D. Unwin)

BNL has participated in a series of NUREG-1150 technical meetings addressing possible improvements in analysis methodology. The NUREG-1150 project management meetings were also attended by BNL representatives.

Modification of the Zion analysis has been ongoing throughout the current period. The following tasks have received particular priority:

- Reclassification of the Zion accident sequences into modified damage state categories.
- Restructuring and requantification of the Zion containment event tree.

- Preparation for Zion-specific containment loading calculations with use of the CONTAIN code.

- Preparation of Zion uncertainty issue papers for presentation to the NUREG-1150 expert review groups.

16. Thermodynamic Core-Concrete Interactions Experiments and Analysis

16.1 Interfacial Heat and Mass Transfer Processes (G. A. Greene and T. F. Irvine, Jr.)

The purpose of this task is to study the mechanisms of bubble induced heat and mass transfer at a liquid-liquid interface and their effects upon the ex-vessel attack of molten core debris on concrete. This effort is in support of the CORCON and VANESA development program at Sandia National Laboratories.

16.1.1 Heat Transfer Between Stratified Immiscible Liquid Layers Driven by Gas Bubbling Across the Interface

The analysis of fission product release and the quantification of public risk due to severe core damage accidents in light water reactors require detailed analyses of the thermal interactions of molten core debris with structural concrete, as well as analyses of mechanical and vaporization sources of aerosols. These interactions comprise what is referred to as the ex-vessel source term. An integrated computer code package has been developed with which to make these calculations: this is called the Source Term Code Package (Gieseke 1986). The specific computer models which calculate the ex-vessel source term are the CORCON code (Cole et al., 1984) for the analysis of molten core-concrete interactions and the VANESA code (Powers et al., 1986) for the analysis of mechanical and vaporization aerosol formation and decontamination.

The CORCON code treats the core debris as molten and segregated into overlying immiscible layers of core oxides, core metals, and melted concrete slag in a vertical, cylindrical geometry. When the core oxide layer becomes diluted by concrete decomposition products to the extent that it becomes less dense than the metallic layer, these two layers physically invert and the two oxide layers combine into one layer. These layers are continuously sparged by concrete decomposition gases from below which keep the individual layers well mixed and isothermal. It is this gas flux which drives the heat and mass transfer processes between the overlying layers. Separate analyses and experimental evidence have revealed that under a wide range of conditions, bubble-induced entrainment may dominate the interlayer transport processes (Greene et al., 1982a, Greene et al., 1988). However, under conditions in which the rising bubbles are unable to support entrainment, transport processes between layers are controlled by bubble agitation at the liquid-liquid interface. This is currently the strategy of layer modeling in CORCON and VANESA. In the stratified state, fission products and their decay heat would be concentrated in the oxide layer while chemically reactive metals, principally zirconium, and their heats of reaction would be concentrated in the metallic layer. Interfacial heat transfer between layers will determine not only the temperature of each layer, but also the upward-to-downward heat transfer split. This in turn controls the downward concrete erosion vs. upward radiative or boiling heat flux.

The earliest interlayer heat transfer model that was developed for CORCON was a version of the Kondratov model (1966) for heat transfer to a surface with bubble agitation, modified by Blottner (1979) to include two effects: (1) a lower asymptotic limit for natural convection in the absence of

bubbling and, (2) an arbitrary increase in the coefficient of the void fraction term from 0.4 to 50.0 to shift the model into better agreement with some limited experimental data. Blottner's interfacial relationship, applicable for either fluid, is as follows,

$$h_i = k(Pr\ g/\nu^2)^{1/3}(.002748\Delta T + 50\varepsilon^2)^{1/3} . \qquad (1)$$

This relationship can be non-dimensionalized as follows,

$$Nu = (0.00274\ Gr_1 + 50.\ Gr_2)^{1/3}\ Pr^{1/3} \qquad (2)$$

where Gr_1 is the Grashof number based upon the thermal buoyancy and Gr_2 is the Grashof number based upon void fraction-induced buoyancy. Gr_2 is not unlike that derived by Greene, et al. (1980) except that the void fraction dependence is arbitrarily quadratic instead of linear. In nearly all cases, the term involving Gr_1 is much less than the term involving Gr_2, and it may be neglected.

Another model for heat transfer across liquid-liquid interfaces agitated by bubbles was developed by Szekely (1963) based upon surface renewal principles. Assuming periodic destruction of temperature gradients at the liquid-liquid interfaces by the arrival of bubbles, he developed the following relationship for the heat transfer coefficient for either fluid,

$$h_i = 1.69\left(\frac{\rho c k j_g}{r_b}\right)^{1/2} . \qquad (3)$$

This relationship can be non-dimensionalized as follows,

$$Nu = 1.69\ Re^{1/2}\ Pr^{1/2} \qquad (4)$$

where Re is the Reynolds number based on the superficial gas velocity and the volume equivalent bubble radius.

Both of these models were subsequently compared to early experimental data of Werle (1982) and Greene (1982a, 1982b) and found to underpredict not only the magnitude, but also the trend of the heat transfer coefficient with increasing superficial gas velocity (Greene et al., 1982a). As a result of this comparison, the experimental investigation to be described was initiated.

16.1.2 Experimental Apparatus and Procedure

An experimental apparatus with which to investigate heat transfer between immiscible liquid layers with gas agitation was constructed. The apparatus was a Pyrex glass cylinder, 10 cm in diameter and 1 meter deep. The apparatus was insulated to minimize radial heat losses by a two-inch thick cylindrical blanket of Fibrefrax insulation. A porous stainless steel frit was mounted in the base to provide a spatially uniform gas flux from below. Internal heating of the lower fluid layer (mercury) was accomplished by a cartridge heating assembly which penetrated the side of the cylindrical test vessel into the fluid chamber. Power was measured by a precision watt meter. The flow through the porous frit was measured by a bank of air rotameters. Bubble size was characterized photographically as a function of the pressure and flow rate. Over the range of pressure and flow rate covered by these experiments, the volume equivalent bubble radius was correlated to the superficial gas velocity as,

$$r_b \text{ (cm)} = 0.233 + 0.109\ j_g \text{ (cm/s)}. \qquad (5)$$

A vertical traversable thermocouple assembly was installed along the centerline axis of the pool for determination of the temperature distribution in each layer and the temperature difference across layers. Ten thermocouples were aligned at a nominal separation of one inch. Fluid pairs chosen for these non-entrainment interlayer heat transfer tests were mercury-water and mercury-silicone oil. Mercury was chosen as the lower fluid to suppress entrainment and to have a minimal resistance to heat transfer. In this fashion, the overall heat transfer coefficient would be approximately equal to the heat transfer coefficient on the oil or water side of the liquid-liquid interface. Fluid density and viscosity were measured in the laboratory. Specific heat and thermal conductivity values were taken from the literature or from vendor-supplied data. Fluid properties are listed in Table 16.1. The apparatus was charged with the test fluids and power supplied via the immersed cartridge heating assembly. The temperature distribution in the liquids was monitored until steady-state conditions were achieved at a prescribed heat flux. The overall heat transfer coefficient was calculated as the net power input divided by the interfacial temperature difference and the cross-sectional area. The superficial gas velocity was calculated as the volumetric gas flux divided by the cross-sectional area. Each data point to be presented represents an average value of from five to as many as thirteen tests, with the individual data variations being in most cases less than 6%.

16.1.3 Experimental Results

The experiments were performed in three series as listed in Table 16.2. The superficial gas velocity covered the range of 0.30 - 8.35 cm/s and the measured heat transfer coefficient varied from 2986 to 50216 W/m^2K. The dimensional experimental data for the three fluid pairs are shown in Figure 16.1. The experimental data greatly exceed the data of Werle (1982) for the same fluids by as much as a factor of ten. With one exception, the data exceed the model predictions of Blottner (1979) and Szekely (1963) by as much as a factor of 7-14 at the highest superficial gas velocities investigated. The only exception is the comparison of the water/mercury heat transfer data

Table 16.1

Properties of Working Fluids

T (C)	ρ (kg/m^3)	C_p (kJ/kg K)	k (W/mK)	ν ($m^2/s \times 10^6$)	Pr (-)
		WATER			
33	994	4.178	.621	0.76	5.07
35	994	4.172	.625	0.74	4.81
36	993	4.173	.627	0.72	4.71
37	993	4.174	.628	0.71	4.60
38	993	4.175	.630	0.70	4.51
39	993	4.175	.631	0.69	4.41
40	992	4.176	.633	0.67	4.32
41	992	4.176	.634	0.66	4.23
45	990	4.175	.640	0.62	4.00
		10 cs SILICONE OIL			
56	906	1.715	.134	6.85	79.4
63	901	1.715	.134	6.30	72.6
77	890	1.715	.134	4.63	52.8
82	887	1.715	.134	3.96	44.9
		100 cs SILICONE OIL			
56	946	1.715	.154	51.3	540.
61	941	1.715	.154	47.8	501.
72	932	1.715	.154	44.0	457.
78	928	1.715	.154	43.1	445.

Table 16.2

Listing of Experimental Data

	Run	$h(W/m^2K)$	$j_g(m/sx10^2)$	T(C)	Nu	Re	Pr
Water/mercury	1	8823	0.30	37	37.9	11.4	4.60
	2	14424	0.59	45	67.6	28.5	4.00
	3	14309	0.88	40	74.6	43.2	4.32
	4	15842	1.17	37	90.8	59.5	4.60
	5	20831	1.47	39	128.7	83.6	4.41
	6	27907	2.05	38	203.8	134.7	4.51
	7	31039	2.65	41	254.6	208.8	4.23
	8	27766	3.23	39	259.6	277.8	4.41
	9	32458	4.38	36	367.5	434.9	4.71
	10	38158	5.63	37	516.5	675.9	4.60
	11	38946	6.28	36	571.5	808.1	4.71
	12	42805	7.21	35	698.6	993.8	4.81
	13	50216	7.75	33	873.3	1101.3	5.07
10 cs Oil/mercury							
	14	5177	0.30	56	104.3	1.18	79.4
	15	5796	0.60	56	129.8	2.63	79.4
	16	7196	0.90	56	177.2	4.34	79.4
	17	8146	1.22	63	224.9	7.17	72.6
	18	9609	1.52	63	286.8	9.65	72.6
	19	10784	2.13	63	378.2	15.9	72.6
	20	14395	2.81	77	580.1	32.8	52.8
	21	14347	3.41	77	642.4	44.2	52.8
	22	16870	4.64	77	931.6	74.2	52.8
	23	20674	6.06	82	1373.0	136.2	44.9
	24	24980	6.74	82	1808.0	165.1	44.9
	25	31604	7.74	82	2547.0	211.1	44.9
	26	29105	8.35	77	2476.0	205.6	52.8
100 cs Oil/mercury							
	27	2986	0.33	61	52.4	0.19	501.0
	28	3750	0.61	56	73.1	0.35	540.0
	29	4338	0.91	61	93.0	0.63	501.0
	30	4924	1.21	56	115.1	0.85	540.0
	31	6052	1.52	61	157.2	1.27	501.0
	32	7073	2.13	61	215.9	2.09	501.0
	33	7885	2.80	78	276.5	3.51	445.0
	34	9382	3.43	72	371.6	4.76	457.0
	35	10930	4.63	72	525.2	7.79	457.0
	36	14082	6.03	78	813.8	12.5	445.0
	37	18328	6.70	78	1142.0	14.9	445.0
	38	20566	7.71	78	1429.0	19.1	445.0
	39	24737	8.34	72	1831.0	21.6	457.0

to that of Blottner (1979), which lies within a factor of two below the data. This behavior is shown in Figures 16.2-16.4 for the three fluid pairs investigated. The heat transfer coefficient was cast as a Nusselt number and the superficial gas velocity as a Reynolds number based upon the volume equivalent bubble radius and the properties of the water or oil layer. The Prandtl number was similarly chosen as that of the water or oil layer. The correlation that was developed to predict interlayer heat transfer between overlying immiscible liquid layers agitated by rising bubbles is shown in Figure 16.5. The form of the correlation is,

$$Nu = 1.95\ Re^{.72}\ Pr^{.72} \qquad (6)$$

and is the relationship recommended for CORCON-MOD2 for interlayer heat transfer.

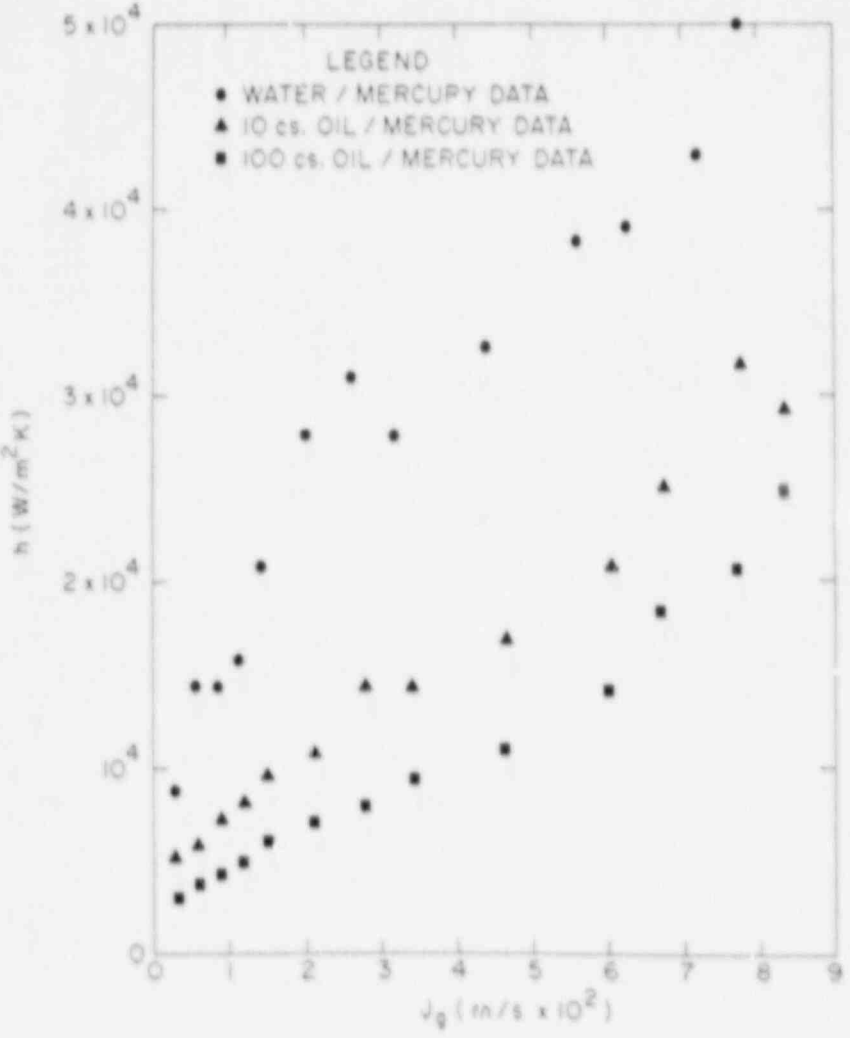

Figure 16.1 Interfacial Heat Transfer Coefficients vs. Superficial Gas Velocity for Stratified, Sparged Fluid Layers

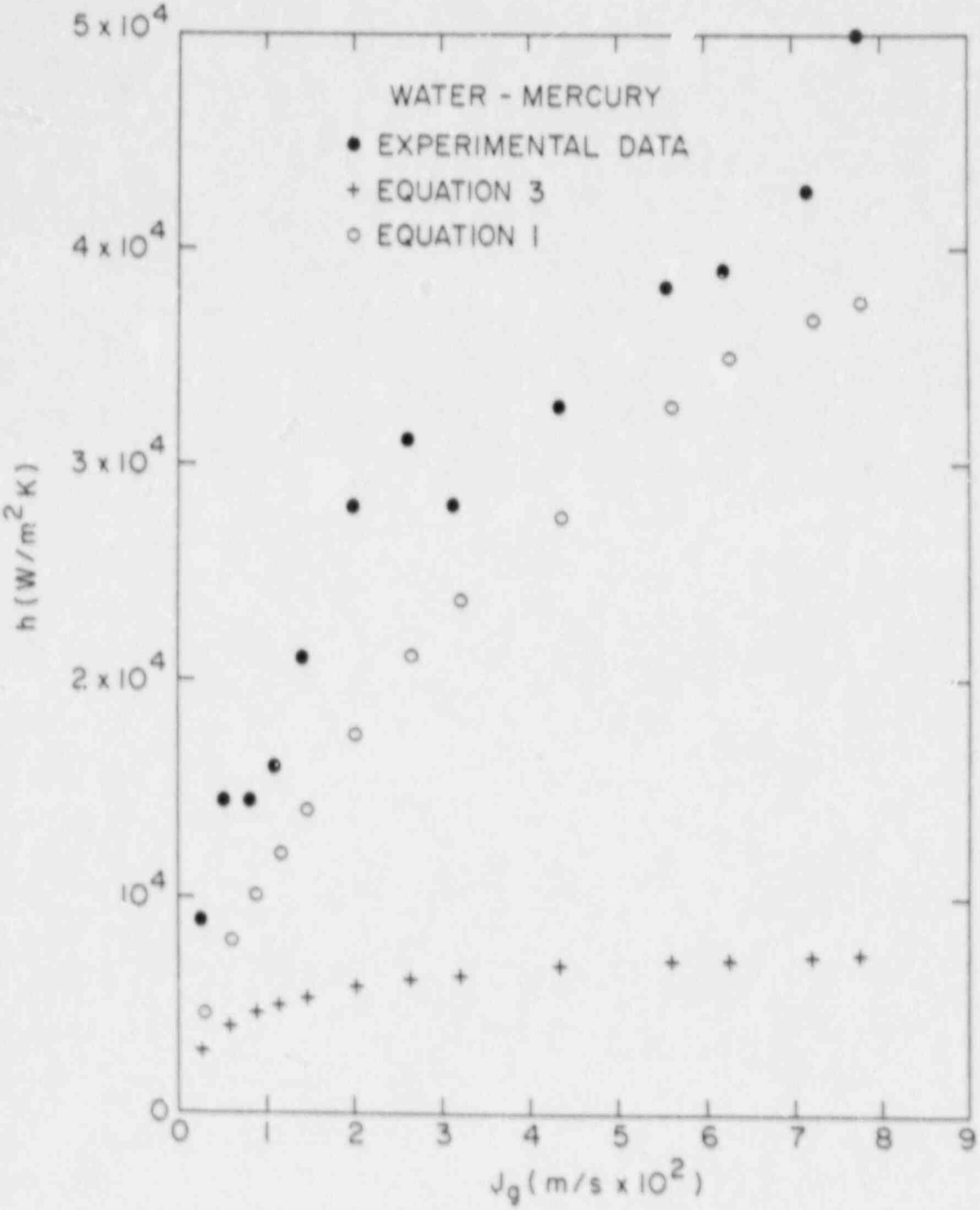

Figure 16.2 Comparison of Water/Mercury Interfacial Heat Transfer Data to Equations 1 and 3

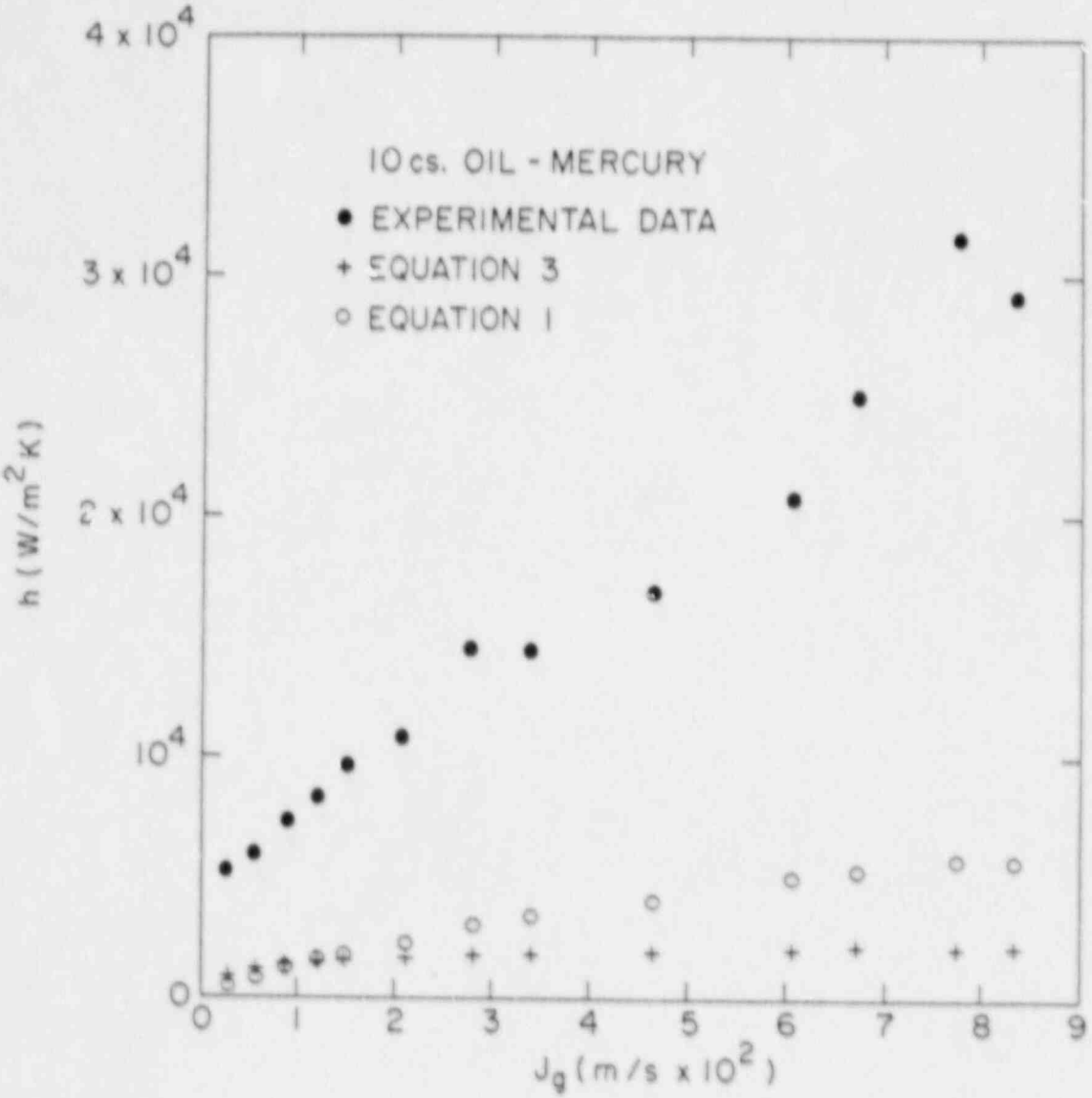

Figure 16.3 Comparison of 10 cs Oil/Mercury Interfacial Heat Transfer Data to Equations 1 and 3

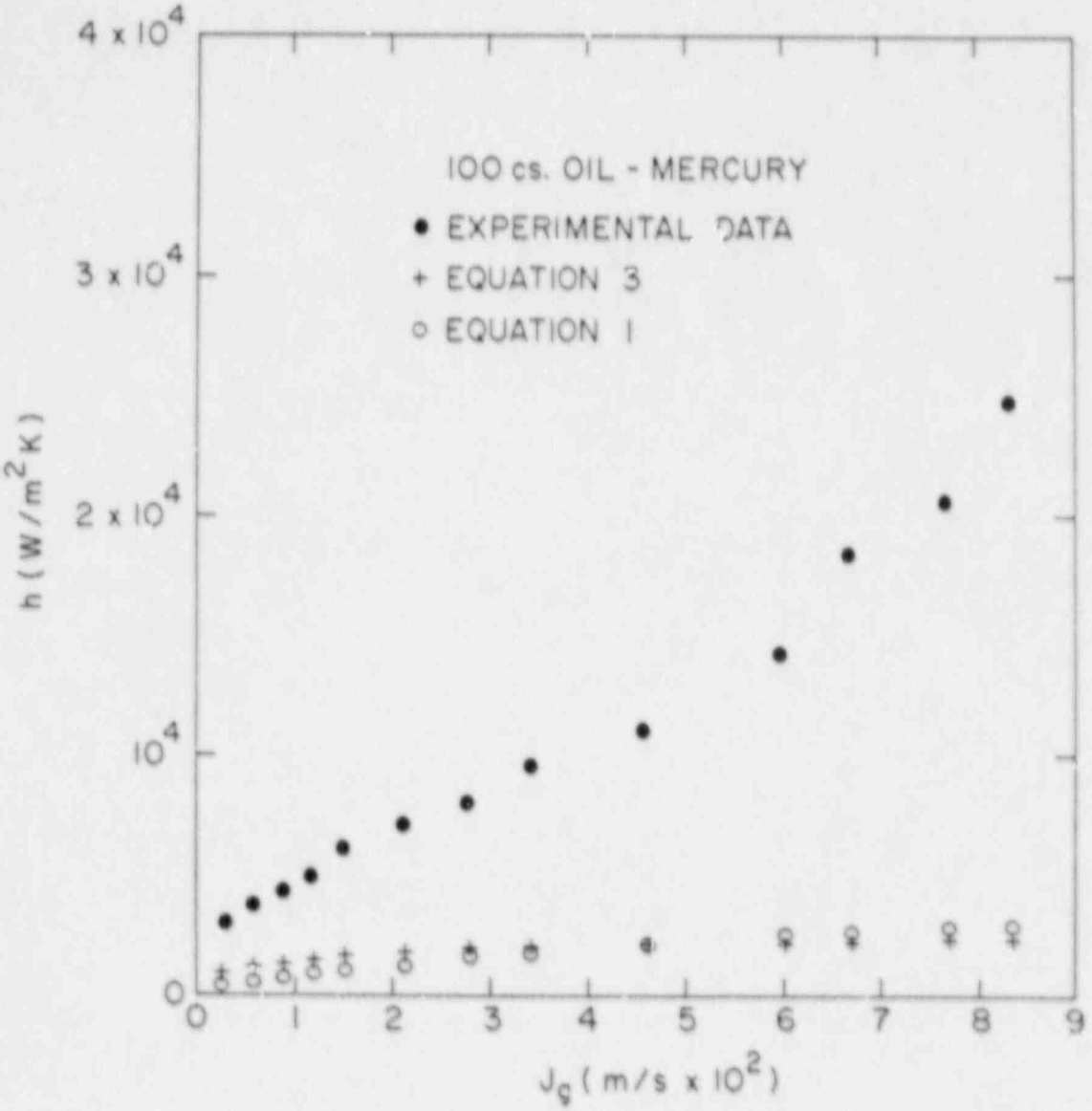

Figure 16.4 Comparison of 100 cs Oil/Mercury Interfacial Heat Transfer Data to Equations 1 and 3

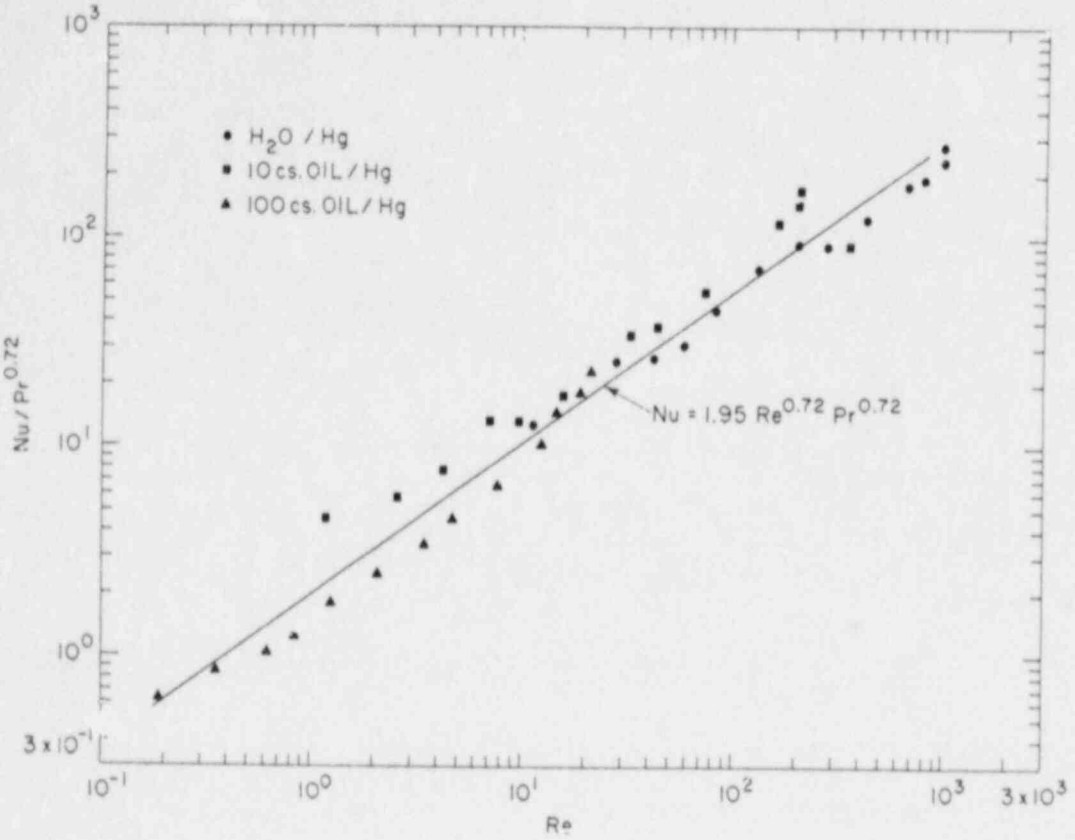

Figure 16.5 Dimensionless Correlation of Interfacial Heat Transfer Data

16.2 Heat Transfer in Core-Concrete Interactions: Boiling from Submerged Porous Surfaces (M. R. Duignan and G. A. Greene)

The purpose of this task is to study the mechanism of boiling and non-boiling heat transfer from simulated core debris crusts and concrete surfaces with a non-condensable gas flux, and their effect on the ex-vessel core-concrete interaction. This effort is in support of the CORCON and VANESA development program at Sandia National Laboratories.

16.2.1 Background

A test apparatus is being designed and constructed to investigate the interaction of simulated concrete decomposition gases on boiling and non-boiling heat transfer to an overlying liquid pool. The apparatus is being designed to support a high heat flux from a flat, horizontal surface with non-condensable gas flux through the surface into the overlying liquid pool. The gas flux will pass through the film boiling interface, simulating the effect of concrete decomposition gases on film boiling of reactor coolant over a pool of crusted core debris.

16.2.2 Preparations to Make Final Measurements to Obtain Baseline Film Boiling Heat Transfer

With the previous failure of the boiling chamber of the test apparatus, a new chamber was proposed, designed and constructed. The chamber incorporated the feature of minimizing its mass near the heat transfer plate by transferring the hold down ring (which secures the chamber to the heat transfer plate) from the base of the chamber to its top. This new chamber has a thinner wall than the original and allows a more effective control of the heat transfer across the vertical wall than just simply adding insulation (e.g., the application of active cooling directly to the outside of the chamber). Also, the thinner wall allowed for better visual observations of the film boiling during experimentation.

A complete set of measurements was made using the new boiling chamber to compare with the previous heat transfer data. The results were similar to those previously reported, but the new boiling chamber stood up better during the thermal cycling caused by experimentation. To eliminate the nucleate boiling on the vertical wall of the boiling chamber, which was now quite visible through the new chamber, two modifications were made:

1. The base of the boiling chamber would be sufficiently subcooled to just eliminate the boiling on the vertical wall.

2. The vertical wall of the chamber would have its thermal resistance increased such that the heat flow from the heat transfer plate would not be diverted up the wall of the chamber to support nucleate boiling.

16.2.3 Modifications to the Boiling Chamber

Three major modifications were made to the chamber to obtain verifiable baseline film boiling data: 1) a constant test fluid level device was incorporated, 2) the passive thermal heat resistance was increased around the lower inside periphery of the boiling chamber and, 3) a cooling coil was placed around the outside base of the boiling chamber.

Some uncertainties in the heat transfer measurements came from the changing test fluid level during experimentation. To minimize those uncertainties a constant level device was designed and constructed such that the test fluid could be delivered to the boiling chamber at a preset flow rate while maintaining the incoming fluid at its saturation temperature. Several tests were taken to assure that a proper fluid level and temperature could be maintained during experimentation.

A thin (several mils) layer of a polyimide substance was applied to the lower inside periphery of the boiling chamber. This substance is made to withstand temperatures up to 400°C over long periods of time while maintaining a low thermal conductivity. The addition of the polyimide substrate increased the thermal resistance of the vertical chamber wall to impede the heat flow from the heat transfer plate to wall surface, thus suppressing the nucleate boiling. Several tests were made to determine the polyimide suitability and durability during experimentation.

A flattened tube was formed to fit around the lower outside base of the boiling chamber as an active means of cooling the wall section where nucleate boiling was occurring. Between the tube and the outside chamber wall a high thermal conductivity paste was applied to assure good heat transfer. This cooling coil system included a constant temperature fluid reservoir, peristaltic pump, flow meter and several temperature probes so that thermal conditions could be set up to just eliminate the nucleate boiling from the vertical wall of the chamber while, at the same time, not subcooling the test fluid pool. Several test runs were made with and without active cooling to the coil. The best results were obtained by using the cooling coil without active cooling, i.e., the copper coil itself, open to the atmosphere, acted as a source of cooling that sufficiently suppressed the nucleate boiling to obtain accurate film boiling data to superheats above 500K.

16.2.4 Final Testing and Results of Baseline Data

A complete set of runs was made to obtain the baseline measurements for the non-condensable gas flow experiments. That is, those results represent film boiling over a flat plate when no non-condensable gas traverses the film boundary layer. These results should correspond to previous film boiling heat transfer measurements done by other researchers. Measurements were made for surface superheats of water from 115K to 600K at atmospheric pressure. For superheats less than 550K, active cooling of the cooling coil was not necessary, i.e.,

a) the relative difference between Berenson's film boiling model and the heat transfer as determined by the condensate mass balance was ±20%.

b) the relative difference between Berenson's model and the heat transfer as determined by the heat conduction through the heat transfer plate was ±10%.

For surface superheats above 550K, active cooling was necessary to eliminate nucleate boiling from the vertical wall. To maintain this superheat, the heating coil was at 80% of its full potential. This superheat, 550K, will be the maximum temperature used in subsequent experimentation with non-condensable gas flow.

Before preparing the test apparatus for the next phase of experimentation (effects of a non-condensable gas flow through the film boiling boundary layer) a photographic study of the film boiling mechanism will be performed in the next quarter.

REFERENCES

BLOTTNER, F.G. (1979), "Hydrodynamics and Heat Transfer Characteristics of Liquid Pools with Bubble Agitation," NUREG/CR-0944.

COLE, R.K., KELLY, D.P. AND ELLIS, M.A. (1984), "CORCON-MOD2: A Computer Model for Analysis of Molten Core-Concrete Interactions," NUREG/CR-3920.

GIESEKE, J. (1986), "Source Term Code Package: A User's Guide (MOD1)," NUREG/CR-4589.

GREENE, G.A., SCHWARZ, C.E., KLAGES, J., and KLEIN, J. (1982), "Heat Transfer Between Immiscible Liquid Enhanced by Gas Bubbling," Int. Meeting on Thermal Nuclear Reactor Safety, Chicago, IL.

GREENE, G.A. AND SCHWARZ, C.E. (1982), "An Approximate Model for Calculating Overall Heat Transfer Between Overlying Immiscible Liquid Layers with Bubble Induced Liquid Entrainment," Proceedings of the Fifth Post Accident Heat Removal Information Exchange Meeting, Karlsruhe, FRG.

GREENE, G.A., CHEN, J.C., AND CONLIN, M.T. (1988), "Onset of Entrainment Between Immiscible Liquid Layers Due to Rising Gas Bubbles," Int. J. Heat Mass Transfer (to be published).

GREENE, G.A., JONES, O.C., JR., SCHWARZ, C.E., AND ABUAF, N. (1980), "Heat Removal Characteristics of Volume Heated Boiling Pools with Inclined Boundaries," NUREG/CR-1357.

KONSETOV, V.V. (1966), "Heat Transfer During Bubbling of Gas Through Liquid," Int. J. Heat Mass Transfer, 9, pp. 1103-1108.

POWERS, D.A., BROCKMANN, J.E., AND SHIVER, A.W. (1986), "VANESA: A Mechanistic Model of Radionuclide Release and Aerosol Generation During Core Debris Interaction with Concrete," NUREG/CR-4308.

SZEKELY, J. (1963), "Mathematical Model for Heat or Mass Transfer at the Bubble-Stirred Interface of Two Immiscible Liquids," Int. J. Heat Mass Transfer, 6, pp. 417-422.

WERLE, H. (1982), "Enhancement of Heat Transfer Between Two Horizontal Liquid Layers by Gas Injection at the Bottom," Nuclear Technology, 59, pp. 160-164.

17. Containment Performance Design Objective

(C. Park)

17.1 Background

The initial objectives of this project were to develop a containment performance objective (CPO) for light water reactor (LWR) containment buildings and implementation guidance for possible incorporation into the Nuclear Regulatory Commission's Safety Goal Policy Statement. This work was completed during 1986 and reported in NUREG/CR-2331, Volume 6, Number 3.

17.2 Objectives

During the current reporting period the project was redirected to providing NRC staff with technical support to help define what might constitute "a large release" of radioactive materials during a severe accident in a LWR.

17.3 Project Status

In order to assess the feasibility of various possible definitions of a "large release" it was decided to use data developed as part of the Zion risk rebaselining study. This study was reported in the "Reactor Risk Reference Document," draft NUREG-1150. Based on the Zion release data and consequence calculations a regressed model was developed. The model was extensively used to test possible definitions of a "large release" in terms of either health effects or total radioactivity released. The results of the calculations were transmitted to the NRC staff.

18. Review of the Core-Melt Evaluation for the Westinghouse Standard Plant (SP-90)
(M. Khatib-Rahbar)

18.1 Background (M. Khatib-Rahbar)

Consideration of severe accidents beyond the traditional design basis, including full core melt accidents, is an important part of NRC's overall safety assessment of nuclear facilities. It is therefore becoming an important ingredient in specific licensing actions and in generic rulemaking proceedings. Also the consideration of features to mitigate the consequences of core melt accidents for nuclear facilities continues to be a major specific licensing activity. The NRC now requires that new standard plant designs provide a probabilistic risk assessment (PRA) as part of the preliminary design approval application. This project will provide support to the NRC staff review of those aspects of the PRA for the Westinghouse Standard Plant (SP/90) related to the core meltdown evaluation. A separate project (reported in Chapter 21 of this document) is addressing the SP/90 accident sequence evaluation.

18.2 Objectives (M. Khatib-Rahbar)

The objectives of this project consist of:

1. To better understand the progression of core melt sequences up to and including associated core melt related phenomenology and the implementation of these processes (and their uncertainties) into an overall assessment of containment loading and failure modes for SP/90. The impact of mitigation strategies on containment loading and failure modes will also be factored into the assessment.

2. To determine the radiological source term suspended in the containment, the effects on engineered safety features (E.S.Fs) and mitigation features of this source term, and finally, the release characteristics of this source term following containment failure for SP/90.

3. To develop an overall capability to assess the radiological consequences as a function of the assumptions regarding accident sequences, phenomenology and mitigation hardware. These radiological consequences will be further analyzed in the context of the SP/90 review with a full appreciation of its regulatory implications.

18.3 Containment Loading Studies (K. Araj)

SP/90 Plant specific containment loading studies were performed for a number of significant accident sequences using the STCP and the CONTAIN codes. CONTAIN is a state-of-the-art containment analysis tool that provides an integrated treatment of containment thermohydraulics, core debris-concrete interactions, and fission product aerosol transport phenomena.

The transient event in the complete loss of coolant injection was simulated using CONTAIN Version 1.06. This class of accident (named a TE sequence) was found to be a major contributor to the SP/90 core melt frequency.

The containment calculations showed that the pressure predictions using MARCH, MAAP and CONTAIN lie within a 10 psia band. However, there are differences in the code predictions most noticably during the long-term pressure behavior MARCH and MAAP, after cavity dryout time, predicted an increasing pressure while a steady pressure level was predicted by CONTAIN. The reason for this difference is under evaluation and CONTAIN calculations will be extended beyond 34 hours to ascertain the nature of this difference.

The dominant accident scenarios in the SP/90 plant belong to a class of accidents in which the reactor coolant system remains at elevated pressure following core melt. If the RCS boundary remains intact, melt-through of the vessel lower head might be followed by high pressure melt ejection. Theoretical and experimental evidence suggests that under these circumstances large fractions of the molten corium could be finely dispersed into the containment with rapid heat transfer to the atmosphere leading to rapid pressurization. This phenomena has been called direct containment heating (DCH).

A number of calculations, employing complex computer models such as MELPROG/TRAC and SCDAP/RELAP, have underscored the possibility of the development, during the course of core degradation, of natural convection currents which may result in overheating and failure of the RCS pressure boundary. Thus the RCS could be depressurized prior to core debris breaching the reactor vessel bottom head. If this phenomena occurs then the possibility of DCH is eliminated. However, given the state-of-the-art computer predictions of natural circulation effects, it is premature to totally dismiss the class of accidents in which pressure-driven melt expulsion might occur. A simple adiabatic, one-volume, DCH load calculation for the SP/90, involving 100% dispersal of the corium, with attendant zirconium oxidation indicated peak pressure of the order 144 psi and gas temperature of 3000 K.

In view of the importance of the DCH scenario to the risk profile of SP/90 and the large uncertainties imbedded in a simplified adiabatic one-volume representation of the containment, a more realistic calculation has been started using CONTAIN-IDHM (a preliminary version of CONTAIN Interim Direct Heating Model), developed at Sandia National Laboratories (SNL).

In the IDHM, those DCH phenomena which are reasonably well understood are treated with mechanistic models. Poorly understood phenomena are, on the other hand, treated parametrically. The models for DCH are integrated with other models for containment thermal-hydraulics, and aerosol phenomena which have been implemented in the standard versions of CONTAIN.

The core debris may undergo chemical reaction and exchange heat with the atmosphere; radiation heat transfer from the debris to the structures is also modelled. The debris is modelled as a single "field" of drops, of a user specified size, with all drops in a given cell being characterized by a single drop size, composition and temperature.

The interaction of the debris with structures is simulated in the IDHM by "trapping". The effect of "trapping" is to remove the debris from the atmosphere at a rate, λ_{tr}, specified by the user.

18.4 Containment Event Tree Analysis (T. Ishigami, K. Araj, S. Kim)

The input preparation for the Containment Event Tree (CET) analysis continues. It is anticipated that two sets of CET analyses will be performed, namely with DCH included and without DCH in order to determine the impact of DCH on the SP/90 risk profile.

19. Review of Containment Response Analyses in the Shoreham Probabilistic Risk Assessment

(K. R. Perkins, J. W. Yang, J. Pires and W. T. Pratt)

19.1 Background

As part of the review of the Containment Response Analysis in Shoreham PRA, two unique tasks were identified for independent analytical evaluation:

(1) the structural capability of the Shoreham primary containment and the likely failure locations if failure occurs, and

(2) the potential for ex-vessel steam explosions, which might occur after a severe accident has progressed to the point at which the core melts through the reactor pressure vessel.

19.2 Project Objective

The primary objective of this project is to provide an independent assessment of specific features of the Shoreham containment response analysis submitted by the applicant in support of the Shoreham Probabilistic Risk Assessment (PRA).

19.3 Project Status

During this reporting period two draft evaluation reports were completed and submitted to the NRC for review. The first evaluation report provided a finite element analysis of the Shoreham containment structure. The results indicate that the Shoreham containment will fail at the intersection of the basemat and the wetwell wall at about 135 psig.

The second draft report addresses the question of the possible pressure rise due to fuel-coolant interaction after core debris flows into the downcomers in the pedestal region. The report concludes that under the limiting assumptions postulated by Corradini et al., the magnitude of a steam explosion appears to be sufficient to reach the failure threshold of the pedestal wall. There are a number of mechanisms identified in the Shoreham PRA which would tend to limit the fuel mass involved in a steam explosion. Specifically, freezing of the molten corium on the drywell floor (for a gradual melt release) or freezing on the downcomer walls and countercurrent steam production will tend to restrict the rate of corium flow into the wetwell. In spite of the above arguments, it does not appear that the possibility of a significant steam explosion in the Shoreham wetwell has been precluded. (It should be noted that the fuel mass postulated by Corradini corresponds to about a one foot long slug of fuel in each of the four downcomers.)

Even if a steam explosion occurs which exceeds the failure limit of the pedestal wall, it is likely that such failures will result in localized cracking of the concrete, which may not prevent the pedestal from continuing to support the reactor vessel. A detailed structural analysis would have to be

performed for the Shoreham pedestal befc : its failure threshold with regard to load bearing capacity could be accurately characterized.

REFERENCES

CORRADINI, M. L. et al. (1985), "Ex-Vessel Steam Explosions in the Mark II Containment," Appendix C of NUREG-1079.

SCIENCE APPLICATIONS, INC. (1983), Probabilistic Risk Assessment, Shoreham Nuclear Power Station, SAI-372-83-PA-01, June 1983.

20. Fission Product Releases and Radiological Consequences of Degraded Core Accidents

(M.Khatib-Rahbar and H. Nourbakhsh)

20.1 Background (H. Nourbakhsh)

The source term to containment is defined as the quantity, timing, and chemical form of the fission product species released to the reactor containment building atmosphere during core damage accidents.

The traditional source term assumption used in the licensing process in the United States has been based on data that was obtained by burning irradiated uranium metal in air. This data formed the basis for the TID-14844 document published in 1962.

The current U.S. Nuclear Regulatory Commission (USNRC) regulatory framework treats design basis events in a nonmechanistic manner with respect to radiological source terms. Significant research activity in the area of severe accidents has been undertaken following the accident at Three Mile Island Unit 2. Updated fission product source term methods have been developed and published in NUREG-0956.

20.2 Fission Product Release Characteristics Into Containment Under Design Basis and Severe Accident Conditions (H. Nourbakhsh, M. Khatib-Rahbar, R.E. Davis)

In order to formulate a consistent and simplified approach for the estimation of radiological releases to containment for accidents involving significant fuel damage the available light water reactor source term information was reviewed. The phenomenological aspects of degraded core accidents were assessed and key factors affecting fission product release characteristics into containment were identified.

A simplified formalism for source term releases to containment was proposed. Two basic assumptions govern the validity of the proposed formalism; firstly, the fission product species are grouped according to their respective chemical form and release characteristics and, secondly, the accident conditions must be categorized into appropriate severe accident attributes which govern the release. These include: (1) Reactor type (BWR vs. PWR), (2) RCS, pressure prior to vessel breach (high vs. low), (3) concrete aggregate (limestone vs. basaltic), and cavity/pedestal condition (dry vs. flooded). Appropriate decontamination factors (DFs), depending on the path of release, were also applied.

The relevant parameters, including the timing of release, were based upon the results of the recent Source Term Code Package calculations performed in support of NUREG-0956 and draft NUREG-1150 studies.

Generic fission product releases from reactor coolant system (FRCS) and from the melt during core/concrete interaction (FCCI) are tabulated in Tables 20.1 and 20.2. The release fraction for each radionuclide group which is assigned to an accident category generally is taken as the highest STCP calculated fraction from all of those accident sequences into the release category.

The duration of these releases to containment have also been selected through an assessment of the existing STCP calculations. In-vessel releases generally occur within 40 minutes for pressurized water reactors (PWRs) and 1.5 hours for boiling water reactors (BWRs). These releases are assumed to be initiated with the gap release following initial core melt. The major in-vessel releases are then assumed to start after an additional 10 minutes into the accident. Although the release from core/concrete interaction is predicted to extend many hours beyond initiation of molten corium/concrete interaction (MCCI) initiation, generally 90% of the radionuclide releases (except Te) occur within 2 hours for PWRs and 3 hours for BWRs. However, for tellurium an ex-vessel release durations of five hours for PWRs and 6 hours for BWRs was assumed.

DF values of 10, 3 and 1 were assigned when very deep, deep, or shallow water (or dry) pools respectively are overlying the corium during MCCI.

In the simplified formalism for appearance rate into the containment, the fission product releases are treated as being proportional to time. Figure 20.1 shows typical comparisons of the proposed simplified appearance rates for the various radionuclides to an STCP calculation.

Table 20.1 Simplified PWR Fission Product Releases to Containment for Severe Accident Conditions

Groups	FRCS[a]		FCCI	
	H,I	L	Basaltic Concrete	Limestone Concrete
NG	1.0[b]	1.0	0	0
Cs, I	0.35	0.9	0	0
Te	0.3	0.65	0.15	0.35
Sr, Ba	2×10^{-3}	0.01	0.15	0.4
Ru, Ce, La	3×10^{-5}	3×10^{-5}	6×10^{-3}	0.02
Release Duration	40 mins.		2 hrs.[c]	

a) H, I and L refer to high, intermediate or low RCS pressure, respectively.
b) All entries are fractions of the initial core inventory.
c) Except for Te where the duration of ex-vessel release is extended to 5 hours.

Table 20.2 Simplified BWR Fission Product Releases to Containment for Severe Accident Conditions

Groups	FRCS[a]		FCCI	
	H,I	L	Basaltic Concrete	Limestone Concrete
NG	1.0[b]	1.0	0	0
Cs, I	0.7	0.8	0.15	0.15
Te	0.1	0.15	0.12	0.5
Sr, Ba	6×10^{-3}	6×10^{-3}	0.2	0.7
Ru, Ce, La	3×10^{-5}	3×10^{-5}	6×10^{-3}	0.06
Release Duration	1.5 hrs.		3 hrs.[c]	

a) H, I and L refer to high, intermediate or low RCS pressure, respectively.
b) All entries are fractions of the initial core inventory.
c) Except for Te where the duration of ex-vessel release is extended to 6 hours.

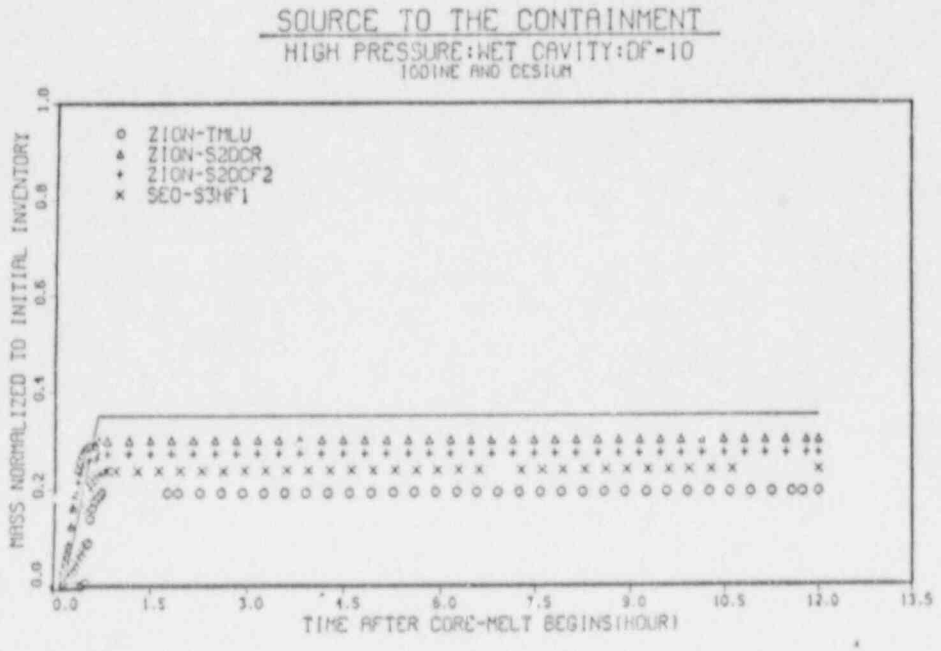

Figure 20.1 I-Cs Cumulative Release Fraction to a PWR Containment (High RCS Pressure, Limestone Concrete, Wet Cavity: DF=10)

21. Review of the Accident Sequence Evaluation for the Westinghouse Standard Plant (SP/90)

(C. Guey, L. Arrietta, R. Youngblood, C. Park, R. Fitzpatrick, T-L. Chu)

21.1 Background

Part of the Commission's Severe Accident Policy requires that new standard plant designs provide a probabilistic risk assessment (PRA) as part of the Preliminary Design Approval (PDA) application. This program support the NRC staffs evaluation of the PDA application for the Westinghouse SP/90 standard plant design. This project addresses the accident sequence evaluation in the SP/90 PRA. A separate project (reported in Chapter 18 of this document) is addressing the SP/90 PRA core meltdown evaluation.

21.2 Program Objectives

BNL will perform a comprehensive review and evaluation of the SP/90 PRA to determine whether the accident sequence frequencies reflect appropriate use of probabilistic risk assessment methods, specific design features, and reliability data. BNL will evaluate the defensibility of the PRA's accident sequence frequency estimates and the uncertainty in core damage frequency induced by uncertainty in failure probabilities with respect to (1) use of state-of-the-art risk assessment methods, (2) thoroughness and comprehensiveness of analysis, (3) availability and appropriate use of data, and (4) modelling assumptions. BNL will include various aspects of the study up to the point of the calculation of core damage frequency, including methodology, assumptions, data, information sources, models, plant design, completeness of the analysis, and any other area where inconsistencies may arise which could have a appreciable impact on results. BNL will perform an evaluation of the PRA interfacing assumptions regarding the balance of plant (BOP) design. BNL will make a limited assessment of the impacts of possible alternative assumptions identified in the review. To the extent feasible, BNL will consider spatial information in evaluating systems interactions and dependencies.

21.3 Technical Approach

BNL conducted a preliminary accident sequence evaluation of the SP/90 PRA including requantification. The preliminary results obtained from the requantification were documented in a draft report dated September 1986. The draft report has undergone both NRC and Westinghouse review and BNL is currently evaluating and responding to the comments as appropriate.

The BNL plant model is being modified where necessary to develop the final results and insights.

21.4 Project Status

At the end of the period, effort was underway to complete an updated draft report based upon new input from Westinghouse. Current results have not been presented because they are of a preliminary predecisional nature.

IV. DIVISION OF REACTOR AND PLANT SYSTEMS

SUMMARY

Code Maintenance (RAMONA-3B)

Currently, only the CDC-7600 version of the RAMONA-3B transient code is available. The code has been upgraded to FORTRAN 77, which will allow the code to run on IBM, CRAY, or CDC machines. An update of the code manual is also being prepared to reflect the code changes made for version 4.0 to 10.0.

Assessment and Application of TRAC-BF1 Code

The code assessment and application activity was redirected toward supplying technical support for the evaluation of TRAC-BF1/MOD1 uncertainty. A procedure of applying CSAU to TRAC-PF1/MOD1 was established and BNL's contribution toward this application was defined. A USNRC account umber at the INEL computing facility was also established to run the TRAC-BF1 and the TRAC-PF1/MOD1.

Plant Analyzer Development for BWR/2 and BWR/6 and Maintenance for BWR/4

The LWR Plant Analyzer Program is being conducted to develop and operate an engineering plant analyzer capable of performing accurate, real-time and faster than real-time simulations of plant transients and Small-Break loss of Coolant Accidents (SABLOCAs) in LWR power plants. The plant analyzer is intended to provide a needed, cost-effective and convenient alternative to widely used, but expensive and time-consuming, power plant simulations employing FORTRAN codes and large mainframe or super computers. The plant analyzer development is based chiefly on a unique combination of advanced modeling techniques with modern minicomputer technology.

The plant analyzer program was at first directed toward reactor safety analyses, but it is also suitable for on-line plant monitoring and accident diagnosis, for accident mitigation, further for developing operator training programs and for assessing and improving existing and future training simulators. The plant analyzer has been modified for on-line training in emergency response. Major assets of the Plant Analyzer are its low cost, unsurpassed convenience of operation and high speed of simulation. Major achievements of the program are summarized below.

Existing training simulator capabilities and limitations regarding their representation of the Nuclear Steam Supply System have been assessed previously. Simulators reviewed at the time have been found to be limited to steady-

state simulations and to restricted quasi-steady transients within the range of normal operating conditions.

A special-purpose, high-speed peripheral processor had been selected for the plant analyzer, which is specifically designed for efficient systems simulations at real-time or faster computing speeds. The processor is the AD10 from Applied Dynamics International (ADI) of Ann Arbor, Michigan. A PDP-11/34 Minicomputer serves as the host computer to program and control the AD10 peripheral processor. Both the host computer and the peripheral processor have been operating at BNL since March 15, 1982.

A four-equation model for nonequilibrium, nonhomogeneous, two-phase flow in a typical BWR/4 had been implemented on the AD10 processor. It is called HIPA-BWR/4 for High-Speed Interactive Plant Analysis of a BWR/4 power plant. The implementation of HIPA-BWR/4 had been carried out in the high-level systems simulation language MPS10 of the AD10.

It had been demonstrated during the last quarter of 1982 that the AD10 special-purpose peripheral processor can produce accurate simulations of a BWR design base transient at computing speeds up to 10 times faster than real-time and 110 times faster than the CDC-7600 mainframe computer carrying out the same simulation. Only the BNL Plant Analyzer has achieved this gain in computing speed relative to the CDC-7600 computer. The plant analyzer interacts on-line with the user, with instrumentation and with controls, by processing both analog and digital input and output data. All calculations are digital.

After the successful completion of this feasibility demonstration, work has continued to expand the simulation capability for simulating the dynamics of the entire nuclear steam supply system as well as the entire balance of plant (steam lines, turbines, condensers and feedwater trains, and containment systems).

Models have been developed and implemented for point neutron kinetics with seven feedback mechanisms and seven automatic scram trip initiations, for thermal conduction in fuel elements, for steam line dynamics capable of simulating acoustical effects from sudden valve actions, for turbines, condensers, feedwater preheaters and feedwater pumps and for emergency cooling systems.

Models have been developed and implemented for the feedwater controller, the pressure regulator and the recirculation flow controller. Twenty-eight parameters for initiating control systems and valve failures and for selecting set points can be changed on-line from a 32-channel control panel. Sixteen dedicated analog output lines are provided for the simultaneous display of 15 selected parameters in labeled diagrams versus time. All input-output channels are addressed approximately 200 times per second. A silent movie has been produced to show how the plant analyzer is operated and how it responds to on-line analog signals.

During the first reporting period of 1984, we presented the comparison of plant analyzer results with published results from GE for 10 different ATWS

events as a part of developmental assessment. The assessment showed that the plant analyzer is capable of simulating ATWS. The plant analyzer has been generalized to simulate any BWR-4 power plant in response to input data changes from the keyboard.

During the second reporting period of 1984, we continued the developmental assessment of the plant analyzer by comparisons against GE, TRAC-BD1, RELAP-5, and RAMONA-3B code results. The results showed that the plant analyzer is capable of realistically simulating a large class of plant transients efficiently and at very low cost.

During the third reporting period of 1984, we implemented the capability of simulating flow reversal, and demonstrated successfully the simulation of boron injection and the subsequent cessation of fission power. Several transients were simulated to demonstrate the plant response to manual depressurization and HPCI flow reduction during an ATWS event (Cheng et al., 1986). These simulations were carried out to assess the efficacy of proposed emergency procedure guidelines. The results indicate that the fission power can be reduced without boron injection and core uncovery, by lowering the pressure and by lowering the coolant level in the downcomer and thereby reducing the core flow rate.

A detailed final report documenting the BWR plant analyzer [Wulff, Cheng, Lekach and Mallen, 1984] has been printed and distributed.

During the fourth reporting period of 1984, we demonstrated that with the plant analyzer one can simulate, evaluate and document with hard-copy prints, in less than four days, thirty-seven different transients, induced by both single and multiple failures or events. We achieved the ability to operate the plant analyzer remotely at BNL from an IBM Personal Computer, equipped with 256 K byte memory, an RS-232 serial port, a 1200 baud modem, a Plantronics PC+ Colorplus color graphics adapter card and a standard R-G-B color monitor.

During the first reporting period in 1985, we have demonstrated that the BNL Plant Analyzer can now be accessed and operated remotely from anywhere in the United States. There were seven demonstrations given in Washington, DC, two in California, one in Idaho and one for a utility in New York. Work has started for on-line support of personnel drills in the NRC Emergency Operations Center. The Tektronix 4115B graphics terminal has been received and installed to generate animated mimics of flow and control diagrams.

During the second reporting period in 1985, we have developed the models for drywell and wetwell responses to discharge from pipe leaks and from the safety and relief valves. We began to expand tabulations of thermophysical properties and related functions toward low pressures in the vessel, and we completed the level tracking simulation in the downcomer.

During the same reporting period we have demonstrated for the first time the remote access and simulation capabilities of the plant analyzer from

Europe across the Atlantic. We have demonstrated that the plant analyzer maintains steady-state conditions without drift for over 20 hours (having four and fourteen decimal place precision for general arithmetic and for integrations, respectively).

During the third reporting period in 1985, we have simulated the first four-hour-long transient in support of a drill at the NRC Emergency Operations Center. We have continued to develop and implement models for simulating processes in the containment building. Graphics capabilities have been developed for continuous data display during indefinitely long transients. Data can be displayed in either S.I. or British units. A log in procedure has been implemented for off-site customers for the BNL Plant Analyzer. The first operation assessment tests have been performed with the new Version 4 of MPS-10.

During the last reporting period in 1985, we have continued with the model implementations for long-term power plant simulations in support of emergency drills. The BNL Plant Analyzer was shown to be the first simulation facility which accomplished the on-line, remote-access simulation of four different transients during a 25-minute-long presentation at the 13th Water Reactor Safety Information Meeting. A one-month-long lecture series was started in December at the National Tsing Hua University (NTHU) under the provisions of the USA-ROC Technical Exchange Program. The lectures covered the modeling principles, the computing methods and the computer architecture employed in the plant analyzer.

During the first reporting period in 1986, we completed the scaling of all containment response models and began the program coding. Five different critical quality and critical heat flux correlations have been compared under three different reactor conditions, and a suitable correlation has been selected for implementation in the HIPA code. The lecture series at the National Tsing Hua University has been completed. As a result of these lectures and of presentations at Taiwan Power Company (Taipower) and at the Institute of Nuclear Energy Research (INER), Taipower expressed its intent to participate in the development of a plant analyzer in Taiwan, in cooperation with BNL (USA), NTHU and INER (Taiwan).

During the second reporting period in 1986, we have completed the implementation of the containment simulation and started its validation. The simulation capability has been expanded to low reactor vessel pressures, down to 2 bar. The previously selected model for computing the minimum critical power ratio has been implemented and successfully tested.

The Plant Analyzer served for the second time to simulate a four-hour-long transient, this time caused by an off-site power loss at the Fermi-2 power plant. This simulation was the basis for an emergency drill at the NRC Emergency Operations Center.

As the first facility ever, the BNL Plant Analyzer was able to produce simulation results within one day. The transient, caused by a feedwater pump

speed excursion at LaSalle-2 power station, and three variations on the incident scenario were computed within hours of the NRC request and graphical results transmitted to the NRC via facsimile.

LILCO has continued to use the BNL Plant Analyzer for simulating the Shoreham power plant. Niagara Mohawk is preparing the BNL Plant Analyzer for simulating the Nine Mile Point-1 BWR/2 power plant.

During the third reporting period in 1986, we continued to validate the containment simulation. A critical flow model has been formulated and implemented for break flows from the steam line, the recirculation loop and the feedwater line.

The remote access capabilities have been demonstrated by operating the Plant Analyzer from Taiwan and from Korea. A proposal has been drafted, submitted to, and revised for, the Taiwan Power Company which has decided to cooperate with BNL in the PWR Plant Analyzer Development. The Korea Advanced Energy Research Institute has also expressed its interest to participate in this development.

The BNL Plant Analyzer can now be accessed from both IBM PC XT and AT computers. A new graphics feature allows the storage in the IBM PC of up to 10 graph segments during long-time simulations and then to combine them into a single graph.

The Plant Analyzer has also been demonstrated in remote access mode as part of a technical paper presentation.

The Plant Analyzer has been maintained and operated in support of two utilities: Niagara Mohawk and Long Island Lighting Company. Technical assistance has been provided in preparing for these utilities plant-specific input data files and selected initial conditions. Documentation of user guides has been continued to aid in the preparation of input data.

During the previous reporting period, Niagara Mohawk Power Corporation has been assisted in setting up the Plant Analyzer for its Nine Mile Point 2 BWR/2 plant. Work has been started to prepare the Plant Analyzer for simulating the Cofrentes BWP/6 plant of the Hidroelectrica Espanola in Valencia, Spain, for the Consejo de Seguridad Nuclear in Madrid, Spain.

During the current reporting period, the BWR/4 version of the Plant Analyzer has been validated against actual plant data for a recirculation pump trip test and a generator load rejection test conducted at the Browns Ferry Unit 1 (BF-1) Nuclear Power Station.

The BWR/2 version of the Plant Analyzer pertaining to the Nine Mile Point Unit 1 (NMP-1) Nuclear Power Station has been developed and validated against plant data and the RETRAN code.

Work was continued on the CSN (Spain) project. The control systems and the recirculation flow dynamics for the Cofrentes BWR/6 plant of Hydroelectrical Espanola SA, Spain, have been developed and programmed. Independent verification of the control system response has also been performed.

BNL has continued to promote the establishment of international cooperative programs for PWR power plant simulations.

Procedures for Evaluating Technical Specifications (PETS)

During this reporting period, the project stressed activity in response to Generic Issues B-56 and B-61. The PETS program has developed methodologies and demonstrated through application the effectiveness of adaptive testing and cumulative downtime strategies. Risk effective surveillance test intervals were analyzed for diesel generators, an PC-based software was developed for implementation of such approaches.

The approaches can be applied not only to diesels, but to any component with suitable data. Incorporation of the approaches in personal computer (PC) software which can provide tools for the regulator or plant personnel for determining acceptable diesel test intervals for any plant specific or generic application is discussed. The FRANTIC III computer code was run to validate the approaches and to elevate specific issues associated with determining risk-effective test intervals for diesels.

Operational Safety Reliability Research

Work during this reporting period largely focussed on (1) extending the reliability program process identified in FY 1986, to include defensive strategies against common-cause failures and (2) soliciting cooperation with an operating utility and evaluating through a trial application the effectiveness of a reliability program applied to a normally-operating system. In addition, select members of the project team were engaged in documenting for the NRC guidance for evaluating reliability programs for diesel generators that would be submitted by licensees in response to Unresolved Safety Issue (USI) B-56.

Risk-Based Performance Indicators

During this reporting period, the project was largely engaged in (1) refining methods to relate currently used performance indicators more closely to risk and (2) developing methods for risk-based performance indicators applied to monitor the unavailability of selected safety systems. In both of these areas, BNL provided a description of the risk-based method, a procedure guide for implementing the method, and where appropriate PC-compatible software for subsequent use by the NRC.

Methods for incorporating additional risk considerations with the current set of performance indicators identified by NRC's interoffice task group, concentrated on risk-weighting scrams, safety system actuations, significant events, and safety system failures. The procedure employed did not rely on whether the plant had a PRA associated with it. As such, simple, albeit conservative rules were developed to quantify the risk impact of operational events. A draft report was prepared that provides a methodology for quantifying the risk associated with operational events. This draft report also documents the risk models employed, the spreadsheet developed and the process for incorporating the approach to any plant. To date, the method has been applied to three plants, viz, Surry, Limerick, and Beaver Valley.

Study of Beyond Design Basis Accidents in Spent Fuel Pools (Generic Issue 82)

This project addresses NRC/RES concerns regarding the significance of possible fission product releases that may result from loss of integrity accidents in spent fuel pool studies including a review and evaluation of assumed propagation mechanisms. The objective of this work is to obtain estimates of the likelihood of spent fuel pool accidents and the concomitant risk. An additional objective is to identify the predominant mechanism for fuel pool failure and fission product release.

Development of Technical Basis for Severe Accident Guidelines and Procedural Criteria for Existing BWR Plants

This project is intended to provide assistance to the NRC in formulating an approach for individual plant examinations (IPEs) to determine whether particular accident vulnerabilities are present. Specifically, the objectives of this effort are: (1) to assist the RES/DRPS staff in the review of NUREG-1150 and the IDCOR analyses for two boiling water reactor (BWR) reference plants, namely, Peach Bottom (a BWR with a Mark I containment) and Grand Gulf (a BWR with a Mark III containment), (2) to help develop the accident prevention and accident mitigation guidelines for these two plant types as well as for BWRs with Mark II containments, and (3) to assist in the review of the IDCOR IPE methodology.

Development of Technical Basis for Severe Accident Guidelines and General Criteria for Existing PWR Plants

This project is intended to provide assistance to the NRC in developing an approach for the Individual Plant Examination (IPE) Program. Specifically, the objectives of this effort are: (1) to assist the RES/DRPS staff in review of NUREG-1150 and the IDCOR analyses for two pressurized water reactor (PWR) reference plants, namely, Sequoyah (a PWR with an ice-condenser containment)

and Zion (a PWR with a large-dry containment), (2) to help develop the accident prevention and accident mitigation guidelines for these two plant types and (3) to assist in the review of the IDCOR IPE methodology.

Interfacing Systems LOCA at LWRs

In this program, BNL staff are conducting a study to provide a technical basis for the resolution of Generic Issue 105. This generic issue deals with potential accidents that involve the failure of isolation valves between the high pressure primary system of the nuclear reactor and the low pressure auxiliary systems. Such accidents are usually called interfacing systems loss-of-coolant accidents (LOCAs). This study deals with both pressurized water reactors (PWRs) and boiling water reactors (BWRs). The study focuses on six representative reactors (three PWRs and three BWRs) and where possible identifies the generic applicability of the plant-specific findings. In addition, a generic analysis is performed to investigate the cost-benefit aspects of imposing a testing program that would require some minimum level of leak testing of the pressure isolation valves on plants that presently have no such requirements.

Improved Reliability of Residual Heat Removal Capability in PWRs as Related to Resolution of Generic Issue 99

In this program, BNL staff are performing a study to develop a technical basis for NRC resolution of Generic Issue 99. Generic Issue focuses on the risk associated with loss of residual heat removal events at pressurized water reactors (PWRs) during shutdown. Numerous loss of residual heat removal events have occurred at PWRs in the USA, which were terminated prior to damaging the reactor core. This study estimates the risk from loss of residual heat removal events and investigates ways of lowering this risk.

Support for Containment Loading Studies

In this program BNL is performing analyses of containment loads for selected LWR configurations in conjunction with cooperative efforts under way with the NRC staff and various expert groups within the Committee on the Safety of Nuclear Installations (CSNI). Specifically, the project is providing support to an international effort being undertaken by the task group on ex-vessel severe accident thermal-hydraulics, which is sponsored by CSNI's Principal Working Group (PWG #2).

Support for TRAC-PF1/MOD1 Uncertainty Analysis

The USNRC is developing the Code Scaling, Applicability and Uncertainty (CSAU) Methodology for estimating quantitatively the uncertainty in code predictions of importance reactor safety parameters, such as the Peak Clad Temperature (PCT) in a Large Break Loss of Coolant Accident (LBLOCA). The CSAU Methodology is being applied first to the TRAC-PF1/MOD1 computer code, simulating an LBLOCA, to demonstrate the feasibility of the Methodology.

BNL analyzed three primary uncertainties arising from uncertainties in modeling fuel stored energy and thermal response, in modeling critical break flow and in modeling pump performance degradation under two-phase flow conditions.

The steady-state temperature distribution and the stored energy in nuclear fuel elements were computed by analytical methods and used to rank, in the order of importance, the effects on stored energy from statistical uncertainties in modeling parameters, in boundary and in operating conditions. An integral technique was used to calculate the transient fuel temperature and to estimate the uncertainties in predicting the fuel thermal response and the peak clad temperature during a large-break loss of coolant accident.

It was shown that the blowdown peak is dominated by fuel stored energy alone or, equivalently, by linear heating rate. Gap conductance, peaking factors and fuel thermal conductivity are the three most important fuel modeling parameters affecting peak clad temperature uncertainty.

The bias in TRAC modeling of critical break flow was determined as the ratio C_D of measured to predicted critical mass flow rates. Twelve Marviken blowdown tests were used to find the C_D. Modeling uncertainty in TRAC break flow calculations was obtained as the standard deviation of C_D.

The bias in TRAC pump modeling is determined from scale extrapolation of pump degradation data, taken from 1/20, 1/5, and 1/3 scale pumps. It is shown that pump degradation is the smaller, the larger the pump is.

22. Code Maintenance (RAMONA-3B) (U.S. Rohatgi)

This project consists of improvement and maintenance of the BWR plant transient code RAMONA-3B. The code employs three-dimensional neutron kinetics coupled with parallel hydraulic core channels and is complete with jet pump, recirculation pump, steam separator, steam line with all necessary valves, safety injection system and limited plant control and protection system. Under user option, the code can also be used with one-dimensional (axial) neutron kinetics. The code is most suitable for analyzing the BWR core and systems transients where the coupling between neutron kinetics and thermal hydraulics is important (e.g., ATWS, CRDA, etc.). The RAMONA-3B code along with the FRAM and BLEND codes can be modified to produce 1-D cross sections for any other code with one-dimensional neutron kinetics model, such as TRAC-BF1. The code is available to any U.S. organization, on a royalty-free basis, for the analysis of U.S. reactors.

The major activities performed during two quarters (April to September) are as follows:

22.1. RAMONA-3B User Manual (L.Y. Neymotin)

The manual preparation has continued during this period. The first five chapters are currently being typed. At present, three chapters and three appendices remain to be completed.

22.2. RAMONA-3B Conversion (S. Heller, L.Y. Neymotin)

Since the CDC-7600 computer at BNL is being phased out with a deadline of the end of September 1987, work has been initiated on the code conversion to the newly installed mainframe computer IBM-3090. At the same time the code is being converted into the FORTRAN-77 standard version. The conversion is essentially complete and the code can now run on CDC, CRAY, or IBM mainframes with minor modifications.

23. Assessment and Application of TRAC-BF1 Code (U.S. Rohatgi)

This project includes the independent assessment of the latest released version of the LWR safety codes such as TRAC, RELAP5 and RAMONA-3B, and the application of these codes to the simulation of plant accidents and/or transients. The other activities in this project are participation in ICAP, meeting connected with scaling and uncertainty analysis, and any current issues in which our expertise can contribute towards their resolution.

Major activities performed during two quarters (April to September) are as follows:

23.1 Technical Support for Uncertainty Analysis for TRAC-PF1/MOD1 (U.S. Rohatgi and W. Wulff)

Dr. U.S. Rohatgi attended a two-day meeting on code uncertainty evaluation methodology development on April 7-8, 1987. Two reports, one describing BNL assessment of TRAC-PF1 with separate effects tests and their relevance for TRAC-PF1/MOD1, and another describing the differences between constitutive relationships in TRAC-PF1 and TRAC-PF1/MOD1 were prepared. A QA document for TRAC-PF1/MOD1 was received and reviewed. The comments were sent to NRC. Dr. W. Wulff and Dr. U.S. Rohatgi attended a senior management meeting to discuss the uncertainty evaluation methodology and QA document on April 27-28, 1987 in Idaho Falls.

A procedure was developed to implement USNRC methodology for evaluating the uncertainty in the prediction of peak clad temperature (PCT) in the blowdown phase by the TRAC-PF1/MOD1 code. This procedure was presented to the USNRC in Washington, D.C. by Dr. Wulff. The meeting was also attended by Dr. U.S. Rohatgi. The tasks to be performed by Brookhaven National Laboratory in support of this uncertainty analysis were finalized and the work was started.

BNL will assess the uncertainty of the blowdown peak clad temperature caused by uncertainty in fuel stored energy and fuel thermal response and the uncertainties of recirculation pump performance and of critical flow through the break.

23.2 TRAC-BF1 Assessment

A USNRC account has been set up at INEL to run the TRAC-BF1 code there. Various steps to familiarize with INEL computing facility has been taken. The assessment of TRAC-BF1 will begin with the approval of the USNRC.

24. Plant Analyzer Development for BWR/2 and BWR/6 and Maintenance for BWR/4 (W. Wulff)

24.1 Introduction

This program is being conducted to develop and operate an engineering plant analyzer, capable of performing accurate, real-time and faster than real-time simulations of plant transients and Small-Break Loss of Coolant Accidents (SBLOCAs) in LWR power plants. The engineering plant analyzer has been developed by utilizing a modern, interactive, high-speed, special-purpose peripheral processor, which is designed for time-critical systems simulations. The engineering plant analyzer currently supports safety analyses and NRC staff training, but it can also serve as the basis of technology development for nuclear power plant monitoring, for on-line accident diagnosis and mitigation, and for upgrading operator training programs and existing training simulators.

Below is a brief summary of previous results and a detailed summary of achievements during the current reporting period.

24.2 Assessment of Existing Training Simulators (W. Wulff and H. S. Cheng)

The assessment in 1981 of then current simulator capabilities consisted of evaluating qualitatively the thermohydraulic modeling assumptions in the training simulator and comparing quantitatively the predictions from the simulator with results from the detailed systems code RETRAN.

The results of the assessment have been published earlier in three reports (Wulff, 1980; Wulff, 1981a; Cheng and Wulff, 1981). It had been found that the reviewed training simulators were limited to the simulation of steady-state conditions and quasi-steady transients within the parameter range of normal operations.

The comparison between PWR simulator and corresponding RETRAN results, carried out for a reactor scram from full power, showed significant discrepancies for primary and secondary system pressures and for mean coolant temperatures of the primary side. Good agreement was obtained between simulator and RETRAN calculations for only the early part (narrow control range) of the water level motion in the steam generator. The differences between simulator and RETRAN calculations have been explained in terms of modeling differences (Cheng and Wulff, 1981).

24.3 Acquisition of Special-Purpose Peripheral Processor and Ancillary Equipment (A.N. Mallen, R.J. Cerbone and S.V. Lekach)

The AD10 had been selected earlier as the special-purpose peripheral processor for high-speed, interactive systems simulation through integrating large systems of nonlinear ordinary differential equations. A brief description of the processor has been published in a previous Quarterly Progress Report (Wulff, 1981b). A PDP-11/34 DEC computer serves as the host computer. An IBM Personal Computer is used for graphics displays and for remote access via commercial telephone line and standard modem.

Two AD10 units, coupled directly to each other by a bus-to-bus interface and equipped with a total of 14 task-specific processors and one megaword of

memory, have been installed with the PDP-11/34 host computer, two 67 megabyte disc drives, a tape drive and a line printer. On-line access is facilitated by a model 4012 Tektronix storage oscilloscope terminal and a 28-channel signal generator. The system is accessed remotely via one DEC Writer terminal and up to four ADDS CRT terminals, two of which are also equipped with line printers. The IBM Personal Computer is used as a terminal and also to access the PDP-11/34 host computer remotely via commercial telephone lines and to generate labeled, multicolored graphs from AD10 results. A Tektronix 4115B multicolor graphics terminal had been installed for direct on-line display of system parameters generated by the AD10 at real-time or faster computing speeds, in the form of animated flow and control diagrams.

24.4 Model Implementation on AD10 Processor and Developmental Assessment

At first, a four-equation slip flow model for nonhomogeneous, nonequilibrium two-phase flow had been formulated and supplemented by constitutive relations from an existing BWR reference code, then scaled and adapted to the AD10 processor to simulate the Peach Bottom-2 BWR power plant (Wulff, 1982a). The resulting High-Speed Interactive Plant Analyzer code (HIPA-PB2) has been programmed in the high-level language MPS10 (Modul Programming System) of the AD10. After implementing the thermohydraulics of HIPA-PB2 on the AD10, we compared the computed results and the computing speed of the AD10 with those of the CDC-7600 mainframe computer. We achieved engineering accuracy at simulation speeds one hundred times larger than that of the CDC-7600 with the low-cost AD10 minicomputer (Wulff, 1982b).

It has been demonstrated (Wulff, 1982b) that (i) the high-level, state equation-oriented systems simulation language MPS10 is superior to FORTRAN and it compressed 9,950 active FORTRAN statements into 1,555 calling statements to MPS10 modules, (ii) the hydraulics simulation occupies one-fourth of available program memory, (iii) the difference between AD10 and CDC-7600 results is only approximately +5% of total parameter variations during the simulation of a severe licensing base transient, (iv) the AD10 is 110 times faster than the CDC-7600 for the same transient, and (v) the AD10 simulates the BWR hydraulics transients up to 10 times faster than real-time process speed. It has been demonstrated that even after the inclusion of models for neutron kinetics, thermal conduction in fuel, balance of plant dynamics and controls, the AD10 still achieves 9 times real-time simulation speed for all transients reported earlier (Wulff, 1983c). The program includes now more than 4,500 calling statements to MPS10 modules (subroutines).

After the feasibility demonstration, we converted the original slip flow model to the drift flux model and expanded the simulation capabilities. The expanded version is called HIPA-BWR/4 and simulates all BWR/4 reactor plants with Mark I containments. The simulation includes neutron kinetics (point kinetics), thermal conduction in fuel elements, reactor hydraulics, acoustical effects in the steam lines and the safety and relief valve logic (Wulff, 1982c; 1983a and Wulff et al., 1984), and further, the balance of plant components, such as the turbines, condensers, feedwater trains, containment and suppression pool, as well as the control and plant protection systems as shown in Figure 24.1 (Wulff, 1984). The schematic in Figure 24.2 shows the control systems which are simulated in HIPA-BWR/4. Also included in the simulation is the boron tracking capability (Wulff, 1983d; 1984a) and the prediction of the minimum critical power ratio (Wulff, 1986a).

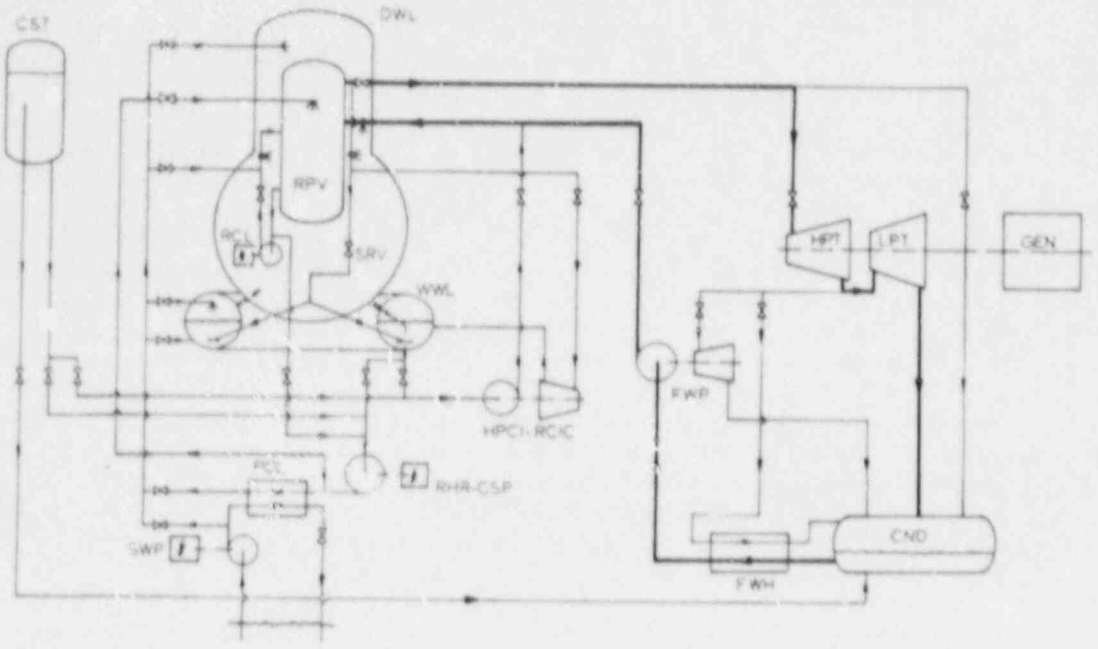

Figure 24.1 Overall Flow Schematic for Plant Analyzer Simulations of BWR/4 Plants with Mark I Containments

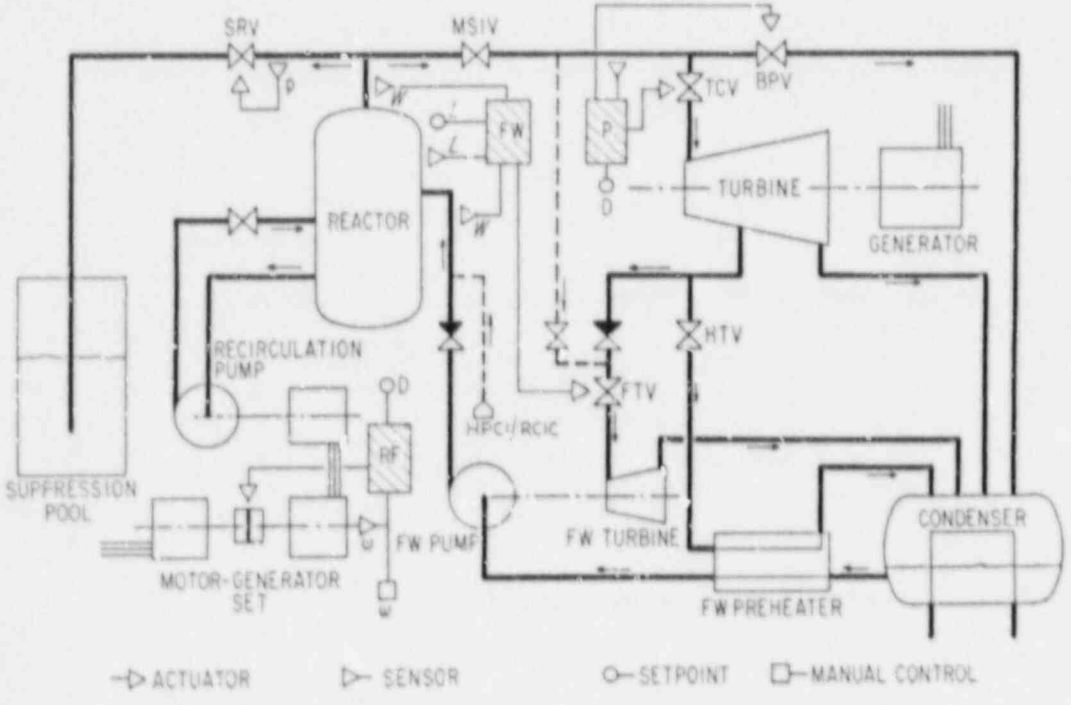

Figure 24.2 Primary Flow Schematic and Control Blocks for BWR Simulation; FW - Feedwater Controller, P - Pressure Controller, RF - Recirculation Flow Controller

Extensive developmental assessment has been carried out for HIPA-BWR/4. Thirty-seven transients have been documented (Wulff, 1984a; 1984b and Wulff et al., 1984) comprising the comparisons of plant analyzer results with calculations from GE, TRAC-BD1, RELAP5 and RAMONA-3B. The comparisons have shown that the plant analyzer can simulate a large number of severe abnormal transients and that it produces the same results as TRAC, RELAP5 and RAMONA-3B for a large class of transients, but at a considerably lower cost and in a much shorter time: 37 transients have been simulated, checked for consistency and documented with hard-copy graphs, using the plant analyzer, in less than four days by two staff members.

The graphics capabilities allow the on-line display of two parameter variations versus (indefinitely long) time on the four-color monitor of the IBM PC. The parameters are arbitrarily selected and displayed in separate colors on labeled diagrams. The graphics capabilities permit the storage of either 15 selected parameters in IBM PC memory or of 150 parameters on disc, while a simulation is being performed, respectively, at the simulation speed nine times or four times greater than real-time process speed.

NRC staff has maintained, however, that the two-parameter display by the IBM PC is inadequate to convey a complete picture on the overall conditions of the plant. A higher graphics resolution on a larger monitor screen is needed to display dynamically animated flow and control diagrams, showing coolant levels, valve alignments and automatic trip conditions for pumps, valves and control systems. To display such signals generated by the AD10 system, a Tektronix 4115B terminal had been authorized and installed late in 1985 and was being programmed. Unfortunately, however, the NRC decided in March 1986 to request the transfer of BNL's Tektronix 4115B terminal to Scientech in Idaho Falls. The graphics development work on the Tektronix 4115B terminal is, therefore, terminated. The terminal has been transferred to Scientech.

Finally, we developed the software for remote access of the plant analyzer via commercial telephone lines, using the IBM personal computer. The necessary accessories and a condensed user guide for remote access were reported earlier (Wulff, 1984d). We demonstrated in the previous reporting period that the plant analyzer is fully operational from the keyboard of the IBM. Two arbitrarily selected parameters are displayed as functions of time during the calculation, while 150 additional parameters are stored on disk in the host computer for later replay. All operator actions and malfunctions can be entered on-line without interrupting the simulation. The plant response to input changes is instantly displayed. Up to 15 successive time plots of the same two parameters can now be stored in the IBM PC and combined into one plot. One can also page back during a simulation to any previously displayed plot, without interrupting the simulation.

The remote access and simulating capabilities of the plant analyzer have been demonstrated successfully at several locations in the U.S., in Europe and in East Asia. Even though the plant analyzer has only 16-bit precision ($\pm$0.00003) for all arithmetic operations except integration (48-bit precision), it has been shown to maintain steady-state conditions free of drift for 20 hours.

Specific activities during the current reporting period are described below in Sections 24.5, 6, 7, 8, and 9.

24.5 Documentation (H. S. Cheng)

The basic description of the BNL Plant Analyzer can be found in the BWR Plant Analyzer report [Wulff, Cheng, Lekach and Mallen, 1984]. This report describes the mathematical models for neutron kinetics, thermal conduction in fuel and structures, thermohydraulics of two-phase flow coolant dynamics in the pressure vessel, the steam line dynamics, turbines, condenser, feedwater preheater, feedwater pumps, valves, motor-generator sets for recirculation, recirculation pumps, control systems, protection systems and boron transport. The report also contains a description of the special-purpose computer, the AD10, and its direct access operation. Since the publication of this report, all thermophysical property relations as given in Section 3.3.10.5 have been replaced by the full relations of the standard ASME Steam Tables [Meyer, McClintock, Silvestri and Spencer, 1977].

Extensions to the level tracking model [Wulff, 1985a] and models for computing Minimum Critical Power Ratio (MCPR) [Wulff, 1986a] and for critical flow through breaks for liquid water, two-phase mixture and pure vapor [Wulff, 1986b] have been published earlier.

Important containment modeling aspects are also presented in previous quarterly progress reports [Wulff, 1985c, 1986b]. Remote access capabilities of the Plant Analyzer are found in [Wulff, 1985b, 1985d].

A computer-based input data directory is now available which contains 412 input parameters, describing component geometry, operating parameters, component characteristics, processes (kinetics parameters), control parameters, specifying trip set points and safety systems parameters, and, finally, defining run specification parameters [Internal Memorandum, Cheng to Plant Analyzer Files, "Revision 1 of Input Parameters for HIPA-BWR4," October 3, 1986]. This directory is treated as a "living document" and distributed to users of the Plant Analyzer either via standard floppy disk (IBM PC-compatible), or via remote access to the Plant Analyzer. Printed copies are also available upon request.

A second computer-based document [Internal Memorandum, Cheng to Plant Analyzer Files, "Steady-State Guidelines for BNL Plant Analyzer," October 8, 1986] has been developed to aid new users in obtaining initial conditions for the BWR Plant Analyzer. This memorandum is also distributed via floppy disk or by telephone from the Plant Analyzer. This and the above memoranda are accessible to all users who have an IBM PC set up for remote operation of the Plant Analyzer.

A catalog has been completed for all the functions which are pretabulated and stored in the Plant Analyzer for high-speed interpolation during a simulation. Of particular interest are all plant-specific functions, such as those describing motor, pump or valve characteristics, as these functions are part of the input data set. This new catalog facilitates the use of the Plant Analyzer for any other BWR plant.

During this reporting period, we documented the results of validations against plant data from BF-1 in two memorandums.

24.6 Validation of Plant Analyzer

24.6.1 Recirculation Pump Trip

During this period, we performed HIPA-BWR/4 validations against the plant data from BF-1. The first validation was done against a Recirculation Pump Trip (RPT) test (Dallman, 1987) initiated from the full power conditions. The results are presented in Figures 24.3 through 24.8 along with the test data. The transient is characterized by a pump coastdown as shown in Figure 24.3. The Plant Analyzer simulation closely follows the test data.

Discussion of Results

The RPT induces a rapid reduction in the core inlet flow as illustrated in Figure 24.4. The agreement with the plant data is quite good. The decrease of core inlet flow resulted in more steam generation in the core, causing a rapid decrease in the reactor power due to void feedback, which is counteracted by Doppler feedback. Both the void and the Doppler feedback coefficients must be right to produce the correct reactor power response as shown in Figure 24.5.

The decreasing reactor power causes a rapid reduction in the steamline flow as seen in Figure 24.6, and hence the system pressure (Figure 24.7). The data comparison for the steamline flow is very good. However, the BPA tends to overpredict the system pressure relative to the test data. The maximum discrepancy in only 6 psi, so the agreement is considered fairly good.

The downcomer collapsed liquid level is most difficult to predict. The comparison with the plant data is not as good as the other parameters, as shown in Figure 24.8. The qualitative agreement is good, but the test data are, on the average, a few inches higher than the BPA prediction, with the maximum discrepancy of about 5 inches.

24.6.2 Generator Load Rejection

The second validation was done against a generator load rejection (GLR) test (Forkner, 1981), also initiated from the full power conditions. Figures 24.9 through 24.14 show the comparisons between the Plant Analyzer simulations and the test data. The transient is characterized by a sharp reduction in steam flow after the Turbine Stop Valve (TSV) fast closure at 1.81 s as shown in Figure 24.9. The BPA simulation closely follows the test data until 7 s. Thereafter, the predicted flow starts to decrease and reduces to zero at 10 s when the MSIVs are fully closed, whereas the test data indicate that about 15% of steam flow remains. It is thought that the steamline flow described by the data is erroneous after 10 s. Flow cannot reach the flow measuring devices once the MSIVs have closed.

Figure 24.10 shows the system pressure response to the generator load rejection. The BPA simulation compares favorably with the test data, with BPA slightly overpredicting the peak. The initial decline in pressure is due to the opening of the bypass valves. The ensuing rapid overpressurization is the result of the fast closure of the TSV at 1.81 s. This pressurization is limited by the relieving action of the Bypass Valve (BPV) and two Safety Relief

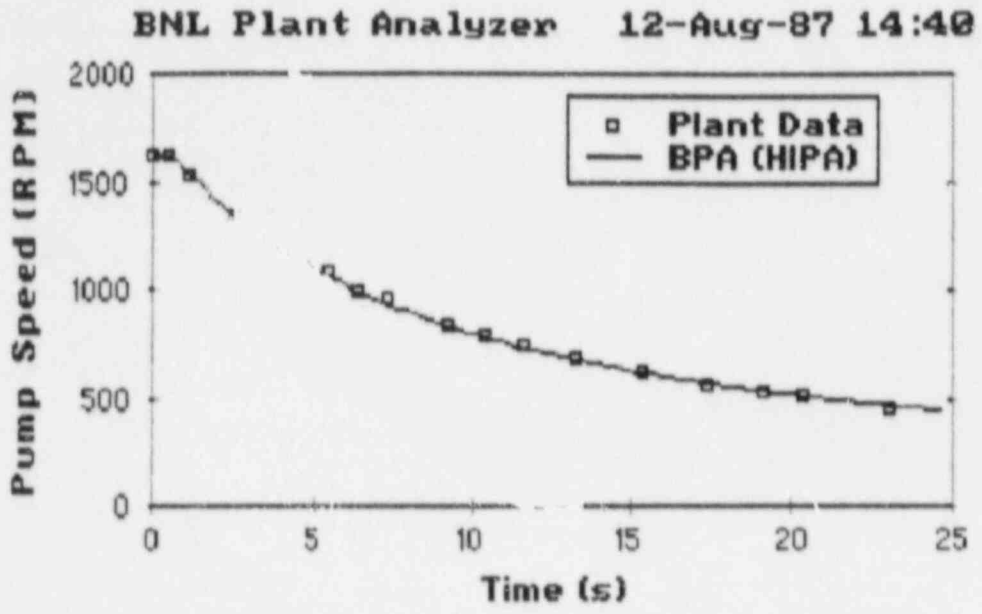

Figure 24.3 Pump Trip Test Data Comparison - Pump Speed

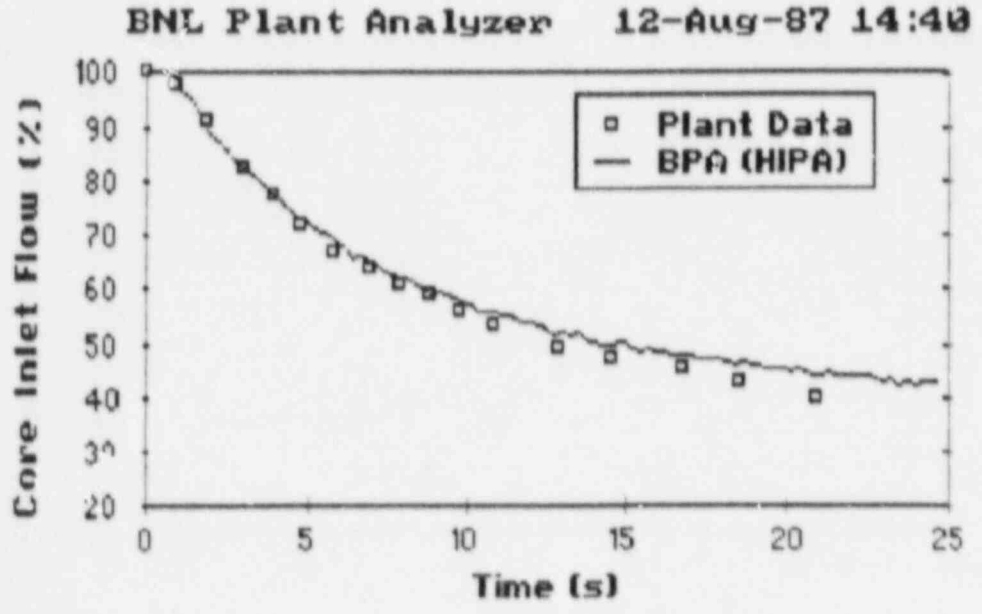

Figure 24.4 Pump Trip Test Data Comparison - Core Inlet Flow

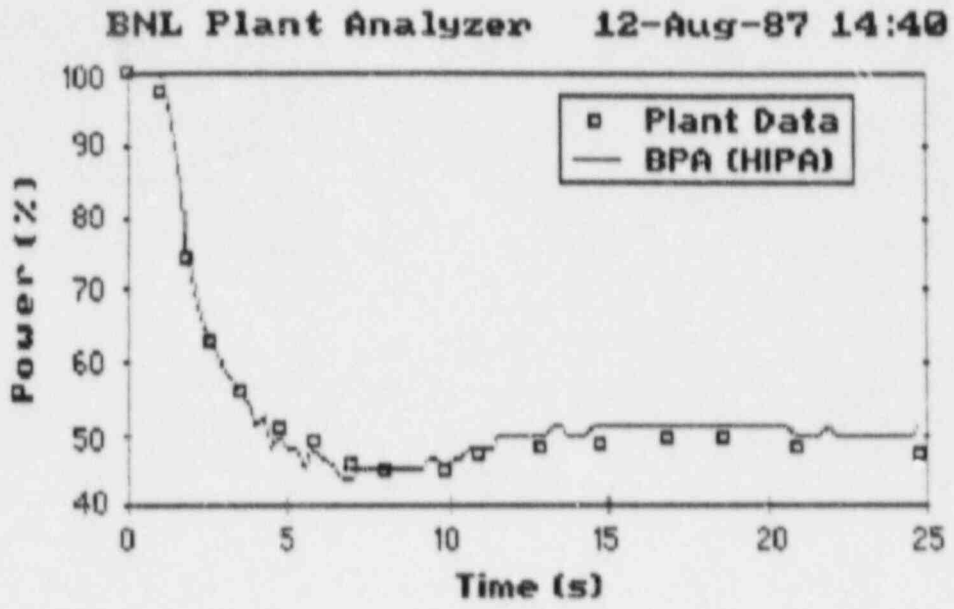

Figure 24.5 Pump Trip Test Data Comparison - Reactor Power

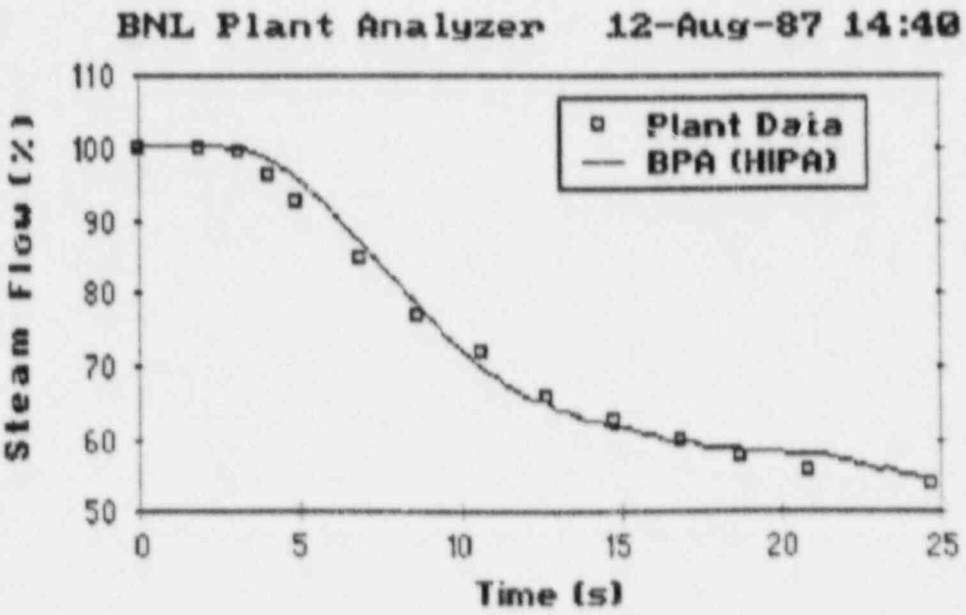

Figure 24.6 Pump Trip Test Data Comparison - Steam Line Flow

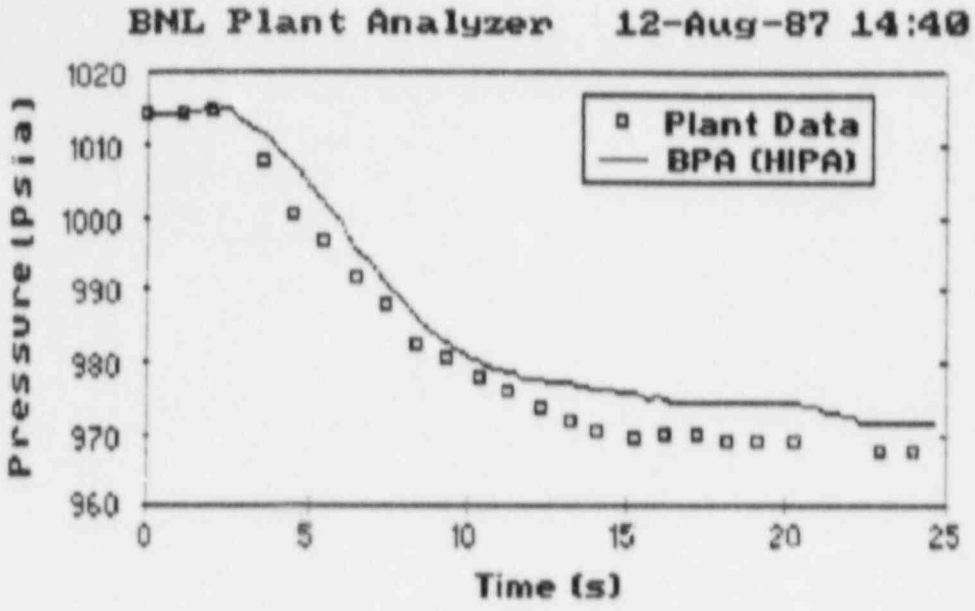

Figure 24.7 Pump Trip Test Data Comparison - System Pressure

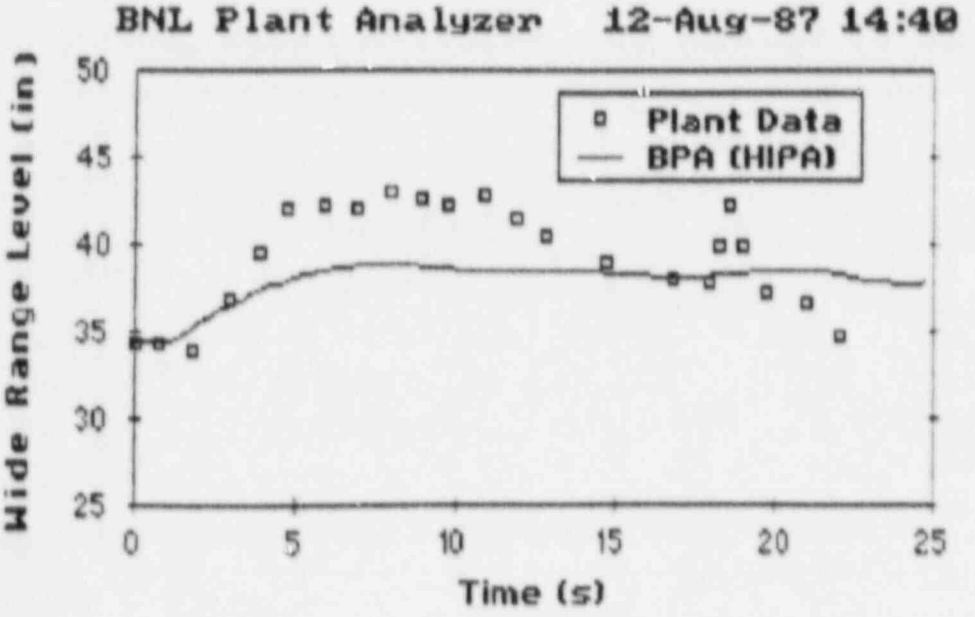

Figure 24.8 Pump Trip Test Data Comparison - Water Level

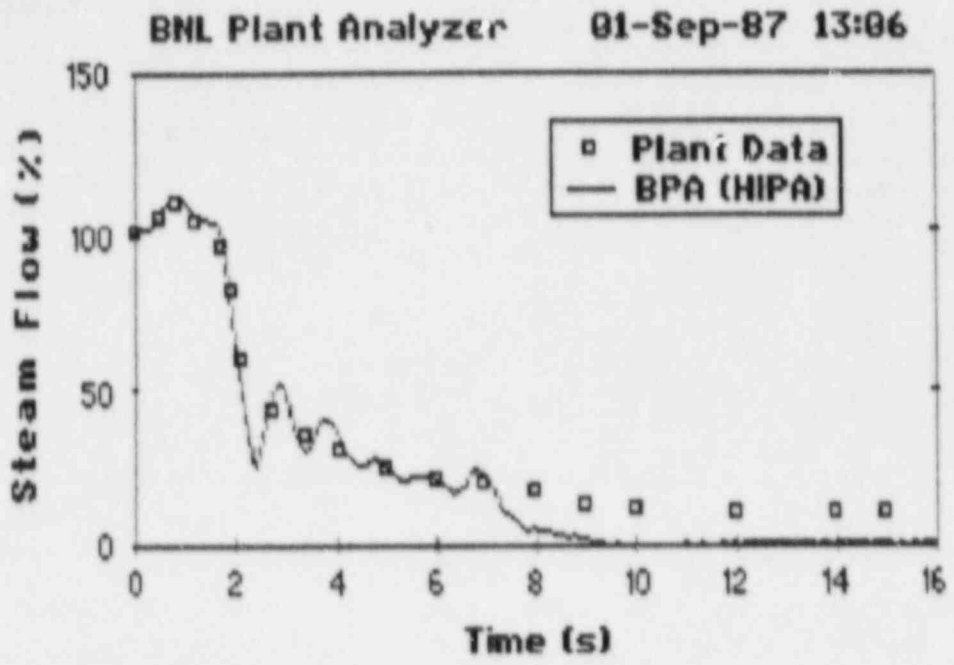

Figure 24.9 Generator Load Rejection Test - Steam Line Flow

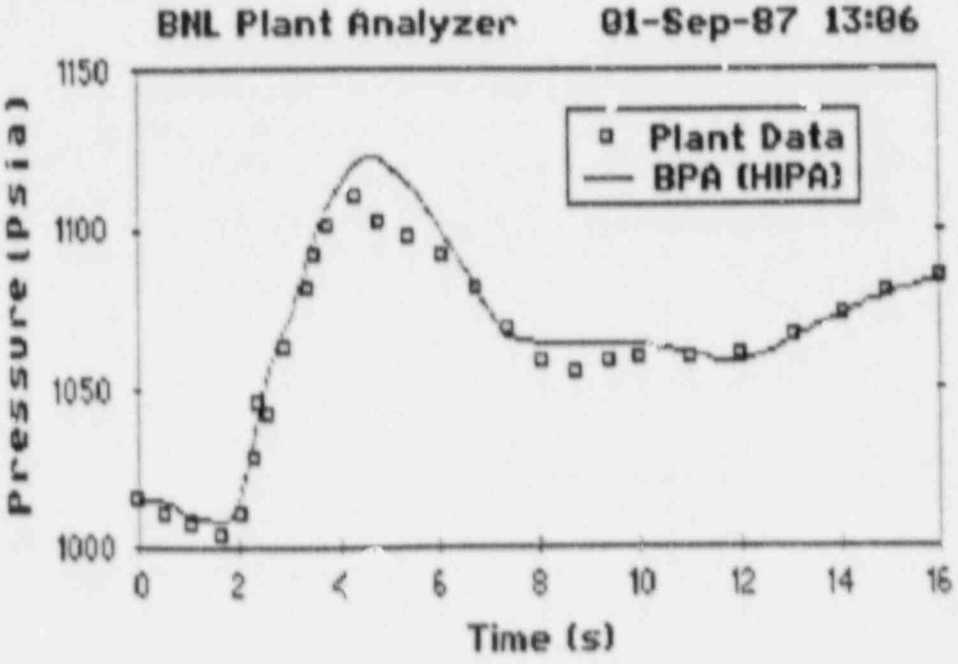

Figure 24. 10 Generator Load Rejection Test - System Pressure

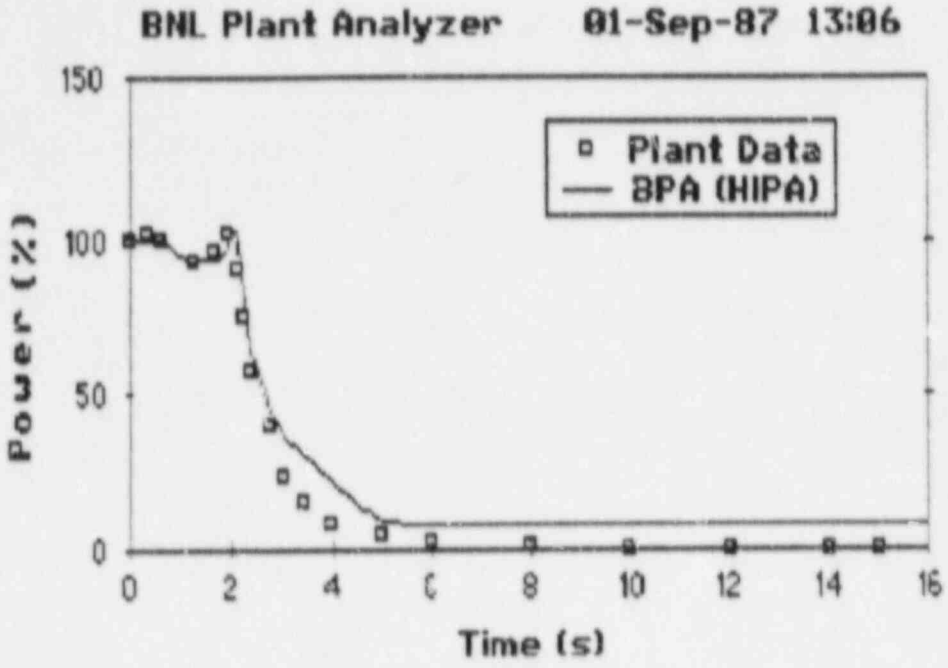

Figure 24.11 Generator Load Rejection Test - Reactor Power

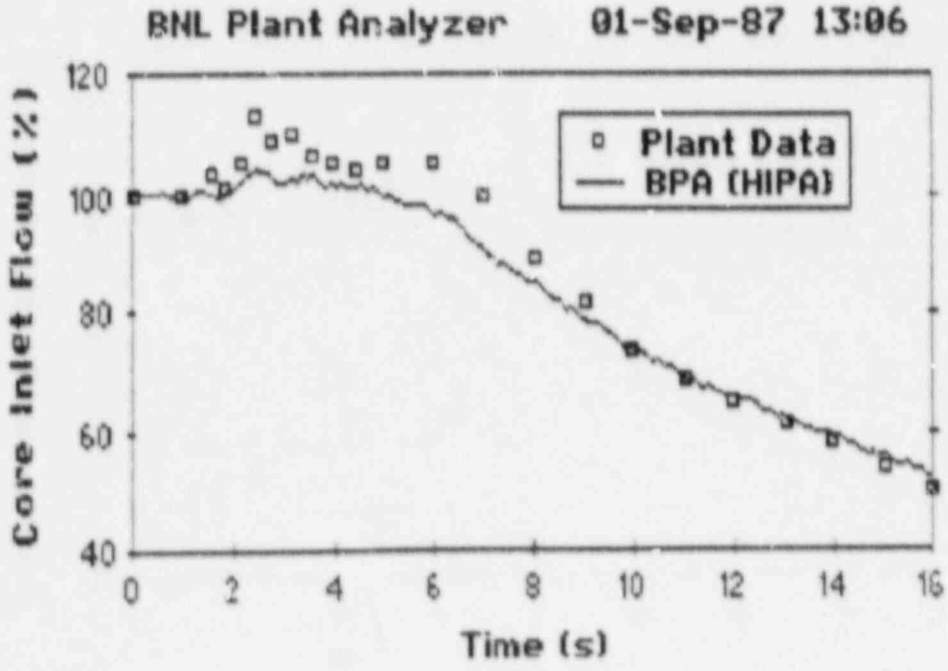

Figure 24.12 Generator Load Rejection Test - Core Inlet Flow

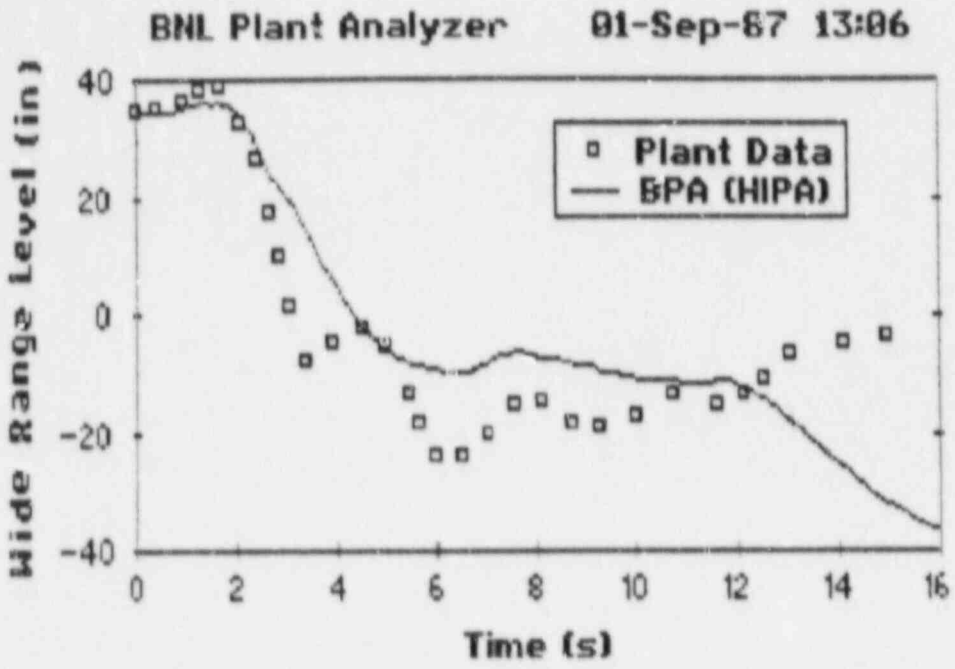

Figure 24.13 Generator Load Rejection Test - Water Level

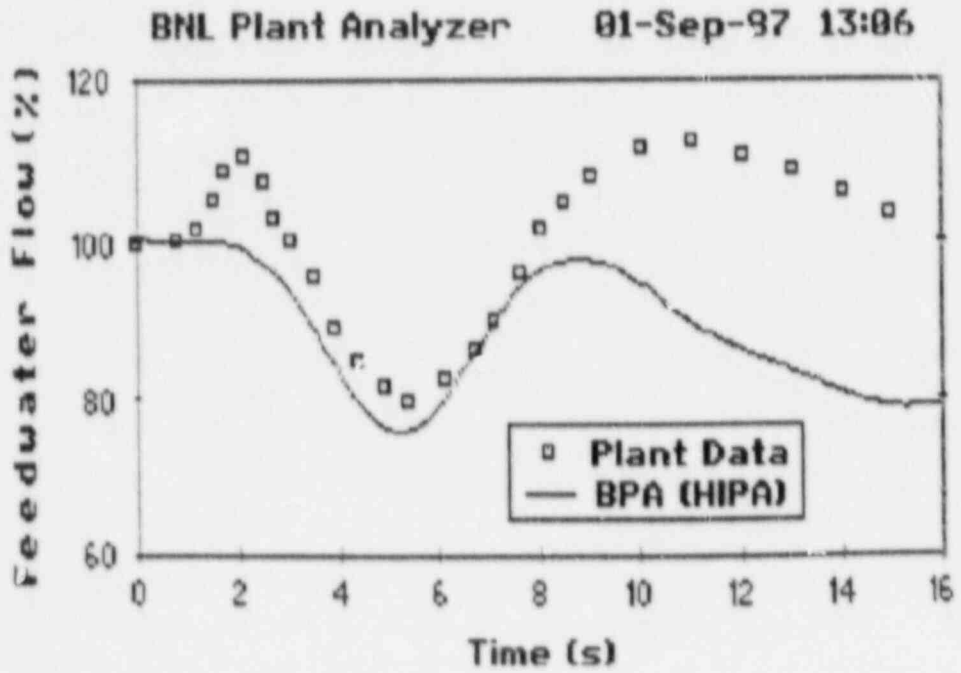

Figure 24.14 Generator Load Rejection Test - Feedwater Flow

Valves (SRVs). The MSIV closure causes the pressure to flatten out at 8 s. The repressurization at 12 s is due to the reclosing of the SRVs.

Figure 24.11 shows the reactor power response to the GLR. The initial dip in the reactor power is the result of more steam production in the core, as seen in Figure 24.9, induced by the initial pressure decline (see Figure 24.10). The small power spike at 2 s is due to the void collapsing caused by the rapid overpressurization but is arrested by reactor scram at 1.63 s with 0.27-s delay. The reactor power decreases rapidly after the scram to the decay heat level. Note that the test data are interpreted from the Average Power Range Monitor (APRM) signals which do not include the decay heat. Overall, the agreement between the BPA simulation and the test data is good.

The core inlet flow response to the load rejection is shown in Figure 24.12. The BPA simulation compares favorably with the test data. This implies the adequacy of the recirculation flow dynamics of BPA, consistent with the finding in the comparison of the BPA simulation with the recirculation pump trip test data.

The comparisons in the water level and feedwater flow responses are not as favorable. Figure 24.13 shows the wide range level response. The predicted level does not fall off as rapidly as the test data nor low enough to initiate the L2 low level trip (about -24 in.) at 6.4 s. In fact, the L2 setpoint was adjusted in the simulation to initiate the trips (MSIV closure and RPT) as indicated in the test. Figure 24.14 shows the feedwater flow response to the GLR. While the BPA simulation follows the same transient behavior as the test data, it does not predict the overshoot at 2 s and generally underpredicts the feedwater flow. The reason for the discrepancies is not fully understood at present. The overshoot could be predicted by reducing the damping coefficient of the Feedwater Turbine Valve (FTV) actuator, but the feedwater flow would become more oscillatory.

24.6.3 BWR/2 Assessment

The BWR/2 version of the Plant Analyzer (HIPA-BWR/2) has also been benchmarked against plant data from a tubine trip test conducted at the Nine Mile Point-1 Nuclear Power Station (NMP-1). The results are presented in Figures 24.15 through 24.19, which are reproduced here from the MS Thesis of M. Byram (1987).

The power response from the test data and the HIPA results can be seen in Figure 24.15. It should be noted that the power response from the test data is fission power, while the power response from HIPA is the thermal power. This should make little difference, since the fission power is proportional to the thermal power and is presented here as relative power. The difference lies in the prediction of decay heat which can be seen in the HIPA calculations, but not in the plant data, as the power goes to zero at approximately 5 s into the transient.

In the turbine trip test data it can be seen that the fission power for the test was initially 117.5% of rated, so that as soon as the power rose due to the turbine trip causing a rise in pressure and a subsequent collapse of core voids, the reactor scrammed on high fission power at 120% of rated. This was simulated in HIPA by setting the high fission power setpoint to 102.5% of

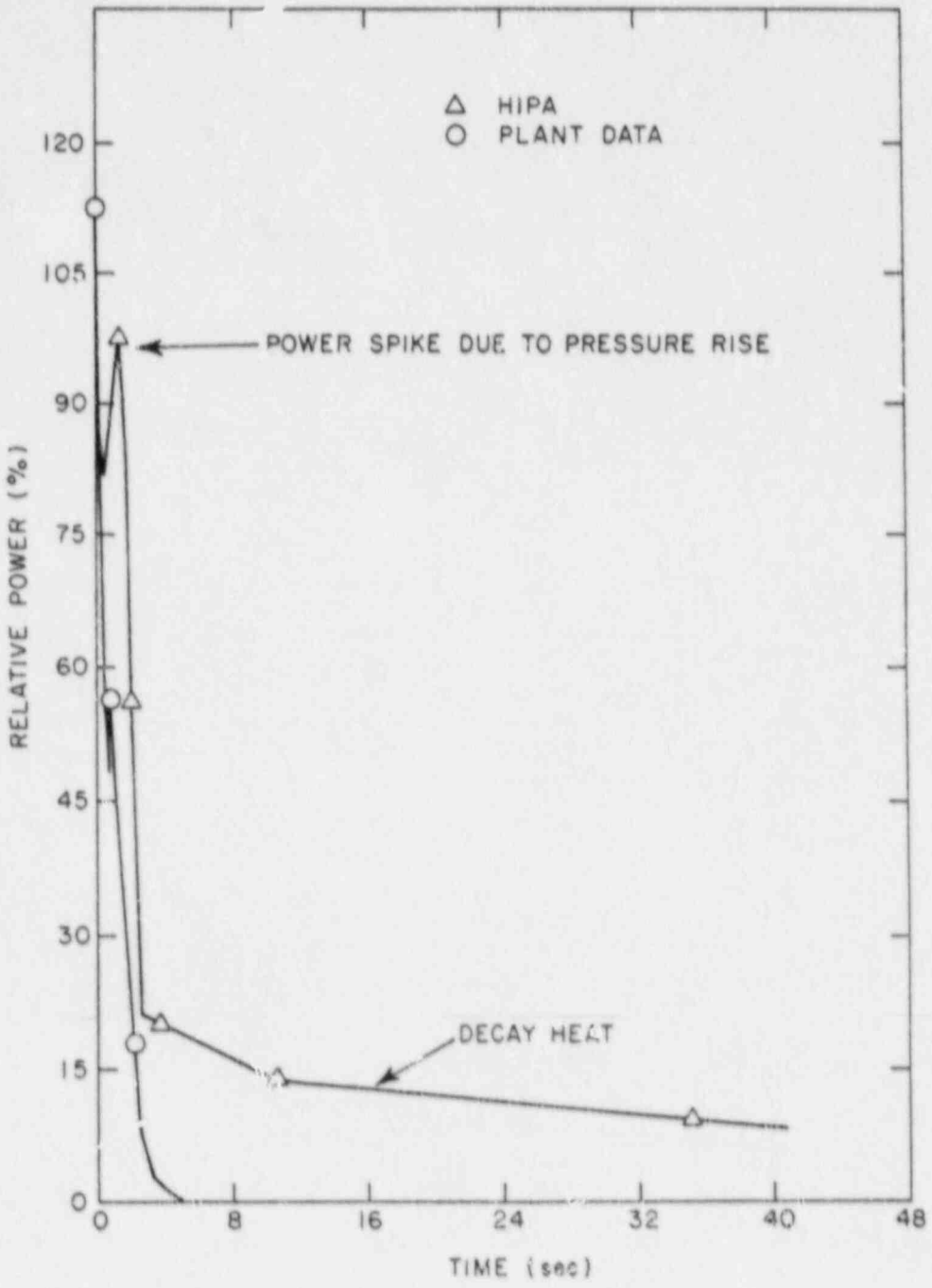

Figure 24.15 Power Response in Turbine Trip with Bypass Transient

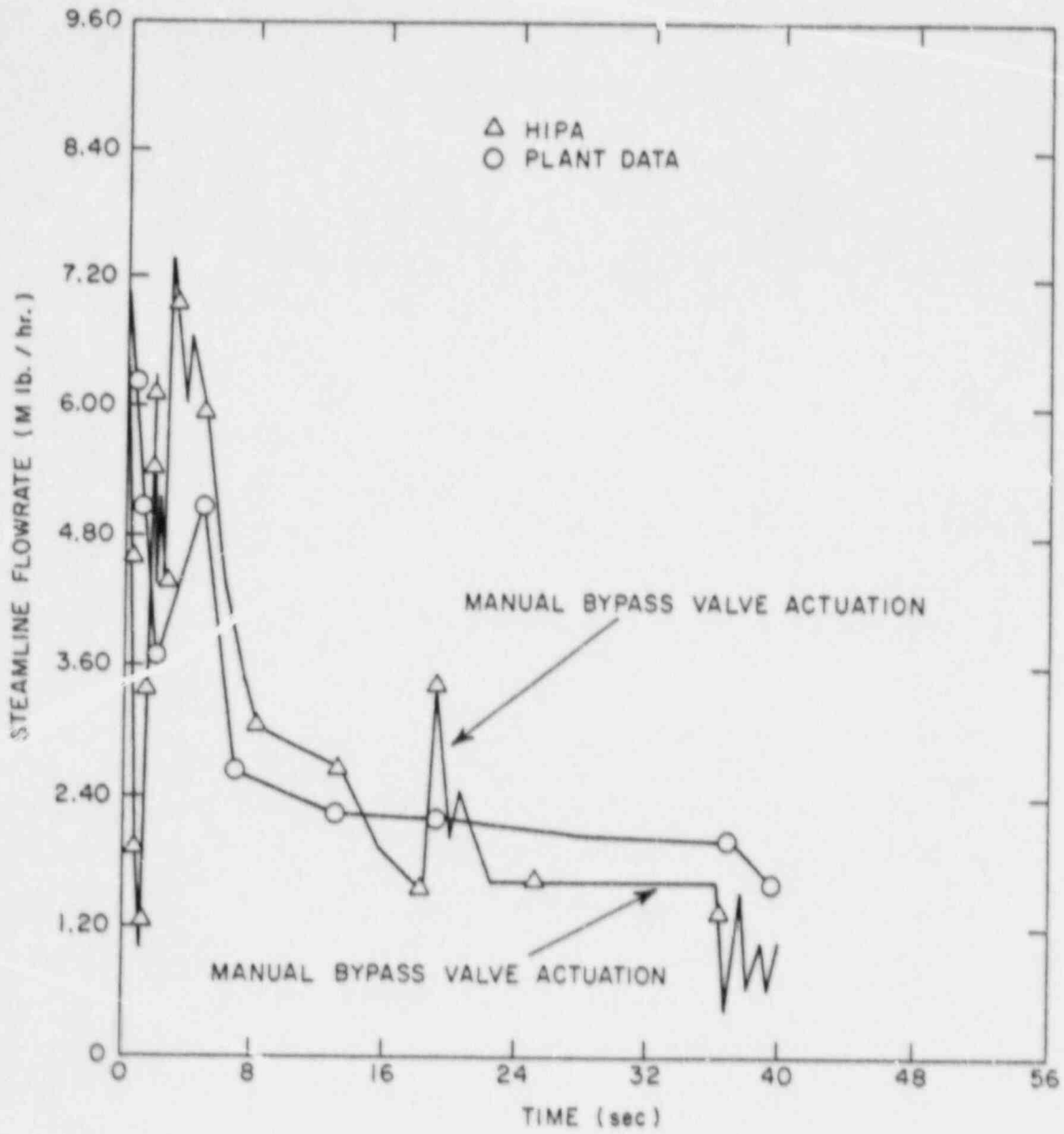

Figure 24.16 Steam Flow Response in Turbine Trip with Bypass Transient

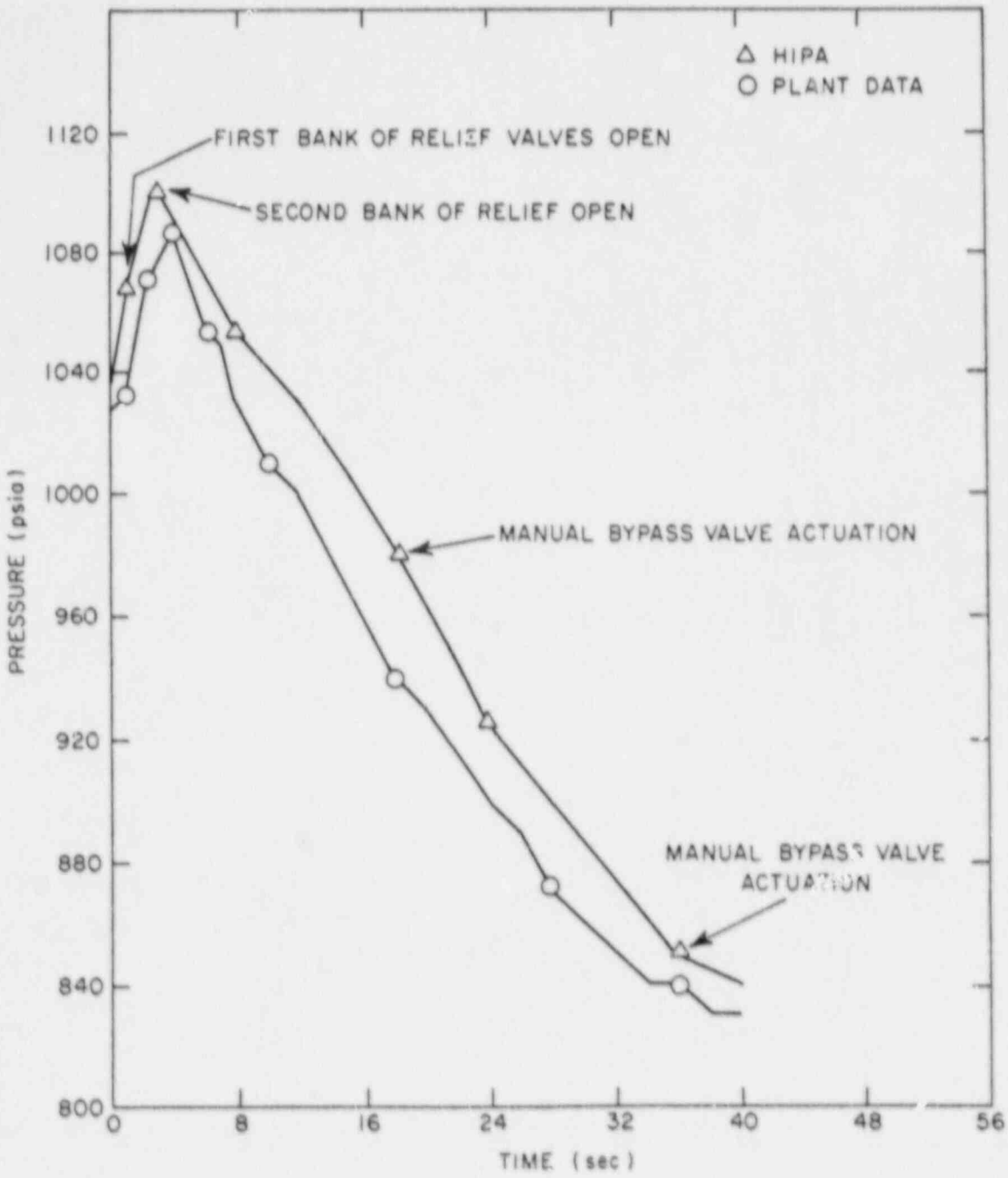

Figure 24.17 Pressure Response in Turbine Trip with Bypass Transient

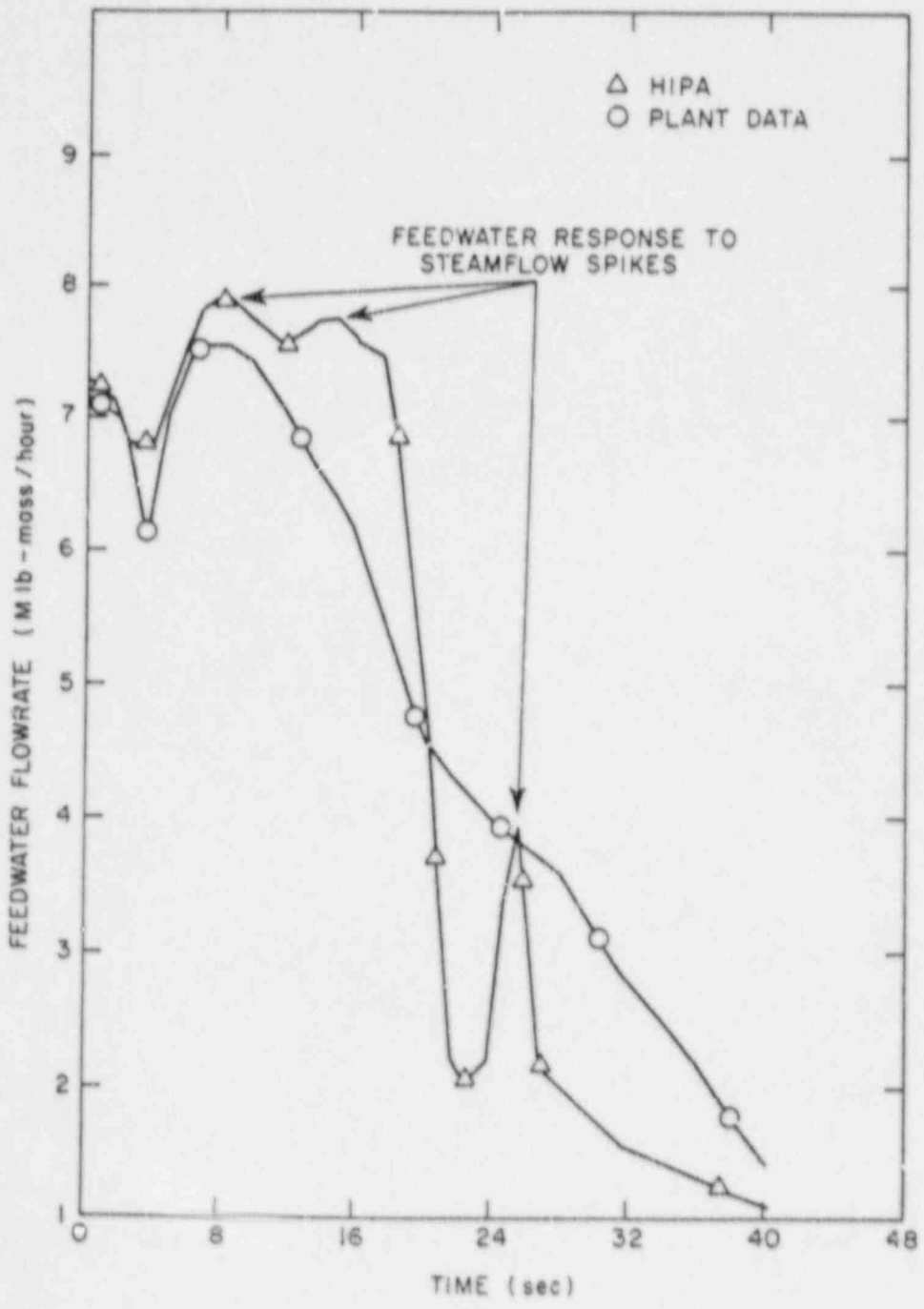

Figure 24.18 Feedwater Flow Response in Turbine Trip with Bypass Transient

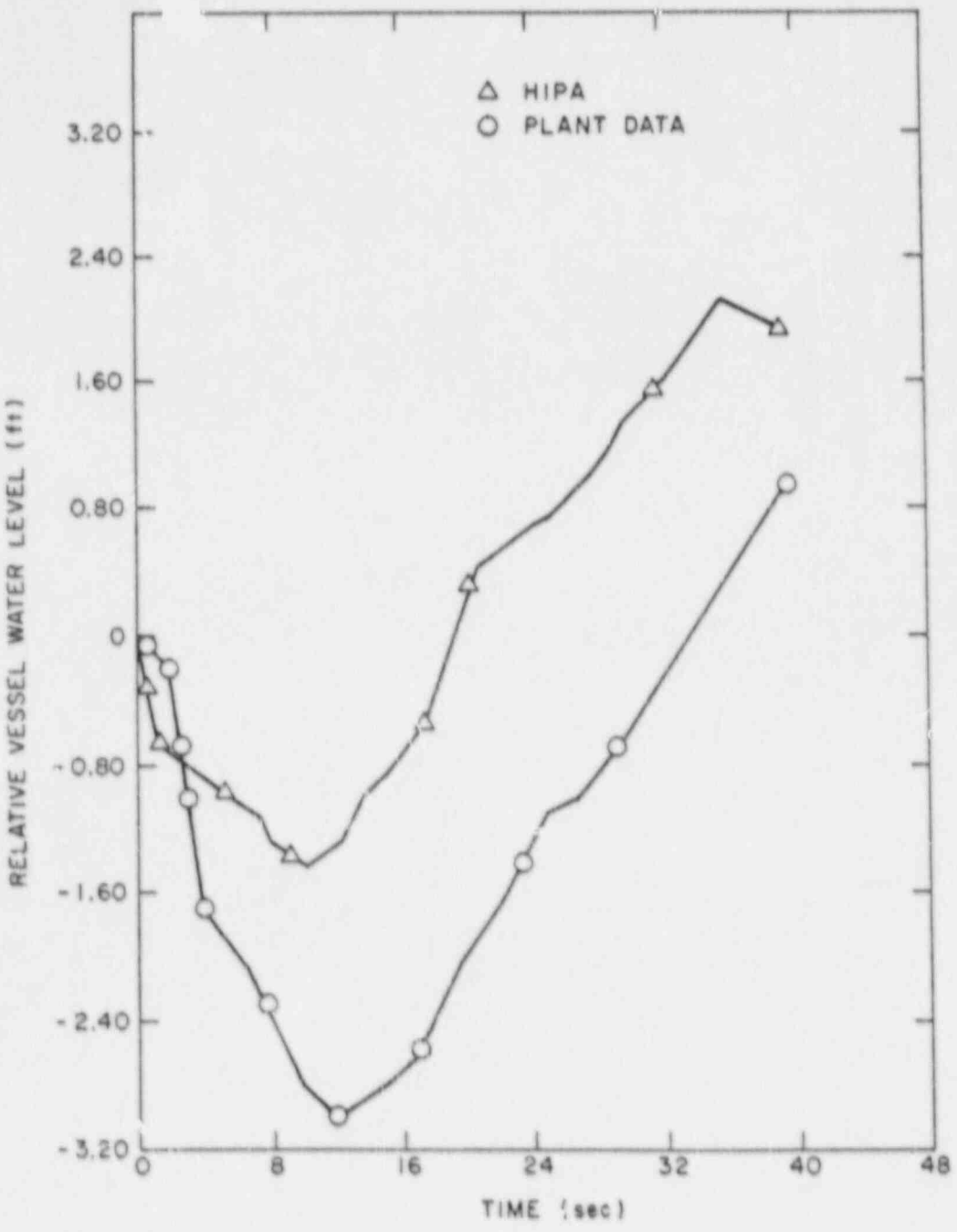

Figure 24.19 Reactor Vessel Water Level Response in Turbine Trip with Bypass Transient

rated. This setting caused a scram so quickly that the power rise was not detected. Both sets of data also show a power spike about one second after the turbine trips due to the pressure rise and subsequent collapse of voids in the core.

The fission power level in the plant data is seen to fall off to zero by about 5 s after the power spike. The HIPA results predict the thermal power to have fallen to approximately 7% of rated after 40 s.

The steam flow response is shown in Figure 24.16. A change in the steam flow is usually in direct response to a change in power level but can also be due to valve actuations in the steam flow path. A good example of the steam flow spike due to valve actuation can be seen at about 19 s into the transient as the bypass valve is closed from its original setting.

Both data and predictions show a sudden fall in steam flow on closure of the turbine control valve. However, HIPA predictions indicate a sharper fall than the plant data. The HIPA results also predict a higher peak steam flow rate with two lesser peaks preceding the largest one, and one lesser peak following it. This is a reasonable prediction when compared to the power spikes. The peak steam flow predicted by HIPA is 101% of the initial steam flow while the peak for the plant data was given to be 71% of the initial steam flow, both of these peaks occurring at about 6 s into the transient.

HIPA and the plant data agree as the steam flow falls after the peaks occur and settles down to around 25% of the initial steam flow. The HIPA results, however, exhibit a more sporadic steam flow due to the manual bypass valve actuation at approximately 19 and 35 s into the transient.

The system pressure response is shown in Figure 24.17. Here the HIPA results agree fairly well with the plant data as the pressure is seen to peak at approximately the same time for all three sets of data. After the turbine stop valve was closed and the turbine bypass was opened, the plant data show that the system pressure rose from 1028 psi to approximately 1087 psi over 3 s, yielding a pressurization rate of 19.7 psi/s. The analyzer predicted a similar pressurization rate of 20.3 psi/s as the pressure rose from 1031 psi to 1098 psi over 3.3 s. Plant data reveal that the first bank of relief valves was actuated at 1075 psi as the setpoint had drifted from 1090 psi. This was seen in the HIPA results as well. In addition, the HIPA results predicted a second relief valve actuation at 1095 psi.

After the turbine trip, the plant went into the hot shutdown mode and passed pressure control to the mechanical pressure regulator and the bypass opening jack. This was modeled in HIPA by interactive control of the bypass valve. Subsequent to pressure peaking, at about 4 s after the turbine trip, the plant data give a depressurization rate of 10.13 psi/s up until 19 s. During the same period, HIPA predicts a depressurization rate of 8.28 psi/s. After this point, the pressure continues to drop at a slightly faster rate and then begins to stabilize at about 840 psi. It should be noted here that the MSIV closure setpoints were lowered in HIPA from 850 psi to a much lower value to model the hot shutdown mode in the plant data.

It can be seen from Figure 24.18 that the feedwater flows predicted by the analyzer give similar trends as the plant data. The dependence of the feedwater flow on the steam flow can be seen as the feedwater flow dips at about 5 s after the turbine trip in response to the steam flow decreasing at the very beginning of the transient. The feedwater flow is seen to drop to a lower point for the plant data due to the larger duration of the steam flow at very low levels, with HIPA predicting only a 0.5 Mlbm/h drop in feedwater flow for a duration of about 2 seconds. The plant data give a drop of 1.09 Mlb/h but for only a small fraction of a second as it rises to a peak of 7.52 Mlb/h at about 8 seconds. HIPA also predicts the subsequent rise in the feedwater flow rate to a level of 7.91 Mlb/h at approximately the same time. However, HIPA predicts two peaks as the two peaks in the steam flow are responded to.

After the feedwater peak occurs at approximately 8 seconds into the transient, the feedwater control system switches into HPCI mode as the turbine driven pump coasts down. Since the plant was placed into the hot shutdown mode, the data suggest that the HPCI system was shut off after initiation. In HPCI mode, the control of feedwater flow switches from the three element control of: steam flow, feedwater flow, and reactor vessel level, to control of the feedwater motor driven pumps on reactor vessel level. HIPA results, however, reveal that the feedwater system here is completely separate from the HPCI system and that it continues to operate in the three-element control mode after turbine trip. This results in a more sporadic feedwater flow curve than seen in the plant data, but because the steam flow falls off in the overall trend, so does the feedwater flow, matching the plant data's trends fairly well. The spike in the feedwater flow around 25 seconds is due to the spike in the steam flow around 20 seconds.

The results for the prediction of the reactor vessel water level response to the transient are presented in Figure 24.19. It can be seen that the trends from the HIPA results and the plant data agree reasonably well, as HIPA predicts a minimum to occur at approximately 11 seconds, and the plant data give a minimum at about 12 seconds. The magnitude of these minima differ by over 1.5 feet, however, as HIPA predicts -1.43 ft and the plant data give a minimum of -3.00 ft below the normal water level. It is difficult to explain this, since there is no information available on the core average void behavior from the plant data. Perhaps the core average void predicted by HIPA is calculated to be higher than that of the turbine trip data, not allowing the level to drop to the same position as seen in the plant data. In any case, the level predicted by HIPA responds the same as that of the plant after the minimum occurs, with the plant giving a rise of 0.139 ft/s compared to 0.138 ft/s as predicted by HIPA over the period of 26 seconds after the minimum level prediction. HIPA predicts the level to fall off at about 38 seconds probably due to a collapse of voids, following a sudden influx of cold feedwater at about 26 seconds.

24.7 Remote Access User Service (I.S. Cheng and A.N. Mallen)

Niagara Mohawk has continued to use the BNL Plant Analyzer for the Nine Mile Point-1, BWR/2 power plant. BNL has assisted in the conversion from BWR/4 to BWR/2 recirculation systems, that is from pump-speed control to flow control by control valve.

The Consejo de Seguridad Nuclear in Spain, Madrid, has an engineer visiting at BNL. His objectives are to set up the BNL Plant Analyzer for simulating the Cofrentes BWR/6 power plant in Valencia, Spain, and to facilitate remote access from Madrid to the Plant Analyzer.

Plant and operating parameters have been compiled for the Cofrentes reactor. Controls for pressure and for feedwater regulations of the Cofrentes BWR/6 plant have been compared with the currently implemented controls for the purpose of identifying differences and needed modifications in the control models. The comparison is based on control block diagrams used previously for computer simulations of the Cofrentes control system. It has been found that valve actuators are represented by first-order (inertia-free) systems in the Cofrentes reference diagrams while the HIPA code of the Plant Analyzer employs second-order systems. Also, the Cofrentes control system contains in the pressure regulator a compensator for the acoustic effects in the steam line. HIPA does not have such a compensator.

Work has been completed on the changes needed in the recirculation flow regulation (power regulation) for the Cofrentes BWR/6.

24.8 Promotional Activities

The BWR Plant Analyzer has been presented and demonstrated to representatives from the International Atomic Energy Agency in Vienna, from Electricite de France (EdF) and to a class of nuclear engineering seniors from Manhatton College.

The Taiwan Power Company (TPC) is expecting governmental approval of the cooperative program for developing BWR and PWR simulation capabilities on the AD100 special-purpose peripheral processor from Applied Dynamics International in Ann Arbor, Michigan. The program involves besides BNL and TPC also the Institute of Nuclear Energy Research (INER) and the National Tsing-Hua University (NTU).

The New York Power Authority [member utility of the Empire State Electric Energy Research Corporation (ESEERCO)] is preparing to use the Plant Analyzer for its Fitzpatrick plant. ESEERCO is evaluating BNL's proposal for PWR simulation.

Grumman Aerospace Corporation has decided not to bid on the development of a nuclear reactor control and instrumentation test facility for Bettis Atomic Power Laboratory because the scope of the development was limited by Bettis to existing technology and did not allow for the utilization of advanced developments as intended by Grumman and BNL.

24.9 Future Plans

Model assessments and needed improvements will be continued. Work will be continued to adapt the Plant Analyzer to the Cofrentes plant.

The Plant Analyzer will be presented and demonstrated to domestic industries and foreign institutions interested in nuclear power simulation for the purpose of promoting cooperative programs directed toward PWR simulations.

REFERENCES

BYRAM, M. E. (1987), "Modification of Brookhaven National Laboratory BWR Plant Analyzer to Accommodate BWR/2 Design of Nine Mile Point-1 Nuclear Power Station," Master Thesis, Rensselaer Polytechnic Institute, Troy, NY, September 1987.

CHENG, H. S. and WULFF, W. (1981), "A PWR Training Simulator Comparison with RETRAN for a Reactor Trip from Full Power," Informal Report, BNL-NUREG-30602, Brookhaven National Laboratory, September 1981.

CHENG, H. S., WULFF, W., MALLEN, A. N., and CAZZOLI, E. G. (1986), "A Dynamic Simulation of Long-Term BWR/4 MSIV Closure ATWS with Emergency Procedure Guidelines," 2nd Int. Topical Meeting on Nuclear Power Plant Thermal Hydraulics and Operations, Tokyo, Japan.

DALLMAN, R. J. (1987), "Severe Accident Sequence Analysis Program - Anticipated Transient Without Scram Simulations, for Browns Ferry Nuclear Plant Unit 1," NUREG/CR-4165, EG&G-2379, Idaho National Engineering Laboratory, May 1987.

FORKNER, S. L. (1981), "BWR Transient Analysis Model Utilizing the RETRAN Program," TVA-TR81-01, Tennessee Valley Authority, December 1981.

ISHII, M. (1977), "One-Dimensional Drift-Flux Model and Constitutive Equations for Relative Motion Between Phases in Various Two-Phase Flow Regimes," Argonne National Laboratory, Argonne, IL., ANL-77-47.

MEYER, C. A., McCLINTOCK, R. B., SILVESTRI, G. J. and SPENCER, R. C., Jr., "ASME Steam Tables," Third Edition, The American Society of Mechanical Engineers, 345 East 47th Street, New York, NY 10017.

WULFF, W. (1980), "PWR Training Simulator, An Evaluation of the Thermohydraulic Models for its Main Steam Supply System," Informal Report, BNL-NUREG-28955, September 1980.

WULFF, W. (1981a), "BWR Training Simulator, An Evaluation of the Thermohydraulic Models for its Main Steam Supply System," Informal Report, BNL-NUREG-29815, Brookhaven National Laboratory, July 1981.

WULFF, W. (1981b), "LWR Plant Analyzer Development Program," Ch. 6 in Safety Research Programs Sponsored by the Office of Nuclear Regulatory Research, Quarterly Progress Report, April 1-June 30, 1981; A. J. Romano, Editor, NUREG/CR-2231, BNL-NUREG-51454, Vol. 1, No. 1-2, 1980.

WULFF, W., CHENG, H. S., LEKACH, S. V. and MALLEN, A. N. (1984), "The BWR Plant Analyzer," Final Report, BNL-NUREG-51812, NUREG/CR-3943.

WULFF, W. (1982a), "LWR Plant Analyzer Development Program," Ch. 5 in Safety Research Programs Sponsored by the Office of Nuclear Regulatory Research, Quarterly Progress Report, January 1-March 31, 1982; A. J. Romano, Editor, NUREG/CR-2331, BNL-NUREG-51454, Vol. 2, No. 1, 1982.

WULFF, W. (1982b), "LWR Plant Analyzer Development Program," Ch. 5 in Safety Research Programs Sponsored by the Office of Nuclear Regulatory Research, Quarterly Progress Report, July 1-September 30, 1982; compiled by Allen J. Weiss, NUREG/CR-2331, BNL-NUREG-51454, Vol. 2, No. 3, 1982.

WULFF, W. (1982c), "LWR Plant Analyzer Development Program," Ch. 5 in Safety Research Programs Sponsored by the Office of Nuclear Regulatory Research, Quarterly Progress Report, October 1-December 31, 1982; compiled by Allen J. Weiss, NUREG/CR-2331, BNL-NUREG-51454, Vol. 2, No. 4, 1982.

WULFF, W. (1983a), "LWR Plant Analyzer Development Program," Ch. 5 in Safety Research Programs Sponsored by the Office of Nuclear Regulatory Research, Quarterly Progress Report, January 1-March 31, 1983; compiled by Allen J. Weiss, NUREG/CR-2331, BNL-NUREG-51454, Vol. 3, No. 1, 1983.

WULFF, W. (1983b), "LWR Plant Analyzer Development Program," Ch. 5 in Safety Research Programs Sponsored by the Office of Nuclear Regulatory Research, Quarterly Progress Report, July 1-September 30, 1983; compiled by Allen J. Weiss, NUREG/CR-2331, BNL-NUREG-51454, Vol. 3, No. 3, 1983.

WULFF, W. (1983c), "NRC Plant Analyzer Development," Proc. Eleventh Water Reactor Safety Research Information Meeting, held at National Bureau of Standards, Gaithersburg, MD, Oct. 24-28, 1983, U.S. Nuclear Regulatory Commission. To be published.

WULFF, W. (1983d), "LWR Plant Analyzer Development Program," Ch. 5 in Safety Research Programs Sponsored by the Office of Nuclear Regulatory Research, Quarterly Progress Report, October 1-December 31, 1983; compiled by Allen J. Weiss, NUREG/CR-2331, BNL-NUREG-51454, Vol. 3, No. 4, 1983.

WULFF, W. (1984a), WULFF, W., (1984b), "LWR Plant Analyzer Development Program," Ch. 5 in Safety Research Programs Sponsored by the Office of Nuclear Regulatory Research, Quarterly Progress Report, April 1-June 30, 1984; compiled by Allen J. Weiss, NUREG/CR-2331, BNL-NUREG-51454, Vol. 4, No. 2, 1984.

WULFF, W. (1984c), "LWR Plant Analyzer Development Program," Ch. 5 in Safety Research Programs Sponsored by the Office of Nuclear Regulatory Research, Quarterly Progress Report, July 1-September 30, 1984; compiled by Allen J. Weiss, NUREG/CR-2331, BNL-NUREG-51454, Vol. 4, No. 3, 1984.

WULFF, W. (1984d), "LWR Plant Analyzer Development Program," Ch. 4 in Safety Research Programs Sponsored by the Office of Nuclear Regulatory Research, Quarterly Progress Report, October 1-December 31, 1984; compiled by Allen J. Weiss, NUREG/CR-2331, BNL-NUREG-51454, Vol. 4, No. 4, 1984.

WULFF, W. (1985a), "LWR Plant Analyzer Development Program," Ch. 4 in Safety Research Programs Sponsored by the Office of Nuclear Regulatory Research, Quarterly Progress Report, January 1-March 31, 1985; compiled by Allen J. Weiss, NUREG/CR-2331, BNL-NUREG-51454, Vol. 5, No. 1, 1985.

WULFF, W. (1985b), "LWR Plant Analyzer Development Program," Ch. 4 in Safety Research Programs Sponsored by the Office of Nuclear Regulatory Research, Quarterly Progress Report, April 1-June 30, 1985; compiled by Allen J. Weiss, NUREG/CR-2331, BNL-NUREG-51454, Vol. 5, No. 2, 1985.

WULFF, W. (1985c), "LWR Plant Analyzer Development Program," Ch. 4 in Safety Research Programs Sponsored by the Office of Nuclear Regulatory Research, Quarterly Progress Report, July 1-September 30, 1985; compiled by Allen J. Weiss, NUREG/CR-2331, BNL-NUREG-51454, Vol. 5, No. 3, 1985.

WULFF, W. (1985d), "LWR Plant Analyzer Development Program," Ch. 5 in Safety Research Programs Sponsored by the Office of Nuclear Regulatory Research, Quarterly Progress Report, October 1-December 31, 1985; compiled by Allen J. Weiss, NUREG/CR-2331, BNL-NUREG-51414, Vol. 5, No. 4, 1985.

WULFF, W. (1986a), "LWR Plant Analyzer Development Program," Ch. 5 in Safety Research Programs Sponsored by the Office of Nuclear Regulatory Research, Quarterly Progress Report, January 1-March 30, 1986; compiled by Allen J. Weiss, NUREG/CR-2331, BNL-NUREG-51454, Vol. 6, No. 1, 1986.

WULFF, W. (1986b), WULFF, W., (1984b), "LWR Plant Analyzer Development Program," Ch. 5 in Safety Research Programs Sponsored by the Office of Nuclear Regulatory Research, Quarterly Progress Report, April 1-June 30, 1986; compiled by Allen J. Weiss, NUREG/CR-2331, BNL-NUREG-51454, Vol. 6, No. 2, 1986.

WULFF, W., CHENG, H. S., and MALLEN, A. N. (1986), "BWR Plant Analyzer Development at BNL," Proc. 14th Water Reactor Safety Information Meeting, NBS, Gaithersburg, MD, NUREG/CR-0081.

25. Procedures for Evaluating Technical Specifications (PETS)
(John L. Boccio and Pranab K. Samanta)

25.1 Background

Technical Specifications (TS) are design and procedural limits that impose explicit restrictions on the operation of nuclear power plants and on the maintenance of safety systems in a pre-accident condition. A number of problems with TSs have evolved over the years and there is general agreement that TS are complex and difficult to implement. As pointed out in NUREG-1024[1], these problems are largely due to the absence of specific criteria regarding the content of the TS. Numerous items have therefore been included within the TS that are of vastly differing levels of safety importance; in some cases, requirements were inconsistent. Other concerns, besides being complex and difficult for control room operators to implement, have been expressed regarding the lack of technical basis for test frequencies and allowed downtimes of components which are symptomatic to accelerated component wear, added maintenance, unnecessary test downtimes, introduction of human errors, and the added potential of common-cause errors.

To address these concerns and to place TS on a more rational basis, the U.S. nuclear industry and the U.S. NRC have embarked on parallel and coordinated efforts. One of NRC's initiatives was to establish a broad-based research program to examine the issues that arise in addressing various alternative means for evaluating the safety implications of current TS and in seeking ways to improve on the current posture of TS.

25.2 Objective

The objectives of the PETS Program are to develop and demonstrate methodologies to utilize reliability and risk techniques in evaluating the scope, detailed requirements, and safety impact of plant TSs, and to explore alternative approaches to structuring TSs to make them more effective in controlling overall risk. The procedures developed are to provide a quantitative basis for revising the TSs and for responding to licensee submittals.

25.3 Summary of Prior Efforts

The PETS Program evolved from an ongoing research project at BNL (Time Dependent Reliability Modeling, FIN A-3230) for developing and applying a methodology to evaluate operating procedures for safety systems in standby and operating modes and to perform sensitivity analyses to various testing, operating, and maintenance strategies. A series of computer codes, FRANTIC I, II, and III, were developed through this study and were designed to predict the time-wise variation of safety system unavailability as a function of different maintenance strategies. Optimized testing intervals could also be gleaned through sensitivity studies employing the FRANTIC-series of codes. In the process of developing and demonstrating risk-based approaches for addressing specific TS safety issues, BNL has, through the PETS program, been investigating the utility of the FRANTIC codes along with the other risk and reliability methods. The development and modification of the FRANTIC code to facilitate its use in AOT

and STI evaluation has continued. Specific features have been added and others are planned to evaluate the effect of realistic test schedules in nuclear power plants.

At its initiation, the primary objective of the PETS program was to develop and demonstrate an overall procedure for determining AOTs and STIs, to propose AOTs and STIs for select specific cases, to provide a procedures guide for implementing TS analysis procedures, and to develop and demonstrate risk-based guidelines for utilizing cumulative downtime allocments to control component downtime as suggested in resolution of Generic Issues B-56 and B-61. The PETS program identified[2] a number of safety issues which impact the determination of AOT and STI requirements. The significance of these documented safety issues was evaluated using the emergency cooling system of the Limerick nuclear power plant as an example. A report[3] describing the findings was issued for review and comment which showed how existing Probabilistic Risk Analysis (PRA) models can be used to address AOT risks as well as providing a preliminary indication as to how a technical review of licensee-submitted TS exemption request should be conducted if the submittal employs probabilistic approaches. Throughout this study, PETS identified the need to develop regulatory review strategies that should not only cover probabilistic implementation approaches (in which risk is explicitly calculated and used as the basis for exemption requests) but should also address those deterministic methods/approaches where risk considerations serve as a more implicit underlying basis for seeking changes in a specific TS.

Using the PRA for Arkansas Nuclear One - Unit 1 as the basis for measuring the risk impact of testing and maintenance activities, the PETS program has also evaluated a complete set of the AOT and STI requirements of the plant's TS. Using core-melt frequency as the risk measure and a pre-defined numerical criterion that is based on the safety goal criterion for the frequency of core melt, this aspect of the study has shown not only which component's downtimes can be relaxed (increased) but also demonstrated a method for determining the risks associated with a given AOT. This report[4] also provides an evaluation of the STI risk at this plant.

Based on the above work, the program focussed on developing methodology guides for modification of AOTs and STIs based on the insights gained through the evaluation of safety issues using the emergency cooling systems of the Limerick plant and through the application to the ANO-1 technical specification requirements. Reports[5-6] were issued which were intended to provide guidance to licensees and to result in uniformity in the TS submittals. The reports covered the regulatory decision process in AOT and STI modifications, and methodology guidance for AOT and STI risk evaluations. These reports are currently planned to be more specific and detailed based on industry and NRC needs for streamlining both the development of licensee submittals and the review of those submittals.

The PETS program conducted a three-day course through the Technology Transfer Program for the NRC staff involved in tech spec modification. The course focused on risk-based evaluation of AOTs and STIs and also on review considerations for licensee submittals of requested changes.

In summary, the PETS activity has involved various aspects of AOT and STI requirements and more than twenty reports have been published. The PETS findings have provided a risk perspective on AOT/STI requirements and cover the following areas (including those requiring additional effort for developing an implementation approach in the regulatory process):

- the expected risk contributions associated with present tech specs,
- the maximum risk contributions allowed by present tech specs,
- approaches to address the maximum contributions allowed by present tech specs,
- proper evaluations of the risk contributions associated with tech specs,
- effects of PRA uncertainties in evaluating risk contributions from tech specs,
- numerical criteria to assess the acceptability of risks associated with tech specs,
- the risk effects of removing downtimes and test intervals from tech specs,
- utilizing allowed cumulative outage times as a means of controlling downtime risks,
- utilizing risk approaches to revise standardized tech specs and plant-specific tech specs,
- the feasibility of performance based tech specs, and
- the effects of aging on the adequacy of risk control by tech specs.

Each of these areas and the findings resulting from PETS research are discussed in a project status summary report (BNL A-3230 9-22-87) that gives the conclusions reached, the issues that remain, and tasks needed to address the issues or to implement the developed approaches into regulatory practices.

25.4 Work Performed During Period

During this reporting period, the project stressed activity in response to Generic Issues B-56 and B-61. The PETS program has developed methodologies and demonstrated through application the effectiveness of adaptive testing and cumulative downtime strategies. Risk effective surveillance test intervals were analyzed for diesel generators, and PC-based software was developed for implementation of such approaches.

From a risk standpoint, the objective of diesel generator surveillance tests is to control the risk arising from failures which can occur while the diesel is on standby. At the same time, risks from test-caused failures and test-caused degradations also need to be controlled. Risk-acceptable test intervals balance these risks in and attempt to achieve an acceptable low, overall risk.

Risk and reliability approaches were developed which allow risk-acceptable test intervals to be determined for any diesel. These approaches, along with the data required to apply them, are described in Reference 8. The approaches can be applied not only to diesels, but to any component with suitable data. Incorporation of the approaches in personal computer (PC) software which can provide tools for the regulator or plant personnel for determining acceptable diesel test intervals for any plant specific or generic application is discussed in the report. The FRANTIC III computer code was run to validate the approaches and to evaluate specific issues associated with determining risk-effective test intervals for diesels.

Figure 25.1 is a characteristic plot obtained from the calculational approaches which were developed. The figure plots diesel accident unavailability and diesel test unavailability versus surveillance test interval (in hours). The diesel accident unavailability (denoted by "Accident") is the probability that the diesel will fail to perform its function in an accident. The diesel test unavailability (denoted by "Test") is the probability that the diesel will fail in a surveillance test as carried out under present technical specifications. The reliability parameters for this example diesel are indicated in the figure caption, although they are not necessary to understand the basic behaviors shown in the figure.

The figure shows several important results. The diesel accident unavailability can never be less than the diesel test unavailability but can be significantly higher. The test unavailability is the performance measured in a surveillance test under present plant-specific or generic technical specifications. The accident unavailability is higher than the test unavailability because it includes all contributions which can cause the diesel to be unavailable in accident, test, maintenance, and repair unavailabilities.

In addition to being significantly higher than the test unavailability, the accident unavailability shows significantly different behavior as the test intervals are changed. Test unavailability continually decreases as the test interval is decreased, a result that is consistent with the requirements in Regulatory Guide 1.108 to test more frequently whenever problems arise.

The accident unavailability, however, shows a clear optimal region, and the unavailability increases if the test interval is increased or decreased from this optimal region. In particular, the accident unavailability can be unacceptably high if the test interval is too short. With regard to controlling the accident unavailability, Regulatory Guide 1.108 is consequently not an especially effective approach; following the Guide can cause the accident unavailability to increase and become unacceptably high. Reference 8 presents approaches which can be used to effectively determine test intervals that maintain the accident unavailability at or near the lowest achievable levels.

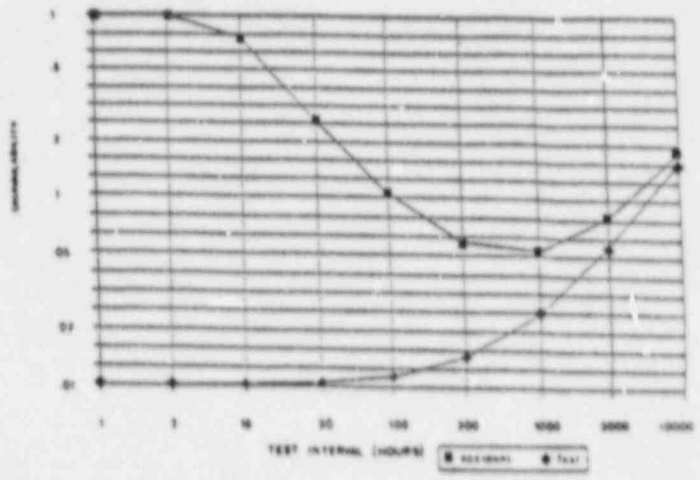

Figure 25.1 Unavailability vs test interval (lambda = 3E-05, P = 1E-02, K = 10, and downtime = 72

Figure 25.2 is a histogram of diesel accident and diesel test unavailability collected from specific plants. The data (Table 25-1) are rough but indicate the relative sizes of the two unavailabilities. Test unavailabilities may satisfy NRC goals, while the accident unavailabilities can be significantly higher. The extra contributions to accident unavailability are not directly controlled by present technical specifications. The approaches in the report can be used to improve control over these extra contributions.

Using the approaches documented, diesel accident unavailability can be more effectively monitored and controlled on a plant-specific or generic basis. Test intervals can be made more risk effective than they are now, producing more acceptable accident unavailabilities, and avoiding the possible deleterious effects of Regulatory Guide 1.108. The methods presented are one step toward performance-based technical specifications, which more directly control risks.

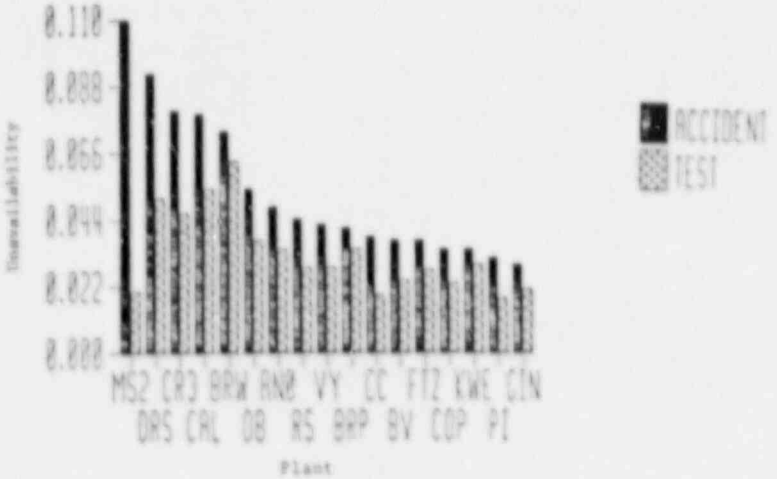

Figure 25.2 Diesel accident unavailability vs. test unavailability

Table 25-1. Reported Unavailabilities by Plants

Unit	Specific Diesel	Unavailability		
		Downtime	Test	Accident
ANO #1	1	1.4E-2	3.4E-2	4.8E-2
Beaver Valley (BV)	1	1.3E-2	2.4E-2	3.7E-2
Big Rock Pt (BRP)	1	7.0E-3	3.4E-2	4.1E-2
Brunswick (BRW)	1	7.0E-3		
	2	6.0E-3	6.3E-2	7.3E-2
		8.0E-3		
		2.0E-2		
Calvert Cliffs (CC)	11	2.0E-2		
	12	2.2E-2	1.9E-2	3.7E-2
	21	1.4E-2		
Cooper (COP)	1	1.2E-2		
	2	1.0E-2	2.3E-2	3.4E-2
Crystal River-3 (CR3)	A	5.2E-2	4.6E-2	8.0E-2
	B	1.5E-2		
Davis-Besse (DB)	1	2.2E-2	3.7E-2	5.3E-2
		1.1E-2		
Dresden (DRS)	2	4.0E-2		
	2/3	4.4E-2	5.1E-2	9.2E-2
	3	4.0E-2		
Farley (FRL)	1B	9.0E-3		
	1C	8.0E-3	1.3E-2	2.0E-2
	1/2A	7.0E-3		
	2C	4.0E-3		
Fitzpatrick (FTZ)	A	8.0E-3	2.7E-2	3.6E-2
	B	6.0E-3		
	C	9.0E-3		
	D	1.6E-2		
Calhoun (CAL)	1	3.2E-2	5.4E-2	7.7E-2
	2	1.8E-2		
Ginna (GIN)	A	7.0E-3	2.1E-2	2.9E-2
	B	9.0E-3		

Table 25-1. Reported Unavailabilities by Plants (Cont'd)

Unit	Specific Diesel	Unavailability		
		Downtime	Test	Accident
Hatch (HAT)	1A	7.0E-3		
	1B	2.0E-2		
	1C	9.0E-3	1.9E-2	2.8E-2
	2A	5.0E-3		
	2C	3.0E-3		
Indian Point 2 (IP2)	21	NG	5.0E-3	
	22			
	23			
Indian Point 3 (IP3)	31	1.0E-2		
	32	7.0E-3	1.0E-2	1.8E-2
	33	7.0E-3		
Kewaunee (KWE)	1A	5.0E-3	2.9E-2	3.4E-2
	1B	5.0E-3		
LaCrosse (LCR)	1A	1.4E-2	4.3E-2	1.6E-2
	1B	9.0E-3		
Maine Yankee (MYK)	1A	4.0E-3	2.8E-2	2.8E-2
	1B	3.0E-3		
Millstone 1 (MS1)	D6	1.5E-2	3.5E-3	1.9E-2
Millstone 2 (MS2)	1211	9.8E-2	2.0E-2	1.2E-1
	1311	8.1E-2		
Nine Mile Point (NMP)	102	3.0E-3		
	103	2.0E-3	7.6E-3	1.0E-2
North Anna (NA)	1H	1.4E-2	1.1E-2	2.4E-2
	1J	1.3E-2		
Palisades (PLS)	1	8.0E-3	1.5E-2	2.4E-2
	2	1.0E-2		
Peach Bottom (PBT)	1	8.0E-3		
	2	8.0E-3	4.5E-3	1.2E-2
	3	8.0E-3		
	4	8.0E-3		

Table 25-1. Reported Unavailabilities by Plants (Cont'd)

Unit	Specific Diesel	Unavailability		
		Downtime	Test	Accident
Point Beach (PBC)	30	1.3E-2	1.1E-2	2.2E-2
	40	1.0E-2		
Prairie Island (PI)	1	1.0E-2		
	2	1.5E-2	1.8E-2	3.1E-2
Quad-Cities (QC)	1	3.0E-3		
	1/2	7.0E-3	1.6E-2	2.1E-2
	2	5.0E-3		
Rancho Seco (RS)	A	1.6E-2	2.8E-2	4.4E-2
	B	1.6E-2		
Robinson (ROB)	2A	1.3E-2	8.0E-3	2.0E-2
	2B	1.1E-2		
St. Lucie	1A	1.1E-2	(NG)	
	1B	1.0E-2		
Surry (SUR)	1	1.0E-2		
	2	5.0E-3	1.0E-2	1.7E-2
	3	6.0E-3		
Trojan (TRJ)	1	9.0E-3	3.0E-3	1.2E-2
	2	8.0E-3		
Vermont Yankee (VY)	1A	1.3E-2	2.8E-2	4.2E-2
	1B	1.4E-2		
Yankee (Rowe) (YR)	1	2.0E-3		
	2	3.0E-3	3.4E-3	1.8E-2
	3	1.3E-2		

25.5 References

1. NUREG-1024, "Technical Specifications - Enhancing the Safety Impact," November 1983.

2. Vesely, W.E. and Boccio, J.L., "The Use of Risk Analysis for Determining AOTs and STIs: Issues and Review Considerations," BNL Technical Report A-3230 9-20-85, September 1985.

3. Samanta, P.K. and Wong, S.M., "AOT Risk Analysis and Issues: Limerick Emergency Coolant Systems," BNL Technical Report A-3230 2-25-85, February 1985.

4. Samanta, P.K., Wong, S.M., and Carbonaro, J., "Risk-Based Evaluations of AOT and STI Requirements at ANO-1 Nuclear Power Plant," 1986 Annual ANS Meeting, Vol. 52, p. 510-511.

5. Samanta, P.K. et al., "Risk Methodology Guide for AOT and STI Modifications," BNL Technical Report A-3230 12-02-86, December 1986.

6. Vesely, W.E., "Procedures to Define Numerical Criteria to Assess Risks Associated with Technical Specification Modifications," BNL Technical Report A-3230 6-5-86, June 1986.

7. Vesely, W.E., Samanta, P.K., and Boccio, J.L., "White Paper Summarizing the Major Findings of the PETS Program on Risk Analysis of Technical Specifications," BNL Technical Report A-3230 9-22-87, September 1987.

8. Vesely, W.E. et al., "Evaluation of Diesel Unavailability and Risk Effective Surveillance Test Intervals," NUREG/CR-4810, BNL-NUREG-52022, May 1987.

26. Operational Safety Reliability Research
(John L. Boccio)

26.1 Background

Despite NRC regulations and fixes made after the TMI accident and the Salem automatic-trip failure, operational events keep happening. A possible reason is that in the past NRC requirements have emphasized prescriptive requirements to correct identified problems; and have not been life-cycle oriented to prevent system reliability degradation and future problems. Therefore, the Commission has directed the staff to place high priority on development of capabilities to foresee problems through monitoring of performance data and to shift regulatory emphasis away from detailed prescriptive requirements toward more general, performance-based requirements.

Several regulatory issues involve finding ways to present reliability degradation and future problems, possibly through more effective use of reliability engineering/management. Examples of such issues are:

- How to prevent multiple failures such as occurred at Davis Besse in 1985 (i.e., improved strategies to prevent common-cause failures).
- How to evaluate industry responses to NRC requirements to maintain or improve reliability of EDGs (GI B-56) and RCP seals (GI-23).
- How can reliability engineering methods be used in Tech Spec improvements to help focus surveillance on important equipment/failure models/errors, and to help improve maintenance effectiveness.
- How to structure reliability engineering/management to selectively use aging research results to systematically prevent degradation and to help develop criteria for license renewal.
- In the long range, how to implement the safety goal policy so that utilities systematically prevent degradation and continually achieve safe performance, while NRC monitors plant performance to verify the safety goals are met.

Previous work under this project has helped to identify the essential elements and process of reliability engineering that are considered useful for achieving and maintaining plant safety during the plant lifetime. Additional research is planned to develop criteria and to evaluate methods for applying reliability engineering/management to the resolution of individual issues.

26.2 Objective

The objective of this project is for BNL to evaluate the effectiveness of reliability engineering/management methods to help achieve and maintain high availability of safety systems and low frequency of transients (and faults) in operating reactors. The research planned for FY 1988 emphasizes evaluation of reliability engineering methods through practical trial applications.

26.3 Summary of Prior Efforts

To meet the basic objective of this project, BNL has divided the effort into nine major tasks. These tasks were formulated so that interim products will be useful to the NRC. In broad terms, these tasks can be classified as: 1) plan development, 2) reliability program element/attribute effectiveness evaluation and modification through case studies, initial trial use, and comparison with generic issues, abnormal occurrences, and accident precursors, and 3) further evaluation/modification through broader trial use and peer review.

The nine major tasks are:

Task (1) - Development of initial project plan.

Task (2) - Evaluation of reliability program effectiveness vs outstanding generic issues, abnormal occurrences and accident precursors.

Task (3) - Identification of successful reliability program attributes and its potential effectiveness through case studies of utility practices.

Task (4) - Reliability techniques development and integration.

Task (5) - Evaluation of reliability program effectiveness, practicality, and attributes through initial trial application on an example system at one plant.

Task (6) - Reliability program description update based on case studies and initial trial use.

Task (7) - Further evaluation of reliability program elements/attributes through broader application to several systems in a trial application at one plant.

Task (8) - Publication.

In previous years, BNL completed Tasks 1, 2, 3, 5, 6, and parts of Task 7. The following reports have been issued:

1. Operational Safety Reliability Research Project Plan, BNL Technical Report A-3282 1/5/85, January 1986.

2. Evaluation of the Potential Effectiveness of a Reliability Program on Safety Issues Resolution, Volume 1 - Generic Safety Issues, BNL Technical Report A-3282 1/15/86, January 1986.

3. Evaluation of the Potential Effectiveness of a Reliability Program on Safety Issues Resolution, Volume 2 - Abnormal Occurrences, BNL Technical Report A-3282 9/15/85, September 1986.

4. Trial Application of Reliability Technology to Emergency Diesel Generators at Trojan, BNL Technical Report A-3282 4/30/86, April 1986.

5. Evaluation of Reliability Technology Applicable to LWR Operational Safety (Draft for Comment), NUREG/CR-4618, May 1986.

6. A Reliability Centered Surveillance Concept for Nuclear Power Plant Standby Safety Equipment. BNL Draft Technical Report A-3282 12-09-86, December 1986.

7. Methodology Evaluation for Identification and Prevention of Reliability-Related Common Causes. Letter Report, May 1987.

8. Evaluation of Reliability Program Elements/Techniques Through Application to a Normally Operating System, Draft Program Plan Letter Report, July 1987.

Based upon the FY 1986 work, NRC issued a draft document, "Evaluation of Needs for Implementation of Reliability Technology in the Regulatory Program," which describes possible regulatory applications to help prevent future accidents from occurring.

26.4 Work Performed During Period

Work during this reporting period largely focussed on (i) extending the reliability program process identified in FY 1986, to include defensive strategies against common-cause failures and (ii) soliciting cooperation with an operating utility and evaluating through a trial application the effectiveness of a reliability program applied to a normally-operating system. In addition, select members of the project team were engaged in documenting for the NRC guidance for evaluating reliability programs for diesel generators that would be submitted by licensees in response to Unresolved Safety Issue (USI) B-56. The following highlights the work conducted through this project during the reporting period.

26.4.1 Guidelines for Using Reliability Programs to Defend Against Common-Cause Failures

To provide a reliability program-based defense against common-cause failures, the study has shown that the following reliability tools are required:

- techniques for identifying potential common-cause failures,
- techniques for prioritizing these identified common-cause failures,
- guidance for determining which of the identified common-cause failures should be defended against, and
- guidance for indicating what type of defenses are likely to be successful against the various types of common-cause failures.

Work centered on identifying the requisite techniques and integrating them within the framework provided by a reliability program structure[1] in order to defend against common-cause failures. To develop the above techniques and guidance around this framework, it is necessary to first develop a reliability center for common-cause, i.e., to classify the reliability characteristics of common-cause failures in such a way that the above techniques can be accomplished. A major objective of this task is to initiate development of such a reliability center for common-cause failures. In addition to the framework provided in Reference 1, this study builds upon work in the common-cause area that was conducted jointly by the NRC, EPRI, and the Systems Reliability Directorate (SRD) of the United Kingdom (UK). The techniques and methods put forth by this joint study[2] are primarily oriented toward quantifying common-cause events that have been a priori identified. The techniques introduced in this study are considered to be an extension of this work in that (i) they can provide systematic ways of identifying potential common-cause failures, (ii) they can provide a systematic way of prioritizing these failures, and (iii) they can give guidance as to the type of defenses against the identified common-cause failures that would be expected to be successful.

Work continues in providing this identification process and in generating guidance for defensive strategies. Figure 26.1 depicts the process being investigated for identifying the reliability program activities needed to defend against common-cause failures.

26.4.2 Trial Application - Normally Operating System

Much effort was spent during this reporting period in soliciting industry involvement in the development of a reliability program for a normally operating system. To date, the project has acquired verbal agreement to participate in this activity from one utility, viz, Consolidated Edison of New York. Based on previous NRC staff recommendations, the system chosen for subsequent investigation is the component cooling water system at the Indian Point 2 site. The scope of this effort includes the following work in cooperation with utility and site personnel: analyzing data on the system performance to identify failures that have occurred, analyzing the design/operations/maintenance programs to identify potential failures, prioritizing importance of components in order to identify critical components and failure modes, identifying possible reliability improvements particularly through changes in operation/surveillance/maintenance, and if such changes are approved by the utility, evaluating the effectiveness of the proposed changes for preventing potential problems from occurring.

To date, basic operating information on this system has been provided by the utility, and data analysis is underway.

26.4.3 Review Guidance - Diesel Generator Reliability Program

A document that provides the NRC with guidance for evaluating diesel generator reliability program submitted by licensees for review was drafted[3] during this reporting period. Table 26-1 summarizes the scope of review to be

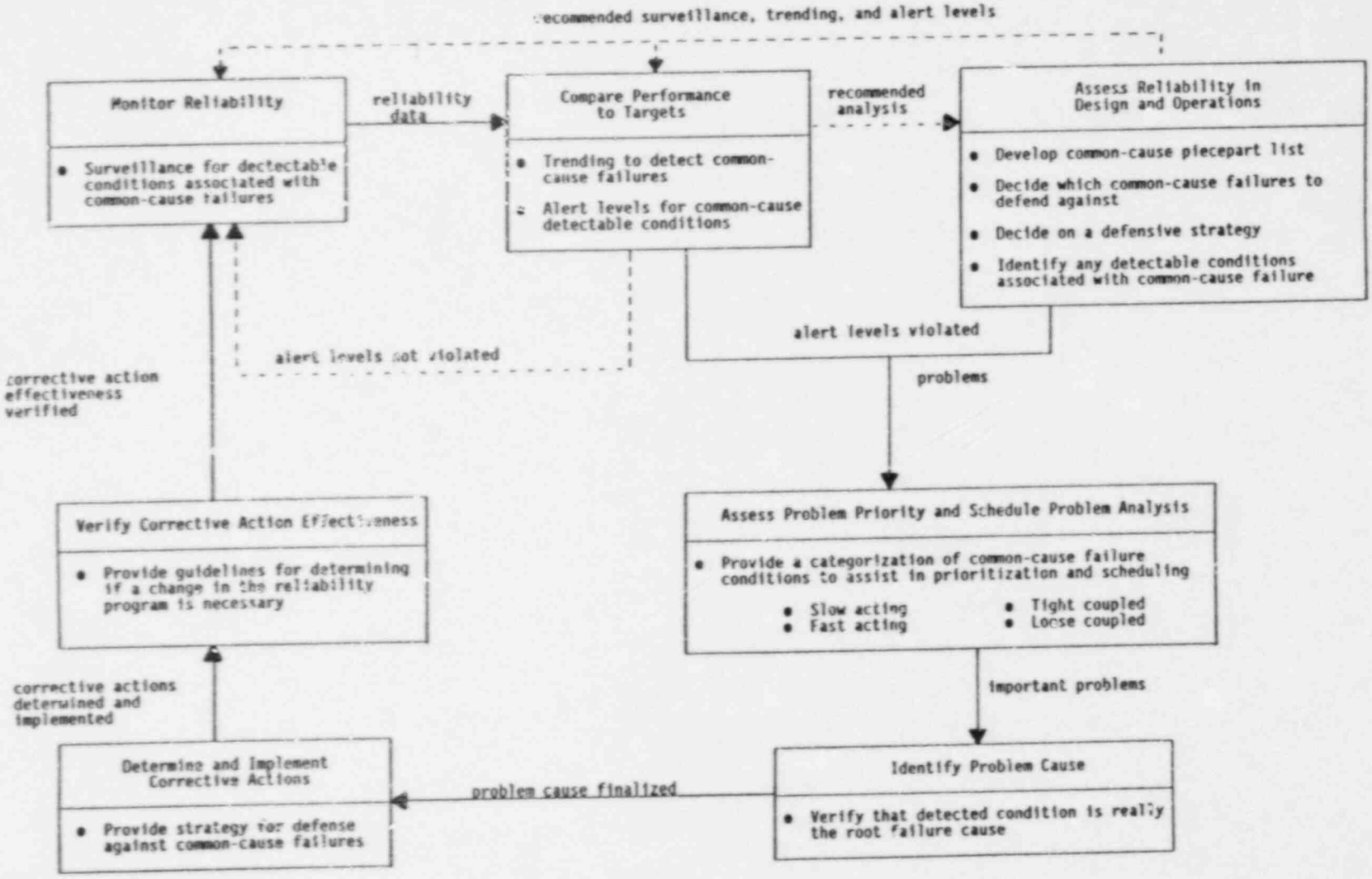

Fig. 26.1. reliability program activities to defend against common-cause failures

Table 26.1. Diesel Generator Reliability Program Critical Review Items

A. EDG Reliability/Availability Target

Assure that the reliability/availability target for the diesel generator has been established, and that calculational measures have been defined that can be evaluated and compared to the target.

B. EDG Surveillance Needs

Assure that the diesel generator equipment boundary has been defined, and that the diesel generator reliability program has specified a task for analyzing the surveillance needs of this equipment

C. EDG Performance Monitoring

Assure that the reliability program specifies a task to monitor diesel generator performance, using both statistical trending and engineering data, to spot degradations in performance.

D. EDG Maintenance Program

Assure that the diesel generator maintenance program has a reliability focus that includes preventive maintenance, prioritization of maintenance actions and spare parts considerations.

E. EDG Failure Analysis and Root Cause Investigation

Assure that there is a task to systematically reduce identified diesel generator problems to correctable causes.

F. Problem Closeout

Assure that the diesel generator reliability program requires a formal problem closeout procedure, and that this procedure involves both (1) establishing criteria for problem closeout when a reliability problem is detected, and (2) providing for any special monitoring activity to assure that the criteria have been satisfied by the corrective action.

G. Data Collection and Utilization

Assure that a data gathering, storage, and retrieval system with sufficient capabilities to support all other features of the reliability program is in place or will be implemented as part of the diesel generator reliability program.

H. Responsibilities and Management Controls

Assure that there are clear line responsibilities and management controls in place that identify responsible individuals for implementing and operating the diesel generator reliability program, and assure that these individuals are qualified to perform the functions for which they are responsible.

provided for emergency diesel generator reliability programs. The items delineated in this table are those that should be explicitly discussed in any reliability program written documentation. As such, these so-called critical review items are discussed at great length in the cited reference. An acceptable diesel generator reliability program will have to address the basic issues associated by each of the critical review items. Efforts spent during this quarter have been to identify these issues further and to provide a checklist for reviewing reliability programs for this system. For example, the report shows how reliability/availability targets for the diesel system can be defined and attempts to clarify the measures necessary to evaluate achievement of this target. To judge the acceptability of diesel generator performance, the progression of failures as well as the overall failure history should be used. Proposed interim failure evaluation criteria are presented in Reference 3 and summarized in this quarterly progress report in Table 26-2. In this example, the progression of failures is very important for interpreting the failure data and for evaluating false alarm rates. All combinations of the evaluation criteria are shown for this example, and their interpretations are summarized in the cited table.

26.5 References

1. Azarm, M.A., and Lofgren, E.V., et al., "Effectiveness of Reliability Technology Applicable to LWR Operational Safety," NUREG/CR-4618, BNL-NUREG-51995, May 1986, revised December 1987.

2. Mosleh, A., and Fleming, K.N., et al., "Procedures for Treating Common-Cause Failures in Safety and Reliability Studies," Volume 1, April 1987, Pickard, Lowe and Garrick, Inc.

3. Lofgren, E.V., et al., "Diesel Generator Reliability Program: Review Guidance," Science Application International Corporation, September 15, 1987.

Table 26.2. Interim EDG Failure Evaluation Criteria (Proposed) for EDGs with a Reliability Target of 95%

Evaluation Criteria (# Failures/#Demands)	Combinations of Failure Evaluation Criteria								Time Period (1 Demand/2 Wks)	False Alarm Rate
≥ 2/20	Y	Y	Y	N	N	N	N	Y	10 Months	26%
≥ 5/50	Y	Y	N	N	N	Y	Y	N	≈ 2 Years	11%
≥ 10/100	Y	N	N	N	Y	Y	N	Y	≈ 4 Years	3%
Failure Progression	1	2	3	4	5	6	7	8		

Legend: Y = Yes
N = No

Interpretations of the Failure Progressions

	Failure Progression	Interpretation
1.	≥ 2 failures in 20 demands ≥ 5 failures in 50 demands ≥ 10 failures in 100 demands	This is an unacceptable condition requiring immediate action to declare the EDG inoperable. There is strong evidence that the long-term EDG unavailability is larger than the target value, and no evidence that it is improving. The EDG reliability program must be improved or enhanced before the EDG can be declared operable again.
2.	≥ 2 failures in 20 demands ≥ 5 failures in 50 demands < 10 failures in 100 demands	This is an alert condition where action is recommended to declare the EDG inoperable. There is evidence that the EDG is deteriorating over time, and that the current reliability is unacceptable. The action taken may depend on other circumstances and information from the plant.
3.	≥ 2 failures in 20 demands < 5 failures in 50 demands < 10 failures in 100 demands	This is a mild alert condition where no action by the NRC is recommended unless there are other recent indications of EDG deterioration. EDG's with acceptable unavailabilities will display this condition about 26 percent of the time. However, some concern is justified.
4.	< 2 failures in 20 demands < 5 failures in 50 demands < 10 failures in 100 demands	This is an acceptable condition. No concrete evidence of unacceptable EDG performance.
5.	< 2 failures in 20 demands < 5 failures in 50 demands ≥ 10 failures in 100 demands	This is an acceptable condition. There is an indication of a past problem that has probably been corrected. Low level vigilance is prudent to assure continued acceptable operation.
6.	< 2 failures in 20 demands ≥ 5 failures in 50 demands ≥ 10 failures in 100 demands	This is an acceptable condition but one that needs continued vigilance. There is indication that a continuing past problem is being corrected, but the evidence is not convincing enough to warrant a decrease in vigilance.
7.	< 2 failures in 20 demands ≥ 5 failures in 50 demands < 10 failures in 100 demands	This is an acceptable condition but one that needs continued vigilance. The interpretation of this condition is similar to the interpretation of condition 6 above, except that the history of unacceptable performance is less extensive.
8.	≥ 2 failures in 20 demands < 5 failures in 50 demands ≥ 10 failures in 100 demands	The interpretation of this condition is somewhat similar to the interpretation of condition 3, except that there is a history of a performance problem that may have been corrected, or partially alleviated. This situation is an ambiguous one, requiring a more detailed evaluation. The assessment would be different if there were 2 failures in last 50 demands, and 2 failures in last 20 demands, than if there were 4 failures in last 50 demands and 2 in last 20. An alert is indicated by this condition.

27. Risk-Based Performance Indicators
(John L. Boccio and A. Azarm)

27.1 Introduction

AEOD, with assistance from the interoffice of task group for performance indicators, has developed and implemented a set of performance indicators for initial use by NRC. These performance indicators are logically related to safety in a qualitative way, but not in a quantitative way, because a reliability/risk based method for quantitatively evaluating either individual indicators or an aggregated set of indicators was not yet available. As stated in the report of the interoffice task group (and SECY-86-317), the purpose of this research project is to develop such methods for reliability/risk based evaluation of performance indicators and alert levels. The results will be used to strengthen NRC's evaluation and use of performance indicators to identify and trend symptoms of declining performance between SALP reviews.

27.2 Objective

The overall objective of this program is to develop a method for applying reliability and risk technology to help select, interpret, and evaluate quantitative indicators of safety performance and operating plants.

27.3 Summary of Prior Efforts

Research in reliability technology performed by BNL under FIN A-3282 explored how performance indicators and alert levels can be directly tied to plant risk and how these risk-based indicators/alert levels might be used as part of an integrated reliability program for helping to maintain an acceptable level of reactor safety throughout a plant's operating lifetime. A means for developing measures or indicators of plant performance by synthesizing, or combining, lower (or more basic) levels of performance is described in NUREG/CR-4618 along with a statistical approach for trending performance within a window in time that would reduce the effects of false alarms. A hierarchy of alert levels, consistent with severe accident probability, is used to measure performance.

In FY 1986, this project explored further the ways for developing risk-based methodology to evaluate the performance indicators and alert levels. A feasibility study was initiated for identifying, applying and evaluating approaches for enhancing the risk perspectives contained within current NRC indicators and for developing direct indicators of plant performance. Results from these research efforts in FY 1986, in the form of technical reports, letter reports, and memos primarily include:

Program Plan for Risk-Based Performance Indicators; letter report, Boccio to Johnson; dated August 30, 1986, which provided the work breakdown structure, the deliverables planned, and the schedule.

Use of LCO Data for Plant Performance Evaluation; letter, Azarm to Robinson; dated, August 25, 1986, which provides some initial thoughts on the use of data on LCO action statements for evaluating plant performance.

Risk-Based Indicators: Concepts, Utilizations and Issues; letter report, Vesely to Boccio; dated, August 26, 1986, which provided the basic structure and scope of this research project.

27.4 Work Performed During Period

During this reporting period, the project was largely engaged in (1) refining methods to relate currently used performance indicators more closely to risk and (2) developing methods for risk-based performance indicators applied to monitoring the unavailability of selected safety systems. In both of these areas, BNL provided a description of the risk-based method, a procedure guide for implementing the method, and where appropriate PC-compatible software for subsequent use by the NRC.

Methods for incorporating additional risk considerations with the current set of performance indicators identified by NRC's interoffice task group, concentrated on risk-weighting scrams, safety system actuations, significant events, and safety system failures. The procedure employed did not rely on whether the plant had a PRA associated with it. As such, simple, albeit conservative rules were developed to quantify the risk impact of operational events. The process taken is depicted in Figure 27.1, and a draft report[1] was prepared that provides a methodology for quantifying the risk associated with operational events. This draft report also documents the risk models employed, the spreadsheet developed and the process for incorporating the approach to any plant. To date, the method has been applied to three plants, viz, Surry, Limerick and Beaver Valley.

The output of the software provides the analyst with a conservative estimate of the conditional core-melt probability for the event being analyzed. It is intended through the use of this methodology to provide an aggregate risk-based measure of performance using current indicators over a time period (T). The table below shows a relative ranking used by this procedure guide to binoperational events.

Risk Impact Category	Exposed Risk Description
Very High	$R>10^{-3}(T)$
High	$10^{-3}(T)>10^{-4}(T)$
Medium	$10^{-4}(T)>R>10^{-5}(T)$
Low	$R<10^{-5}(T)$

Currently, the NRC is exploring the practicality of implementing this approach within its current trending programs.

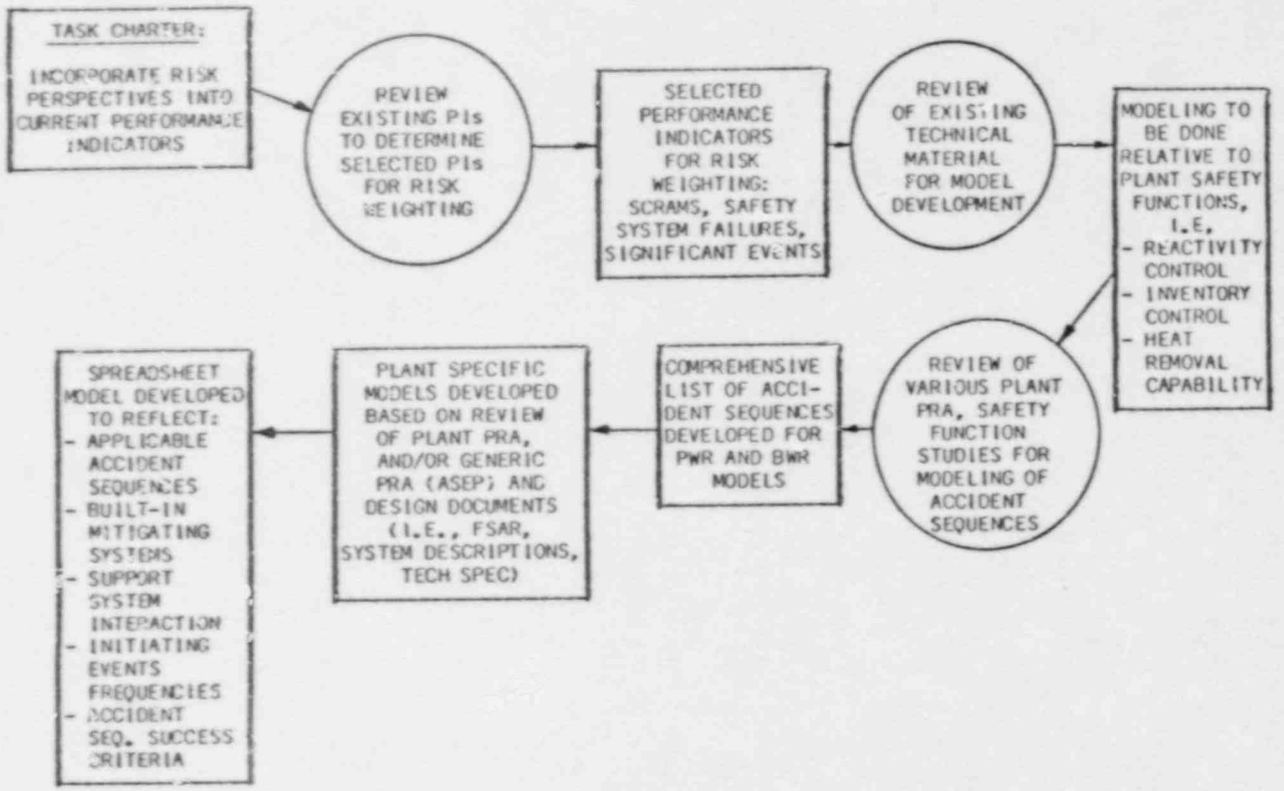

Fig. 27.1. Incorporate risk perspectives into current performance indicators

In addition to developing methods for risk weighting NRC's current set of performance indicators, this project has been engaged in developing indicators for monitoring the unavailability of select safety systems. A report[2] was prepared during this reporting period that presents system unavailability indicators which can be constructed from observing downtime occurrences of systems or trains.

Alternative indicators are presented which utilize different types of recorded downtime data. The formulations are presented for each indicator along with the unavailability contributions which are specifically monitored. The response times are also given for the different types of downtime data which can be recorded. The response time, which is the average time between observed downtimes, determines the time required to detect trends. Based on the response times and other evaluations that are performed, recommendations are made as to the most efficient indicators to use for given applications.

Table 27-1 illustrates the response times for given train reliability parameters for the different types of downtime data which can be recorded. In the report other tables and figures are given for other train reliability parameters. The general conclusions from all these tables are the same: train downtime data provide significantly faster response times than system downtime data.Furthermore, recording all unscheduled downtimes provides faster response times than recording only catastrophic failures. By recording all unscheduled downtimes of a train, trends can be detected on the order of months instead of years, when only system downtimes are recorded.

Figure 27-2 illustrates the options which are identified in the report for monitoring train unavailability and for recording train downtime data. Based on the report's findings, the items which are circled represent the most efficient options for monitoring train unavailability and hence system unavailability. The efficient options are first to monitor only the unscheduled downtime contributions to the unavailability as opposed to monitoring both scheduled and unscheduled downtime contributions, and to monitor only the frequency of these unscheduled downtimes. To monitor the unscheduled downtime contributions, the times of individual downtimes should be recorded as opposed to recording only the number of downtimes. Finally, the times of all unscheduled downtimes should be recorded as opposed to recording only catastrophic failures.

The options at the two lowest levels of Figure 27-2 should be carried out if at all possible, that is one should record what other equipment is already down when a downtime occurs, and one should record the causes of the downtime. The fact that other equipment is already down, such as for testing or maintenance, can have orders of magnitude impact on the unavailability. Also, one should record the causes of downtime with as much detail as is feasible. The classification system in the Nuclear Plant Reliability Data System (NPRDS) is an example of a useful cause classification system. Recording the various causes of downtimes is important not only to diagnose problems, but to evaluate common cause failure potentials and to predict generic implications of the downtimes.

Table 27.1. Average Times Between Recorded Downtimes for Different Situations and for Different Types of Downtimes Recorded

TYPE OF DOWNTIME RECORDED	PRESENT GENERIC DATA (SYSTEM UNAVAILABILITY = 3×10^{-4})*	SYSTEM UNAVAILABILITY INCREASES BY A FACTOR OF 4	SYSTEM UNAVAILABILITY INCREASES BY A FACTOR OF 16	SYSTEM UNAVAILABILITY INCREASES BY A FACTOR OF 100
CATASTROPHIC FAILURES OF THE SYSTEM ONLY RECORDED	96 YEARS	23 YEARS	6 YEARS	1 YEAR
ANY UNSCHEDULED DOWNTIME OF THE SYSTEM RECORDED	10 YEARS	2.5 YEARS	7 MONTHS	1 MONTH
CATASTROPHIC FAILURES OF A TRAIN ONLY RECORDED	3 YEARS	1.5 YEARS	8 MONTHS	3 MONTHS
ANY UNSCHEDULED DOWNTIME OF A TRAIN RECORDED	4 MONTHS	2 MONTHS	1 MONTH	2 WEEKS

*BASED ON A TWO TRAIN SYSTEM WITH GENERIC SYSTEM UNAVAILABILITY OF 3×10^{-4}. EACH TRAIN HAS A CATASTROPHIC FAILURE RATE OF 4×10^{-5} PER HOUR, A CORRECTIVE MAINTENANCE RATE OF 3×10^{-4} PER HOUR, MONTHLY TESTING AND AN AVERAGE DOWNTIME DURATION OF 8 HOURS. A CATASTROPHIC FAILURE OF THE SYSTEM IS DEFINED HERE AS BOTH TRAINS CATASTROPHICALLY FAILING. A CATASTROPHIC FAILURE OF A TRAIN IS A COMPLETE LOSS OF FUNCTION OF THE TRAIN.

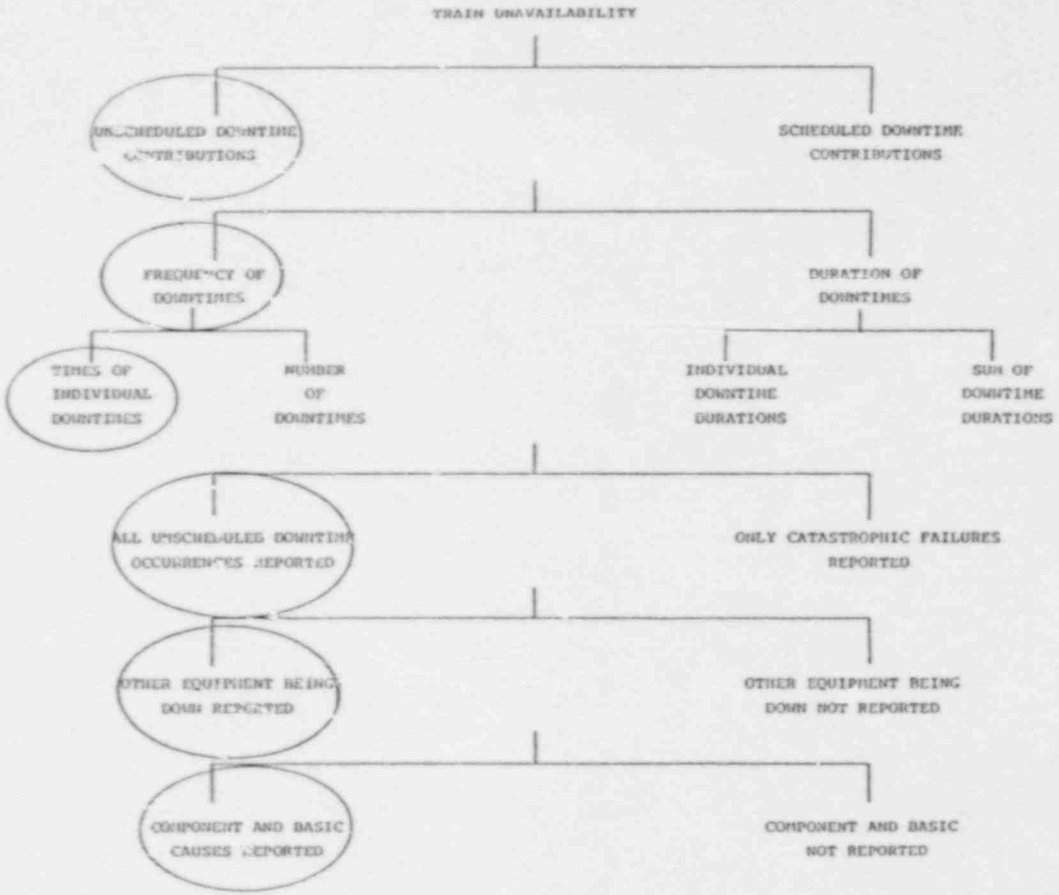

Fig. 27.2. Options in monitoring train unavailability

Even though the above options represent the most efficient ones, the report's findings are also that all information on the downtimes should be recorded if feasible. Particularly the duration of the downtime and, for catastrophic failures, the time since the last test of the train should be recorded if feasible. The downtime durations give a more accurate estimate of the train and system availability, and also can be used to investigate relationships between maintenance and availability. The time since the last test for catastrophic failures gives the undetected downtime during which the failure existed, which is a major contributor to the unavailability.

With regard to the downtime reporting frequency, the report's findings are that the times of downtimes should be reported as quickly as possible to detect abrupt degradations in unavailability. The supplemental information on the downtime occurrences, such as the causes of the downtime, can be provided later. Examples are provided to test whether the indicators can track time trends and anomalous swings in the frequency and unavailability performance of a train or a system.

27.5 References

1. Azarm, M.A., and J.F. Carbonaro, "Incorporating Risk Perspectives into Present Indicators Using Risk Categorization Scheme: Procedure Guide," March 1987.

2. Vesely, W.E., and Azarm, M.A., "System Unavailability Indicators," BNL Technical Report, A-3295 9-30-87, September 1987.

28. Study of Beyond Design Basis Accidents in Spent Fuel Pools (Generic Issue 82)

(V. L. Sailor, K. R. Perkins, J. R. Weeks and H. R. Connell)

28.1 Background

Generic Safety Issue 82, "Beyond Design Basis Accidents in Spent Fuel Pools," was assigned a medium priority in November 1983. In this prioritization, the NRC staff considered three factors that had not been included in earlier risk assessments:

1. Spent fuel is currently being stored rather than shipped for reprocessing or repository disposal, resulting in much larger inventories of spent assemblies in reactor fuel basins than had previously been anticipated,

2. In order to accommodate the larger inventory, high density racking is necessary, and

3. A theoretical model suggested the possibility of Zircaloy fire, propagating from recently discharged assemblies to lower power assemblies in the event of complete drainage of water from the pool.

The Reactor Safety Study concluded that the risks associated with spent fuel storage were extremely small in comparison with accidents associated with the reactor core. That conclusion was based on design and operational features of the storage pools which made the loss of water inventory highly unlikely. In addition it was assumed that the pool inventory would be limited to about one-third of a core.

Subsequent to the Reactor Safety Study, A.S. Benjamin et al. investigated the heatup of spent fuel following drainage of the pool. A computer code, SFUEL, was developed to analyze thermal-hydraulic phenomena occurring when storage racks and spent fuel assemblies become exposed to air.

Calculations with SFUEL indicated that, for some storage configurations and decay times, the Zircaloy cladding could reach temperatures at which the exothermic oxidation would become self-sustaining with possible cladding damage and fission product release. The possibility of propagation to adjacent assemblies (i.e., the cladding would catch fire and burn at a high enough temperature to heat neighboring fuel assemblies to the ignition point) was also identified. Under very restricted flow conditions, SFUEL predicted that spent fuel stored for up to 3 years (and having a correspondingly low decay heat) could become involved. Cladding fires of this type could occur at temperatures well below the melting point of the UO_2 fuel. The cladding ignition point is about 900°C compared to the fuel melting point of 2880°C.

There is no case on record of a significant loss of water inventory from a domestic, commercial spent fuel storage pool. However, two recent incidents have raised concern about the possibility of a partial draindown of a storage pool as a result of pneumatic seal failures.

The first incident occurred at the Haddam Neck reactor during preparations for refueling with the refueling cavity flooded. An inflatable seal bridging the annulus between the reactor vessel flange and the reactor cavity bearing plate extruded into the gap, allowing 200,000 gallons of borated water to drain out of the refueling cavity into the lower levels of the containment building in about 20 minutes. Gates to the transfer tube and the fuel storage pool were in the closed position, so no water drained from the pool.

The second pneumatic seal failure incident occurred in the Hatch spent storage pool/transfer canal, (the seal failure at Hatch was not in the refueling cavity) which released approximately 141,000 gallons of water and resulted in a drop in water level in the pool of about five feet.

However, the BNL review of these events indicates that they are unique to the plants involved and such events are unlikely to cause a substantial loss of pool inventory for other plants. However, pneumatic seal failures may expose individual fuel bundles during refueling and these events are being investigated as part of Generic Issue 137, "Refueling Cavity Seal Failure."

28.2 Project Objective

The objective of this investigation is to provide an assessment of the potential risk from possible accidents in spent fuel pools. The risks are defined in terms of:

- the probabilities of various initiating events that might compromise the structural integrity of the pool or its cooling capability,
- the probability of a system failure, given an initiating event,
- fuel failure mechanisms, given a system failure,
- potential radionuclide releases, and
- consequences of a specified release.

This study generally follows the logic of a typical probabilistic risk analysis (PRA); however, because of the relatively limited number of potential accident sequences which could result in the draining of the pool, the analyses have been greatly simplified.

28.3 Project Status

During this reporting period, extensive comments on the draft report were received from the NRC Project Manager. These comments were evaluated and integrated into the final report (NUREG/CR-4982). The major conclusions are summarized in the next section.

28.4 Results

The likelihood and consequences of various spent fuel pool accidents have been combined to obtain the risks which are summarized in Table 28.1. The population dose results are insensitive to the fission product release because they are driven by decontamination levels assigned within the consequence model used (namely the CRAC2 code). The health physics models in the CRAC2 code assign a maximum allowable dose for each individual before the

Table 28.1 Estimated Risk for the Two Spent Fuel Pools from the Two Dominant Contributors

Accident Initiator	Spent Fuel Pool Fire Probability/Ry	Health Risk[1] (Man-rem/Ry)	Interdiction[1] Risk (Sq. Mi./Ry)
Seismic induced PWR pool failure	2.6×10^{-4}-1.6×10^{-10}	600-Neg.*	.011-Neg.
Seismic induced BWR pool failure	6.5×10^{-5}-4×10^{-11}	156-Neg.	.003-Neg.
Cask drop[2] induced PWR pool failure	3×10^{-5}-3×10^{-12}	70-Neg.	.001-Neg.
Cask drop[2] induced BWR pool failure	8×10^{-6}-8×10^{-13}	20-Neg.	4×10^{-4}-Neg.

*Neg. - Negligible.

[1]The upper end of the risk ranges assumes no fire propagation from the last fuel discharge to older fuel. However, the fission products in the last fuel discharge were assumed to be released during the fire with no fission product decontamination on structures.

[2]After removal of accumulated inventory resumes. Presently, most plants are accumulating spent fuel in the pool without shipping to permanent storage. (Note that many new plants have pool configurations and administrative procedures which would preclude this failure mode.)

contaminated area is reoccupied. This allowable dose for the returning population is the dominant contributor to total exposure given in Table 28.1 and limits the utility of the dose calculation. Thus the land interdiction area is included in Table 28.1 as a more sensitive representation of the severity of the postulated accident.

The unique character of fuel pool accidents (potentially large releases of long lived isotopes) makes it difficult to compare directly to reactor core melt accidents. There are no early health effects. The long-term exposure calculations are driven by assumptions in the CRAC modeling and the results are not very sensitive to the size of the fission product release. There is substantial uncertainty in the fission product release estimates. These uncertainties are due to both uncertainty in the accident progression (fuel temperature after clad oxidation and fuel relocation occurs) and the uncertainty in fission product decontamination.

A number of potential preventive and mitigative measures were identified, but because of the large uncertainty ranges in Table 28.1, the potential benefits of such measures are also uncertain and plant specific. A cost benefit analysis has not been performed. Rather, the phenomenological insights, developed during the investigation, have been used to generate a list of possible risk reduction measures. Calculations with the SFUEL code indicate that, for those plants that use a high density storage rack configuration, a factor of five reduction in the fire probability (given loss of pool inventory) can be achieved by improved air circulation capability. This reduction factor is based upon the time period after discharge for which SFUEL predicted that the decay heat is sufficient to initiate a clad fire. Considering the large uncertainty in risk, a plant specific cost/benefit analyses should be performed before such risk reduction measures are implemented.

REFERENCES

U.S. NUCLEAR REGULATORY COMMISSION (1983), "A Prioritization of Generic Safety Issues," Division of Safety Technology, Office of Nuclear Reactor Regulation, NUREG-0933, pp. 3.82-1 through 6.

U.S. NUCLEAR REGULATORY COMMISSION (1975), "Reactor Safety Study, An Assessment of Accident Risk In U.S. Nuclear Power Plants," NUREG-75/014, (WASH-1400), App. I, Section 5.

BENJAMIN, A. S., et al. (1979), "Spent Fuel Heatup Following Loss of Water During Storage," Sandia National Laboratories, NUREG/CR-0649, (SAND77-1371).

PISANO, N. A., et al. (1984), "The Potential for Propagation of a Self-Sustaining Zirconium Oxidation Following Loss of Water in a Spent Fuel Storage Pool," Draft Report, Sandia National Laboratories, (Note: the project ran out of funds before the report was published.)

U.S. NUCLEAR REGULATORY COMMISSION, IE Bulletin No. 84-03: "Refueling Cavity Water Seal," Office of Inspection and Enforcement, August 24, 1984.

LICENSEE EVENT REPORT, LER No. 84-013-00, Haddam Neck, Docket No. 50-213, "Failure of Refueling Pool Seal," 09/21/84.

BAKER, G. (1986), "Hatch Error Releases 141,000 Gallons of Spent Fuel Pool Waters," Nucleonics Week, Vol. 27, No. 50, pgs. 3-4.

CROFF, A. G. (1983), "ORIGEN2: A Versatile Computer Code for Calculating the Nuclide Composition and Characteristics of Nuclear Materials," Nuclear Technology, Vol. 62, pp. 335-352.

RITCHIE, L. T., et al. (1983), "Calculations of Reactor Accident Consequences Version 2, CRAC2: Computer Code User's Guide," Sandia National Laboratories, NUREG/CR-2326 (SAND81-1994).

29. Development of Technical Basis for Severe Accident Guidelines and Procedural Criteria for Existing BWR Plants

(K. R. Perkins, W. T. Pratt, W. J. Luckas, J. R. Lehner and R. G. Fitzpatrick)

29.1 Background

The U.S. Nuclear Regulatory Commission (NRC) has formulated an approach for a systematic safety examination of existing plants to determine whether particular severe accident vulnerabilities are present and what changes are desirable to ensure that there is no undue risk to public health and safety.

The Industry Degraded Core Rulemaking Program (IDCOR) selected four reference plants for detailed analysis: Peach Bottom, Grand Gulf, Sequoyah, and Zion. The IDCOR analyses performed for the reference plants have been documented together with the methodology used for the analyses and the technical basis supporting the methodology.

Parallel with the IDCOR work, the NRC under the Severe Accident Research Program (SARP), performed risk assessments, audit calculations, sensitivity studies, and uncertainty analyses for five plants. The five plants considered by SARP were Peach Bottom, Grand Gulf, Sequoyah, Zion, and Surry.

The purpose of this effort is to review all of the IDCOR and SARP analyses performed for the reference plants, understand the reasons for the differences, and then use the experience gained from these reviews for identifying plant features and operator actions that were found to be important for either preventing or mitigating severe accidents in each plant type.

29.2 Project Objectives

Three basic goals for this severe accident program apply equally to all plant types:

- Goal 1: Mitigate fission-product releases.
- Goal 2: Control the frequency of high-consequence sequences.
- Goal 3: Reduce high core-damage frequency.

The aim was, therefore, to identify specific plant features, operator actions and their important attributes which could be used to achieve these goals during the examination of individual plants.

29.3 Project Status

Based on an extensive review of prior severe accident investigations, the authors have identified a detailed list of plant features, operator actions and their important attributes which can be used to assess the capability of individual boiling water reactor (BWR) plants to cope with severe accidents. Although much of the work is based on probabilistic risk assessments (PRAs), the plant features, operator actions and associated attributes are deterministic in nature. That is, the list of attributes describe specific features of

key systems and operational procedures which have been found helpful in reducing the likelihood of severe accidents. The project takes into account detailed severe accident experiments and analyses performed by the NRC/RES, the nuclear power industry and foreign governments.

During the reporting period three draft reports have been assembled which identify the plant features, operator actions and associated attributes which have been found to be important for the three BWR containment types (Mark I, Mark II, and Mark III). These draft reports were submitted to the NRC and the ACRS staff for review. Substantial comments were received and will be incorporated into the revised reports.

During this reporting period a draft report was prepared by [illegible] Consultants, R. J. Budnitz and V. Joksimovich, on the "Content of PRA S[illegible] for Future LWRs." This report is under review by both BNL and NRC st[illegible]

30. Development of Technical Basis for Severe Accident Guidelines and General Criteria for Existing PWR Plants

(K. R. Perkins, W. T. Pratt, J. R. Lehner, W. J. Luckas and R. G. Fitzpatrick)

30.1 Background

The U.S. Nuclear Regulatory Commission (NRC) has formulated an approach for a systematic safety examination of existing plants to determine whether particular severe accident vulnerabilities are present and what changes are desirable to ensure that there is no undue risk to public health and safety.

The Industry Degraded Core Rulemaking Program (IDCOR) selected four reference plants for detailed analysis: Peach Bottom, Grand Gulf, Sequoyah, and Zion. The IDCOR analyses performed for the reference plants have been documented together with the methodology used for the analyses and the technical basis supporting the methodology.

Parallel with the IDCOR work, the NRC under the Severe Accident Research Program (SARP), performed risk assessments, audit calculations, sensitivity studies, and uncertainty analyses for five plants. The five plants considered by SARP were Peach Bottom, Grand Gulf, Sequoyah, Zion, and Surry.

The purpose of this effort is to review all of the IDCOR and SARP analyses performed for the reference plants, understand the reasons for the differences, and then use the experience gained from these reviews for identifying plant features and operator actions that were found to be important for either preventing or mitigating severe accidents in each plant type.

30.2 Project Objectives

Three basic goals for this severe accident program apply equally to all plant types:

- Goal 1: Mitigate fission-product releases.
- Goal 2: Control the frequency of high-consequence sequences.
- Goal 3: Reduce high core-damage frequency.

The aim was, therefore, to identify specific plant features, operator actions and their important attributes which could be used to achieve these goals during the examination of individual plants.

30.3 Project Status

Based on an extensive review of prior severe accident investigations, the authors have identified a detailed list of plant features, operator actions and their important attributes which can be used to assess the capability of individual pressurized water reactor (PWR) plants to cope with severe accidents. Although much of the work is based on probabilistic risk assessments (PRAs), the plant features, operator actions and associated attributes are deterministic in nature. That is, the list of attributes describe specific

features of key systems and operational procedures which have been found helpful in reducing the likelihood of severe accidents. The project takes into account detailed severe accident experiments and analyses performed by the NRC/RES, the nuclear power industry and foreign governments.

During the reporting period two draft reports have been assembled which identify the plant features, operator actions and associated attributes which have been found to be important for the two PWR containment types (ice condenser and large dry). These draft reports were submitted to the NRC and the ACRS staff for review. Substantial comments were received and will be incorporated into the revised reports.

31. Interfacing Systems LOCA at LWRs

(G. Bozoki, P. Kohut, T-L. Chu, R. Fitzpatrick)

31.1 Background

The term "interfacing system LOCA" (ISL) refers to a class of nuclear plant loss-of-coolant accidents in which the interface between the Reactor Coolant System (RCS) pressure boundary (isolation valve, piping wall, etc.) and a supporting system of lower design pressure is breached. A subclass of these accidents takes on special concern when the flow path affects the availability of the safety systems needed to mitigate the accident. This can occur by directly overpressurizing the safety system possibly outside primary containment, thus establishing discharge of coolant directly to the environment. Depending on the configuration and accident sequence, the Emergency Core Cooling System (ECCS) as well as other injection paths may fail, resulting in a core melt with containment bypass.

The Reactor Safety Study[1] (WASH-1400) pointed out that a subclass of these types of accidents, called V-events,* can be significant contributors to the risk resulting from core damage. In spite of numerous analyses conducted in various PRAs, both the probability and the consequence estimates for interfacing system LOCA (ISL) sequences continue to be subject to substantial uncertainties. Depending on assumed valve failure modes, common cause contribution, valve monitoring, test and maintenance strategies, and statistical data handling methods, the total core damage frequency due to ISL accidents may vary from 10^{-4} to 10^{-8}/reactor year. The radiological consequences are also subject to large variations due to plant-specific features, the location of the secondary break, and the radionuclide behavior under the particular ISL sequence (e.g., break is below or above water level).

The NRC has taken steps to impose requirements to reduce the frequency of ISLs and has conducted a number of programs (analytical, experimental, inspection) to study various aspects of ISL accidents.

31.2 Project Objectives

The primary goals of the present project are (a) provide technical support to NRC, Reactor and Plant Systems Branch to resolve this issue, (b) investigate the frequency and the effects of ISLs, (c) identify any improvements that would significantly reduce the frequency of ISLs, (d) determine the cost-benefit aspect of the improvements, and (e) determine the effects and the cost-benefit relationship of instituting leak testing programs of the pressure isolation valves for those plants that do not currently have such a requirement.

*The V-events were defined for PWRs and involved the failure of two check valves in series or two check valves in series with an open motor-operated valve.

31.3 Technical Approach

The overall methodology of the project includes the following elements:

- From all the potential ISL flow paths (at the six representative BWR and PWR plants), pathways were identified as candidates where ISLs may occur.
- For the selected pathways, ISL initiator frequencies were calculated by utilizing all available information, including plant visits and new failure data obtained from root cause analysis of experienced pressure isolation valve failures.
- In the PWR analysis, the relief valve capacities were considered in classifying ISL initiators leading to overpressurization of low pressure piping and small LOCAs.
- For each of the identified pathways, event trees were constructed assuming two types of initiators: overpressurization events leading to small or large LOCA and events without overpressurization resulting in small LOCA. The event trees describe the immediate plant response (status of frontline safety systems and support systems), the accident management (thermal hydraulic features of the accident and operator responses) and pipe rupture probabilities. The end states of the event trees were connected to plant specific PRA event trees through a conditional core damage frequency multiplier. Special attention was given to the estimate of pipe rupture probability.
- All accident scenarios resulting in core damage were computed. Scenarios leading to ISLs bypassing containment were further evaluated for health risk by using "scrubbed" and "nonscrubbed" source terms (i.e., characterizing pipe ruptures below or above water level, respectively).
- The sensitivities of core damage frequency and corresponding risks were calculated for each of the scenarios assuming various corrective actions such as:
  a. more frequent leak testing of check valves and motor-operated valves,
  b. application of permanent pressure sensors in the piping between valves,
  c. ensuring the availability of alternate injection sources in addition to the standard ones (RWST, etc.),
  d. improved operator training, and
  e. deferring testing of certain high risk pressure isolation valves until reactor shutdown.
- The sensitivities of core damage frequency and corresponding risks were calculated for each of the reference plants by removing the benefits of leak testing over a protracted period of time.
- Cost-benefit calculations were performed for each of the corrective actions using the risk data obtained with scrubbed and nonscrubbed source terms. In comparing the results, strategies were suggested for determining the optimum method to decrease the occurrence of ISLs and/or mitigate their risk effects.
- A generic cost-benefit calculation was also performed to investigate the effect of instituting a minimum leak testing program for plants that do not currently have such a requirement.

31.4 Project Status

The overall results for this project were being finalized at the close of the period. The results will be issued as two separate NUREG/CR reports (BWR and PWR) during the next reporting period.

Reference

1. "Reactor Safety Study - An Assessment of Accident Risks in Commercial U.S. Nuclear Power Plants," WASH-1400 (NUREG-75/914), USNRC, October 1975.

32. Improved Reliability of Residual Heat Removal Capability in PWRs as Related to Resolution of Generic Issue 99

(T-L. Chu, R. G. Fitzpatrick)

32.1 Background

NRC Generic Issue 99 is concerned with the general problem of loss of residual heat removal (RHR) capability in PWRs during cold shutdown operations. U.S. experience includes numerous partial or total losses of RHR events, attributable to various design- and operationally-related causes. While none of these events resulted in major consequences, it is expected that an extended loss of RHR capability under cold shutdown conditions could be a significant contributor to overall plant risk. Of particular significance is the common cause failure of both RHR loops due to a loss of suction arising from: (a) the inadvertent closure of the RHR suction/isolation valves as a result of the failure or misoperation of the associated valve autoclosure interlocks or (b) an excess lowering of the water level in the reactor vessel during drained-RCS operations. In the absence of prompt mitigative action by the operator, the loss of RHR flow could result in pump cavitation and damage, delayed recovery of RHR capability, and a potential for core uncovery. Additionally, inadvertent closure of the RHR suction valves during solid plant operations, isolates the RCS from the RHR pressure relief valve system and allows for possible challenge of the PORV safety system provided for the low temperature overpressure protection (LTOP) of the reactor coolant system.

32.2 Objective

The objective of this project is to obtain generic estimates of the risk reduction potential provided by various RHR design/operational changes proposed for cost-effective improvement in the reliability of RHR capability in PWRs during plant outage operations.

32.3 Technical Approach

The starting point for the BNL study was NSAC-84,[1] "Zion Nuclear Plant Residual Heat Removal PRA." This probabilistic risk assessment was sponsored by the Electric Power Research Institute in cooperation with Commonwealth Edison Company. The benefits derived from using NSAC-84 as a starting point included a shutdown-specific data base, a detailed plant description for accurate modelling and insights into the progression of various accident sequences. NSAC-84 investigated a number of initiating event categories to provide a broad picture of shutdown risk. The BNL analysis essentially covers the same scope as NSAC-84 except that low temperature overpressurization events were not included in the BNL analysis because they are being addressed under NRC Generic Issue 94.

Modifications applied to the NSAC-84 model included redefinition of the phases of an outage, new estimates of the durations of phases (in particular, the duration that a plant stays in the partially drained condition), and the modelling of human cognitive errors. In the BNL analysis, generic shutdown data were collected and used to estimate the frequencies of initiating

configuration under the assumption that the Zion plant is representative of a majority of the U.S. PWRs.

Because Generic Issue 99 deals primarily with loss-of-cooling events and loss-of-cooling events dominate the preliminary results of this study, the insights will focus upon the loss-of-cooling event results. However, the results for all three initiating event categories will be included.

A containment event tree was developed to assess the integrity of the containment given that a core damage event occurred during shutdown. Due to insufficient data on the top events in the event tree, it could not be fully quantified. Therefore, sensitivity calculations were done to assess the sensitivity of the containment event tree to uncertainty in the top events. Each of the containment event tree end points imply a fission product release path (or release category) from the damaged reactor core to the environment. A range of possible release categories during shutdown were estimated from previous calculations[2] for accidents from power operation. The offsite consequences of the release categories were assessed using the MACCS[3] code. The results of these calculations are presented in the framework of sensitivity study. The sensitivity study addresses the possibilities of 1) having the equipment hatch open and not being above to close it, 2) having a containment penetration open and not being able to seal it, and 3) the potential for reducing the source terms given containment spray availability. The insights derived from the sensitivity study cover potentially beneficial changes to the Technical Specifications.

32.4 Project Status

The results for this project were being finalized at the close of the period. A final report will be issued as NUREG/CR-5015 during the next reporting period.

References

1. "Zion Nuclear Plant Residual Heat Removal PRA," NSAC-84, July 1985.

2. "Reactor Safety Study: An Assessment of Accident Risks in U.S. Commercial Nuclear Power Plants," WASH-1400, NUREG-75/014, October 1975.

3. Chain, D. I. et al., "MELCOR Accident Consequence Code System (MACCS) Users Guide," Sandia National Laboratories (to be published).

33. Support for Containment Loading Studies

(M. Lee and R. Bari)

33.1 Background and Objectives

A considerable amount of information has been developed regarding the thermal-hydraulic phenomena associated with severe accidents as a result of studies which have been conducted over the past several years. These studies have been sponsored by the NRC and by organizations outside this country, notably analytical studies and experimental programs in the United Kingdom, the Federal Republic of Germany, and France. Currently, the NRC staff is considering information from a joint international study on specific containment loading phenomena being pursued under the various expert groups within the Committee on the Safety of Nuclear Installations (CSNI), which is part of the Organization for Economic Cooperation and Development (OECD). In this project BNL is providing the NRC with an evaluation of the remaining issues on thermal-hydraulic phenomena associated with severe accidents based on a comparison of analyses performed by various members of the CSNI expert groups. The evaluation involves not only an assessment of the international community's analyses of containment loading phenomena from severe accidents but also those sponsored by the NRC.

33.2 Work Performed During Period

BNL provided help in finalizing a CSNI report on two international standard problems related to core/concrete interactions (SP-1) and combustible gas distribution (SP-2) in a containment building. Presentations on these two standard problems were also prepared.

BNL prepared a report on "Status of Direct Containment Heating in the United States" and this was presented to the task group at its meeting in May 1987. BNL is participating in a subgroup that is developing an international status report on direct containment heating work in the OECD countries.

BNL prepared a description of severe accident open issues for presentation to the CSNI Principal Work Group (PWG) #2 task group on ex-vessel severe accident thermal-hydraulics. This will be presented to the task group at its meeting in October 1987.

BNL is the coordinator of the third international standard problem (SP-3) on the SURC-4 experiment. BNL will formulate the standard problem calculation and associated reporting formats and prepare the comparison report after results are received from participating countries. Presentations will be made on the problem to the task group and the participants during October 1987.

34. Support for TRAC-PF1/MOD1 Uncertainty Analysis
(W. Wulff and U. S. Rohatgi)

34.1 Introduction

The USNRC is developing the Code Scaling, Applicability and Uncertainty (CSAU) Methodology [USNRC Draft Report, 1987] for estimating quantitatively the uncertainty in code predictions of important reactor safety parameters, such as the Peak Clad Temperature (PCT) in a Large Break Loss of Coolant Accident (LBLOCA). The CSAU Methodology is being applied first to the TRAC-PF1/MOD1 computer code, simulating an LBLOCA, to demonstrate the feasibility of the Methodology.

The project concentrates on determining the uncertainty in predicting Peak Clad Temperature (PCT) as the important parameter because (PCT) characterizes fuel integrity, i.e., the ability of the fuel cladding to retain fission products. Code uncertainties are quantified, therefore, on the basis of the code's ability to predict PCT accurately. During an LBLOCA, the clad temperature reaches, in general, two peaks; one during the earlier blowdown phase, the other one later, after the refill phase. Which one of the two peaks is higher depends on fuel design and coolant loop response characteristics. The clad temperature rises when the fuel element is suddenly surrounded by dry vapor. Then, more stored energy passes from the fuel pellets through the annular gas gap to the clad, then passes from the clad to the vapor, because the convective heat transfer is sharply reduced (dry-out or post-critical heat flux (CHF)). The clad temperature reaches a peak when it decreases due to improved convective cooling after the arrival of liquid in the core or due to a decrease in pellet temperature. In either case, more heat is removed by convection from the clad than is supplied to the clad from the fuel pellet.

The PCT is the higher, the faster the clad temperature rises and the longer it rises. PCT uncertainty can therefore be decomposed into uncertainties of predicting the time rate of clad temperature rise and of predicting the time for liquid arrival in the core. The time rate of clad temperature change depends upon the energy initially stored in the fuel, primarily in the pellet, and upon the thermal response time of the fuel. The initially stored energy depends strongly on fuel parameters and on initial conditions. The thermal response of the fuel depends both on fuel parameters and on coolant conditions. The time for the reappearance of liquid in the core is dominated by break and pump flow characteristics for the first peak and by additional thermohydraulic loop phenomena for the second peak.

Thus, fuel stored energy, fuel thermal response, critical break flow and pump performance degradation under two-phase flow conditions are important and were analyzed in detail. Below in Sections 34.2.1 through 34.2.4 we describe first the effects on PCT uncertainty from fuel stored energy. Sections 34.2.5 through 34.2.7 present the transient fuel response effects, Section 34.3 presents the break flow analysis and Section 34.4 presents the pump performance analysis.

34.2 PCT Uncertainty from Fuel Stored Energy and Thermal Response Uncertainties (W. Wulff)

The objective of the analysis on fuel stored energy is to calculate the individual changes in initial fuel stored energy, associated with the known statistical uncertainties in input data specifications and with documented uncertainties of modeling fuel heat transfer in TRAC-PF1/MOD1. Specifically, the fuel stored energy variations are to be calculated for given 1σ-level uncertainties of:

(i) initial fission power,
(ii) local power peaking factors,
(iii) fuel thermal conductivity,
(iv) cladding thermal conductivity,
(v) gap conductance,
(vi) fuel heat capacity,
(vii) cladding heat capacity,
(viii) radial fission power distribution in pellet, and
(ix) convective film coefficient.

It will then be the objective of the work presented in Section 34.3 to calculate the variations of the peak clad temperature for the early or blowdown peak as they are caused by the uncertainties in the above nine parameters. The analysis is general in principle but evaluated for specific LBLOCA conditions in a Westinghouse plant with 17x17 fuel arrays. The analysis is evaluated for TRAC-PF1/MOD1 models and for reference conditions as computed by TRAC.

The effects from the above statistical uncertainties are then ranked in the order of their relative importance on peak clad temperature predictions.

34.2.1 Steady-State Thermal Analysis of Fuel

The energy stored in fuel pellet and clad was computed by integrating the steady-state temperature distributions in fuel pellet and clad. The temperature distributions we obtained by closed-form integration of the steady-state conduction equation, taking into account the temperature variation of thermal conductivities and the radial variation of fission power in the pellet.

The radii of fuel pellet and cladding were computed from specifications at room temperature and the expressions for thermal expansions in MATPRO [Hagrman et al., 1980]. The expressions given there were first used directly to compute the reference values $k_f(T_{fo})$ and $k_c(T_w)$ for pellet and cladding outer surfaces, respectively, and also to fit a power law and an exponential expression for $k_f(T)$ and $k_c(T)$ in the interior of pellet and cladding, respectively. Details will be presented in NUREG/CP-0091, Vol. 4, p. 23.

The dependencies of gas thermal conductivity and of radiative properties were also taken from MATPRO [Hagrman et al., 1980].

The fission power varies radially in accordance with

$$q_f'''(\xi_f) = \frac{n+2}{n+2(1+m)} \langle q_f''' \rangle_f [1 + m\xi_f^n] \tag{34.1}$$

where q_f''' = local volumetric fission power density

$\langle q_f''' \rangle_f$ = area-averaged fission power density

ξ_f = r/R_1, normalized radius in fuel pellet

R_1 = outer fuel pellet radius

r = radial coordinate

m,n = constants.

The form of Eq. (34.1) constitutes also the best type of fitting Westinghouse data as used in TRAC. The first coefficient on the right-hand side of Eq. (34.1) is needed to assure that averaging reduces Eq. (34.1) to an identity. The coefficients m and n vary in the ranges of $0 \leq m \leq 3$ and $2 \leq n \leq 4$. Specified Westinghouse data require $m = 0.403$ and $n = 3.917$. This means that the fission power density is greater around the periphery of the pellet and that the temperature is more uniform than for constant fission power density.

The Kirchhoff transformation

$$\theta = \frac{1}{k_{ref}} \int_{T_{ref}}^{T} k(T)dT \tag{34.2}$$

was used to convert the nonlinear conduction equation

$$\nabla \cdot (k \nabla T) + q''' = 0 \tag{34.3}$$

into the linear form

$$k_{ref}\nabla^2\theta + q'''(r) = 0 \tag{34.4}$$

The integral $\theta(r)$ of Eq. (34.4) was then solved for the temperature $T(r)$, by using Eq. (34.2).

First we obtained the wall temperature T_w from the known coolant temperature T_∞, the linear heating rate q_f', the given convective heat transfer coefficient $\bar{h}_c$ and the known outer clad radius R_w

$$T_w = T_\infty + q_f'/(2\pi R_w \bar{h}_c). \tag{34.5}$$

With T_w known, the cladding thermal conductivity $k_c(T_w)$ was computed according to MATPRO [Hagrman et al., 1980], then Eq. (34.4) was integrated for the clad to yield $\theta_c(r)$. The result was solved for the cladding temperature $T_c(r)$ and evaluated for $r = R_2$ to give the inner cladding temperature:

$$T_{ci} = T_w + \frac{1}{b_c} \ln\left[1 + \frac{b_c\, q'_f}{2\pi k_c(T_w)} \ln \frac{R_w}{R_2}\right] . \qquad (34.6)$$

where $b_c = -7.7123 \times 10^{-4}\ K^{-1}$ is the exponent of the curve fit $k_c(T) = k_c(T_w) \exp\left[T/T_w\right]^{b_c}$. The temperature difference across the gas gap was computed to account for radiative heat transfer, temperature-dependent gas conductivity and radiative surface properties, thermal expansions and temperature jump distance. Ultimately, the unknown ratio $\eta = T_{fo}/T_{ci}$, containing the known temperature T_{ci}(cf. Eq. (34.6)) and the unknown pellet surface temperature T_{fo} was computed from

$$Y(\eta) = C_1(\eta-1)\left(\frac{\eta+1}{2}\right)^B + \frac{C_2(\eta^4 - 1)}{\phi_1 + (c_1 + C_3\eta)^{-1}} - \phi_o = 0 , \qquad (34.7)$$

where $C_1 = k_g(T_{ci})/t$

$C_2 = \sigma T_{ci}^3$

$C_3 = c_2 T_{ci}$

$\phi_o = q'_f/(2\pi R_1 T_{ci})$

$\phi_1 = (R_1/R_2)(1/\varepsilon_c - 1)$

R_i = pellet radius

ε_c = 0.9151, clad emissivity

$\sigma = 5.6697 \times 10^{-8}\ Wm^{-2}K^{-4}$, Stefan-Boltzmann constant

and $B = 0.7085$ is the exponent in $k_g = A(\bar{T}/1K)^B$, $A = 2.639 \times 10^{-3}$ W/(mK) for the thermal conductivity of the gas in the gap. The constants $c_1 = 0.7856$ and $c_2 = 1.5263 \times 10^{-5} K^{-1}$ define fuel pellet emissivity by $\varepsilon_f = c_1 + c_2 T_{fo}$. Equation (34.7) is solved iteratively by the Newton-Raphson method. With T_{fo} found, the thermal conductivity of the pellet surface, $k_f(T_{fo})$, was computed in accordance with MATPRO [Hagrman et al., 1980].

With T_{fo} and $k_f(T_{fo})$ known from Eq. (34.7), the pellet temperature distribution $T_f(\xi_f)$ was computed from the integral of Eq. (34.4) and the inversion of Eq. (34.2). Setting $\xi_f = r/R_1$, one finds this result:

$$T_f(\xi_f) = T_{fo}\{1 + \frac{b_f + 1}{4T_{fo}k_f(T_{fo})}[R_1^2(q_f''')_{c\ell}][1 + \frac{4m}{(n+2)^2}$$

$$-\xi_f^2(1 + \frac{4m}{(n+2)}\xi_f^n)]\}^{1/(b_f+1)}, \qquad (34.8)$$

where $(q_f''')_{c\ell}$ is the fission power density at the centerline and given from Eq. (34.1) with $\xi_f = 0$:

$$R_1^2(q_f''')_{c\ell} = (n+2)q_f'/\{\pi[n+2(1+m)]\}. \qquad (34.9)$$

The symbols m and n in Eqs. (34.8) and (34.9) are defined by Eq. (34.1), while $b_f = 0.762303$ defines the thermal conductivity in the pellet interior via $k_f(T) = k_f(T_{fo})[T/T_{fo}]^{b_f}$

The maximum error from curve fits for k_c and k_f as used in Eq. (34.2) is less than 1%.

34.2.2 Comparison of Results from Closed-Form Integration with TRAC Results

Thermal conductivity and temperature distributions produced by TRAC-PF1/MOD1 were compared, respectively, with cited references in the TRAC document [NUREG/CR-3858, LA-10157-MS, 1986] and with closed-form integrations.

The TRAC document [NUREG/CR-3858, LA 10157-MS, 1986] claims that the fuel thermal conductivity is computed in TRAC in accordance with Reference [Hagrman et al, p. 23, 1980], but it is not. Evaluating the expressions in the TRAC document [Hagrman et al, pp. 501 and 502, 1980] for a fuel with 95% of theoretical density, one obtains the comparison with the MATPRO formulation [Hagrman et al, p. 22, 1980] as shown in Table 34.1 below. Also shown are the results of an extremely simple correlation given by [Malang, 1975], which is not only better than the TRAC formulation, but also produces results which are closer to the experimental data than the results from MATPRO; see [Wulff et al., p. 3-33, 1984]. Table 34.1 shows that the values calculated by TRAC are too low and should result in higher fuel temperatures than those obtained with the MATPRO values. It will be shown below that this is not the case.

All the equations for material properties, for solving Eq. (34.7) iteratively and for the temperature distributions, Eqs. (34.5, 6 and 8) were programmed on an HP-41/CX pocket calculator. The programs were executed to calculate the fuel temperature distribution in that rod and at that location, where TRAC computed the largest clad temperature at full power and under steady-state conditions in a Westinghouse PWR with 17x17 fuel arrays. It was

Table 34.1 Comparison of TRAC and MATPRO Results for Thermal Conductivity

Temperature K	Thermal Conductivity W/(mK)		
	MATPRO	TRAC	MALANG
300	8.28	7.56	8.91
500	6.09	5.42	6.08
750	4.47	4.03	4.38
1,000	3.58	3.23	3.45
1,250	3.03	2.73	2.89
1,500	2.68	2.39	2.55

the intent to have, for the reference calculation, the same conditions as in the TRAC-PF1/MOD1 calculation. These conditions are as follows:

linear heating rate, nominal		18.303 kWm^{-1}
local radial peaking factor		1.111
local axial peaking factor		1.050
hot rod peaking factor		1.215
linear heating rate, effective	q'_f =	25.942 $kWm^{-2}K^{-1}$
convective heat transfer coefficient	$\bar{h}_c$ =	40.05 $kWm^{-2}K^{-1}$
coolant temperature	T =	599.44 K
pellet radius, cold	R_{of} =	4.0960 mm
gap width, cold		0.0380 mm
outer clad thickness, cold		4.750 mm
pellet radius, @ full power	R_1 =	4.11994 mm
inrer clad radius	R_2 =	4.14058 mm
outer clad radius	R_w =	4.75756 mm
clad thickness (hot)		0.616981 mm

Since the convective heat transfer in TRAC is computed with the cold-value of outer clad radius, the heat transfer coefficient $\bar{h}_c$ had to be adjusted so that $(\bar{h}_c)_{TRAC}(R_w)_{COLD} = \bar{h}_c \cdot R_w$. The effective gap width was computed to produce the same gap conductance as produced in the TRAC code: $h_{gp} = 10.960$ $kWm^{-2}K^{-1}$. The same surface roughness and temperature jump distance (total of 4.4 μm) as in TRAC was employed and a gap width of 20.639 μm was obtained (not listed in TRAC output lists).

Table 34.2 below shows the comparison between the results from closed-form integrations and from TRAC.

The comparison reveals that the TRAC-computed centerline temperature is too low, even though the surface temperatures have been made to agree fairly well and even though the thermal conductivity k_f of the fuel is too low in TRAC as discussed above. Since the centerline temperature increases by approximately 16.4 K for a reduction in fuel thermal conductivity by 0.1 W/(mK),

Table 34.2 Comparison Between Closed-Form Integration and TRAC-PF1 Solutions

Location	Temperature (K)		
	Closed-Form Int.	TRAC	Difference
Fluid (T_∞)	599.440	599.440	
Outer Clad Surf. (T_w)	621.109	620.174	-0.94
Inner Clad Surf. (T_{ci})	654.932	654.08	-0.85
Pellet Surface (T_{fo})	746.368	746.295	-0.07
In Fuel Pellet at			
$r/R_1 = \sqrt{3}/2$	868.137	867.944	-0.19
$\sqrt{2}/2$	999.148	996.880	-2.27
$\sqrt{1}/2$	1,140.99	1,137.60	-3.39
0	1,296.16	1,290.75	-5.41

and since, according to Table 34.1 above, the mean difference between MATPRO and TRAC values of thermal conductivity is -0.46 W/mK), it appears as if TRAC had a total computational error of -(4.6 · 16.4 + 5.2) K = -80 K for the center line temperature. Notice that if TRAC accounts for fuel cracking or other phenomena which reduce the thermal conductivity but are not accounted for in the closed-form integration, then the deficit of the centerline temperature can only be larger.

34.2.3 Stored Energy

The thermal energy stored in fuel pellet and cladding is computed with respect to the energy at the coolant temperature T_∞. It is the sum of energies stored in fuel pellet and in cladding, namely

$$E = E_f + E_c \quad , \tag{34.10}$$

where

$$E_f = 2\pi \int_0^{R_1} \rho_f \int_{T_\infty}^{T_f(r)} [c_p(T)]_f \, dT \, r \, dr \tag{34.11}$$

$$E_c = 2\pi \int_{R_2}^{R_w} \rho_c \int_{T_\infty}^{T_c(r)} [c_p(T)]_c \, dT \, r \, dr \tag{34.12}$$

and ρ_f = 10,011.5 kg/m^3, fuel density [10]

ρ_c = 6,487/5 kg/m^3, clad density [10]

c_p = specific heat at const. pressure.

subscripts f and c designate fuel and clad, respectively. Specific heat as a function of temperature was computed on the basis of expression and tables given in MATPRO [Hagrman et al., pp. 9 and 206, 1980]. For UO_2 was computed $[c_p(T_{fo})]_f$ from the cited reference and $[c_p(T)]_f$ was curve-fitted by $[c_p(T)]_f = [c_p(T)]_f = [c_p\ (T_{fo})]_f\ [1+1.5299K^{-1}\ (T_f - T_{fo})]$, with an error of less than 0.6%. For zircaloy, the tabulated data [Hagrman et al., 1980] were curve-fitted by $[c_p(T)]_c = 80.20769\ J/(kgK)[T/1K]^{0.220247}$, with a maximum error of 0.6% and the coefficient of determinateness of 0.998.

The integrals of Eqs. (34.11) and (34.12) were numerically evaluated on an HP-41CX programmable pocket calculator, using its built-in quadrature algorithm. This algorithm was executed to guarantee six significant digits. With the conditions listed in Section 34.2.2 above, the following results were obtained:

E_f = 66.5903 kJ/m,

E_c = 1.4005 kJ/m and

E = 67.9908 kJ/m.

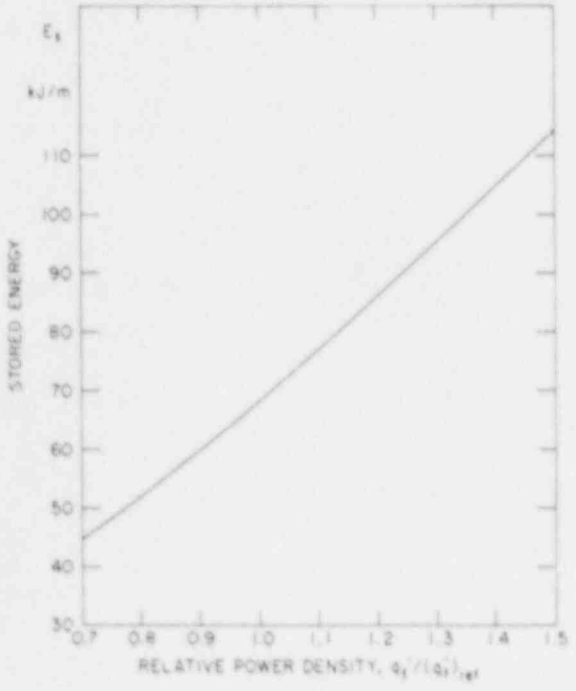

Figure 34.1 Stored Fuel Energy vs Fission Power

Figure 34.1 shows the dependence of fuel stored energy E on normalized linear heating rate or fission power, the fission power being normalized by the value listed in Section 34.2.2 above.

It was indicated in Section 34.2.2 that the TRAC code appears to underpredict the fuel centerline temperature by 80K. With Eq. (34.10), one can determine the corresponding deficiency in fuel stored energy. TRAC appears to underpredict fuel stored energy by 6.05 kJ/m or by 8.9% of its reference value relative to the coolant temperature (E = 0 for $\langle T_f \rangle_f = \langle T_c \rangle_c = T_\infty$).

34.2.4 Uncertainties in Predicting Fuel Stored Energy

Expressions for thermophysical properties and transfer laws are derived from experimental data with known random errors. Secondly, reactor and fuel conditions

are specified, but with statistical uncertainty. Thirdly, the mathematical models in TRAC-PF1/MOD1 were found to differ (cf. Table 34.1) from the documented models. The TRAC models have systematic errors because of such differences, because of parameter adjustments and because of numerical approximations (computational errors). Parameter adjustments and computer errors are being assessed by comparison with data [USNRC Draft Report, 1987]. Their consequences are known, but only within statistical error bounds.

Thus, even though a computer code execution is deterministic, the statistical uncertainties in input data specifications and the often unpredictable consequences from systematic errors cause computer results to be afflicted with essentially random errors, the magnitudes of which must be estimated with quantifiable confidence.

In this section are summarized the uncertainties in fuel-related parameter specifications. They were taken from previously published uncertainty analyses, from the available code documentation and from [Hagrman et al., 1980].

Uncertainties of Input Data Specifications. In the category of input data are (i) the initial power level or linear heating rate, (ii) the power distribution, (iii) the fuel dimensions at cold conditions and (iv) the condition of the fuel (burn-up conditions). Table 34.3 below summarizes the fuel-related input parameters, their 1-σ uncertainties, associated probability distributions and the references. Unknown probability distributions are specified as uniform because equal probabilities reflect the maximum of ignorance.

Table 34.3. Uncertainties in Input Data

Parameter	1-σ Uncertainty	Distribution	Reference
Fission Power	±2%	Normal	[Sheron, 1987] Table 2
Peaking Factors			
Local Axial	±0.7%	Normal	[Sheron, 1987] Table 2
Local Radial	±2.5%	Normal	[Sheron, 1987] Table 2
Pellet Radius (cold)	±0.1%	Uniform	[Laats, 1981] Table 2
Clad Radii (cold)	±0.1%	Uniform	[Laats, 1981] Table 2
Neutron Flux Depression			
m (Eq. 34.1)	±0.05	Uniform	Estimated
n (Eq. 34.1)	±0.3	Uniform	Estimated

The uncertainty in fission power reflects the random error of matching the calorimetric balance of the plant with instrument readings. Even though it is not a code uncertainty, it must be part of the peak clad temperature uncertainty. Peaking factor uncertainties account for random errors in specifying power distributions in the core. [B. W. Sheron, 1987] implied normal distributions for power and peaking factors. These have been adopted here also.

Errors in pellet and cladding dimensions are random fabrication errors. Since quality control eliminates large deviations, a uniform distribution is suggested here. However, for the purpose of this analysis, these size uncertainties and the uncertainties of surface roughness [Laats, 1981, Table 2] are combined later into the gap conductance uncertainty, to which is assigned also a uniform probability distribution.

Uncertainties for fission power variation within the fuel pellet are estimated. No data could be found.

Modeling Uncertainties. Modeling uncertainties arise from random differences between heat transfer and thermophysical property measurements and the correlations used to represent the measurements in the computer code. Systematic differences, however, between the mathematical models in the code and the experimental data are code-specific and presented below. In the category of fuel-related modeling uncertainties are the uncertainties from (i) fuel pellet thermal conductivity, (ii) cladding thermal conductivity, (iii) fuel pellet heat capacity, (iv) cladding heat capacity, (v) filler gas thermal conductivity, (vi) thermal expansion or gap width, (vii) radiative surface properties and (viii) convective heat transfer coefficients. Table 34.4 below summarizes 1-σ level uncertainties, approximate distributions and source references for these parameters.

The probability distributions in Table 34.4 are specified as normal whenever they are unknown or known to be approximately normal.

The uncertainty of fuel thermal conductivity, k_f, is specified in [Hagrman, 1980, p. 24] for all fractions of theoretical fuel density. For the fraction of 94.9%, Hobson's data as listed in [Hagrman, 1980] are (0.32 ± 0.09)W/(mK) higher than the MATPRO correlation, in the temperature range between 547K and 1,330K. However, for this analysis we adopt the more universally applicable error range as specified in [Hagrman, 1980].

Error brackets for heat capacities, (ρc_p), were computed from uncertainties specified for specific heats in Reference [Hagrman, 1980, p. 10 (of 8/81 revision) and 211] and the densities given below in Eq. (34.13). The uncertainty for Eq. 34.12 density is trivial (±0.5% of theoretical density for fuel [Laats, 1981, Table 2]) and therefore ignored.

The uncertainties for important parameters affecting the gap conductance are combined into an overall gap conductance uncertainty, based on Eq. (3) and on the assumption of independence between the dominant gap width and gas conductivity uncertainties:

$$\Delta h_{gp} = \sqrt{\Delta_1^2 + \Delta_2^2} \, . \qquad (34.13)$$

Table 34.4. Uncertainties of Fuel-Related Parameters

Parameter	1-σ Uncertainty	Distribution	Reference
Fuel thermal cond., k_f	±0.2 W/(mK)*	Uniform	[Hagrman, 1980] p. 24
Clad thermal cond., k_c	±1.01 W/(mK)	Normal	[Hagrman, 1980] p. 218
Fuel heat capacity, $(\rho c)_f$	±30.035 kJ/(m^3K)	Uniform	[Hagrman, 1980] p. 10†
Clad heat capacity, $(\rho c)_c$	±64.875 kJ/(m^3K)	Uniform	[Hagrman, 1980] p. 211
Gas thermal cond., k_g	±0.0131 W/(mK)	Uniform	[Hagrman, 1980] p. 485,† [Chambers et al., 1982] p. 15
Effective gap width, t	±20.98 μm	Skewed	[Steck et al, 1980] pp. 31 & 92
Pellet emissivity, ϵ_f	±7%	Uniform	[Hagrman, 1980] p. 48.6
Clad emissivity, ϵ_c	±0.10	Uniform	[Hagrman, 1980] p. 237
Convective heat transf., single-phase, forced, turb.	-5% to +35%	Uniform	[Lellouche, 1987] p. 18 [Dittus et al., 1930]

*Notice that Hobson's data listed in Table A-2.VII [Hagrman, 1980], are incorrectly plotted in Figure A-2.4.
†Revision 8/81.

Here, the uncertainty from gas conductance uncertainty, Δk_g = 0.0131 W/(mK) is

$$\Delta_1 = \Delta k_g / t = 634.7 \text{ W/(m}^2\text{K)} , \qquad (34.14)$$

the effective gap width, t, being computed to be t = 25.039 μm, and from the gap width uncertainty, one finds

$$\Delta_2 = h_{gp} - \frac{k_g}{t + \Delta t} = 4{,}992.0 \text{ W/(m}^2\text{K)} . \qquad (34.15)$$

The gas thermal conductivity, k_g, is evaluated with the mean gas temperature computed from the values given in Table 34.2. The nominal gap conductance is h_{gp} = 10.960 kW/(m^2K) as in the TRAC code. The gap width uncertainty, Δt, is taken from [Steck, 1980] as shown in Table 4. Uncertainties from radiative heat transfer are ignored because the entire contribution from radiative heat transfer to gap conductance is only 0.4% at normal full power conditions.

Substitution of Eqs. (34.14) and (34.15) into Eq. (34.13) yields the 1-σ uncertainty of gap conductance which is

$$\Delta h_{gp} = 5{,}032.2 \text{ kW/}(m^2K) \qquad (34.16)$$

and amounts to 45.9% of the nominal gap conductance.

Gap conductance uncertainty is dominated by the uncertainty of effective gap width. The effective gap width uncertainty, Δt, is slightly smaller than the effective gap width t itself, but approximately as large as the physical gap width δ. There is no general agreement in the literature concerning gap width uncertainties; most error ranges have been assumed without basis. [Sheron, 1987, Table 2] lists an "assumed RMS error" of 25% for gap conductance, which appears low. In contrast, [Lassmann and Hohlefeld, 1987] more recently compared nearly a thousand gap conductance measurements with results from the URGAP computer code. The measurements were taken primarily from extremely well-controlled out-of-pile experiments, and URGAP "has been fitted to the data of [Ross and Stoute, 1962], [Dean, 1962] and [Campbell et al., 1977]." Under such rather ideal but atypical conditions, [Lassmann and Hohlefeld, 1987] obtained the gap conductance uncertainty of 33.4% (1-σ level). [Cunningham et al., 1978] concluded also from experiments that the gap width uncertainty is approximately 50% (p. C-2), based on an initial gap width of 229 μm (p. A-1) and a mean gap closure by 63% (p. C-2). This leaves, under normal full-power conditions (in a BWR fuel pin), a gap width of 108 μm with an uncertainty of 50 μm. [Cunningham et al., 1978] add a 100% uncertainty (p. C-6) in temperature jump distance uncertainty and a 10% uncertainty in the gap width coefficient of their STORE computer code. This tends to support the uncertainty analysis by [Steck et al., 1980] for PWR conditions, i.e. the reference from which Eq. (34.16) was derived.

For uncertainties of convective film coefficients, it was pointed out by [Lellouche, 1987] that when heat transfer coefficients appropriate for conditions inside circular tubes are used for heat transfer in tube bundles, then the heat transfer coefficients are consistently under estimated. This being the case in the TRAC code, the ±20% range of 1-σ level uncertainties suggested by the comparison of the Dittus-Boelter correlation with data [Dittus, 1930], has been shifted to {-5%, +35%} to account for the above enhancement of heat transfer regimes with phase change. This is addressed in Section 34.2.5 later.

Systematic Modeling Errors in TRAC-PF1/MOD1. Based on presently available code documentation [NUREG/CR-3858, LA-10157-MS, 1986] and on the written responses from Los Alamos National Laboratory to specific questions posed by the author, TRAC-PF1/MOD1 has four systematic errors related to its fuel modeling:

1. The thermal conductivity is too low as shown in Table 34.1 (cf. [NUREG/CR-3858, LA-10157-MS, 1986, p. 50]. The mean bias is -0.46 W/(mK) relative to the correlation given in MATPRO [Hagrman, 1980, p. 23]. The consequences should have been an excess of initial fuel stored energy of approximately 6 kJ/m or 9%, and a 13% increase in pellet thermal response time. As pointed out in Section 34.2.2, however, TRAC results show a slight deficit of 1% in fuel stored energy when compared with results from closed-form integration. The cause for this discrepancy might be computational error; the exact cause cannot be identified without additional code documentation. The increase in thermal response time, on the other hand, appears to be corroborated indirectly by comparing the thermal response of the cladding as computed by TRAC and by the analysis presented in Section 34.2.5 below.

2. The gap width is increased from approximately 14 μm to 21 μm (under hot conditions). The adjustment is suggested in the TRAC LBLOCA report [Fujita, 1983, p. 17], to achieve vendor-specified initial fuel-stored energy. The magnitude of the adjustment given here is inferred from hand calculations because the necessary documentation is lacking in TRAC output listings. It is possible, by gap width adjustments, to obtain the correct initial fuel stored energy, but not without changing the pellet and cladding response times. It will be shown in Section 34.2.5, that any increase in gap width, i.e. decrease in gap conductance, increases blowdown peak clad temperature. This is true only in the vicinity of the fuel conditions calculated in TRAC for full-power conditions, but it shows that stored energy and with it pellet temperature is more important for peak clad temperature than gap conductance. Whether TRAC results are conservative, however, can only be determined from calculations carried out with correct fuel thermal conductivity, without significant computational error and without gap width adjustments.

3. Thermal expansion in radial direction are computed incorrectly in TRAC [NUREG/CR-3858, LA-10157-MS, 1986, p. 70], because (i) the formula for radial displacements is evaluated with the absolute temperature instead of with the excess temperature above the temperature of the strain-free state and (ii) total radial displacements are added to radii from previous time steps, rather than to radii of cold conditions. One should suspect documentation errors here, but it was not possible to resolved this issue without better documentation.

4. The calculation of two-phase flow heat transfer coefficients in TRAC-PF1/MOD1 [NUREG/CR-3858, LA-10157-MS, 1986, p. 81, Eq. (140), p. 83, top equation; p. 63] is incorrect because (i) the equation on page 63 is wrong and (ii) a mixture heat transfer coefficient is assigned to the liquid phase, while the vapor phase heat transfer coefficient is not zero.

(i) Los Alamos National Laboratory claims [Boyack, 1987], with unspecified references to M. Ishii and J. M. Delhaye, that the equation on page 63 of [NUREG/CR-3858, LA-10157-MS, 1986] for combining phasic heat transfer coefficients is derived by averaging. No reference for this averaging is offered. Since the equation contains neither a phasic perimeter fraction, nor a phasic wetted area fraction, nor a phasic wall residence time fraction, it is absolutely impossible to derive the equation in [NUREG/CR-3858, LA-10157-MS, 1986] on page 63, nor Eq. (98) on p. 58 (for solid structures) either by space or by time averaging.

(ii) Los Alamos National Laboratory concedes [Boyack, 1987], that mixture and vapor heat transfer coefficients should not added as in the TRAC code, but they claim that it is permissible to add them because the liquid convective heat transfer coefficient $(\bar{h}_c)_\ell$ is at least 100 times greater than that for vapor, $(\bar{h}_c)_v$. This claim is wrong in principle (one does not introduce unnecessary errors, because they are small); it is also wrong because 25 randomly selected TRAC results, obtained from a PWR LBLOCA calculation, show that during the blowdown phase $(\bar{h}_c)_\ell/(\bar{h}_c)_v = 16 \pm 14$, $(1\text{-}\sigma)$.

This systematic error does not affect single-phase coolant conditions, whence it does not affect the initially stored energy but it does affect the transient calculations and the peak clad temperature.

The Resultant Uncertainties in Fuel Stored Energy. Table 34.5 summarizes the changes caused in fuel stored energy by varying the dominating fuel-related parameters, each one individually, by its $1\text{-}\sigma$ uncertainty. The second columns shows the parameter values for normal conditions, as they were used to obtain the results in Table 34.2, and the stored energy given in Section 34.2.3. The third column shows the parameter changes which bring about an increase in fuel stored energy and which correspond to a $1\text{-}\sigma$ variation. Notice that the convective film coefficient was reduced by 20%, one-half of the total variation listed in Table 34.4. Column four shows the extreme values used to calculate the changes in stored energy, while column five lists the corresponding values for stored energy. The last column shows the changes in stored energy relative to the reference value of E = 67.991 kJ/m.

The values in Table 34.5 serve four purposes. Firstly, they serve to rank the parameters in their order of significance in affecting stored energy. Notice that, the convective film coefficient is in eighth place because it is assumed that its minimum value is only 5% below its computed reference value (on account of heat transfer enhancement in rod bundles, and because such a 50% decrease would increase the stored energy only by 0.313 kJ/m. Clearly, uncertainties in gap conductance, peaking factors and fuel thermal conductivity have the most serious influence on stored energy.

Table 34.5. Elements of Stored Energy Uncertainty

Parameter	Reference Value	1σ Change†	Max./Min. Values	E, Stored Energy kJ/m	$E - (E)_{ref}$ kJ/m
Gap Conductance	10.960 $kWm^{-2}K^{-1}$	-5.028 $kWm^{-2}K^{-1}$	5.932 $kWm^{-2}K^{-1}$	84.928	16.937
Peaking Factors	1.41736	x1.03218	1.46297	70.675	2.685
Fuel Thermal Cond.	4.392 $Wm^{-1}K^{-1}$	-0.2 $Wm^{-1}K^{-1}$	4.186 $Wm^{-1}K^{-1}$	70.475	2.484
Power	486.49 MW/m^3	+2%	496.22 MWm^{-3}	69.655	1.664
Fuel Heat Capacity	3.028 $MJm^{-3}K^{-}$	+30.035 $kJm^{-3}K^{-1}$	3.059 MJ $m^{-3}K^{-1}$	68.651	0.661
Cladding Thermal Cond.	16.735 $Wm^{-1}K^{-1}$	-1.01 $Wm^{-1}K^{-1}$	15.728 $Wm^{-1}K^{-1}$	68.455	0.464
Burn-Up M N	0.4034 3.9167	-0.05 -0.30	0.3534 3.6167	68.346	0.355
Convective Film Coeff.	40.05 $kWm^{-2}K^{-1}$	-20%	32.04 $kWm^{-2}K^{-1}$	69.241	1.251
Cladding Heat Capacity	2.145 $MJm^{-3}K^{-1}$	+64.875 $kJm^{-3}K^{-1}$	2.210 MJ $m^{-3}K^{-1}$	68.033	0.042

†cf. Tables 3 and 4.

Secondly, the values listed in the third and last columns of Table 34.5 serve to estimate the sensitivity of fuel stored energy on modeling parameters. The ratio of listed stored energy change over a listed parameter change is an approximation to the partial derivative of stored energy with respect to that parameter and can be used to estimate the stored energy change for different parameter changes.

Thirdly, if one assumed that the conditions of linear error propagation are met, one could estimate the uncertainty in fuel stored energy from

$$\sigma_E = \sqrt{\sum \sigma_i^2} = 17.7 \text{ kJ/m} , \qquad (34.17)$$

which is 26.1% of the reference value E = 67.991 kJ/m. The σ_i values in Eq. (34.17) are the values in the last column of Table 34.5, except that for convective heat transfer only 1/4 of the tabulated value is used (corresponding to the low range shown in Table 34.4). It must be pointed out, however, that Eq. (34.17) is only a rough estimate since the conditions of linear error propagation are not strictly met.

The fourth and last purpose served by Table 34.5 is to show that the effects of parameter variations on fuel stored energy can be simulated by simply varying the fission power or the power peaking factor. Since this is easy to carry out in the TRAC code for a large number of fuel elements, it is a powerful technique for developing response surfaces in support of statistical uncertainty analyses, because this technique saves computing resources. One needs to select from Table 34.5 the amount of needed change in stored energy for a given change of any of the listed parameters, and then to determine from Figure 34.1 the multiplies for peaking factor which is to be used for the steady-state calculations of initial conditions.

Conclusions Regarding Fuel Stored Energy Uncertainty

1. Initial fuel stored energy can be computed efficiently from closed-form integration of the steady-state conduction equation, taking into account the dependence of thermophysical properties on temperature and the radial variation of fission power due to neutron flux depression.

2. The uncertainty in fuel stored energy is dominated by uncertainties in gap conductance, peaking factors and fuel thermal conductivity.

3. The fuel stored energy per unit of length of fuel pin, in the fuel pin with the highest clad temperature at full-power conditions in a Westinghouse PWR core with 17 x 17 fuel arrays and 160,000 Md/t burnup is 68 kJ/m. The standard deviation of the stored energy is approximately 26%.

4. It is possible to approximate the effects on stored energy of all important uncertainties from fuel-related modeling parameters by corresponding variations in peaking factors.

34.2.5 Analysis of Fuel Thermal Response

It is recognized that peak clad temperatures are the higher the larger the initial fuel stored energy is and the more easily this stored energy can pass from the fuel pellet into the cladding. Also, one and the same change or uncertainty in important fuel modeling parameters can increase the stored energy while retarding the energy transfer from pellet to clad, thereby representing opposing mechanisms which determine peak clad temperature. Gap conductance and thermal conductivity of fuel pellets are two such important modeling parameters.

It is the purpose of this section to determine the effects which the parameters listed in Table 34.5 have on peak clad temperature. It is of particular interest to know which of these parameters have opposite effects on peak clad temperature and on fuel stored energy.

We seek the transient fuel and cladding temperature by integrating the transient conduction equation

$$\rho c_p \frac{\partial T}{\partial \tau} = \bar{k} \frac{1}{r} \frac{d}{dr} \left(r \frac{dT}{dr} \right) + q_f''' \qquad (34.18)$$

in the two regions of pellet and cladding, using subscripts f for fuel and c for clad. We introduce new symbols

$\overline{\rho c}_p = \rho c(\langle T \rangle)$, mean volumetric heat capacity and

$\bar{k} = k(\langle T \rangle)$, mean thermal conductivity,

both evaluated, respectively, for fuel and clad with the area-averaged temperatures.

Solution Technique

Equation (34.18) is first converted, by area averaging into one ordinary differential equation each for pellet and for clad, as shown in [Wulff et al., 1985]. The result is

$$\frac{d\langle T_f \rangle_f}{d\tau} = \frac{\langle q_f''' \rangle_f}{(\overline{\rho c}_p)_f} - \frac{2\bar{k}_g}{R_1 (\overline{\rho c}_p)_f} \frac{T_{fo} - T_{ci}}{\ln \frac{R_2 + g_c}{R_1 - g_f}} \qquad (34.19)$$

$$\frac{d\langle T_c \rangle_c}{d\tau} = \frac{\bar{k}_g}{s R_m (\overline{\rho c}_p)_c} \frac{T_{fo} - T_{ci}}{\frac{R_2 + g_c}{R_1 - g_f}} + \frac{R_w}{R_m} \frac{\bar{a}_c}{s^2} N_{Bi} (T_\infty - T_w), \qquad (34.20)$$

where $c = R_2 - R_1$ cladding thickness

$R_m = (R_1+R_2)/2$ mean radius of clad

$\bar{\alpha}_c = \bar{k}_c/(\overline{\rho C_p})_c$, thermal diffusivity of clad

$N_{Bi} = s\bar{h}_c/\bar{k}_c$ Biot number of clad

g = temperature jump distance

and all other symbols have been defined previously. Integration of Eqs.(34.19) and (34.20) yields the area-averaged temperatures $\langle T \rangle$ for fuel pellet and cladding. However, one needs to calculate the surface temperatures T_{fo}, T_{ci} and T_w, in order to integrate Eqs. (34.19) and (34.20).

These three temperatures are computed by approximating the transient temperature distributions in pellet and clad by two separate power polynomials in radius r. The polynomials have time-dependent coefficients which are computed to satisfy the above-mentioned seven boundary conditions of heat flux and temperature continuity. plus two requirements imposed by the definition of averaging. The total of nine conditions defines the three temperatures T_{fo}, T_{ci} and T_w, all in terms of $\langle T_f \rangle_f$, $\langle T_c \rangle_c$ and T_∞, and also six time-dependent polynomial coefficients [Wulff, 1985]. The three surface temperatures are:

$$T_{fo} = F_1\langle T_f \rangle_f + F_2\langle T_c \rangle_c + F_3 T_\infty \tag{34.21}$$

$$T_{ci} = \langle T_f \rangle_f - \Omega_1(\langle T_f \rangle_f - T_{fo}) \tag{34.22}$$

$$T_w = [(\Omega_4-\Omega_3)T_\infty - T_{fo} + (\Omega_3+1)T_{ci}]/\Omega_4, \tag{34.23}$$

where $F_1 = (\Omega_1-1)[\Omega_4(\Omega_3-\Omega_2) - \Omega_5(\Omega_3+1)]/G$

$F_2 = \Omega_3\Omega_4/G$

$F_3 = -\Omega_3\Omega_5/G$

$$G = \Omega_1\Omega_3(\Omega_4-\Omega_5) + (1-\Omega_1)(\Omega_2\Omega_4+\Omega_5)$$

$$\Omega_1 = 4\lambda_f\gamma_3+1 \quad , \quad \Omega_4 = \Omega_3(N_{Bi}+2)/2$$

$$\Omega_2 = \gamma_6-2\gamma_5 \quad , \quad \Omega_5 = \gamma_6(\Omega_4-\Omega_3)$$

$$\Omega_3 = 2\lambda_c\gamma_4$$

$$\lambda_f = \bar{k}_f/\bar{k}_g \quad , \quad \lambda_c = \bar{k}_c/\bar{k}_g$$

$$\gamma_3 = \ln[(R_2+g_c)/(R_1-g_f)]$$

$$\gamma_4 = \gamma_3 R_2/s$$

$$\gamma_5 = (3R_2+2s)/[3(2R_2+s)]$$

$$\gamma_6 = (4R_2+3s)/[6(2R_2+s)] \ .$$

All γ-values are fixed for fixed geometry; λ-, Ω-, F- and G- values vary with temperature. One can integrate Eqs. (34.19) and (34.20) with Eqs. (34.21) through (34.23). The fuel center line temperature is given by

$$T_c = 2\langle T_f\rangle_f - T_{fo} \ . \tag{34.24}$$

The expressions for temperature distributions (parabolic in pellet and cladding, logarithmic in gap) can be found in [Wulff, 1985]. They are not needed here. However, Eqs. (34.19) and (34.20) need initial values for $\tau = 0$. They are derived to render the derivatives in Eqs. (34.19) and (34.20) to be zero [Jones, 1980]. They are computed from:

$$\langle T_f(0)\rangle_f = (V_1U_{22} - V_2U_{12})/(U_{11}U_{22} - U_{12}U_{21}) \tag{34.25}$$

$$\langle T_c(0)\rangle_c = (V_2U_{11} - V_1U_{21})/(U_{11}U_{22} - U_{12}U_{21}), \tag{34.26}$$

where $V_1 = \dfrac{s/R_w}{N_{Bi}} \cdot \dfrac{R_1^2\langle q_f'''(0)\rangle_f}{2\bar{k}_f} + T_\infty \dfrac{\Omega_3-F_3[(1+\Omega_3)\Omega_1-1]}{\Omega_4}$

$$V_2 = \frac{R_1^2 \langle q'''(0) \rangle_f}{2\bar{k}_g} \gamma_3 - T_\infty F_3 (1-\Omega_1)$$

$$U_{11} = \{(1+\Omega_3)[1+\Omega_1(F_1-1)]-F_1\}/\Omega_4$$

$$U_{12} = F_2[(1+\Omega_3)\Omega_1-1]$$

$$U_{21} = (1-\Omega_1)(F_1-1)$$

$$U_{22} = F_2(1-\Omega_1),$$

and $\langle q'''(0) \rangle_f$ is the initial, area-averaged fission power; all other symbols are defined below Eq. (34.24).

Equations (34.19) and (34.20) were integrated on an HP-41CX programmable pocket calculator, using a fourth-order Runge-Kutta integration algorithm†. The HP-41CX executes all expressions for properties, Eqs. (34.25) and (34.26) for initial conditions and Eqs. (34.21) through (34.24) for fuel and cladding temperatures. The integration step size of 50 milliseconds guarantees a computing accuracy of $\pm$0.05K; five significant digits remained unaltered during eighty integration steps or 4 second of a null transient which was started from Eqs. (34.25) and (34.26).

Results were computed for two sets of boundary conditions. One set approximates the fission power and coolant conditions as calculated by the TRAC code while simulating an LBLOCA for reference Westinghouse PWR plant conditions. The other set consists of limiting step changes in coolant conditions to show the effects from DNB delay (departure from nucleate boiling) or from dryout delay, and also with changes of time for scram initiation. The results are presented in the following two subsections.

34.2.6 Effect of Fuel Parameter Uncertainty on Peak Clad Temperature

Eighteen transient fuel temperature calculations have been performed to assess the effects of parameter variations on thermal response and on peak clad temperature. The results are shown in Table 34.6.

---

†The Runge-Kutta algorithm was coded for the HP-41CX as part of this project. It needs 26 memory registers. The number of nonlinear ordinary differential equations, $\dot{Y} = f(x,Y)$, that can be integrated is free and depends only on the complexity of f and the number of available registers (max. 896).

Table 34.6 Thermal Response of Fuel and Peak Clad Temperature Change

Parameter	Step Change		TRAC Blowdown B.C.	
	Initial Clad Temperature Rise K/s	Change of Initial Temp. Rise K/s	Peak Clad Temp. K	Change in Peak Clad Temp. K
Gap conductance	724.2	-7.2	884.8	52.4
Peaking factor	753.0	21.6	843.0	10.6
Fuel thermal conductivity	731.3	-0.1	847.5	15.1
Power	744.9	13.5	839.0	6.6
Fuel heat capacity	731.4	0	833.3	0.9
Cladding thermal cond.	732.0	0.6	833.9	1.5
Convective heat trans. coef.	722.0	-9.4	849.5	17.1
Cladding heat capacity	710.0	-21.4	833.5	1.1
Reference case	731.4	---	832.4	---

The first set of nine calculations was carried out to obtain the initial time rate of mean clad temperature rise from Eq. (34.20). Initial steady-state conditions were computed, according to Eqs. (34.25), (34.26) and (34.21) through (34.24), first with the parameters from TRAC-PF1/MOD1 as listed in Section 34.2.2, and then with all but the burn-up parameters (not modeled in Eqs. (34.19) and (34.20)) shown in Table 34.5, changed by the same 1-σ uncertainty as listed in Table 34.5. The transient was induced by changing the following three boundary conditions from initial values

$$T_\infty = 599.44\text{K}, \quad \bar{h}_c = 40.05\ \text{kW/(m}^2\text{K)} \qquad \text{for } \tau < \tau' = 0 \tag{34.27a}$$

$$\langle q'''_f \rangle_f = 486.49\ \text{MW/m}^3 \qquad \text{for } \tau < \tau'' = 0 \tag{34.27b}$$

to

$$T_\infty = 666.80\text{K}, \quad \bar{h}_c = 0.8805\text{kW/(m}^2\text{K)} \qquad \text{for } \tau \geq \tau' = \tag{34.28a}$$

$$\langle q'''_f \rangle_f = 2?.24\ \text{MW/m}^3 \qquad \text{for } \tau \geq \tau'' = 0, \tag{34.28b}$$

which are the highest vapor temperature, the lowest heat transfer coefficient, both as calculated by TRAC-PF1/MOD1 for an LBLOCA blow-down phase, and 5.6% of initial power, representing the mean fission power during the first two seconds. The symbols τ' and τ'' are, respectively, the time of DNB and of scram initiation. The results are shown in the second and third columns of Table 6. The second column shows the initial mean clad temperature rise, $d\langle T_c \rangle_c/dt$ at $\tau = 0$. The third column shows the effect of parameter variations on the

response of the cladding, relative to that of the reference calculation, which is shown in the last line. Indeed, gap conductance, fuel thermal conductivity, convective film coefficient and cladding heat capacity, when changed so as to increase fuel stored energy, decrease, as expected, the rate of thermal response by the cladding. This suggest that these four parameters have opposite effects on stored energy and peak clad temperature.

Figure 34.2 shows the transient outer cladding temperature, $T_w(\tau)$ under reference conditions and with boundary conditions as specified by Eqs. (34.27) and (34.28). This figure suggests that the initial slope might not dictate the peak of the clad temperature T_w. In fact, as shown in the first two columns of Table 34.6, the opposite effects suggested by the results in the second and third columns are unimportant with regard to peak clad temperature.

Far more importantly, Figure 34.2 shows that during the blowdown phase the clad temperature is limited by vapor cooling, without the arrival of droplets. The clad temperature peaks even when the pessimistic cooling conditions, Eqs. (34.28), prevail at once after scram and then remain. The blowdown peak clad temperature is almost unaffected by reactor pump degradation or by transition of critical break flow from subcooled to two-phase flow conditions, except in the highly unlikely event that liquid injection at core entrance should occur in less than approximately two seconds after dryout or departure from nuclear boiling (DNB). Aside from this exception, the blow-d peak clad temperature is dictated by fuel stored energy alone or, equivalently, by the linear heating rate (cf. Figure 34.1). Whence, blow-down peak clad temperature measurements are not affected by scale distortions outside the core in a test facility.

Turning now to the second set of transient fuel temperature calculations, we describe how the last two columns in Table 34.6 were obtained. Another reference and eight repeat calculations were carried out with the 1-σ parameter variations listed in Table 34.5, only one parameter being varied at a time, to show the effects of these parameter variations on blow-down peak clad temperature. These nine parametric calculations were carried out, however, with boundary conditions representative of the ones imposed by the TRAC-PF1/MOD1 code during blow-down, on the fuel pin segment which had the highest clad temperature at full-power steady-state conditions. Figures 34.3, 34.4, and 34.5 for cooling rate, liquid temperature and vapor temperature, respectively were generated by TRAC and used to derive these approximate boundary conditions for coolant temperature, T_∞, heat transfer coefficient, $\bar{h}_c$, and fission power, $\langle q'''_f \rangle_f$:

$$T_\infty(\tau) = 599.44K - (21.41K/s)\tau \tag{34.29}$$

$$\bar{h}_c(\tau) = 40.05kW/(m^2K)\cdot f_1(\tau), \tag{34.30}$$

where $f_1(\tau) = 1+(0.9812\ s^{-1})\tau$ for $0 \leq \tau \leq 0.47s$

$= \text{Max}\{0.022314,\ 2.13745-(1.43886\ s^{-1})\}$

for $0.47s \leq \tau < 4s$

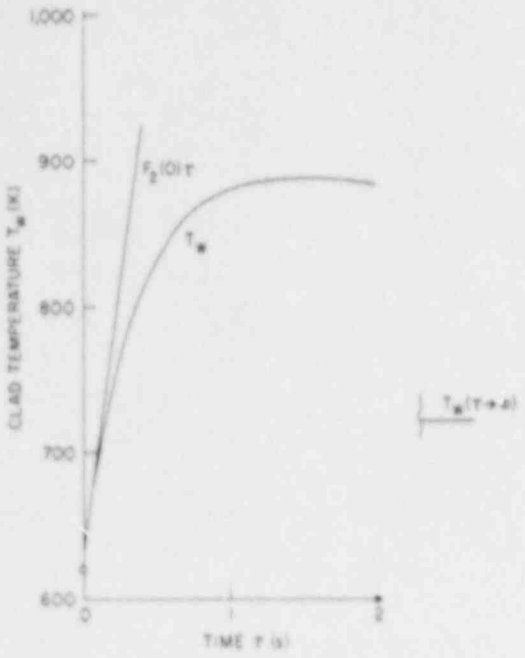

Figure 34.2 Transient Outer Clad Temperature for Step Change in Boundary Conditions at Time $\tau = 0$

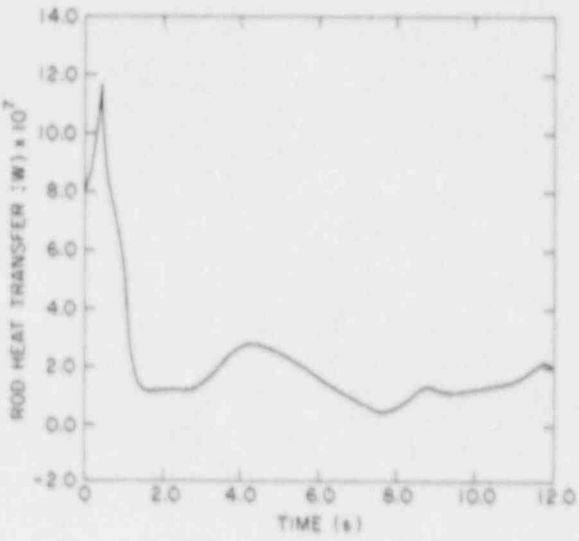

Figure 34.3 TRAC-Computed History of Heat Transfer Rate from Fuel Rod During LBLOCA for Rod Location With Greatest Initial Clad Temperature

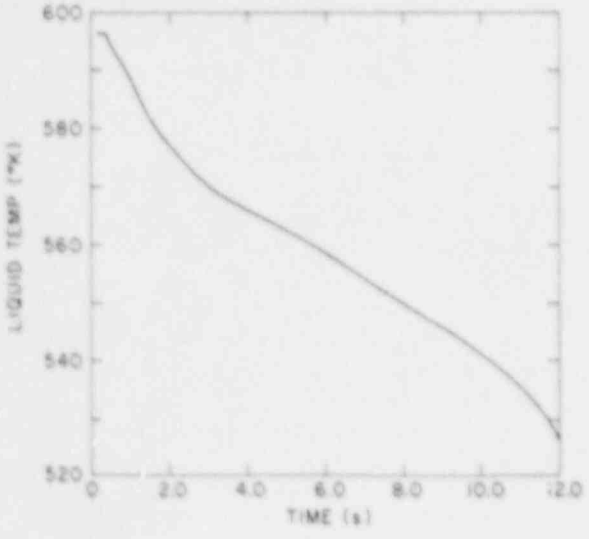

Figure 34.4. TRAC-Computed History of Liquid Temperature at Fuel Rod During LBLOCA for Rod Location With Greatest Initial Clad Temperature

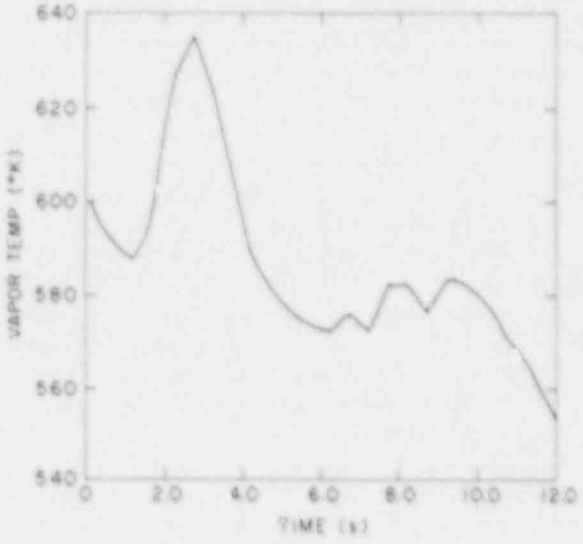

Figure 34.5. TRAC-Computed History of Vapor Temperature at Fuel Rod During LBLOCA for Rod Location With Greatest Initial Clad Temperature

and

$$\langle q_f''' \rangle_f = 486.49\ \text{MW/m}^3 \qquad \text{for } 0 \le \tau \le t'' = 0.2\text{s}$$

$$= 486.49\ \text{MW/m}^3\ [1.236-(1.180\ \text{s}^{-1})\tau \qquad \text{for } t'' \le \tau \le t'' + 0.8\text{s}$$

$$= 27.24\ \text{MW/m}^3 \qquad \text{for } t'' + 0.8\text{s} \le \tau \le 4.0\text{s}$$

(34.31)

All boundary conditions start out with steady-state initial conditions. The TRAC-computed cooling recovery at 2.81s after break initiation is intentionally omitted; the cooling rate is kept constant instead.

The outer clad temperature history, $T_w(\tau)$, obtained with these reference conditions and with all parameters in Table 34.5 at their nominal values is shown as the solid curve, marked REF, in Figure 34.6. The comparison with TRAC results shows that the TRAC-computed peak clad temperature is approximately 28K lower and appears 0.4 seconds later than shown in Figure 34.6. The shape of the curve from TRAC, however, is the same as that of the solid curve in Figure 34.6, except for a small reduction in slope at the time (1.47s) of a computer restart.

The fourth column in Table 34.6 shows the peak clad temperatures obtained by changing the listed parameters by the 1-σ uncertainties listed in Table 34.5. The last column shows the corresponding changes in peak clad temperature relative to the reference value of 832.4K, given in the last line. In contrast to the conclusion arrived at from the thermal response rate differences in the third column of Table 34.6, all parameter changes which produce an increase in stored energy produce also an increase in peak clad temperature. This shows clearly that energy storage is more important for peak clad temperature than are heat transfer rates.

After taking the square root of the sum of squares (cf. Eq. (34.17) for stored energy) of all the differences in the last column of Table 34.6, one obtains a rough estimate for the 1-σ uncertainty in peak clad temperature of 41.4K, as it results from the uncertainty of fuel-related parameters. This estimate is offered here with caution, because it is based on linear error propagation, of which the requirements can be met only approximately by the peak clad temperature modeling analysis. The dash-dot curve at the top in Figure 34.6 shows the expected peak clad temperature when all the 1-σ changes of fuel-related parameters combine statistically. The curve is drawn for the 1-σ uncertainty in gap conductance of 46%. The intermediate dash curve is drawn for the gap conductance uncertainty of 35% as proposed by [Lassmann and Hohlefeld, 1987]. No attempt is made to assign confidence limits to these peak clad temperature uncertainties as these limits are the subject of an ongoing effort by the USNRC.

However, as before for stored energy, the peak clad temperature differences given in Table 34.6 can serve, along with their corresponding parameter changes listed in Table 34.5, to estimate the sensitivity of peak clad temperature on each of the fuel-related parameters. Finally, one can recognize the

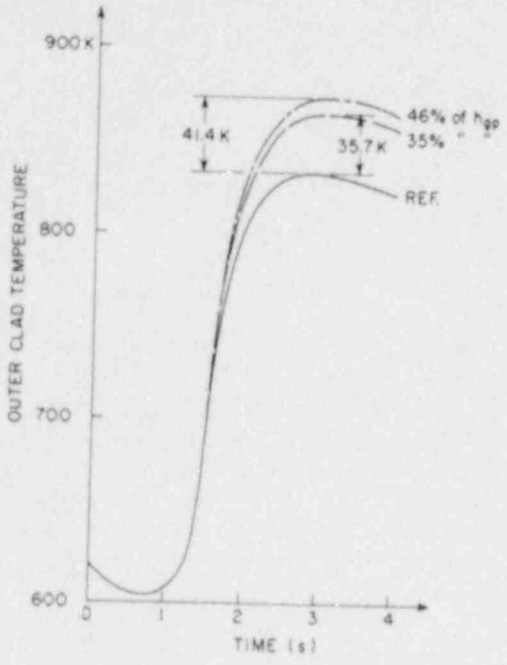

Figure 34.6. Peak Clad Temperature Change Due to Uncertainties in Fuel-Related Parameters

order of importance for the parameters concerning their effect on peak clad temperature; the order is the same as for fuel stored energy, as far as the three most important parameters are concerned. Notice that in this ordering the change of peak clad temperature due to a change in convective heat transfer coefficient should be divided by four because the coefficient is expected to change in the range from -5% to +35%, while the difference in peak clad temperature was obtained for -20%, as shown in Table 34.5.

Notice in Figure 34.6 that the clad temperature peaks without recovery of cooling due to droplet injection. This confirms the conclusions reached before for Figure 34.2, but now also for boundary conditions which approximate those computed by TRAC-PF1/MOD1.

34.2.7 Effect of Hydraulics Parameters on Peak Clad Temperature

In this section are presented the results from transient fuel temperature calculations carried out with limiting step changes in boundary conditions for the purpose of assessing the effects on peak clad temperature from (i) changes in heat transfer coefficients, (ii) delay of the time when DNB or dry-out occurs, and (iii) delay of the time when scram is initiated.

The Effect of Heat Transfer Coefficients can be seen by comparing the curves for outer clad temperature, $T_w(\tau)$, in Figures 34.7 and 34.8. These curves curves were computed with all parameters in Table 34.5 at their nominal values, with fission power as described by Eqs. (34.31), with the coolant temperature T_∞ as specified by the first of Eqs. (34.27a) and (34.28a) and with

$$\begin{aligned} \bar{h}_c &= 40.05\ \text{kW/(m}^2\text{K)} && \text{for } 0 \le \tau \le \tau' \\ \bar{h}_c &= 227.1\ \text{W/(m}^2\text{K)} && \text{for } t' \le \tau \le 4\text{s in Fig. 34.7} \\ &= 56.8\ \text{W/(m}^2\text{K)} && \text{for } t' \le \tau \le 4\text{s in Fig. 34.8} \end{aligned} \tag{34.32}$$

The lowest value of $\bar{h}_c$ computed during blowdown by TRAC-PF1/MOD1 is 880.5 W/(m^{2}K). This is for single-phase, turbulent vapor flow, with* the velocity of 4.62 m/s, at the pressure of 81 bar and the vapor temperature of 666.2K. Turbulent free convection by dry vapor would represent the pessimistic extreme in velocity calculation and produce 164 W/(m^{2}K). Thus, the heat transfer coefficient $\bar{h}_c$ used for Figure 34.7 is slightly more than 1/4 of the minimum TRAC computed value; in Figure 34.8 it is ~1/15 and even only ~1/3 of the free convection value. This is extremely low.

The clad temperature peaks in Figures 34.2 and 34.7 reaches its asymptotic value $T_w(\infty)$ from above, in Figure 34.8 it approaches its asymptotic temperature from below. The clad temperature is limited by vapor cooling; a maximum occurs when the asymptotic wall temperature

$$T_w(\infty) = (T_v)_{max} + R_1^2 \langle q'''_{decay} \rangle_f / [2R_w(\bar{h}_c)_{min}] \tag{34.33}$$

is below the initial mean pellet temperature $\langle T_f(o) \rangle_f$, where

$(T_v)_{max}$ = maximum vapor temperature
R_1 = pellet radius
R_w = outer clad radius
$\langle q'''_{decay} \rangle_f$ = decay power density in pellet
$(\bar{h}_c)_{min}$ = minimum heat transfer coefficient

Early arrival of liquid can turn down the clad temperature only if the heat transfer coefficient is unrealistically low or if the liquid arrives unrealistically early.

*Dittus-Boetter, $N_{Re} = 78{,}000$, $N_{Pr} = 1.12$.

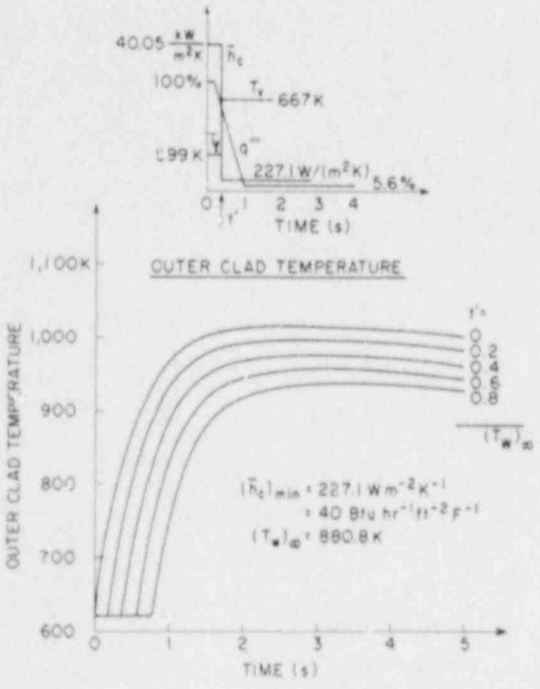

Fig. 34.7 Effect of DNB Delay Time t' on Peak Clad Temperature for Low Heat Transfer Coefficient, $\bar{h}_c$ = 227 Wm^2K^{-1}

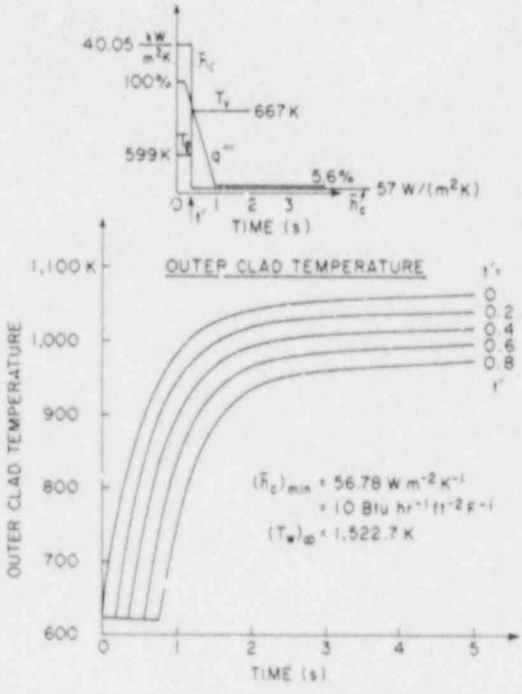

Fig. 34.8 Effect of DNB Delay Time t' on Peak Clad Temperature for Extremely Low Heat Transfer Coefficient, $\bar{h}_c$ = 56.8 $Wm^{-2}K^{-1}$

The Effect of DNB or Dry-Out Delay is shown also in Figures 34.7 and 34.8. The delay t' is measured from break initiation as shown in the top sketches of Figure 34.7 and 34.8.

Any delay in DNB or dry-out delays the temperature rise (horizontal shift of curves) and the peak by approximately the same amount t'. Moreover, any such delay reduces also the peak (vertical shift of curves), because extended cooling of the clad under pre-DNB conditions reduces the stored energy in the fuel prior to the temperature excursion.

The Effect of Scram Delay relative to the appearance of DNB or dry-out is shown in Figure 34.9 The three curves are obtained with t' = 0.2s in Eqs. (34.27a) and (34.28a). The middle curve is obtained with the fission and decay power history described by Eq. (34.31) with t" = 0.2s, the top and bottom curves, respectively, with t" = 0.3s and 0.1s.

An advance in scram initiation reduces the peak clad temperature by approximately 300 K/s, while a delay of scram initiation increases the peak clad temperature by approximately 120 K/s.

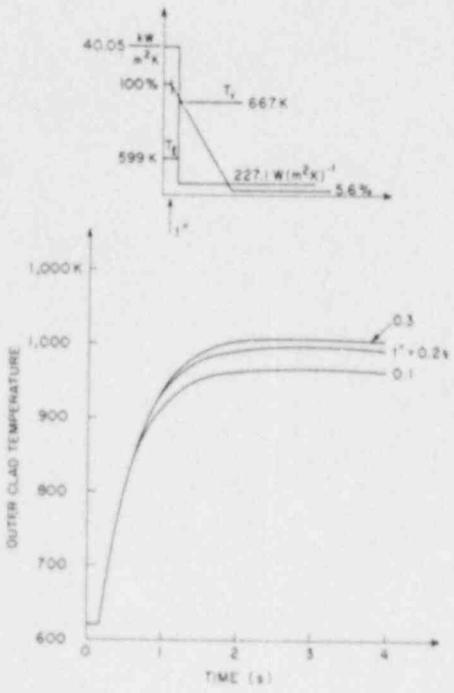

Figure 34.9 Effect of Scram Delay on Peak Clad Temperature

In conclusion, the above effects from variations in heat transfer coefficient in DNB or dry-out delay and scram delay include all effects from hydraulic and system-related parameters on the blowdown peak clad temperature, because droplet cooling is unimportant under realistic blowdown conditions. The effects from systematic modeling errors (cf. Section 34.2.4) on peak clad temperature uncertainty is not quantified here, because the necessary modeling documentation for TRAC-PF1/MOD1 is not available at this time.

Confidence limits for peak clad temperature will be developed in an ongoing USNRC project. The work will be extended from blowdown to reflood peak clad temperature. More details of this analysis can be found in NUREG/CP-0091, Vol. 4, p. 23.

34.2.8 Conclusions on Fuel Model Related Uncertainties

The analysis presented here leads to these major conclusions:

1. The peak clad temperature during blowdown is limited by effective single-phase vapor cooling to less than 880K.

2. The blowdown clad temperature peaks, under all credible circumstances, before the arrival of liquid droplets in the core. Therefore, the peak clad temperature during blowdown is not affected by reactor loop characteristics (break flow or pump degradation). It is governed instead by fuel stored energy or, equivalently, by linear heating rate. It depends only slightly on vapor velocity which affects the convective heat transfer coefficient after DNB or dry-out.

3. Fuel stored energy and peak clad temperature during blowdown depend primarily on three fuel-related modeling parameters, with this order of significance: gap conductance, power peaking factor and fuel thermal conductivity. Uncertaintites in stored energy and blowdown peaking factors are affected primarily by the uncertainties in these three parameters and potentially by systematic modeling errors in predicting these three parameters.

4. As a result of Conclusions 2 and 3, blowdown peak clad temperature measurements are not affected by scaling distortions outside the reactor core (in downcomer, pumps, steam generators, etc.). Since test facilities with nuclear fuel (LOFT etc.) have full-scale fuel pins from the view point of transient radial conduction, it can be stated that blowdown experiments with nuclear fuel yield the blowdown peak clad temperature without scale distortion.

5. The expected uncertainty in fuel stored energy is found to be 26%, based on 1-σ uncertainties in all governing parameters. Based on the same parameter uncertainties, the blowdown peak clad temperature has an uncertainty of 42K (1-σ level).

6. Based on its published documentation, the TRAC-PF1/MOD1 computer code has systematic modeling errors in fuel thermal conductivity, gap conductance and convective film coefficients. The first two errors compensate during steady-state, but not during transient calculations. The third error applies only to two-phase flow and heat transfer conditions. Additional documentation is needed to quantify the effects on peak clad temperature from these errors. Particularly, the TRAC output listing of fuel-related parameters is inadequate for code validation (FORTRAN) and for assessing the causes and effects of observed discrepancies.

34.3 Uncertainties in Modeling and Scaling of Critical Break Flow (U.S. Rohatgi and W.-S. Yu)

The coolant inventory in the reactor system is controlled by the break flow rate. However, a more significant role of the break flow rate is its influence on the distribution of the liquid inventory during the blowdown phase. The fuel rod clad starts to heat up at the time of break as the flow stagnates in the core. However, around 2.3 seconds after break initiation, the break flow decreases below the flow through the pumps in the intact loops, after the break flow changes from subcooled to two-phase critical flow. This results in the restoration of some liquid flow into the core, in core-wide rewet, and in the occurrence of the first peak of the clad temperature in the blowdown phase.

The purpose of the break flow analysis presented here is to determine bias and uncertainty in TRAC-PF1/MOD1 predictions of critical break flow rates, based on experimental data from twelve Marviken tests.

34.3.1 The Critical Flow Model in TRAC-PF1

TRAC-PF1/MOD1 has three models for critical flow. One is for subcooled liquid, the second is for two-phase flow conditions and the third one is for single-phase vapor. This report deals with the first and second models, because the third model is irrelevant for peak clad temperature predictions.

Subcooled Critical Flow is computed in TRAC from a modified Bernoulli equation, as described in Appendix D on page 530 of [NUREG/CR-3858, LA-10157-MS, 1986]. This TRAC code document gives in Eq. (D-9) the critical velocity for subcooled liquid, calculated for the break plane location, as the velocity V_e:

$$V_e = \text{Max}\left\{a_{HE}, \sqrt{V_c^2 + 2\,(p_c - p_e)/\rho_m}\right\}, \qquad (34.34)$$

where a_{HE} is the sound speed of homogeneous two-phase mixtures, V_c and p_c are the velocity and pressure at the nearest upstream computational cell center, while p_e and ρ_m are the break plane pressure and the mixture density at a location not specified in the TRAC documentation. A number of questionable explanations are given to justify Eq. (34.34). They can be found in Section II-B of Appendix D, in [NUREG/CR-3858, LA-10157-MS, 1986]. Particularly, the second argument of the maximizing function in Eq. (34.34) produces a velocity which is neither related to the pressure wave propagation velocity, nor does it satisfy a mass flux maximizing condition. Therefore, it is not clear why Eq. (34.34) should always produce a critical mass flow rate.

Equation (34.34) applies in TRAC, whenever the void fraction α_c at the upstream cell center nearest to the break satisfies $\alpha_c < 0.01$. The break plane pressure p_e is computed in TRAC on the basis of the nonequilibrium flashing model by [Jones, 1980] (who used Alamgir and Lienhard's earlier work). The pressure p_e is computed from Eq. (D-10) of [NUREG/CR-3858, LA-10157-MS, 1986] according to:

$$p_e = p_s - \text{Max}\{0, \Delta p\}\,. \qquad (34.35)$$

Here p_s is the saturation pressure (at unspecified location), and:

$$\Delta p = 0.258\,\frac{\sigma^{1.5}\left(\frac{T_\ell}{T_{crit}}\right)^{13.76}}{1 - \frac{\rho_g}{\rho_\ell}}\sqrt{\left[1 + 13.25\left(\frac{-Dp/Dt}{1.01325\times10^{11}}\right)\right]^{0.8}/(kT_{crit})}$$

$$-0.070\left(\frac{A_e}{A_c}\right)^2 \rho_\ell\, V_e^2\,, \qquad (34.36)$$

where σ, k, T and ρ designate surface tension, Boltzmann constant, temperature and density, respectively, all quantities must be expressed in S.I. units. Subscripts g, ℓ and crit designate gas, liquid and thermodynamic critical, while subscripts e and c are, as before, designating break plane and upstream cell center locations. The locations associated with subscripts g and ℓ are also not specified in [NUREG/CR-3858, LA-10157-MS, 1986].

Notice that Eq. (34.36) contains the limiting critical velocity V_e, that substitution of Eq. (34.36) first into Eq. (34.35) and then into Eq. (34.34) renders Eq. (34.34) implicit in the velocity V . The TRAC code document [NUREG/CR-3858, LA-10157-MS, 1986] fails to indicate the method by which V_e is computed from Eqs. (34.34, 34.35 and 34.36), with T_ℓ, ρ_ℓ and p_s all dependent on V_e.

Notice also that [NUREG/CR-3858, LA-10157-MS, 1986] fails to specify the method for computing the substantial derivative Dp/Dt. The RELAP5 code documentation shows the same model for critical flow of subcooled liquid* [Ranson, 1981, p. 79] as TRAC and specifies:

$$Dp/Dt = (\rho_\ell V_e^3/A_e)(dA/dx)_e \ , \qquad (34.37)$$

where $(dA/dx)_e$ is the variation of cross sectional area with respect to axial distance at the break. Obviously, Eq. (34.37 fails to produce nonequilibrium pressure undershoot for breaks in straight pipes.

Finally, it must be pointed out that [NUREG/CR-3858, LA-10157-MS, 1986] fails to indicate how V_e , as computed from Eq. (34.34), limits the mass flux as computed from the field equations in TRAC.

Two-Phase Critical Flow is computed in TRAC from the condition that the maximum value of the real part of the characteristic roots λ_i, associated with the field equations:

$$\underline{\underline{A}}\partial\underline{U}/\partial t + \underline{\underline{B}}\partial\underline{U}/\partial x = \underline{C} \qquad (34.38)$$

is zero [NUREG/CR-3858, LA-10157-MS, 1986, p. 528]. The field equations are the mass balances of an inert gas and the two-phase mixture, the phasic momentum balances and the mixture entropy balance for isentropic flow. $\underline{\underline{A}}$ and $\underline{\underline{B}}$ in Eq. (34.38) are 5x5 matrices and the state variable vector $\underline{U}$ has the components of inert gas pressure p_g, vapor pressure p_v, void fraction α and phasic velocities v_ℓ and v_g. The source vector $\underline{C}$ is unimportant for all but the entropy equation. In TRAC it is completely ignored.

The characteristic roots λ_i are computed numerically from the characteristic equation:

$$\det\left[\underline{\underline{A}}\lambda + \underline{\underline{B}}\right] = 0. \qquad (34.39)$$

*Aside from a factor of 2 discrepancy in the last term of Eq. (34.37).

The numerical scheme [NUREG/CR-3858, LA-10157-MS, 1986, p. 530] involves also the maximization of the mass flux at the location of the break plane. Thus, the two-phase critical flow model in TRAC contains two independent choking criteria, but not the standard compatibility criteria of quasi-steady critical flow (see Reocreux, NUREG-TR-0002, Vol. 1, p. 75).

The above two-phase flow choking criterion is imposed in TRAC for $\alpha_c > 0.1$ at the nearest upstream cell center. In the range of $0.01 \leq \alpha_c \leq 0.1$, a linear interpolation with respect to α_c is used between the critical flows calculated from Eq. (34.34) and from Eq. (34.39).

34.3.2 Purpose of Critical Flow Model Evaluation

The objective is to quantify the modeling deficiency, or uncertainty, in the TRAC-PF1/MOD1 critical flow model, as applied to PWR and LBLOCA conditions. The deficiency measure of the model is defined as the multiplier C_D, which is a ratio of measured over predicted critical flow rates:

$$C_D = \frac{\text{measured flow rate}}{\text{predicted flow rate}} \quad . \qquad (34.40)$$

The uncertainty in the model is represented by the standard deviation of C_D.

34.3.3 Procedure for Critical Flow Uncertainty Analysis

[Abdollahian et al., 1982] in a study of Marviken Critical Flow tests, concluded that for large size pipes ($D > 0.3$m and $L/D > 1.5$), the subcooled critical flow was independent of diameter (D) and length (L), and only depended on the inlet stagnation conditions as shown here:

$$G_c = f\,(P_o, T_o)$$

where G_c, P_o, T_o are critical mass flux, stagnation pressure and temperature at the inlet to the pipe. However, for small pipes, the subcooled critical mass flux does depend upon L/D. For PWRs, the cold leg diameter is around 0.7m and the distance between the RC pump discharge to the vessel is on the order of 8D ($L/D \approx 8$). This implies that if the break is located anywhere between $L/D = 1.5$ to 6.5 from either the vessel or the pump, the break flow will only depend upon the conditions of the fluid entering the broken pipes and not on the pipe length or diameter, and C_D will reflect any dependence of TRAC-PF1 critical flow models on the pipe geometry (L,D).

It is the purpose of the study to quantify the uncertainty in the critical flow model of TRAC-PF1/MOD1 as applied to PWRs. It was decided to use available test data from nearly full-scale facilities. The Marviken tests satisfied the large-scale requirement, as the test section diameters varied from 0.2m to 0.5m, the nozzle lengths varied from 0.3D to 3.7D and inlet subcooling temperatures varied from 5K to 50K. Furthermore, these tests produced measurements of pressure and temperatures at 0.7m above the nozzle entrance, which makes it possible to model only the test section near the break. This affords the break flow prediction to be unaffected by phenomena

taking place in the rest of the test facility. The mass flux data were obtained from the pitot-static method. The errors in the mass flux measurements were ±3 to 10% for the subcooled flow and ±8 to 15% for two-phase flow. For the work reported here, 12 tests were selected from [Marviken Results Test 12 through Test 25, 1979] and are listed in the first four columns of Table 34.7.

Separate TRAC-PF1/MOD1 nodalization models for each test were set up. These models consisted of two cells (0.35m each) in the discharge pipe, one cell for the converging section, a number of equal-size cells in the straight section of the nozzle. The cell lengths, ΔL, in the straight section varied between 0.2 and 0.5 m. They were approximately equal to the test section diameter and also equal to the cell length used in standard PWR plant simulation.

Marviken Critical Flow tests are transient tests (blowdown) and the mass flow rate data are available at every 0.1 second interval up to 1.0 second, then at every 0.5 second up to 3.0 seconds, and at every second thereafter. The first ten seconds of these tests, for which the inlet fluid was subcooled, were predicted by the TRAC code. Comparisons between the predicted mass flow rates with the experimental mass flow rates were made for the times for which the void fraction in the last cell before the BREAK component was less than 0.03. This generated a number of C_D values per test for subcooled critical flow. A mean value $\langle C_D \rangle$ and standard deviations were computed for each test from this set. Similarly, a set of C_Ds for two phase choking were computed for each test from the cases for which the void fraction in the last cell before the BREAK component was greater than 0.07. The mean value $\langle C_{D,2\phi} \rangle$ and the standard deviations, 2ϕ, were computed from each $C_{D,2\phi}$ set of each test for two-phase choking. Only one-fourth to one-third of all data points fell into the two-phase choking regime. It should also be noted that some of the inlet temperature data were spurious and the corresponding data were omitted.

34.3.4 Results and Conclusions for Critical Flow Uncertainty

As the purpose of this study is to provide a mean value of C_D and standard deviation for application to PWRs, the mean values for C_D were plotted as a function of D, inlet subcooling ΔT and aspect ratio L/D. It was observed from these plots that mean $\langle C_D \rangle$ for subcooled choking and two-phase choking had no discernable trend with D or subcooling, but it did show a trend with L/D. This can be verified from Table 34.7.

A curve fit was obtained for $\langle C_D \rangle$ for subcooled choking as shown in Figure 34.10.

$$\langle C_D \rangle = 0.696 \exp\left(0.649 \left(\frac{L}{D}\right)^{-0.168}\right) \qquad (34.41)$$

However, as this curve did not pass through all the data points, the standard deviations were computed using the mean values $\langle C_D \rangle$ and the C_D data at each L/D. The resulting standard deviations have been plotted in Figure 34.11 as function of L/D and show a distinct trend. A curve fit was generated for the standard deviation:

Table 34.7 Summary of Marviken Test Specifications and C_D Coefficients*

	Test Section		Liquid Subcooling	Subcooled Flow	Two-Phase Flow
Test No.	L/D†	D(m)	ΔT(k)	$\langle C_D \rangle$	$\langle C_D \rangle$
12	3.0	0.3	30	1.115	
13	3.0	0.2	30		1.111
15	3.6	0.5	30	1.219	
16	3.6	0.5	30	1.258	
17	3.7	0.3	30	1.146	
18	3.7	0.3	30	1.157	
19	3.7	0.3	5	1.11	1.309
20	1.5	0.5	5		1.54
21	1.5	0.5	30	1.364	
22	1.5	0.5	50	1.35	
24	0.3	0.5	30	1.533	1.92
25	1.7	0.3	5	1.18	1.485

*See Eq. (34.31) for definition
†L is length of test section

$$s = 0.9\exp\left(-1.737\left(\frac{L}{D}\right)^{0.227}\right) \tag{34.42}$$

A similar procedure was followed for two phase critical flow model and the curve fit for $C_{D,2\phi}$ and standard deviation are shown in Figures 34.12 and 34.13 and are also described by the following expressions:

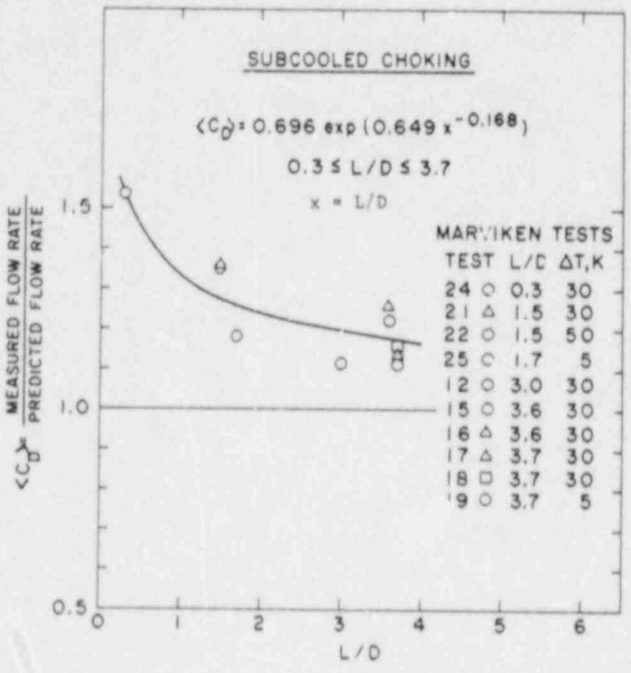

Figure 34.10 $\langle C_D \rangle$ as Function of L/D for Subcooled Choking

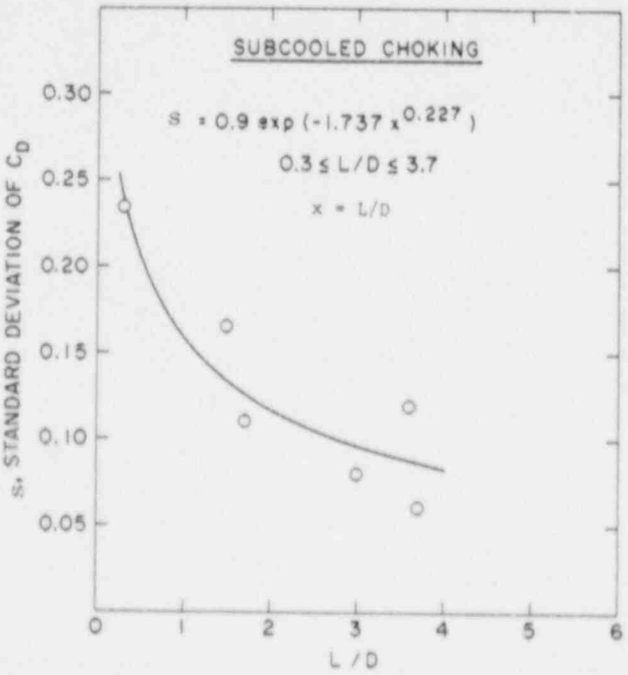

Figure 34.11 Standard Deviation s of C_D as Function of L/D for Subcooled Choking

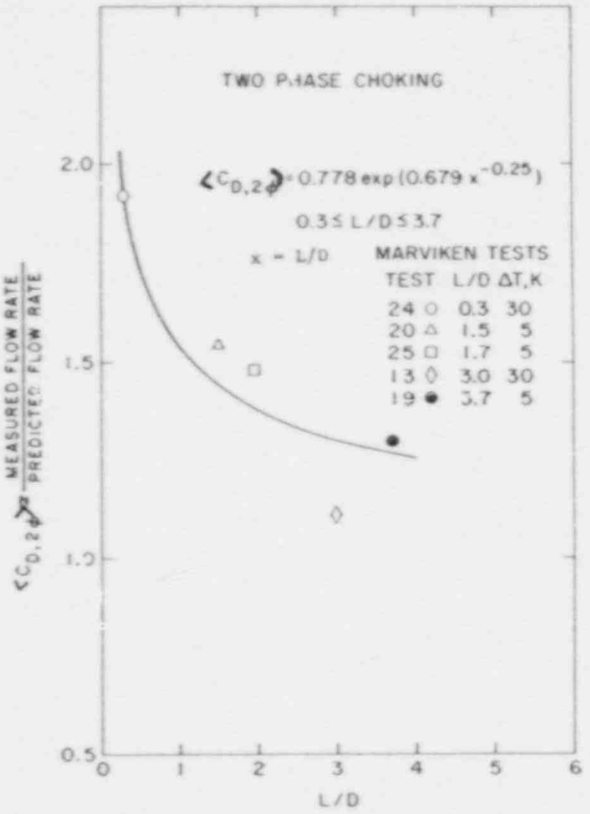

Figure 34.12 $\langle C_{D2\phi} \rangle$ as Function of L/D Two-Phase Choking

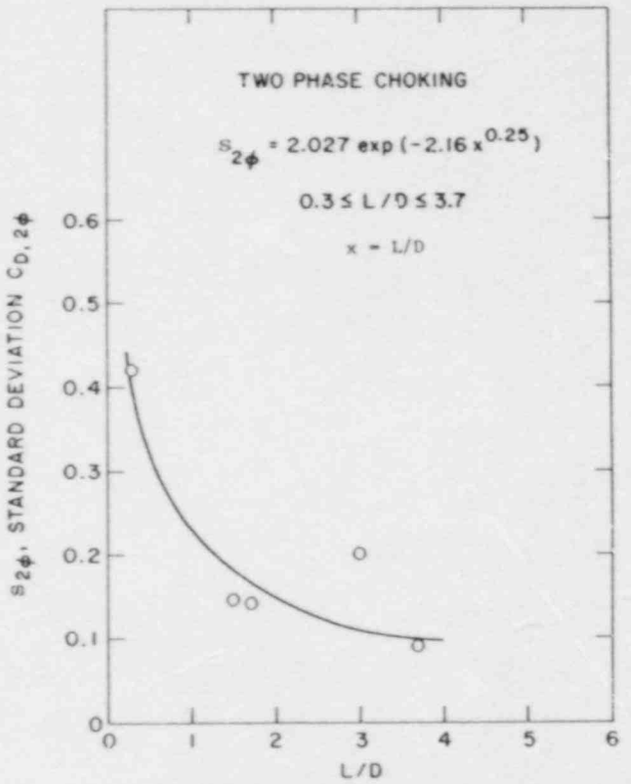

Figure 34.13 Standard Deviation $s_{2\phi}$ of $C_{D2\phi}$ as Function of L/D for Two-Phase Choking

$$\langle C_{D,2\phi} \rangle = 0.778\exp\left(0.679\left(\frac{L}{D}\right)^{-0.25}\right) \quad (34.43)$$

$$s_{2\phi} = 2.027\exp\left(-2.16\left(\frac{L}{D}\right)^{0.25}\right) \quad (34.44)$$

These $\langle C_D \rangle$s must be used directly in the TRAC input deck through the options in the NAMELIST. Once the location of the break has been selected, L/D can be calculated, one from the distance of the break from the vessel and the other from the distance of the break from the pump discharge, and C_Ds can be obtained from the above equations. The response surface (± s range) for statistically combinine uncertainties must be obtained by adding to, and subtracting from, C_D one standard deviation, and the measurement errors. The correction for the measurement errors of C_D in subcooled choking should be ±0.1 and in the two-phase choking regime it should be ±0.15.

34.4 Uncertainty in Pump Model (U.S. Rohatgi)

During a hypothetical large break LOCA in PWR, the reactor coolant pump plays an important role in determining the timing of restoring the core inlet flow after core flow reversal at the time of the pipe rupture. The flow into the downcomer and finally at the core inlet is a result of the competing influences of the vessel side cold leg break flow and intact loop cold leg flows into the downcomer due to the pumps in these loops. The core inlet flow is restored when the broken cold leg flow decreases below the total flow in the intact loops. The pump motor could be on or off depending upon the supply of AC power. In the case of loss of AC power, the pump will start to coast down. However, the pump has enough stored kinetic energy that it continues to transfer energy to the fluid, although at a decreasing rate. During the early part of the transient (up to first peak) the intact loop pump flows are close to single-phase flows and there will be no appreciable degradation in the pump performance. The situation changes as the transient proceeds; the primary coolant will have more vapor voids, leading to two phase flow through the pump and a corresponding performance degradation.

The objective of this study is to provide single-phase and fully degraded two-phase homologous curves and the degradation multipliers for head and torque for the Westinghouse full-size pump (specific speed 5200 rpm $(gpm)^{0.45}/(ft)^{0.75}$) and their uncertainties as required for assessing the TRAC-PF1/MOD1 pump model.

34.4.1 Pump Model in TRAC

TRAC-PF1/MOD1 has a pump model [NUREG/CR-3858, LA-10157-MS, 1986] which is based on the model developed by Idaho National Engineering Laboratory (INEL) from the Semi-Scale test data. The model is general enough to apply to any other pump for which single phase homologous curves, two-phase fully degraded homologous curves and degradation multipliers as a function of void fraction (α) are available for the pump head and hydraulic torque. The pump head is computed as follows:

$$H_{2\phi} = H_{1\phi} + M(\alpha)\ (H_{DEGRAD} - H_{1\phi}) \tag{34.45}$$

where $H_{2\phi}$, $H_{1\phi}$, H_{DEGRAD}, $M(\alpha)$ are two-phase head, single-phase head, fully degraded head and degradation multiplier respectively. The last three items in this list have to be supplied through input. The $M(\alpha)$-function interpolates between the single-phase head curve and the fully degraded, or lowest, two-phase head curve. The static pressure rise across the pump can be computed from the head, $H_{2\phi}$, and inlet density, ρ, as given here:

$$\Delta P = H_{2\phi} \cdot \rho_{in} \cdot g \tag{34.46}$$

The head curves in the model are in the form of homologous curves with homologous variables as defined here:

$$\begin{aligned} &(H/H_{ref})/(Q/Q_{ref})^2 \text{ vs. } (\Omega/\Omega_{ref})/(Q/Q_{ref}),\ (\Omega/\Omega_{ref})/(Q/Q_{ref}) \leq 1.0 \\ &(H/H_{ref})/(\Omega/\Omega_{ref})^2 \text{ vs. } (Q/Q_{ref})/(\Omega/\Omega_{ref}),\ (Q/Q_{ref})/(\Omega/\Omega_{ref}) \leq 1.0 \end{aligned} \tag{34.47}$$

A similar description is available for estimating the hydraulic torque for the pump:

$$T_{2\phi} = T_{1\phi} + N(\alpha)\ (T_{DEGRAD} - T_{1\phi}) \tag{34.48}$$

where $T_{2\phi}$, $T_{1\phi}$, T_{DEGRAD} and $N(\alpha)$ are two-phase, single-phase, and two-phase fully degraded torques, and torque degradation multiplier. $T_{1\phi}$ and T_{DEGRAD} are supplied through input tables or homologous curves. The homologous curves for torque are of the following form:

$$\begin{aligned} &\beta = T/T_{ref} \\ &\beta/(Q/Q_{ref}) \text{ vs. } (\Omega/\Omega_{ref})/(Q/Q_{ref}),\ (\Omega/\Omega_{ref})/(Q/Q_{ref}) < 1.0 \\ &\beta/(\Omega/\Omega_{ref}) \text{ vs. } (Q/Q_{ref})/(\Omega/\Omega_{ref}),\ (Q/Q_{ref})/(\Omega/\Omega_{ref}) \leq 1.0 \end{aligned} \tag{34.49}$$

The single-phase torque estimated from the homologous curves is corrected for the density if that is different from the rated density:

$$T = T_{ref}\ (\rho/\rho_{ref})\beta\ . \tag{34.50}$$

The torque obtained from the homologous curves is used to compute the pump speed.

The TRAC-PF1/MOD1 pump model is very simple and requires most of the information through the input. However, this model does not allow for the effect of three important parameters: specific speed, pressure and geometry. In general the pump head for two phase flow is a function of the following variables:

$$H_{2\phi} = H_{2\phi} (Q/Q_{ref}, \Omega/\Omega_{ref}, \alpha, P, N_s, Geom), \qquad (34.51)$$

where P, and N_s are pressure and pump specific speed.

Figure 34.14 shows homologous head curves as a function of void fraction for various pumps of different specific speeds and sizes at the rated condition of flow and speed. It can be seen from this figure, that there is a significant effect of pump design. The RS111 pump, which has the highest specific speed and is closer to the axial flow pump design, undergoes the least degradation. However, the effect of the specific speed and geometry can be eliminated from the expression for the head if the data are available for the right type of pump:

$$H_{2\phi} = H_{2\phi} (Q/Q_{ref}, \Omega/\Omega_{ref}, \alpha, P) \qquad (34.52)$$

The TRAC-PF1/MOD1 pump model also does not account for pressure effects. Figure 34.15 shows the effect of pressure on degradation for CE pump [Kennedy et al., 1980]. It is clear from this figure that degradation increases at low pressures.

The TRAC-PF1/MOD1 model as described earlier interpolates between single phase head curve and corresponding fully degraded head curve through a degradation multiplier which is only a function of void fraction. It has been observed [Seeberger and Schneider, 1986] that the same degradation multiplier function cannot be used for all flows and the lack of accounting for all the influences in the model will lead to a larger uncertainty in the model.

In summary, the current TRAC model for reactor coolant pumps cannot account for effects of inlet pressure, specific pump speed and pump size.

34.4.2 Analysis of Pump Modeling Uncertainty

The single phase performance curves for the pump head and the hydraulic torque for full size pumps or small scale pumps of the same specific speed are known with good accuracy (error <2%). Also for pumps with the same specific speed, the effect of the size is negligible and the single-phase curves from small-size pumps could be used for large-size pumps. However, the two-phase performance curves depend on many flow parameters and pump size which are not accounted for in TRAC-PF1/MOD1. Therefore, TRAC has large uncertainties in the results for the pump. All these uncertainties are combined in the uncertainty of the degradation multipliers.

34.4.2.1 Available Pump Models

There are two semi-empirical models available in the literature; the EPRI model and the KWU model. The EPRI model [Furuya and Maekawa, 1987] consists of a set of two-phase flow balance equations written in rotating coordinates for the impeller. The model contains available constitutive relationships for interfacial mass and momentum transfer, which were developed for the pipe flow. The model predicts the pump performance for various fluid conditions and pump speeds, but only near the design conditions for flow rate and pump speed. The EPRI model has been applied to a variety of pumps and some of the predictions are shown in Figures 34.16 and 34.17 for CREARE and C-E pumps. There is a large spread in the experimental data for void fractions below 0.5. However, the EPRI model predicts the trends for head degradation.

The EPRI model cannot be used to assess the uncertainty in the TRAC pump model because it requires pump design data which are proprietary and generally not available.

The second semi-empirical model is the KWU model [Seeberger and Schneider, 1986] which was developed for the Federal Ministry for Research and Technology, West Germany. Unlike the EPRI model, the KWU model does not imply integration of balance equations along the rotor channel, but does account for the important phenomena which cause the performance degradation. The model generates the degradation functions in terms of non-dimensional groups, using test data. The data are generally available only for small-scale pumps. The model has the potential to predict the performance of PWR pumps from subscale data. However, the KWU model does not account for condensation in the impeller, and there is some uncertainty about the allocation of head degradation among the three phenomena of slip, phase separation and compressibility. This model is simple and requires only impeller diameter and the test data from subscale pumps.

The KWU model application requires test data directly for developing the TRAC-PF1 model parameters. There is no accounting for pressure, flow rate and pump speed in the TRAC model. The resulting TRAC code uncertainty is reflected in the large spread of the computed degradation multipliers which can only be functions of inlet void fraction.

There is an additional limitation, as the test data are only available for small size pumps at specific pump speeds which differ from that of the full-scale PWR pump. Table 34.8 compares test pumps and summarizes all the data available. There are two possible approaches to use the KWU model; use the CE (1/5 scale, N_s = 4200) and KWU (1/5 scale, N_s = 6700) data to bracket the Westinghouse pump (N_s = 5200), or use the Westinghouse proprietary pump (1/3 scale, N_s = 5200) data directly. It was decided to follow the latter approach, as it produced data for the largest test pump available and at the correct specific speed. However, the data were taken at low pressure, and some data for air-water mixtures, which implies that a model developed from these data will overpredict the degradation for PWR LBLOCA conditions and will be conservative.

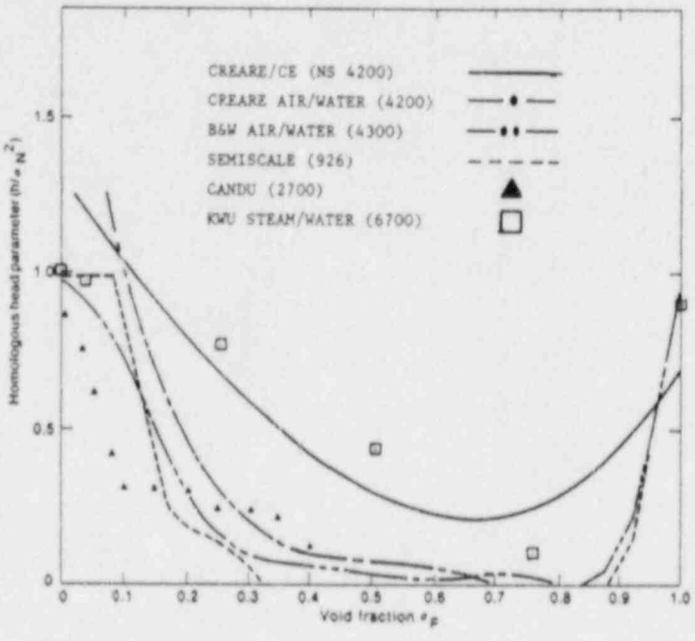

Figure 34.14 Comparison of Two-Phase Head for Various Pumps at Their Design Conditions

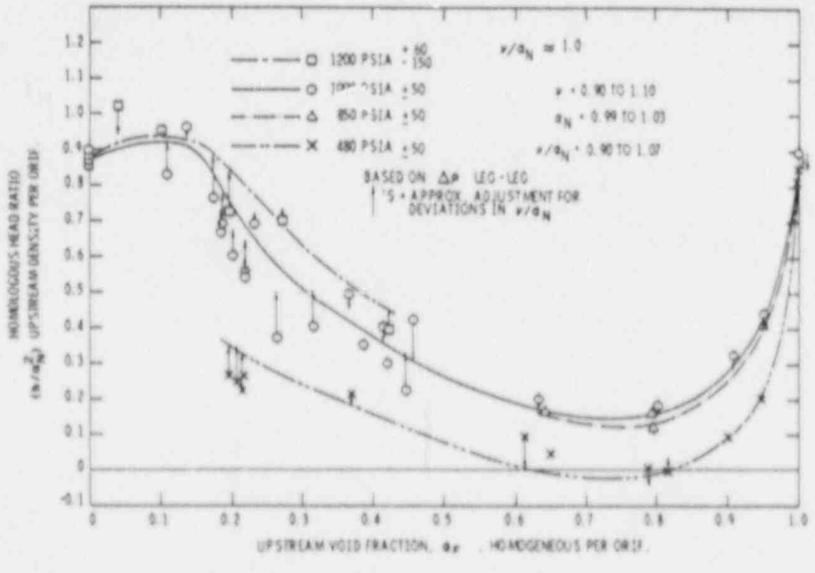

Figure 34.15 Effect of System Pressure on Two-Phase Flow Performance of CE Pump

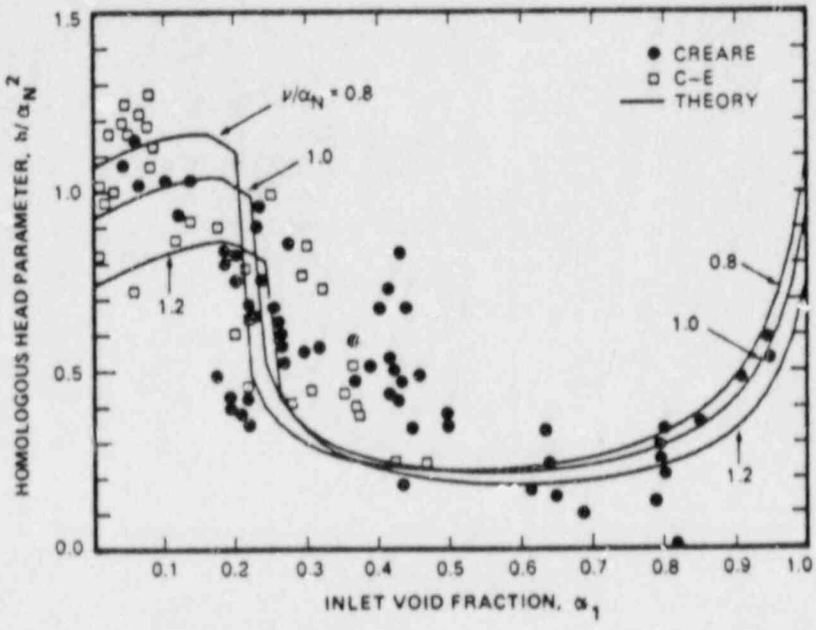

Figure 34.16 Comparison of the Head between the Theory and Experimental Data for a Mixed-Flow Pump for υ/α_N between 0.8 and 1.2 (steam/water case) (Furuya, 1987)

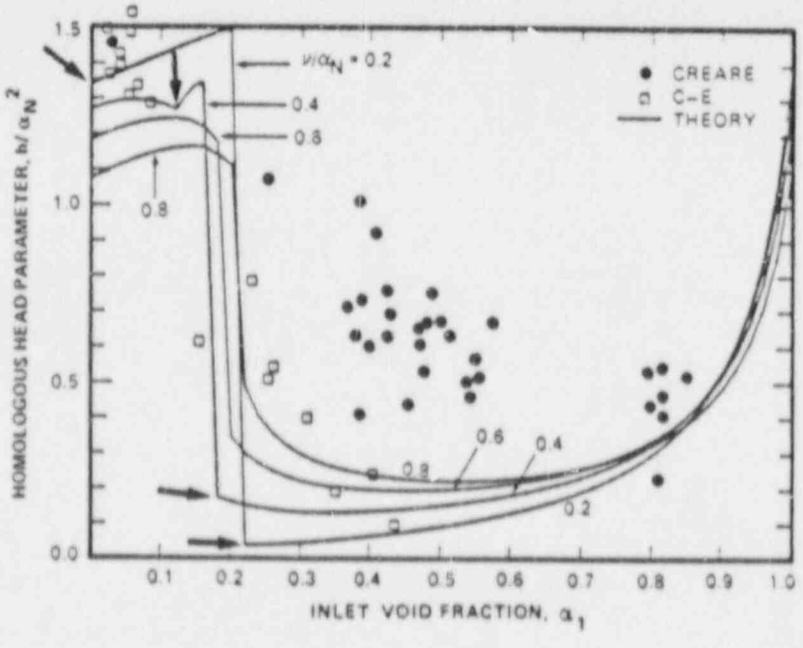

Figure 34.17 Comparison of the Head between the Theory with Inlet Pressure Variation and Experimental Data for Mixed-Flow Pump for υ/α_N between 0.0 and 0.8 (steam/water case) (Furuya, 1987)

34.4.2.2 TRAC Pump Model Assessment.

The model developed from the Westinghouse data consists of the single-phase and fully degraded homologous curves for head and torque, and of the mean value and the standard deviation of degradation multipliers, representing the modeling uncertainty.

The model developed from the Westinghouse pump data is for the correct specific speed, but it needs a correction for the size effect to represent the full-size pump. In order to estimate the size effect, the data from CE (1/5 scale) [Kennedy et al., 1980] and CREARE (1/20 scale) [Swift, 1982] pumps were analyzed in the range of $0.0 \leq (Q/Q_R)/(N/N_R) \leq 2.0$. Here Q and N designate volumetric flow rate and rotational pump speed, respectively. Subscript R denotes the normal operating conditions (design conditions). In order to minimize the uncertainty in determining the size effect, the data were grouped in the increment of 0.25 for $(Q/Q_R)/(N/N_R)$. For each of these groups, least-square fit curves for $(H/H_R)/(N/N_R)^2$ or $(H/H_R)/(Q/Q_R)^2$ were obtained as a function of void fraction, for both the CE and CREARE pumps, as shown in Figures 34.18 through 34.21. The R value in these figures is the root-mean square value of the differences between the data and the best-fit curve. The number of data points considered in each curve fit are given in the bracket (#). The root mean square averages of the difference between the two curves for each group of $(Q/Q_R)/(N/N_R)$ were obtained. The conclusion from these numbers is that the size effect is smallest near the design conditions ($(Q/Q_R)/(N/N_R) \approx 1.0$), and that the larger pump degrades less. The difference between the curves would be less if CREARE data were available at the same pressure as that of the CE data.

The CE and CREARE pump data were further analyzed by obtaining mean degradation functions which are shown in Figure 34.22. The CREARE data are available only for void fractions less than 0.5. Figure 34.22 confirms our earlier conclusion that the larger size pump (CE) degrades less. Furthermore, it can also be hypothesized that the effect of size will be less for larger pumps because the length scale of two-phase flow structure will be much smaller than the pump dimensions. There is a definite lack of data at proper pressures and void fractions to make a quantitative estimate of the size effects to correct the model developed from the Westinghouse data.

A recent study was performed [Fujie and Yamanouchi, 1985] to investigate the similarity rules applicable to two phase flow through centrifugal pumps. They studied the flow regime transitions and the interfacial transfer functions in the blade channels. They concluded that for most flow conditions, other than low gas velocity or large liquid velocity, the single phase similarity laws also apply to two phase flows. The conclusion from this study implies that the models developed from small-scale pumps under similar pressure conditions can be used for full-scale pumps.

Based on the argument presented so far, it can be concluded that the pump model along with the uncertainties developed from the Westinghouse pump (1/3 scale) data can be used to represent the full-size pump and that the lack of correction for the size effect and pressure will tend to predict earlier pump degradation and higher peak clad temperature in LBLOCA.

Table 34.8 Rated Pump Parameters and Operating Conditions at Full-Scale and in Five Test Programs

Parameter	Westinghouse PWR	PWR Primary Coolant Pump (Bingham-Williamette)	PWR Primary Coolant Pump (Byron-Jackson)	Westinghouse Pump	B&W Pump	C-E Pump	Creare Pumps	KWU Pump
Scale	1/1	1/1	1/1	1/3	1/3 of Bingham-Williamette Pump	1/5 of Byron Jackson Pump	1/20 of Byron-Jackson Pump	1/5, RS111
Rated Volumetric Flow Rate (gpm)	94,600	104,200	87,000	6210	11,200	3500	181 (219)	3148
Rated Total Head (ft)	290	397	252	64.4	390	252	252	293.7
Rated Speed (rpm)	1190	1190	900	1500	3580	4500	18,000	8480
Specific Speed rpm $(gpm)^{0.5}/(ft)^{0.75}$	5200	4319	4200	5190	4317	4200	4200	6700
Fluid*	S/W	S/W	S/W	A/W & S/W	A/W	S/W	A/W and S/W	S/W
Pressure (psia)	15-2250	15-2250	15-2250	15-420	20-120	15-1250	A/W at 90 S/W at 400	435-1305

* A/W is air/water mixture
S/W is steam/water mixture

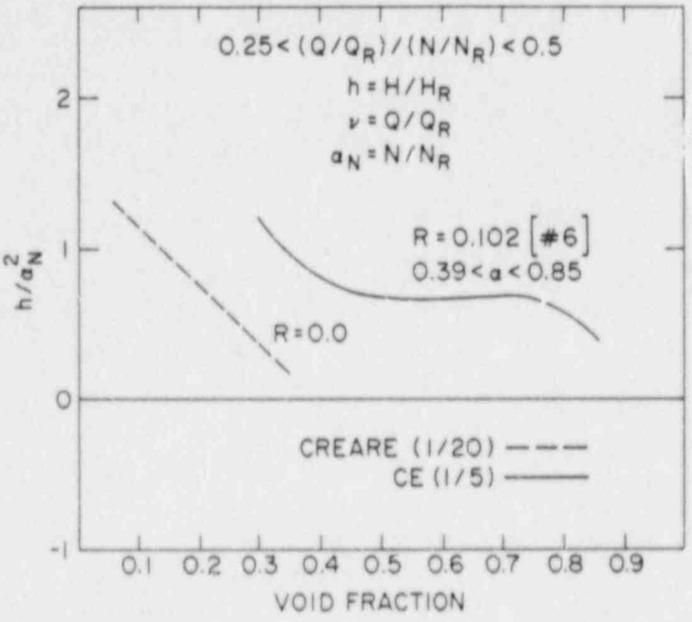

Figure 34.18 Comparison of CE and CREARE Pump Performance for $0.25 < (Q/Q_{ref})/(N/N_R) < 0.5$

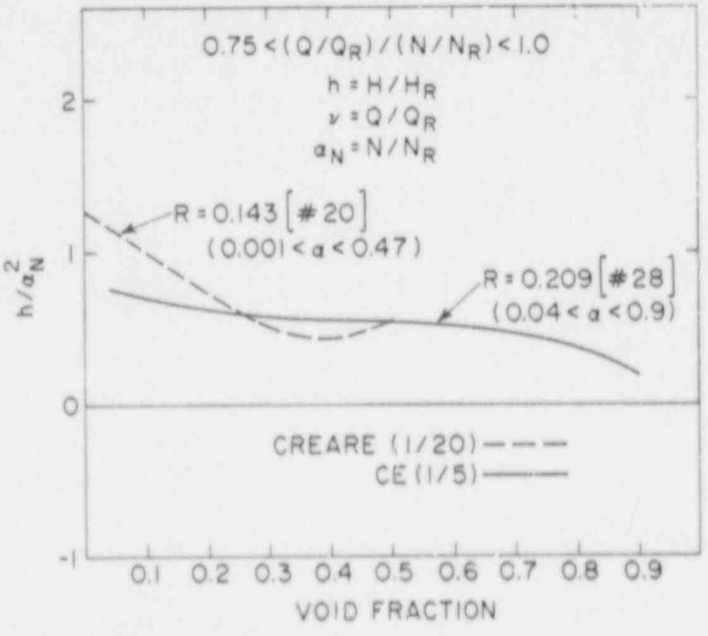

Figure 34.19 Comparison of CE and CREARE Pump Performance for $0.75 < (Q/Q_R)/(N/N_R) < 1.0$

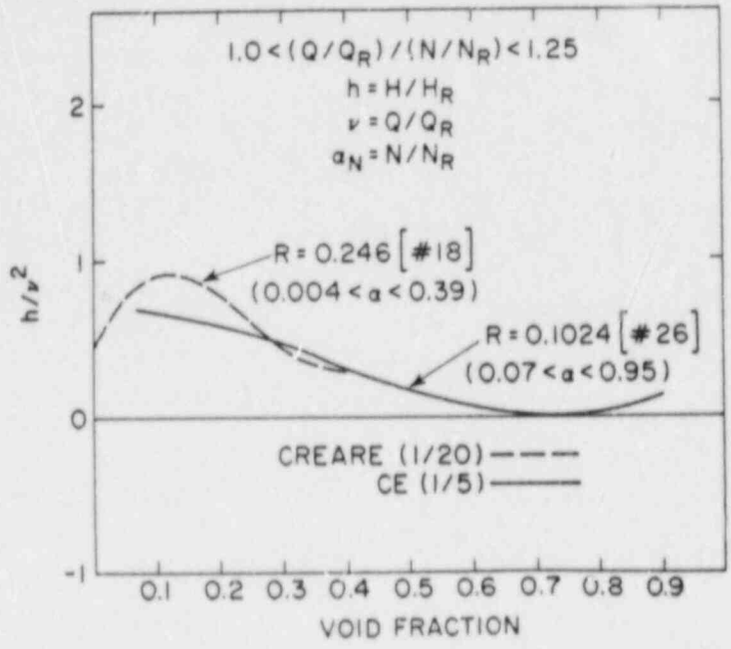

Figure 34.20 Comparison of CE and CREARE Pump Performance for $1.05 < (Q/Q_R)/(N/N_R) < 1.25$

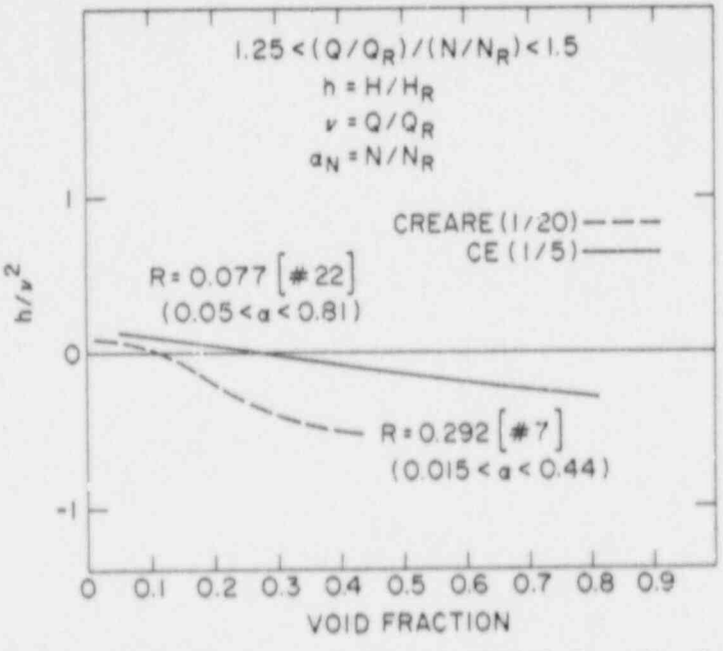

Figure 34.21 Comparison of CE and CREARE Pump Performance for $1.25 < (Q/Q_R)/(N/N_R) < 1.5$

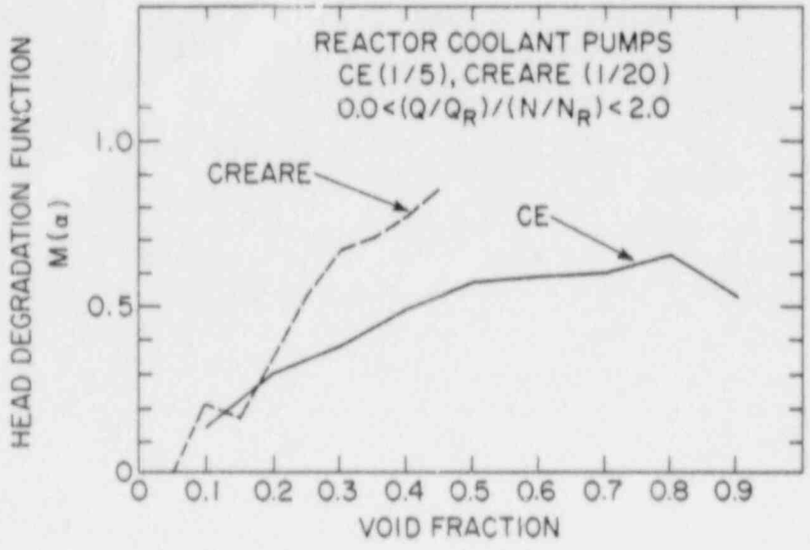

Figure 34.22 Comparison of Head Degradation Functions Developed from CREARE and CE Pump Data

34.4.3 Conclusions Regarding Pump Model Uncertainty

A pump model in the framework of TRAC-PF1/MOD1 were developed from the Westinghouse pump data (1/3). It was also shown that larger pumps will degrade less and that the model developed from low pressure data will overpredict pump degradation. The model developed here will predict early degradation for the pump in LBLOCA which will affect the thermal-hydraulic calculations for the reactor towards estimating higher peak clad temperatures.

A more realistic pump model is needed than the current TRAC pump model, which properly accounts for pressure, flow rate, pump speed and the pump size. The inability to account for these parameters is the largest contributor to the TRAC model uncertainty. There are data available for full-scale CANDU pumps and smaller scale KWU pumps (1/5 scale) which should be utilized. Furthermore, the EPRI model [Furuya and Maekawa, 1987] and KWU semi-empirical [Seeberger and Schneider, 1986] model should be utilized. The current TRAC model also does not account for the energy transfer from the impeller to the fluid in the energy equation and it assumes homogeneous fluid conditions at the pump discharge. These two model weaknesses should also be resolved.

34.5 Future Work

The work on PCT uncertainty caused from fuel modeling in TRAC is completed. Components of PCT uncertainty will be combined statistically through TRAC calculations (response surface) and statistics, in an ongoing USNRC project.

Bias and uncertainty of break flow modeling in TRAC as presented here will be used in the same development of response surface and statistical analysis for predicting overall PCT uncertainty.

The bias for TRAC pump models will also be used in the same analysis for overall PCT uncertainty. Uncertainty in pump degradation has been estimated, but is proprietary information and not presented here.

More detailed documentation is forthcoming in NUREG/CP-0091, Vol. 4.

REFERENCES

ABDOLLAHIAN, D., "Critical Flow Data Review and Analysis," EPRI Report, NP-2192, January 1982.

BOYACK, B.E., "Response to Questions of September 8, 1987," Letter dated September 15, 1987, from Los Alamos National Laboratory to U. S. Rohatgi, Brookhaven National Laboratory.

CAMPBELL, F.R. et al., "In-Reactor Measurement of Fuel-to-Sheath Heat Transfer Coefficients Between UO_2 and Stainless Steel," AECL-5400 (1977).

CHAMBERS, R., W. E. DRISKELL and S. C. RESCH, "Assessment of FRAP-T6 Code Capabilities During Large Break Loss of Coolant Accidents," EGG-CAAD-5829, Idaho National Engineering Laboratory, Idaho Falls, ID (1982).

"Compendium of ECCS Research for Realistic LOCA Analysis," Draft Report, NUREG-1230, Division of Reactor and Plant Systems, U.S. Nuclear Regulatory Commission, Washington, D.C. (1987). See Section 4.3.4.

CUNNINGHAM, M.E. et al., "Stored Energy Calculation: The State of the Art," PNL-2581, Pacific Northwest Laboratory, Richland, WA 99352, operated by Battelle Memorial Institute (1978).

DEAN, R.A., "Thermal Contact Conductance Between UO_2 and Zircaloy-2," CVNA-127, Westinghouse Electric Corporation (1962).

DITTUS, F.W. and L. M. K. BOELTER, "Heat Transfer in Automobile Radiators of Tubular Type," Publications in Engineering, University of California, Berkeley; p. 443 (1930).

FUJIE, H. and A. YAMANOUCHI, "A Study on Applicability of Similarity Rule to Performances of Centrifugal Pumps Driven in Two-Phase Flow," Nuclear Engineering and Design, 85, 1985, pp. 345-352.

FURUYA, O. and S. MAEKAWA, "An Analytical Method for Prediction of Pump Performance Operating in Condensable Two-Phase Flows," Proc. of 1987 ASME/JSME Thermal Engineering Joint Conference, Hawaii, March 1987.

HAGRMAN, D.L. et al., "MATPRO-Version II (Revision 1), A Handbook of Materials Properties for Use in the Analysis of LWR Fuel Rod Behavior," NUREG/CR-0497, TREE-1280, Rev. 1, EG&G Idaho, Inc., Idaho Falls, ID (February 1980).

JONES, JR., O. C., "Flashing Inception in Flowing Liquids," Brookhaven National Laboratory Report, BNL-NUREG-51221, 1980.

KENNEDY, W. C., et al., "Pump Two-Phase Performance Program," EPRI Reports, NP-1556 (Vol. 1-8), September 1980.

LAATS, E.T., "FRAPCON-2 Model Uncertainty Study," EGG-CAAD-5584, EG&G Idaho, Idaho National Engineering Laboratory, Idaho Falls, ID (1981).

LASSMANN, K. and F. HOHLEFELD, "The Revised Urgap Model to Describe the Gap Conductance Between Fuel and Cladding," Nuclear Engineering and Design, 103 (1987), p. 215.

LELLOUCHE, G.S., "Considerations Relative to TRAC-PF1/MOD1 Uncertainty Analysis," distributed to members of the USNRC Technical Program Group, from S. Levy, Inc., 3425 S. Bascom Ave., Campbell, CA 95008-7006, Sept. 18, 1987.

MALANG, S., "Simulation of Nuclear Fuel Pads by Using Process-Controlled Power for Indirect Electrically Heated Rods," ORNL-TM-4712 (GEMP-482), Oak Ridge National Laboratory (1975).

RANSON, V. H., "RELAP5/MOD 1 Manual, Volume 1: System Models and Numerical Methods," NUREG/CR-1826 (1981).

ROSS, A.M. and R. L. STOUTE, "Heat Transfer Coefficient Between UO_2 and Zircaloy-2," CRFD-1075 (1962).

Safety Code Development Group, "TRAC-PF1/MOD1: An Advanced Best Estimate Computer Program for Pressurized Water Reactor Thermal-Hydraulics Analysis," NUREG/CR-3858, LA-10157-MS, Los Alamos National Laboratory, Los Alamos, NM 87545 (1986).

SEEBERGER, G. J. and K. SCHNEIDER, "Development of a Two-Phase Pump Model for the Main Coolant Pumps in Pressurized Water Reactors," Foreign Document I.D. R 917/85/003, NRC Translation 1821, May 1986.

SHERON, B.W., "Bases and Criteria for the Selection of Response Surface Parameters for the Statistical Assessment of LOCA," Enclosure 7, GEW-38-87, U.S. Nuclear Regulatory Commission, Division of Safety, Washington, DC 20555, (301) 492-7588 (1987).

STECK, G.P., M. PERMAN, R. K. BYERS, "Uncertainty Analysis for a PWR Loss-of-Coolant Accident: I. Blowdown Phase Employing the RELAP4/MOD6 Computer Code," NUREG/CR-0940, SAND79-1206, Sandia Laboratories, Albuquerque, NM 87185 (1980).

SWIFT, W. L., "Model Pump Performance Program - Data Report," EPRI NP-2379, May 1982.

"The Marviken Full Scale Critical Flow Tests, Results from Test 12," MXC-212, September 1979, Joint Reactor Safety Experiments in the Marviken Power Station, Sweden.

"The Marviken Full Scale Critical Flow Tests, Results from Test 13," MXC-213, September 1979, Joint Reactor Safety Experiments in the Marviken Power Station, Sweden.

"The Marviken Full Scale Critical Flow Tests, Results from Test 15," MXC-215, September 1979, Joint Reactor Safety Experiments in the Marviken Power Station, Sweden.

"The Marviken Full Scale Critical Flow Tests, Results from Test 16," MXC-216, September 1979, Joint Reactor Safety Experiments in the Marviken Power Station, Sweden.

"The Marviken Full Scale Critical Flow Tests, Results from Test 17," MXC-217, September 1979, Joint Reactor Safety Experiments in the Marviken Power Station, Sweden.

"The Marviken Full Scale Critical Flow Tests, Results from Test 18," MXC-218, September 1979, Joint Reactor Safety Experiments in the Marviken Power Station, Sweden.

"The Marviken Full Scale Critical Flow Tests, Results from Test 19," MXC-219, September 1979, Joint Reactor Safety Experiments in the Marviken Power Station, Sweden.

"The Marviken Full Scale Critical Flow Tests, Results from Test 20," MXC-220, September 1979, Joint Reactor Safety Experiments in the Marviken Power Station, Sweden.

"The Marviken Full Scale Critical Flow Tests, Results from Test 21," MXC-221, September 1979, Joint Reactor Safety Experiments in the Marviken Power Station, Sweden.

"The Marviken Full Scale Critical Flow Tests, Results from Test 22," MXC-222, September 1979, Joint Reactor Safety Experiments in the Marviken Power Station, Sweden.

"The Marviken Full Scale Critical Flow Tests, Results from Test 24," MXC-224, September 1979, Joint Reactor Safety Experiments in the Marviken Power Station, Sweden.

"The Marviken Full Scale Critical Flow Tests, Results from Test 25," MXC-225, September 1979, Joint Reactor Safety Experiments in the Marviken Power Station, Sweden.

WULFF, W., H. S. CHENG and A. N. MALLEN, "Analytical Modeling Techniques for Efficient Heat Transfer Simulation in Nuclear Power Plants," 23rd ASME/AIChE/ANS National Heat Transfer Conference, Denver, CO, BNL-NUREG-35944 (1985). (See Eq. (9) for cladding and Eq. (12) for pellet).

WULFF, W., H. S. CHENG, S. V. LEKACH and A. N. MALLEN, "The BWR Plant Analyzer," NUREG/CR-3943, BNL-NUREG-51812, Brookhaven National Laboratory, Upton, NY 11973 (1984).

NRC FORM 335 (2-84) NRCM 1102, 3201, 3202

U.S. NUCLEAR REGULATORY COMMISSION

BIBLIOGRAPHIC DATA SHEET

SEE INSTRUCTIONS ON THE REVERSE

1. REPORT NUMBER (Assigned by TIDC add Vol. No., if any)
NUREG/CR-2331
BNL-NUREG-51434, Vol. 7, No. 2 & No. 3

2. TITLE AND SUBTITLE
Safety Research Programs Sponsored by Office of Nuclear Regulatory Research, Progress Report, April 1, 1987 - September 30, 1987

3. LEAVE BLANK

4. DATE REPORT COMPLETED
MONTH: May YEAR: 1988

5. AUTHOR(S)
Compiled by Allen J. Weiss

6. DATE REPORT ISSUED
MONTH: June YEAR: 1988

7. PERFORMING ORGANIZATION NAME AND MAILING ADDRESS (Include Zip Code)
Brookhaven National Laboratory
Department of Nuclear Energy
Upton, New York 11973

8. PROJECT/TASK/WORK UNIT NUMBER

9. FIN OR GRANT NUMBER A-3014, 24, 3215, 27, 30, 42, 52, 6E, 70, 81, 82, 86, SO, 93, 94, 95, 98, 3302, 05, 3705, 72, 86, 88, 3801, 06, 21, 25, 27, 28, 29, 49, 61, 3952, 54, D-1679

10. SPONSORING ORGANIZATION NAME AND MAILING ADDRESS (Include Zip Code)
U.S. Nuclear Regulatory Commission
Office of Nuclear Regulatory Research
Washington, D.C. 20555

11a. Type of Report - Progress

b. PERIOD COVERED (Inclusive dates)
April 1 - September 30, 1987

12. SUPPLEMENTARY NOTES

13. ABSTRACT (200 words or less)

The Advanced and Water Reactor Safety Research Programs Quarterly Progress Reports have been combined and are included in this report entitled, "Safety Research Programs Sponsored by the Office of Nuclear Regulatory Research - Progress Report." This progress report will describe current activities and technical progress in the programs at Brookhaven National Laboratory sponsored by the Division of Regulatory Applications, Division of Engineering, Division of Reactor Accident Analysis, and Division of Reactor and Plant Systems of the U.S. Nuclear Regulatory Commission, Office of Nuclear Regulatory Research following the reorganization in February 1987.

14. DOCUMENT ANALYSIS - a. KEYWORDS/DESCRIPTORS
Thermal-Hydraulic Reactor Safety, Severe Accident, TRAC-BF1 Code, Core-Concrete Interaction, Fire Protection, Failure Analysis, Reactor Dosimetry, QUASAR, SP-90, GI-82, GI-99, Advanced Reactors, COMMIX, Plant Analyzer, RAMONA-3B, Protective Action, Source Term, Prob. Risk Assess. Nucl. Plant Aging, MELCOR, PETS, Performance Indicators

15. AVAILABILITY STATEMENT

16. SECURITY CLASSIFICATION
(This page)
(This report)

17. NUMBER OF PAGES

18. PRICE